PB196380

A MANUAL OF
ELECTROSTATIC PRECIPITATOR TECHNOLOGY
PART I - FUNDAMENTALS

SOUTHERN RESEARCH INSTITUTE
2000 9th Avenue S. Birmingham, Alabama 35205

Reproduced by
NATIONAL TECHNICAL
INFORMATION SERVICE
Springfield, Va. 22151

338

STANDARD TITLE PAGE FOR TECHNICAL REPORTS

1. Report No. APTD-0610

2. Govt. Accession No.

3. Recipient's Catalog No.

4. Title and Subtitle

A Manual of Electrostatic Precipitator Technology
Part 1 - Fundamentals

5. Report Date August 25, 1970

6. Performing Organization Code

7. Author(s)

Sabert Oglesby, Jr. and Grady B. Nichols

8. Performing Organization Rept. No.

9. Performing Organization Name and Address

Southern Research Institute
2000 9th Avenue, S.
Birmingham, Alabama 35205

10. Project/Task/Work Unit No.

11. Contract/Grant No. CPA-22-69-73

12. Sponsoring Agency Name and Address

Division of Process Control Engineering
National Air Pollution Control Administration
Cincinnati, Ohio 45227

13. Type of Report & Period Covered

14. Sponsoring Agency Code

15. Supplementary Notes

16. Abstracts

The state of technology of electrostatic precipitation for particulate emission control is reported. This report is intended to serve as a basic handbook on the subject of electrostatic precipitation covering the entire system including fundamental theory, design, operation, and application. Its purpose is to provide a source of information that will be of benefit to the researcher, manufacturer, and user of electrostatic precipitators. The systems study included a review of literature pertaining to electrostatic precipitation, a comprehensive review of precipitator fundamentals, a survey and review of the use of precipitators in each of eight major application areas, and a review of the potential for electrostatic precipitators in new applications. In order to provide information useful to a wide range of users, this manual is organized to present a general review of the precipitation process, with qualitative relationships between the various precipitator functions, and a detailed quantitative analysis of each of the system functions. Particular emphasis is placed on the validity of the theoretical derivations in view of the (over)

17. Key Words and Document Analysis. (a). Descriptors

Air pollution control equipment	Reviews
Electrostatic precipitators	
Design criteria	
Gas flow	
Electric corona	
Electric charge	
Electrical resistivity	
Maintenance	
Manuals	
Handbooks	

17b. Identifiers/Open-Ended Terms

17c. COSATI Field/Group 13/02, 20/03, 09/03

18. Distribution Statement Unlimited

19. Security Class (This Report) UNCLASSIFIED

20. Security Class. (This Page) UNCLASSIFIED

21. No. of Pages 347

22. Price

This report was furnished to the Air
Pollution Control Office by the
Southern Research Institute in fulfillment of Contract No. CPA-22-69-73.

16. Abstracts (cont'd)

assumptions made and the significance of the interaction of variables of importance in precipitator operation. Further discussions include mechanical design considerations, energization equipment, gas flow, operational problems, and the current utilization of precipitators in the major application areas.

A MANUAL OF
ELECTROSTATIC PRECIPITATOR TECHNOLOGY

PART I - FUNDAMENTALS

Prepared Under Contract CPA 22-69-73

for

THE NATIONAL AIR POLLUTION CONTROL ADMINISTRATION
Division of Process Control Engineering
Cincinnati, Ohio

by

Sabert Oglesby, Jr., Director
Engineering Research and
Principal Investigator

and

Grady B. Nichols, Senior Engineer

Southern Research Institute
Birmingham, Alabama
August 25, 1970
10,000-2291-XIII

FOREWORD

This manual of electrostatic precipitator technology was prepared under Contract CPA 22-69-73 for the National Air Pollution Control Administration, Division of Process Control Engineering, with Mr. Timothy W. Devitt serving as Project Officer. The manual is presented in two parts. Part I covers the fundamentals of electrostatic precipitation and Part II covers the application of electrostatic precipitators to control of emissions in various application areas.

Part I of this manual was prepared on the basis of a comprehensive review of precipitator literature and discussions with those active in research in the field of electrostatic precipitation. Part II of the manual was prepared on the basis of information prepared by Research-Cottrell, Inc., Bound Brook, New Jersey, based on records covering installations in the various application areas. These installations include some designed by other precipitator manufacturers, as well as those designed by Research-Cottrell.

To supplement the data furnished by Research-Cottrell, Southern Research Institute conducted a survey of a number of installations in various industries. In some instances, considerable data were available covering both design and performance of the precipitators. In other instances, data were not available. Consequently, the extent and quality of the information covering the application areas varies.

Rust Engineering Company, Division of Litton Industries, Birmingham, Alabama, furnished data on the application of electrostatic precipitators in the pulp and paper industry.

Dr. Harry J. White, Head of the Department of Applied Science, Portland State University, served as consultant on the program and contributed heavily in the review of precipitator fundamentals.

ABSTRACT

This manual is a comprehensive report on the state of technology of electrostatic precipitation for particulate emission control. It is intended to serve as a basic handbook on the subject of electrostatic precipitation covering the entire system including fundamental theory, design, operation, and application.

The purpose of the manual is to provide a source of information that will be of benefit to the researcher, manufacturer, and user of electrostatic precipitators. The information and data are based on an electrostatic precipitator systems study performed under Contract No. CPA 22-69-73 for the National Air Pollution Control Administration.

The systems study included a review of literature pertaining to electrostatic precipitation, a comprehensive review of precipitator fundamentals, a survey and review of the use of precipitators in each of eight major application areas, and a review of the potential for electrostatic precipitators in new applications.

In order to provide information useful to a wide range of users, this manual is organized to present a general review of the precipitation process, with qualitative relationships between the various precipitator functions, and a detailed quantitative analysis of each of the system functions. Particular emphasis is placed on the validity of the theoretical derivations in view of the assumptions made and the significance of the interaction of variables of importance in precipitator operation.

Further discussions include mechanical design considerations, energization equipment, gas flow, operational problems, and the current utilization of precipitators in the major application areas.

TABLE OF CONTENTS
PART I - FUNDAMENTALS

Page No.

DESCRIPTIVE SUMMARY 1

Corona Generation 1
Particle Charging 6
Particle Collection 9
Removal 11
Electrical Energization 12
Systems Analysis 13
Design 14
Mechanical Components 16
Gas Flow 17
Resistivity 18
Measurement of Performance 19
Troubleshooting and Maintenance 20
Electrostatic Augmentation and Unusual Designs 21

CHAPTER 1. CORONA GENERATION 23

1.1 Current Voltage Relationship 30
1.2 Temperature and Pressure Effects 34
1.3 Practical Aspects of Corona Theory on Electrostatic Precipitation 40
1.4 Practical Aspects of Corona Generation 53
Bibliography 55

CHAPTER 2. THE ELECTRIC FIELD 57

2.1 Space Charge Phenomena 57
2.2 Practical Aspects of the Electric Field 66
Bibliography 68

CHAPTER 3. PARTICLE CHARGING 69

3.1 Field Charging 70
3.2 Diffusion Charging 78

Page No.

3.3 Combination of Field and Diffusion Charging 81
3.4 Practical Aspects of Particle Charging 85
Bibliography 95

CHAPTER 4. PARTICLE COLLECTION 96

4.1 Particle Kinetics 96
4.2 Particle Collection with Laminar Gas Flow 103
4.3 Particle Collection with Turbulent Gas Flow 105
4.4 Factors Modifying the Particle Collection in a Precipitator 114
4.5 Practical Aspects of Particle Collection 117
4.6 Recent Modifications to the Deutsch Equation 118
Bibliography 123

CHAPTER 5. GAS FLOW 124

5.1 Introduction 124
5.2 Straighteners 138
5.3 Splitters 139
5.4 Transformation Splitters 139
5.5 Vanes 141
5.6 Diffusion Plates 144
5.7 Modelling 146
Bibliography 151

CHAPTER 6. RAPPING AND REENTRAINMENT 152

6.1 Rapping 152
6.2 Reentrainment 158
Bibliography 165

CHAPTER 7. RESISTIVITY AND CONDITIONING 166

7.1 Volume Conduction 166
7.2 Surface Conduction 167
7.3 Mechanisms of Surface Conditioning 171
7.4 Field Conditioning Studies 177
7.5 Moisture Conditioning 177
7.6 Chemical Conditioning 179
Bibliography 186

Page No.

CHAPTER 8. ELECTROSTATIC PRECIPITATOR SYSTEMS ANALYSIS 187

8.1 Generalized Precipitator Model 188
8.2 Simplified System Model 190
8.3 Example Utilizing Existing Simplified System Model . 193
8.4 Limitations of Existing Model 199
8.5 Model Verification 200

CHAPTER 9. DESIGN METHODOLOGY 203

9.1 Design Method I 203
9.2 Design Method II 214
Bibliography 217

CHAPTER 10. MECHANICAL COMPONENTS 218

10.1 Tubular Type Precipitators 218
10.2 Plate Type Precipitators 218
10.3 Discharge Electrodes 221
10.4 Discharge Electrode Support 227
10.5 Collecting Electrodes 229
10.6 Electrode Cleaning Equipment 233
10.7 Hopper Systems 239
10.8 Dust Removal Systems 239
Bibliography 241

CHAPTER 11. POWER SUPPLIES AND CONTROLS 242

11.1 The Power System 242
Bibliography 265

CHAPTER 12. MEASUREMENTS 266

12.1 Measurement of Gas Flow and Efficiency 266
12.2 Velocity and Gas Volume 266
12.3 Determination of Dust Concentration 268
12.4 Computation 272
12.5 Sources of Error 276
12.6 Measurement of Resistivity 288
Bibliography 297

Page No.

CHAPTER 13. TROUBLESHOOTING AND MAINTENANCE...... 298

13.1 Gas Flow 301
13.2 Rapping 302
13.3 Hoppers and Ash Removal 304
13.4 Troubleshooting Techniques 304
13.5 Maintenance 305

CHAPTER 14. ELECTROSTATIC AUGMENTATION AND UNUSUAL PRECIPITATION DESIGNS........... 311

14.1 Wet Scrubbers 311
14.2 Electrostatically Augmented Packed Bed Filters 314
14.3 Fabric Filter 315
14.4 Mechanical Collection........ 315
14.5 Space Charge Precipitation 316
Bibliography 322

LIST OF FIGURES
PART I

Figure No. Page No.

1.1 Diagram of the Feedback Nature of the Avalanche Process 29
1.2 Theoretical Relationship Between Corona Starting Voltage and Wire Size.................. 33
1.3 Effect of Wire-to-Wire Spacing on Clean Electrode Corona Current..................... 35
1.4 Variations in Clean Electrode Corona Starting Potential With Pressure and Temperature 37
1.5 Electrical Characteristics of Air at 1500°F 38
1.6 Current Voltage Relationships for 15-ft Wire and Pipe Precipitator at High Pressure and High Temperature 41
1.7 Negative Corona Characteristics for Nitrogen-Oxygen Mixtures With Clean Electrodes 42
1.8 Variation of Negative Corona Current With Applied Voltage for Nitrogen-Sulfur Dioxide Mixtures 43
1.9 Variation in Negative Corona Current With Applied Voltage for Air-Water Vapor Mixtures at 400°F and Atmospheric Pressure.......................... 44
1.10 Electric Field and Charged Particle Distribution Within a Corona.............................. 52

3.1 Electric Field Modified by the Presence of an Uncharged Conducting Particle 72
3.2 Induced Electrostatic Charge in Particulate Due to Proximity of Ion 73
3.3 Electric Field After Particle Acquires a Saturation Charge 74
3.4 Number of Elementary Charges Vs. Ion Density and Time for Various Theoretical Analyses 83
3.5 Particle Charging Characteristics—Number of Charges Vs. Particle Size. Comparison Between Hewitt's Experimental Data and Various Charging Theories 84

Figure No. Page No.

3.6 Number of Elementary Charges Vs. Charge Density—Time Product for 0.06μ Radius...... 86
3.7 Electric Field Variations as a Function of Time at a Particular Point in Space Caused by the Variation in the Applied Voltage from the Power Supply.. 87
3.8 Charging Characteristics for Various Waveforms With 3 kV/cm Average Values................ 91
3.9 Charge Vs. Time in a Field of 3 kV/cm Average, With Charging Time Constant as a Parameter Peak/Average = 1.63 94

4.1 Free Body Diagram of Forces Acting on a Negatively Charged Particle in an Electrostatic Precipitator.. 98
4.2 Acceleration Time Constant (τ) as a Function of Particle Diameter 101
4.3 Length of Precipitator Required for 100% Collection for Idealized Laminar Gas Flow in a Pipe Precipitator of Radius, R.................... 104
4.4 Possible Gas Distribution in a Precipitator Duct 108
4.5 Assumed Gas Flow Distribution for Quality Factor Example 113
4.6 Negative Corona Voltage Current Characteristics in Air for a 15-foot Pipe, 20 cm Diameter, 0.277 cm Wire Diameter......................... 116

5.1 Air Friction Vs. Reynolds Number and Roughness 129
5.2 Collection Efficiency as a Function of Flow Velocity 133
5.3 Gas Velocity Profiles......................... 134
5.4 Gas Velocity Contour Plot 135
5.5 Histogram Showing Statistical Velocity Distribution................................ 137
5.6 Elbow Loss as a Function of Radius Ratio 140
5.7 Streamlined Turning Vane Elbow 143

6.1 Acceleration to Remove Dust Down to a Given Remaining Thickness for Fly Ash in British Installations................................ 155
6.2 Shear (Parallel) Rapping Efficiency for Various Precipitated Dust Layers Having About 0.2 Gram of Dust per sq in., as a Function of Maximum Acceleration in Multiples of "g" 156

Figure No. Page No.

6.3 Normal (Perpendicular) Rapping Efficiency for Various Precipitated Dust Layers Having About 0.2 Gram of Dust per sq in., as a Function of Maximum Acceleration in Multiples of "g"..... 157
6.4 Threshold Shear Velocity Vs. Particle Size ... 160

7.1 Plots of Resistivity Vs. 1/kT 168
7.2 Experimental Values of Electron Activation Energy.............................. 169
7.3 Resistivity of Bone-Dry Dusts at Elevated Temperatures.............................. 170
7.4 Effect of Humidity on Particle Resistivity 172
7.5 Conditioned Fly Ash Particle——CERL, England (20,000X) 174
7.6 Unconditioned Fly Ash Particle——Low Sulfur Coal (80,000X) 176
7.7 High-Temperature Psychrometric Chart 178
7.8 Schematic Diagram of SO_3 Conditioning Plant .. 181
7.9 Effect of Ammonia Conditioning on Southern N.S.W. Fly Ash.......................... 184

8.1 Electrostatic Precipitator System Model 189
8.2 Electrostatic Precipitator System Model—Parts Simulated in Computer Program in Heavy Line 191
8.3 Computer System Flow Diagram 194
8.4 Input Particle Size Distribution and Discrete Approximation 196
8.5 Computed Efficiency Vs. Particle Size for Five Installations 202

9.1 Relationship between Precipitation Rate Parameter and Resistivity.................. 207
9.2 Relationship between Precipitation Rate Parameter and Sulfur Content for Electric Utility Installations at a Temperature of 300°F. 208
9.3 Collection Efficiency Vs. Power Rate......... 210
9.4 Relationship between Collection Efficiency and Sectionalization 211
9.5 Linear Relationship between Precipitation Rate Parameter and Power Density for Fly Ash Collectors 215

Figure No.		Page No.
10.1	A Single-Stage Vertical Wire and Pipe Unit	219
10.2	Parallel Plate Precipitator	220
10.3	Weighted Wire Corona Electrodes	223
10.4	Typical Shapes of Stiff Discharge Electrodes	225
10.5	Two Types of Support Structures for Corona Wires	226
10.6	High Temperature Support Bushings, Style 1	228
10.7	High Temperature Support Bushings, Style 2	230
10.8	Various Types of Collection Electrodes	232
10.9	Typical Electromagnetic Rapper Assembly	234
10.10	Typical Electromagnetic Vibrator Assembly	236
10.11	Mechanical Single Impact Rapper	238
11.1	The Power Supply System for Modern Precipitators	243
11.2	Full-Wave Mechanical Recitifier H-V Power Supply	245
11.3	Vacuum Tube Rectifier	246
11.4	Spark Rate Control Circuit from Van Hoesen, et al	249
11.5	Optimum Operating Voltage for a Single Section of a Precipitator	251
11.6	Equivalent Circuit of the Precipitator Collection Electrode System	251
11.7	Time Response of the Precipitator Equivalent Circuit to Various Voltage Waveforms With the Same Peak Amplitude	256
11.8	Half-Wave Mechanical Rectifier H-V Power Supply	258
11.9	Tube Rectifier H-V Power Supply	260
12.1	Sampling Points in a Round Duct	269
12.2	Schematic Arrangement of Dust Sampling Apparatus	273
12.3	Flow Lines in the Vicinity of a Sampling Probe	279
12.4	Accuracy of Anisokinetic Sampling	280
12.5	Accuracy of Velocity Readings for Manometer Accuracy of ± a Inches Water Gage and Standard Air Density	282
12.6	Relationship between True Efficiency Vs. Calculated Efficiency	289
12.7	High Voltage Cell for Measurement of Dust Resistivity	291
12.8	Resistivity-Temperature Relations	292
12.9	Resistivity Probe	294
12.10	Diagram of Apparatus	295
12.11	Resistivity Changes During Site Measurements on Four Different Power Stations	296
13.1	Relationship between Corona Power and Efficiency for Fly Ash Precipitators	299
14.1	The Electrostatic Force between a 10μ Water Droplet and a 0.5μ Dust Particle Charged to Saturation in an Electric Field of 6 kV/cm	313

LIST OF TABLES
PART I

Table No.		Page No.
6.1	Erosion Situations	163
8.1	Input Parameters from Boiler	192
8.2	Precipitator Parameters	192
8.3	Derived Quantities	193
8.4	Comparison between the Measured and Computed Collection Efficiency for Five Fly Ash Precipitators	201
9.1	Representative Precipitation Rates for Various Applications	205
9.2	Rapping Practices	213
12.1	Comparison of Six Measurement Standards	267
12.2	Sources of Measurement Errors	277
12.3	Permissible Error Limits for Glass/Mercury Thermometers	283
13.1	Typical Maintenance Schedule	306

LIST OF SYMBOLS
PART I

A = Collection electrode area or specific area of an object
C = Constant or coefficient
C_p = Current to charge particulate
D = Dust concentration or diffusion coefficient
E = Electric field
F = Force, Farad
K = Aspect ratio, constant
$L_p L_w$ = Length of precipitator or corona wire
N = Densities of various quantities - number per units volume
P = Perimeter, probability
Q = Quality factor or quantity
R = Radius - specific dimension
S = Surface area per gm of dust, circumference
V = Voltage, ionization potential
W = Weight of dust
X = Fraction of molecules ionized

a = Radius corona wire or dust particle
b = Radius collection pipe, wire and pipe precipitator
d = Air density, relative
e = Electronic charge
f = Wire roughness factor, reentrainment factor
h = Height of plates, velocity head
i = Current, per unit length
j = Current, per unit area
k = Boltzmann's constant, coefficient
$\ln$ = Natural logarithm
n = Number of items per unit time
p = Velocity pressure
q = Electrical charge
r = Radius or reduction factor
t = Time
v = Velocity
v_g = Volume flow rate
w = Migration velocity or precipitation rate parameter

α = Ionization coefficient, acceleration, erosion coefficient
β = Constant erosion coefficient
γ = Secondary emission coefficient
δ = Boundary layer thickness
Δ = Increment
ϵ, ϵ_0 = Relative dielectric constant, permittivity of free space
η = Collection efficiency, viscosity
μ = Mobility
ρ = Resistivity, space charge density, gas density
σ = Conductivity
Σ = Summation
τ = Time constant
χ = Concentration ratio
∇^2 = Laplacian operator

TABLE OF CONTENTS

PART II - APPLICATION AREAS

Page No.

DESCRIPTIVE SUMMARY 324

Electric Power Generation 324
Pulp and Paper 328
Iron and Steel Industry 330
Rock Products 337
Chemical Industry 340
Municipal Incinerators 343
Petroleum Industry 344
Nonferrous Metals 345
High Temperature, High Pressure Gas Cleaning 346
New Application Areas 347

CHAPTER 15. ELECTROSTATIC PRECIPITATORS IN THE ELECTRIC UTILITY INDUSTRY 348

15.1 Fly Ash Characteristics 351
15.2 Flue Gas Characteristics 360
15.3 Historical Development of Fly Ash Precipitators 363
15.4 Design of Fly Ash Precipitators 365
15.5 Summary of Precipitator Operating Conditions 383
15.6 Precipitator Installations and Economics 393
15.7 Trends 408
Bibliography 416

CHAPTER 16. ELECTROSTATIC PRECIPITATORS IN THE PULP AND PAPER INDUSTRY 418

16.1 Process Descriptions 421
16.2 Character of Recovery Boiler Particulate Emission 427
16.3 Character of Sulfate Process Flue Gases 432
16.4 Historical Developments of Electrostatic Precipitators for Recovery Furnaces 435
16.5 Precipitator Applications 445
16.6 Summary of Precipitator Operating Conditions 455

Page No.

16.7 Assessment of the State of the Art.................. 462
16.8 General Observations and Discussion of Trends..... 467
Bibliography.................................. 473

CHAPTER 17. ELECTROSTATIC PRECIPITATORS IN THE IRON AND STEEL INDUSTRY................. 474

17.1 Introduction.................................. 474
17.2 Application to Coke Ovens........................ 476
17.3 Application to Sinter Plants........................ 487
17.4 Application to Blast Furnaces..................... 502
17.5 Application to Open Hearth Furnaces.............. 529
17.6 Application to Basic Oxygen Converters............ 546
17.7 Application to Electric Arc Furnaces.............. 567
17.8 Application to Scarfing Machines.................. 584
17.9 Application to Iron Cupolas........................ 592
Bibliography.................................. 604

CHAPTER 18. ELECTROSTATIC PRECIPITATORS IN THE ROCK PRODUCTS INDUSTRY................. 609

18.1 Manufacture of Portland Cement.................. 609
18.2 Character of Emissions from Cement Kilns........ 61
18.3 Electrostatic Precipitators for Control of Cement Dusts.................................. 621
18.4 Electrostatic Precipitators for Gypsum Industry.... 640
Bibliography.................................. 659

CHAPTER 19. ELECTROSTATIC PRECIPITATORS IN THE CHEMICAL INDUSTRY...................... 660

19.1 Major Fields of Application..................... 660
19.2 Sulfuric Acid Production Processes.............. 660
19.3 Design and Operating Parameters for Sulfuric Acid Mist Precipitators.......................... 666
19.4 Sulfuric Acid Mist Precipitator Installations and Cost Data.................................. 675
19.5 Precipitators for the Elemental Phosphorus Industry.................................. 684
19.6 Precipitators for the Phosphoric Acid Industry...... 704
19.7 Precipitators for the Carbon Black Industry........ 722
Bibliography.................................. 728

Page No.

CHAPTER 20. THE APPLICATION OF ELECTROSTATIC PRECIPITATORS IN CLEANING MUNICIPAL INCINERATOR DUSTS 729

20.1 Types of Incinerators 729
20.2 Incinerator Capacities 730
20.3 Refuse Properties 731
20.4 Emission Properties 732
20.5 Incinerator Emission Control 737
20.6 Use of Electrostatic Precipitators on Municipal Incinerators 740
20.7 Economics 752
Bibliography 754

CHAPTER 21. ELECTROSTATIC PRECIPITATORS IN THE PETROLEUM INDUSTRY 755

21.1 Introduction 755
21.2 Catalytic Cracking 756
21.3 Detarring 761
21.4 Development of Electrostatic Precipitators in the Petrochemical Industry 768
Bibliography 785

CHAPTER 22. THE APPLICATION OF ELECTROSTATIC PRECIPITATORS IN THE NONFERROUS METALS INDUSTRY 786

22.1 Historical Development 786
22.2 Nonferrous Metal Processing 788
22.3 Electrolytic Reduction of Aluminum 798
22.4 Production of Primary Copper 799
22.5 Production of Primary Lead 810
22.6 Zinc Reduction 818
22.7 Summary of Precipitator Operation Conditions 822
Bibliography 836

Page No.

CHAPTER 23. THE APPLICATION OF ELECTROSTATIC PRECIPITATORS TO THE CLEANING OF HIGH PRESSURE, HIGH TEMPERATURE GASES..... 837

23.1 High Pressure, High Temperature Processes 837
23.2 Influence of Temperature and Pressure on Precipitator Performance........................ 838
23.3 Precipitators for High Temperature, High Pressure Operation.. 840
23.4 Cleaning of Natural Gas in Pipelines............... 841
Bibliography.. 844

CHAPTER 24. NEW PRECIPITATOR APPLICATIONS......... 845

24.1 Application of Electrostatic Precipitators.......... 856
Bibliography.. 875

DESCRIPTIVE SUMMARY OF PART I

Electrostatic precipitation utilizes the forces acting on electrically charged particles in the presence of an electric field to effect the separation of solid or liquid aerosols from a gas stream. In the precipitation process, dust suspended in the gas is electrically charged and passed through an electric field where electrical forces cause the particles to migrate toward the collection surface. The dust is separated from the gas by retention on the collection electrode and subsequently removed from the precipitator. Various physical configurations are used to accomplish these basic functions of charging, collection, and removal, depending upon the type of application and properties of the dust and gas.

While particles in a gas stream normally have a small inherent electric charge, it is orders of magnitude too small for effective electrostatic collection. Consequently, the precipitation process must provide a means for particle charging. In all commercial precipitator applications, the charging is accomplished by means of a high-voltage, direct-current corona.

CORONA GENERATION

Corona, as applied to electrostatic precipitators, is a gas discharge phenomenon associated with the ionization of gas molecules by electron collision in regions of high electric field strength. The process of corona generation requires a nonuniform electric field, which is obtained by the use of a small diameter wire as one electrode and a plate or cylinder as the other electrode. The application of a high voltage to this electrode configuration results in a high electric field near the wire. The electric field decreases inversely with the radius from the wire surface.

The corona process is initiated by the presence of electrons in the high field region near the wire. Electrons for corona initiation are supplied from natural radiation or other sources and, since they are in a region of high electric field, they are accelerated to high velocities and possess sufficient energy so that on impact with gas molecules in the region, they release orbital electrons from gas molecules. The additional free electrons are also accelerated and enter into the ionization process. This avalanche process continues until the electric field decreases to the point that the electrons released do not acquire sufficient energy for ionization.

Within the region defined by the corona glow discharge, where ionization is taking place, there are free electrons and positive ions resulting from electron impact ionization. The behavior of these charged particles depends upon the polarity of the electrodes, and the corona is termed negative corona if the discharge electrode is negative, or positive corona if the discharge electrode is positive. Both positive and negative corona are used in industrial gas cleaning applications; however, the negative corona is most prevalent within the temperature range of most industrial applications.

In the case of the negative corona, positive ions generated in the corona region as a result of electron impact are attracted toward the negative wire electrode and electrons toward the positive plate or cylinder electrode. Beyond the corona glow region, the electric field diminishes rapidly, and if electronegative gases are present, electrons will be captured by the gas molecules on impact. The negative ions thus generated move toward the collection electrode and serve as the principal means for charging the dust.

In the corona process, there must be a source of electrons to initiate and maintain the avalanche process. The electrons are supplied from naturally occurring ionizing radiation, photoionization due to the presence of the corona glow, and, in the case of high temperature operations, from thermal ionization at the electrode surface. For negative corona, electrons are also provided by secondary emission from the impacts between the positive ions and the discharge electrode. Cosmic and terrestrial radiation provide approximately 20 ion-electron pairs per cubic centimeter of gas per second.

Mobilities of the various charge carriers play an important role in the corona generation process. Electron mobility in high fields is approximately 400 times that for ions. In the negative corona case, the electron mobility is such that sparking would occur when the field required to initiate corona is reached unless the electrons are attached to gas molecules to form a stabilizing space charge.

In most industrial gas cleaning applications, there are sufficient quantities of electronegative gases, such as oxygen, so that practically all of the electrons are attached to gas molecules. Gases such as nitrogen, helium, argon, etc., do not form negative ions, and hence a stable negative corona is not possible in these gases.

In positive corona, the electrons generated by the avalanche process flow toward the collection electrode. Since the positive ions are the charge carriers, they serve to provide an effective space charge, and the presence of an electronegative gas is not required for positive corona. Sources of electrons for initiating and maintaining avalanche in a positive corona are cosmic radiation and photoionization due to the corona glow.

Positive and negative corona differ in several important aspects. In appearance, the positive corona is a rather uniform sheath surrounding the discharge electrode. In contrast, negative corona appears as localized discharges from points on a clean wire and as localized tufts along the dust-coated electrode. The voltage-current characteristics of the negative corona are superior to those of positive corona at the temperature at which most precipitators operate. Higher operating voltages and currents can be reached prior to disruptive sparking. It is postulated that a spark or arc breakdown in the interelectrode space occurs by formation of a streamer originating at the positive electrode surface. In the positive corona, the origin of the streamer would be at the surface of the discharge wire, and hence in a high field region. In the negative corona, the positive electrode is the collection plate and the field near this surface is considerably less than at the discharge electrode; hence a higher voltage would be required for spark propagation.

Negative corona is accompanied by the generation of ozone, and therefore is usually not used for cleaning air in inhabited space. However, most industrial gas cleaning precipitators utilize negative corona because of its inherently superior electrical characteristics which leads to increased efficiency at the temperatures at which they are used.

Geometry of the electrodes, gas composition, and gas conditions have important influences on corona generation. The diameter of the discharge wire and the electrode spacing determine the voltage gradient, and hence the variation in electric field strength. The electric field varies as the reciprocal of the radius near a small diameter wire. Hence, with a very small wire, the electric field near the surface can be quite high, often in the range of 50-100 kV/cm. The avalanche process requires the presence of a high electric field over a given distance. In general, the smaller diameter wire requires a higher electric field strength for initiation of corona. For a given spacing, however, the onset of corona occurs at a lower voltage for the smaller diameter wire. Also, for a given voltage, higher currents are obtained with smaller diameter discharge electrodes.

Temperature and pressure influence the generation of corona by changing the gas density. In the avalanche process, the time available for accelerating an electron between collisions is a function of gas density. With increased molecular spacing, higher velocities can be achieved between collisions. Thus, ionizing energy can be achieved with low electric fields for low gas densities.

A second effect, in the case of the negative corona, is that the increased molecular spacing results in the penetration of free electrons further into the interelectrode region before capture to form a negative ion. This results in an increased average mobility in the interelectrode space, and hence a higher current. Additionally, at very high temperatures (above about 1500°F) thermionic emission increases, further increasing the number of free electrons and the effective average charge mobility. These effects reduce the voltage required for sparkover, so that at high temperatures, positive corona would perhaps give superior voltage-current relationships and improved collection efficiency since electrons move toward the discharge electrode in positive corona.

Corona generation studies of a basic nature are most often made with clean electrodes under laboratory conditions. These conditions are highly idealized in comparison to industrial precipitators. In practical precipitators, the presence of a dust laden gas has several effects on corona generation. First, the dust entering the interelectrode space becomes charged by attachment of negative or positive ions. Because of the much lower mobility of the charged dust, it constitutes a significant space charge. The magnitude of the space charge depends upon the size and quantity of the dust and the magnitude of its charge. The effect of the space charge is to reduce the electric field in the vicinity of the corona glow region and thus it tends to quench the corona and reduce the current. This effect is particularly significant at the inlet section of a precipitator where dust concentrations are highest. Special electrode shapes are often used to minimize this space charge problem at the inlet section.

A second important consideration of the effects of dust on corona generation is the deposits formed on both collection and discharge electrodes. On the collection electrode, dust deposits alter the electric field and sparking conditions as a result of the voltage drop within the dust layer. This effect limits the voltage and current at which the precipitator can operate, and is its chief influence on corona generation.

Dust deposits also form on the discharge electrode in operating precipitators. This deposit can be quite heavy in the case of some types of dust. The effect on corona can be considerable depending on the nature of the deposit and the electrical properties of the dust. If the dust resistivity is reasonably low, the effect of the deposit will be to effectively increase the diameter of the discharge wire. This results in higher voltage required for corona initiation or reduced corona current for a given voltage. If the dust deposit is uneven, an uneven distribution of corona along the length of the wire may result.

If the dust resistivity is high, the effect generally would be to reduce corona current for a given voltage. However, if the deposit is somewhat porous, breakdown of the gas in the interstitial region can occur and the effect of the deposit may be reduced.

The current in a precipitator is carried by free electrons, ions, and charged dust particles. The magnitude of the current carried by each of these is related to the number densities of the carrier, the mobility of the carrier, and the electric field. Mobilities are related to the various physical parameters of the charged particle, but primarily to the charge-to-mass ratio of the carrier. Electrons, with their low mass, have the highest mobility of all the current carriers ($\mu_e \sim 750$ cm^2/volts sec). Oxygen ions would have a lower mobility, about 1/400 that of an electron ($\mu_{O_2^-} \sim 1.9$ cm^2/volts sec), and charged dust particles would have the lowest mobility of all the current carriers (in the range of 0.02 cm^2/volts sec). These mobilities are for conditions normally encountered in commercial installations. It is thus apparent that for a given electric field, the current carried by each of the carriers is in proportion to their mobilities for the same number densities. For a negative corona, the number densities of the charged particles change in traversing the glow region from the discharge electrode surface. At the surface, the positive ion density is greatest, since all of the positive ions from the avalanche process flow to the discharge electrode. At the boundary of the corona glow region, ion generation ceases; hence the concentration of positive ions is zero beyond that point.

The number of free electrons at the wire surface is minimal and increases, because of the avalanche process, to a maximum at the boundary of the corona glow region. Moving into the quiescent zone, free electrons are captured by the electronegative gas molecules. The probability of electron capture is high due to the number of gas molecules present, so that the electron density rapidly decreases beyond the corona glow boundary.

As the electrons from the corona are captured by the gas molecules to form negative ions, the negative ion concentration increases. Traversing further into the interelectrode space, the negative ions attach to the dust particles present to form charged particles. The number of free ions present then decreases as they are consumed in the particle charging process. A considerable fraction of the negative ions present go to charging the dust particles, although due to the difference in mobilities, the percentage of the current due to bound ions is small.

The currents carried by these various carriers can be determined by their number densities, mobilities, and the electric field strength. It should be remembered, however, that the number densities of the various carriers, as well as current, are important in analysis of precipitator operation.

PARTICLE CHARGING

There are two physical mechanisms by which gas ions impart charge to dust particles in the precipitator. Particles in an electric field cause localized distortion of the field so that electric field lines intersect the particles. Ions present in the field tend to travel in the direction of maximum voltage gradient, which is along electric field lines. Thus, ions will be intercepted by the dust particles, resulting in a net charge flow to the particle. The ion will be held to the dust particle by an induced image charge force between the ion and dust particle. As additional ions collide with and are held to the particle, it becomes charged to a value sufficient to divert the electric field lines such that they do not intercept the particle. Under this condition, no ions contact the dust particle and it receives no further charge. The electrostatic theory of the process shows that the saturation value of the charge on the particle is related to the magnitude of the electric field in the region where charging takes place, the size of the particle, and the dielectric constant of the particle. The saturation charge is proportional to the square of the particle diameter, thus larger particles are more easily collected than small ones. This mechanism of charging is called field-dependent charging.

The time required for a particle to acquire a saturation charge is an important factor that is often neglected in precipitation theory. Field dependent charging may be described by an asymptotic final value function, and is dependent upon ion density and mobility. If a single particle is introduced into a high ion density field, charging takes place in milliseconds. However, charging times by the field-dependent regime can be appreciable under practical conditions of large dust loading and low currents.

For small particles (diameter $<0.2\mu$), the field-dependent charging mechanism is less important, and collision between the particles and gas ions is governed primarily by thermal motion of the ion. Equations describing the rate of charging can be derived assuming that charging rate is independent of the magnitude of the electric field. Since ion movement is so greatly influenced by the electric field, the assumption obviously generates considerable error. However, the factors influencing charging rate can be seen under this assumption to be particle diameter, free ion density, and thermal velocity of the ions.

Since the range of thermal velocities has no upper boundary, there is no saturation value associated with diffusion charging. However, as the charge on a particle increases, the probability of impact decreases, so that there is a decreasing charging rate associated with an increasing particle charge. This second charging process is called diffusion charging.

Recent work in the area of diffusion charging has been directed toward obtaining better agreement between experimentally determined values of diffusion charging and those predicted by theory. Studies of the influence of electric field have been made on the basis of approximate solutions to the equations that include the effect of the electric field.

In practical precipitators, field-dependent charging is usually of most interest, but in some applications particles are present in the range where diffusion charging is the predominant mode ($<0.2\mu$ diameter) as well as the area in which both mechanisms are significant. Unified charging equations have been developed covering the size range where both charging regimes are important, and results agree reasonably well with experimental laboratory values.

Particle charging theory indicates several important factors governing precipitator performance. Since the magnitude of the particle charge is dependent upon the magnitude of the electric field in the field-dependent mode, it is important that field strength be kept as high as practical in the region where charging takes place.

A second factor of importance is the rate of charging of the particles. Practical precipitators generally introduce heavy concentrations of uncharged dust in the inlet section of the precipitator. Calculations show that the number of ions required to charge this dust to its saturation value may be large, hence the number of free ions present may be substantially reduced and charging times are not insignificant.

The waveform of the applied voltage is significant, as it influences the peak value of the electric field and the charging time. The saturation value of the particle charge is determined by the peak value of the electric field. However, charging only occurs during the interval of time that the applied field exceeds the self-field corresponding to the charge on the particle. Consequently, longer times will be required to reach saturation for a varying voltage than for a pure d-c voltage. However, the varying voltage is preferable for spark quenching and permits operation at a higher average voltage.

The electric field in a precipitator determines the maximum value of the particle charge due to field-dependent charging and also the force acting on a charged particle. Since the electrical field enters the collection efficiency equations effectively as a squared term, it is important that the magnitude of the field be maintained as high as practical.

The electric field strength is determined by the electrostatic component, which is related to the precipitator geometry and the applied voltage; and by the space charge component, which is related to the presence of charged particles (ions and charged particulate) in the interelectrode space. The design of the precipitator can be varied to alter the geometry of the discharge electrode and the electrode spacing. These factors can determine the magnitude of the electrostatic component. Variations in electrode geometry can also alter the corona current, which in turn influences the electric field by changing the space charge contribution. Equations describing the electric field for clean electrodes have been developed from classical electrical theory. Utilizing these equations, it is possible to predict the field at any location, assuming clean electrodes.

In a practical precipitator, dust accumulations on the collection electrodes limit the maximum voltage, and hence the electric field strength at which the precipitator can operate. The voltage drop across the dust layer is dependent upon the corona current density, the electrical resistivity of the dust, and the thickness of the dust deposit. For high resistivity dusts, the voltage drop across the collected dust layer can be in the neighborhood of 10-20 kV, assuming reasonable current densities and dust deposit thicknesses. Obviously, the electrical energization equipment must be capable of providing sufficient voltage to accommodate this voltage drop, while maintaining adequate voltage across the interelectrode spaces. The effect of the resistivity of the dust layer, however, is more severe than its influence on power supply voltage. The electric field in the dust layer can be quite high for high resistivity dust. This high field region at the anode surface can lead to sparkover at lower applied voltages, thus limiting the maximum operating voltage of the precipitator.

A second condition associated with high dust resistivity can also influence particle charging and the magnitude of the electric field. Once sparking occurs, a crater is formed in the dust layer, and current densities in the localized area can result in localized electric fields that are sufficiently high to initiate a corona emanating from the base of the crater. This corona results in positive ion production and, due to the direction of the electric field, these ions flow toward the discharge electrode. Collisions with dust particles tend to charge them with opposite polarity to that required for collection. Also, collision with negative ions tends to neutralize them, reducing the ion density in the interelectrode space.

If dust resistivity is further increased, a diffuse corona glow will appear over the large areas of the dust surface. Under these conditions the positive ion production by the reverse corona is sufficient to completely disrupt the charging process, and effective precipitation is not possible under these conditions.

PARTICLE COLLECTION

The forces acting on a charged particle in a precipitator are gravitational, inertial, electrical, and aerodynamic. The latter two are the principal ones of importance in electrostatic precipitation.

If a particle is suspended in a laminar gas flow stream in a pipe and wire precipitator, a force due to the electric field and particulate charge will act on the particle in the direction of the collection electrode. This force is opposed by the viscous drag force of the gas. In sufficient time, which is short for small particles, the particle would reach a terminal velocity at which point the electrical and viscous drag forces would be equal. In precipitator terminology, this is called the migration velocity. The other force acting on the particle is the aerodynamic force by the gas stream. The motion of the particle will be along the line defined by the vector sum of these two forces. Under laminar flow, all particles would be collected in a given length of the precipitator and the collection efficiency for shorter lengths would be linearly related to precipitator length.

In practical size precipitators, however, laminar flow is practically never achieved. Consequently, the turbulent gas flow causes particles to follow a random path through the precipitator. The magnitude of the forces due to the turbulent gas flow is large compared to the electrical forces. However, at the boundary layer the gas flow is laminar and particles entering the boundary layer will be collected. The collection efficiency is therefore related to the probability of a particle entering the boundary layer. Studies by Anderson, Deutsch, and White of particle collection in a turbulent gas stream have shown theoretically that collection efficiencies are exponentially related to the collection surface, the gas volume handled, and the migration velocity of a particle. The equation, known generally as the Deutsch-Anderson equation, is of the form $\eta = 1 - \exp\left(-\frac{A}{v_g} w\right)$.

The derivations of the efficiency equation are based on the assumption that there is a reasonably constant distribution of the particles in any cross section of the precipitator due to turbulent mixing of the gas. In addition to this assumption, there are several basic conditions that apply to the derivation of the equation. Utilizing the relation for the theoretical migration velocity $w = \frac{2\epsilon_0 E_0 E_p a}{\eta}$ generally associated with the efficiency equation neglects any contribution of diffusion charging. Also, the calculation is based on a single particle size. The equation also includes no term to account for reentrainment of collected dusts, uneven distribution of the gas flow, or other factors inherent in practical precipitator operation.

A principal practical use of the Deutsch-Anderson equation has been in relating measured collection efficiency to the collecting surface area and gas volume. In such cases, the term w as calculated from the Deutsch-Anderson equation is a parameter, rather than the migration velocity given by theoretical considerations. In this case, it is called effective migration velocity or precipitation rate parameter. The term is useful in describing the effectiveness with which a given dust can be collected, and is widely used in design and analysis of precipitators.

From a theoretical as well as a practical standpoint, the distribution of particles within the precipitator is important. There is some evidence to indicate that particle distribution within the precipitator may not be uniform and that diffusional forces may also play a role in collection efficiency.

REMOVAL

Once collected, the dust or liquid aerosol must be removed from the precipitator. This can be accomplished by flowing a liquid down the collection electrode to wash the collected dust, or by rapping the electrodes to impart an acceleration to dislodge the dust, which falls into a hopper for subsequent removal. Liquid aerosols normally coalesce and drain from the plates so that removal is not a problem.

In dry removal systems, rapping of the collection electrode to remove the dust is normally done on a periodic basis. Successful rapping depends upon accumulation of sufficient thickness of material on the plate so that it falls in large agglomerates into the hopper. There is always some reentrainment of the dust so that effective rapping must minimize the amount of material reentrained in the gas stream.

The accelerations required to remove the collected dust vary with the properties of the dust and gas stream. Forces of cohesion and adhesion consist of molecular (van der Waals), electrical, and mechanical forces. Some dusts adhere tenaciously to the collection surface and require substantial accelerations to dislodge them. Variations in operating temperature, gas composition, or both, can alter the forces required for successful rapping. Electrical forces, which are related to current density and dust resistivity, are also significant in holding the collected material to the plate, and therefore affect the forces required for rapping. Since current densities are higher at the discharge electrode than at the collecting electrode, greater forces are often required to maintain them relatively free of dust deposits than are required at the collection plates.

Reentrainment of the dust during rapping is evidenced by increased dust loadings at the precipitator exit following a rap. To minimize this effect, only small sections of the precipitator are rapped at one time.

ELECTRICAL ENERGIZATION

The function of electrical energization is to provide optimum electrical conditions for particle charging and collection. The energization equipment consists of a transformer to step up the voltage from the normal supply line to between 30-100 kV which is required for precipitation. The particular voltage is a function of electrode (wire-to-plate) spacing, and the spacing is generally chosen to minimize the influence of misalignments of the electrodes resulting from faulty construction, warping, etc. A rectifier, usually of the vacuum tube or silicon type, converts the alternating voltage to d-c to give unipolar ions. An automatic control system is usually provided to maintain optimum voltage conditions for precipitation. The control system can operate from spark rate, secondary or primary voltage, or other parameters.

The power capacity of the energization equipment is determined by the precipitator size or quantity of gas flow, design efficiency of the precipitator, and properties of the dust and gas. The manner in which the power is applied varies with the application, and the policies of the equipment manufacturer. The principal variable is the number of independently powered precipitator sections that make up the total power supply. Increasing the number of sections by using a large number of smaller power supplies is advantageous if the the precipitator is operating in a spark-limited mode, as a higher voltage can be maintained for a given spark rate. The size of the power supply also determines the internal impedance of the supply, hence large power supplies with high current capacities have low impedances, which are not as effective in spark quenching as the smaller, high impedance supplies. Smaller power supply sections also tend to minimize effects of plate misalignment or other localized disturbances. Finally on large systems, the influence of an outgage of a section of the precipitator is not as pronounced in systems comprised of smaller power supply sections if many independent sections are used.

Analysis of the electrical characteristics of a precipitator shows that it consists primarily of a parallel capacitive and resistive load, the value of which is determined by the corona current and voltage. The value of the capacitance is large enough to maintain the voltage at a high level between cycles, even though the power supply is unfiltered. The electrical characteristics of the dust deposit also influence the electrical operation of precipitators. The effect of the filtering characteristics of the dust layer is to smooth out voltage fluctuations so that higher peak voltages can be applied for a given spark rate if the voltage waveform has a high rise rate. On the other hand, charging times may be increased by these voltage waveform alterations, hence for the optimum design, both effects must be considered.

SYSTEMS ANALYSIS

Despite its seeming simplicity, the interaction of the variables makes it difficult to analyze the performance of a precipitator without considering the system as a whole. The systems analysis approach permits a review of the various parameters controlling system performance and permits a rational basis for precipitator design and analysis.

A simplified systems analysis has been developed which relates most of the important variables and permits a computerized method of precipitator analysis or performance evaluation.

The systems model is programmed to determine the collection efficiency for each discrete particle size range for each increment of length of the precipitator by calculating the following: the field strength as a function of radius at each increment of distance through the precipitator, the saturation charge on the dust, the actual charge on the dust at each increment from considerations of the free ion densities, and the amount of material in each size range that is removed at each increment. From this, the total collection efficiency can be calculated.

Comparisons of efficiencies predicted from the systems model with those measured in field tests show good agreement, except where unusual conditions, such as excessive reentrainment, were suspected.

The general philosophy behind the systems model is that it permits a satisfactory calculation of performance based on known theory, whereas theoretical calculations based on very elementary or simplified theory do not. Refinement of the model to include such factors as reentrainment, voltage-current characteristics, sparkover effects, spatial distribution of the dust, diffusion charging, and gas distribution, should permit a more theoretically correct analysis and should give better agreement between measured and calculated performance.

DESIGN

The design of precipitators involves the determination of precipitator size and electrical energization equipment required to give a desired efficiency, the design of a gas flow system to provide acceptable gas flow quality, structural design of the precipitator shell and supports, selection of the rapping equipment, and selection of the electrode configuration.

Present design methodology is generally based upon empirical relations, the values of which have been obtained from experience with similar applications. There are several approaches to the selection of the precipitator size. In general, these methods involve the selection of a precipitation rate parameter and determination of the collection plate area required from the Deutsch-Anderson equation or from design curves based upon field experience. The precipitation rate parameter varies for different applications and often varies considerably within the same application area due to variations in gas and dust properties.

Selection of the precipitation rate parameter can be made on the basis of experience with similar installations or from experimentally derived curves relating precipitation rate parameters to dust properties. For many applications, the range of precipitation rate parameter variations is small (of the order of ± 10%). In such cases, the uncertainty in plate area requirements is of the same magnitude. In other instances, variations can be as high as 400-500%, so that some method for reducing the uncertainty is highly desirable. In general, some property of the effluent from the industrial process has been related to precipitation rate parameter and an empirical relationship is derived to predict the value of the precipitation rate parameter. In the case of fly ash precipitators, sulfur content of the coal and resistivity of the dust are commonly used to establish this value. Particle size distribution is another significant variable, and curves relating precipitation rate parameter with any other variable should be modified to compensate for particle size variations if sufficient data are available.

Power requirements for a precipitator vary with collection efficiency. Selection of the power requirements is generally based on curves relating efficiency with corona power per unit volume of gas flow (watts/cfm). These curves are experimentally developed for each type of application and vary with dust properties. These curves are usually based on total delivered secondary power, and power supply capacity is selected on the basis of a power supply efficiency (from 60-75%) and the standard power supply size that will meet the efficiency requirements.

Sectionalization is also based on empirical information derived from experience. These curves must be consistent with those based on power requirements and on relationships involving collection surface area, since the same efficiencies can be achieved through the use of fewer sections and greater collection area for installations operating in a spark rate limited mode.

Design of the gas flow system is generally based on model studies with large systems, and its importance to good precipitation cannot be overemphasized.

Selection of the number of rappers, type of electrodes, etc., varies among manufacturers and with the type of dust being collected. Structural design is relatively straightforward.

One of the principal difficulties encountered by the users of electrostatic precipitators is the evaluation of bids for specific installations. Although precipitator bids are based on guaranteed performance, there are many examples of precipitator installations that fail to meet design performance by a wide margin. It is not uncommon for bids to vary considerably in the collection surface area, the amount of power and degree of electrical sectionalization, and the type of gas flow distribution systems. The user is therefore faced with the problem of evaluating the adequacy of each design for meeting his requirements. The ability to interpret bids requires experience with the particular type of dust or a method of assessing the effect of the design variations on performance.

A technique for evaluating design parameters for given dust and gas conditions has been developed based on the method of regression analysis. Based on a group of approximately 75 tests on 20 installations, equations predicting the precipitation rate parameter as functions of gas and fuel properties have been developed. An overall correlation coefficient of about 0.85 has been obtained, with maximum uncertainties of about 25% in the precipitation rate parameter for fly ash precipitators. This is rather good agreement since design and performance parameters may vary considerably more than for fly ash collection.

MECHANICAL COMPONENTS

The two general types of precipitators currently used are the tubular and plate types. The tubular precipitator consists of cylindrical collection electrodes with discharge electrodes located on the axis of the cylinder. Gas to be cleaned passes through the annular space between electrodes and the dust is collected on the outer cylinder. This type construction is used in wet electrode systems, in high-pressure, high-temperature applications, in some types of precipitators collecting liquid aerosol particles, and for small dry collection installations.

The plate type precipitator consists of parallel collecting plates with discharge electrodes located between the plates. Collecting electrode plates are usually 12 to 40 feet high and spaced 6 to 12 inches apart. The length of the ducts in the direction of gas travel can vary according to the precipitator design. Total length can be from around 12 to 24 feet or longer for very large installations.

Mechanical components which make up a precipitator are the shell, electrodes, hoppers, rappers, support members, and the necessary electrical feedthrough and support backings.

The shell can be rectangular or cylindrical and can be constructed of steel, tile or concrete. Thermal insulation is usually provided in the case of corrosive gases to maintain the shell above the dew point temperature to minimize corrosion. Design of the shell generally follows straightforward structural engineering practice.

The shell and electrode configurations can be arranged to divide the gas flow and to provide independent sections that can be separately energized. When parallel gas flow paths are provided, each path is referred to as a duct or chamber.

Discharge electrodes in both cylindrical and plate type precipitators are of a variety of types depending upon the application and the precipitator manufacturer. The discharge electrodes can be small diameter (~0.1 inch) wire, square wire, or fabricated structures of various types. The primary consideration in discharge electrode selection is to obtain desirable voltage-current characteristics and to provide mechanical strength for resistance to corrosion and fatigue. In general, American practice is to utilize electrode structures supported at the top, with weights at the hopper end to maintain the electrode taut. Guides are provided to maintain alignment. European practice is generally to use a mast or frame for rigid support of the discharge electrodes. Various discharge electrode configurations can be used with either type of mounting.

Collecting electrodes in plate type precipitators are generally flat plates with various types of stiffeners and baffles. The baffles provide shielding of the collected dust to reduce reentrainment during rapping and to reduce scouring of the plates due to gas flow.

Single impact or vibrational rappers are provided for dust removal in dry type precipitators. Rappers can be electromagnetically, pneumatically, or mechanically actuated. The major requirement for successful rapping is to deliver sufficient impact to the electrodes to dislodge the dust without causing excessive reentrainment. The acceleration required to remove the dust varies with the type of dust and gas composition. Rapping is generally specified in terms of the energy delivered per rap and the number of rappers per square foot for the collecting surface or per length of wire for the discharge electrode.

Dust removal can be through flat bottom pans with scrapers to move the collected material to a screen conveyor or through pyramidal hoppers where it is removed by conveyors or vacuum systems. The latter type is the most prevalent.

GAS FLOW

Gas flow in practical precipitators is well within the turbulent region. When exiting from the process, gas velocity usually is relatively high and often uneven. Gas velocity must be reduced to a relatively low level and turbulence controlled before entering the precipitator for good precipitation. Poor quality gas flow can affect precipitator performance by scouring the plates in localized regions of high gas velocity and by reducing performance due to the exponential relationship between efficiency and gas volume flow.

Often, space limitations preclude more conventional methods of achieving uniform gas flow, and turning vanes, splitters, straighteners, and diffusion plates must be designed to provide adequate gas flow quality.

The Industrial Gas Cleaning Institute recommends a minimum gas flow quality such that 85% of local velocities are within 25% of the mean, with no reading more than ±40% from the mean.

Because of the difficulties in predicting gas flow quality the use of physical models is almost universal. Models are usually constructed of pressed hardwood or acrylic plastic. Smoke streamer patterns and pitot tube transverses are used to indicate gas flow uniformity. Models have been historically constructed $\frac{1}{4}$ to $\frac{3}{8}$ size with the Reynolds number held constant. However, with the trend toward larger plants, models constructed to $\frac{1}{16}$ scale have been used. The use of smaller scale models tends to give less accurate results.

RESISTIVITY

Electrical resistivity of the dust is an important factor in the performance of electrostatic precipitators. If the resistivity of the collected dust is higher than about 2×10^{10} ohm-cm, excessive sparking or reverse corona can occur, thereby limiting precipitator performance.

Two distinct types of electrical conduction occur. One type is conduction by free electrons within the particles. This type of conduction depends upon the electron activation energy (a material property) and temperature. Many industrial dusts are composed of metallic oxides, sulfates, etc., which have low activation energies so that the electrical conductivity is low at temperatures in the range of 300-400°F. At higher temperatures, however, conductivity becomes greater and for most dusts this is the primary conduction mechanism at temperatures above 450-500°F.

The second kind of conduction is conduction over the particle surfaces owing to adsorption of moisture or certain chemicals such as sulfuric acid. Adsorption increases with decreasing temperature and hence particle conductivity also increases with decreasing temperature. Moisture is often referred to as the primary conditioning agent and other chemical adsorbates as secondary conditioning agents.

The role of the secondary conditioning agents is not clearly understood in all cases. It is postulated that the secondary conditioning agent may alter the surface of the dust, thus enhancing the rate of moisture adsorption and hence the conductivity. The effectiveness of the secondary conditioning agent varies with the type of dust. There is evidence that an acid conditioning agent, such as SO_3, is more effective in conditioning a basic dust, whereas a basic conditioning agent, such as NH_3, is more effective in conditioning an acidic dust. There is some evidence that the conditioning agent and moisture adsorb or condense onto the dust surface together to form the conductive layer and subsequently may react with the dust layer to alter the resistivity. Effects of additions of limestone to particulate emission from sources such as power generator boilers and sinter machines tend to indicate that reactions between dust and conditioning agent may detrimentally influence electrical conductivity.

In some instances of high resistivity dust, additions of a conditioning agent to the effluent gas have resulted in substantial reductions in resistivity and enhanced collection. Examples are SO_3 additions to the gas from power generator boilers and ammonia additions to gas from catalytic cracking units used in petroleum refining. However, additions of relatively large quantities of chemical additives have failed to improve performance in some applications. But since secondary conditioning agents are known to be highly specific and selective in effectiveness, there is no appropriate reason for expecting random additives to work. Causes for this condition are not fully understood.

MEASUREMENT OF PERFORMANCE

Measurement of precipitator performance generally includes dust loadings at the precipitator inlet and outlet, gas velocity distribution, electrical current and voltage input to the precipitator, and gas composition. Dust resistivity is an important parameter that should be measured, but often is not.

Dust loadings are normally measured by a sampling probe and a dust collector, such as a thimble. Prior to sampling, a gas velocity distribution traverse is made so that dust samples can be taken isokinetically to minimize selective size collection. Sources of error in sampling are usually attributed to anisokinetic sampling, improper probe handling, dust collection on the walls of the sampling train or dust collector, and errors in gas flow measurement. Sampling procedures require careful attention to detail and the development of skills in the sampling procedures.

Resistivity of the dust sample must be made in-situ to be meaningful. Laboratory measurements may be high by orders of magnitude and often fail to correlate with in-situ values.

In-situ resistivity can be measured by determining the current flow through a given volume of collected dust when a known voltage is impressed across it. Several types of resistivity probes can be used for this purpose. In some types, the dust is deposited electrostatically utilizing a point-plane precipitator. Other type probes utilize a cyclone type mechanical collector. The errors involved include those associated with obtaining a representative sample. Particle size and degree of packing can influence the apparent resistivity of the dust layer.

TROUBLESHOOTING AND MAINTENANCE

Causes for a precipitator to fail to achieve its design efficiency can be due to inadequate design, electrical difficulties, improper gas flow, inadequate rapping, installation problems, electrode misalignment, poor maintenance, or improper operation.

Indications of electrical difficulties can usually be observed from the levels of corona power input. Efficiency is generally related to power input, and if inadequate power densities are indicated, difficulties can usually be traced to dust resistivity, unusually fine particle size, electrode misalignment, improper control operation, or dust accumulation on the electrodes. Improper gas flow can be determined by measurement of the gas flow distribution. Poor gas flow can result from improper design, plugging of distribution plates, build-up of dust on dust walls and turning vanes, etc.

Improper rapping is usually manifest in excessive dust deposits on the collection and discharge electrodes. Adequacy of rapping can be measured by accelerometers mounted on the electrodes. Accelerations required to dislodge the dust vary with type of dust and operating conditions, and rapping must be adjusted to maintain the desired thickness of dust deposit without excessive reentrainment. Visual observation of interior of outlet flue from the precipitator is often a sensitive and revealing method for checking rapper operation.

Maintenance schedules should be set up for inspection, servicing, and repair of critical components. These components include rappers, feed through bushings, transformers, electrodes, ash removal equipment, and electrical controls. Excessive dust deposits, corrosion, broken wires, etc. are common types of difficulties encountered.

ELECTROSTATIC AUGMENTATION AND UNUSUAL DESIGNS

Electrostatic augmentation of fabric filters, packed bed filters, and wet scrubbers has been studied in some detail. Performance of fabric filters varies with the type of dust deposit and the thickness of the deposit. Pressure drop is also generally related to the dust deposit. The filtering action is generally considered to occur by the trapping of dust on the collected layer. If a single particle is too large to pass through an interstitial region, it is trapped on the dust layer and separated from the gas stream.

Electrostatic augmentation involves establishing an electric field between the fabric and another electrode, precharging the dust particle, or both. The effect of electrostatic augmentation is that the interstitial openings in the fabric material function as if they were smaller and hence smaller particles are retained. Its principal advantage has been in the more rapid build-up of the dust layer and somewhat higher efficiency for a given pressure drop.

Loose bed filters are notably inefficient in collection of small particles. However, if charged particles are introduced or if an electrostatic field is impressed across the filter or both, the dust particles will deposit on the filter bed. The effect is to provide increased collection surface area in a two stage precipitator. Greatly increased efficiency can be achieved over that for a conventional loose bed filter. The potential for increased collection surface would indicate the possibility of enhanced collection over a two stage precipitator with the same metallic plate area. The obvious disadvantage is in removal of the collected dust, which would require liquid backwash or circulation and cleaning of the filter material.

Augmentation of wet scrubbers is intended to provide better contact between the particulate and the scrubbing liquid by utilization of the attractive force between the charged particles. The attractive force between a charged dust particle and an oppositely charged liquid droplet varies with the distance of separation. Thus, with separation distances of 10μ, the attractive force is approximately equal to the gravitational force.

The use of the space charge developed as a result of the dust charge or as a result of other charged material has often been the basis of a precipitator concept in which no high voltage is applied to the collection plate.

Fields developed as a result of space charge can be quite high provided the concentration of charged dust is high and there is ample spacing between electrodes. However, as dust is collected, the space charge decreases and collection efficiency decreases. Charged water drops have also been utilized to maintain a higher space charge field. These approaches are more suited to specialized applications and their practicality for industrial gas cleaning has not been demonstrated.

CHAPTER 1
CORONA GENERATION

Since electrical conduction in gases has been a subject of extensive research for many years, the mechanism of conduction is well understood from both the theoretical and experimental standpoints. The research includes studies covering a wide range of pressure, temperature, and electrical field strength for a variety of areas such as plasma physics, electrical high voltage transmission, and electric lighting.

Among the more comprehensive theoretical discussions of gas discharge phenomena are those by von Engel,[1] Wannier,[2] and Loeb.[3,4] White[5] presents a discussion of gas discharge phenomena as applied specifically to electrostatic precipitation. The body of information available about the electrical behavior of gases appears to be sufficient to describe the principles of corona generation as it applies to the electrostatic precipitation process.

The two types of corona used in electrostatic precipitation are classified as negative and positive, depending on the electrical polarity of the corona wire. Negative corona are characterized by greater stability than positive corona, and by higher currents and field strengths at near standard temperature and pressure conditions, which, in turn, lead to increased collection efficiency. As a result, negative corona are used in almost all industrial electrostatic precipitators. This analysis is therefore primarily devoted to the negative corona precipitator. The principal drawback to the use of negative corona is the generation of a significant amount of ozone. Although this has not been considered to be a problem with industrial gas cleaning, it does tend to preclude its use in air conditioning systems.

To understand the phenomenon of the corona discharge, it is necessary to consider the behavior of gases under the influence of an electric field. Although gases are basically nonconductors, there are some free electrons and ions present in the gas due to ionizing radiation which exists in the atmosphere. Cosmic rays and naturally occurring radioactivity produce about 20 ion-electron pairs per cm^3-second. If an electric field is applied to these gases, a small, almost immeasurable, current flows. This current is caused by the flow of the free electrons and ions under the influence of the electric field. Expressed as an equation from electrostatic theory (Coulomb's law):[6]

---

[1] Refer to the bibliography for this chapter.

$$F = qE \tag{1.1}$$

where

F = force,
q = charge on the particle, and
E = electric field strength.

This force drives the charged particles through the gas, resulting in an electric current flow. The motion of the charged particles is governed primarily by the combined effects of the electric field as the driving force, with inertia and viscous forces (collisions between the particles and gas molecules) as the retarding forces. When the particles attain a constant or terminal velocity, the inertia force is reduced to zero, and the two remaining forces result in an average velocity for the particles which is related to the magnitude of the electric field and the gas viscosity. The velocity attained will be that at which the viscous drag force balances the applied electrical force. The constant of proportionality is termed the particle mobility μ.

$$v = \mu E$$

This mobility parameter contains such factors as the charge-to-cross-sectional-area ratio of the particle and the viscosity or density of the host gas.[7]

Orbital electrons in an atom are held to the nucleus by a combination of nuclear, atomic, and electrostatic forces. The resultant binding force is different for each gas species. The magnitude of this binding force is referred to as the binding energy of each species. An electron can be removed from the parent atom by the addition of sufficient energy to exceed the binding energy of that particular gas atom. Thus, collisions between rapidly moving free electrons and orbital electrons can transfer a sufficient quantity of energy to the bound electrons to free them. This leads to the formation of a positive ion and an additional free electron, through a process termed ionization.

Ionization occurs in gases where the electric field is increased to the point that free electrons can be accelerated to a velocity sufficient to ionize an atom. This energy must be supplied in a short interval of time because the free electrons can lose energy through collision. Thus, the electric field must be great enough to supply the ionization energy during the time between inelastic collisions.

The corona is generated by a mechanism which is commonly referred to as electron avalanche. This mechanism becomes effective when the applied electric field exceeds that required to impart a sufficient velocity to the free electrons to cause ionization by collision with the bound electrons in the gas molecules.[8] These newly freed electrons are also accelerated and cause additional ionization. Starting with a single free electron, one ionizing collision will free an additional electron, both of which again are accelerated and collide with other gas molecules to release two additional electrons. This multiplication process continues throughout the region of space where the electric field exceeds the critical value for ionization.

There is always a supply of free electrons available to initiate the avalanche process. These free electrons are supplied by the ionization of gas molecules by either cosmic rays, natural radioactivity, photoionization, or the thermal energy of the gas. If the avalanche mechanism is initiated in a uniform electric field, such as a parallel plate capacitor, the avalanche will continue until a path between the plates becomes ionized and a spark occurs, resulting in an unstable breakdown. If the breakdown occurs in a region with a nonuniform electric field, however, corona will occur only in those regions where the critical field is exceeded. This leads to the conventional corona glow discharge in the region where ionizing collisions are occurring, followed by a quiescent zone where the electric field is insufficient to maintain the avalanche process. These nonuniform fields can be established by the application of a voltage between either a point or wire as one electrode and a plate or concentric cylinder as the other.

Consider, for example, the electric field existing between a wire and a concentric cylinder. From Gauss' law, the field for a condition of no current flow can be described as

$$E = \frac{V}{r \ln \frac{b}{a}} \tag{1.2}$$

where

V = applied voltage,
a = radius of the inner wire,
b = radius of the concentric cylinder, and
r = radius to the point where the value of the field is desired.

As the voltage between the wire and cylinder is increased, the field strength will increase until the electric field at the corona wire reaches that required for corona initiation. This field at which the onset of corona begins is given by a semi-empirical relation by Peek.[9]

$$E_c = 30\ md\left(1 + 0.30\sqrt{\frac{d}{a}}\right)\ \text{kV/cm} \tag{1.3}$$

where

E_c = corona onset field strength,
m = a roughness factor for the wire, $0.5 \leq m \leq 1.0$, and
d = relative air density.

$$d = \frac{T_0}{T} \cdot \frac{P}{P_0}$$

where

T_0 = standard absolute temperature of room air (293°K), and
P_0 = standard atmospheric pressure (760 mm mercury).

T and P are the actual absolute temperature and pressure for which "d" is to be calculated.

Equation 1.3 shows that the electric field required for the onset of corona increases as the diameter of the wire decreases. Small diameter wires result in higher field strength near the surface. However, the magnitude of the field rapidly decreases at increasing distances from the wire. On the other hand, larger diameter wires result in low field strength near the wire surface and the value of the electric field falls off less rapidly away from the wire. It is apparent, therefore, that both the maximum value of the field and the gradient are significant in determining the corona onset field. At very large values of "a", the second term of Equation 1.3 becomes insignificant. Thus, for a very large wire diameter, the magnitude of the corona onset field would approach 30 kV/cm for a smooth wire.

Since this is the breakdown strength for air in a uniform field, sparking would occur, and corona generation would not be possible.

The applied voltage required to generate an electric field of the critical value can be determined by integrating the electric field from the surface of the corona wire to the outer electrode.

$$V = \int_a^b E(r)\,dr = \int_a^b \frac{aE_c}{r}\,dr = aE_c \ln\frac{b}{a}$$

$$= 30\,amd\left(1 + 0.3\sqrt{\frac{d}{a}}\right)\ln\frac{b}{a} \qquad (1.4)$$

When the critical voltage for the onset of corona is reached, free electrons in the vicinity of the wire are accelerated to the ionization energy, and avalanche will occur in the region where the critical field strength is exceeded.

Continuing into the lower field region of the precipitator, the electric field strength decreases as indicated by Equation 1.2, until the electrons no longer exceed the ionization energy. At this point in space, the avalanche process is quenched, no more free electrons are generated, and therefore no more positive ions are present. The edge of this avalanche region is defined by the boundary of the corona glow. Therefore, only negative charges are available to carry the current within the quiescent portion of the precipitator.

Even though the total current is carried by negative charges in the quiescent region of the precipitator, positive ions are active carriers in the corona zone. At the surface of the corona wires the current is carried almost exclusively by the positive ions. The free electrons are produced by the avalanche process in the region surrounding the corona wire, with the exception of secondary electrons. Thus, from the principle of current continuity, the current is carried by a combination of positive ions and secondary electrons in the region immediately surrounding the corona wire, but is carried solely by negative charges in the quiescent zone.

The behavior of the negative charges in the low field region is governed by the characteristics of the host gas. The presence of an electronegative gas such as oxygen, chlorine, and sulfur dioxide, serves the function of building up a space charge by attaching and retaining the free electrons generated by the avalanche. These electrons are held to the gases because the gas atom is at a lower energy state when a negative ion is formed. The mobility of the negative ion is almost the same as for the positive ion. The negative ions drift slowly, in comparison to free electrons, toward the collection electrode giving rise to a significant space charge.

The conditions necessary for the maintenance of a stable negative corona include a copious source of electrons near the discharge electrode and an effective space charge in the passive zone between the electrodes. The space charge is necessary to stabilize the avalanche region in the corona by bringing about an equilibrium condition between the electric field and the electron multiplication region. In the absence of a sufficient limiting space charge, the avalanche process would grow until sparking occurred.

In the negative corona discharge, the electron avalanche mechanism produces large numbers of free electrons near the discharge electrode; however, due to their relatively high mobility, ~400 times that of ions, the free electrons are quickly swept to the anode and do not form a space charge unless electronegative gases are present. In the presence of electronegative gases, an effective space charge is built up by the attachment of free electrons to the gases.

The positive ions created in the avalanche process move to and impact with the corona electrode. These impacts provide an additional source of electrons by the process of secondary emission.

Secondary emission is a statistical process whereby a small percentage of the ion impacts results in a new free electron. Approximately one out of every thousand positive ions produces a free electron at standard gas conditions. The rate of generation is related to the electric field in the vicinity of the corona electrode and to the electrode material. This does not limit the corona generation process, however, because the avalanche mechanism provides many positive ions for each original electron through electron multiplication.

Figure 1.1 is a graphical representation of the corona discharge showing the feedback nature of the process.

There are two stages in the development of a corona. If the corona is brought about by slowly increasing the applied voltage, the location of the first corona point will be determined primarily by the geometry of the

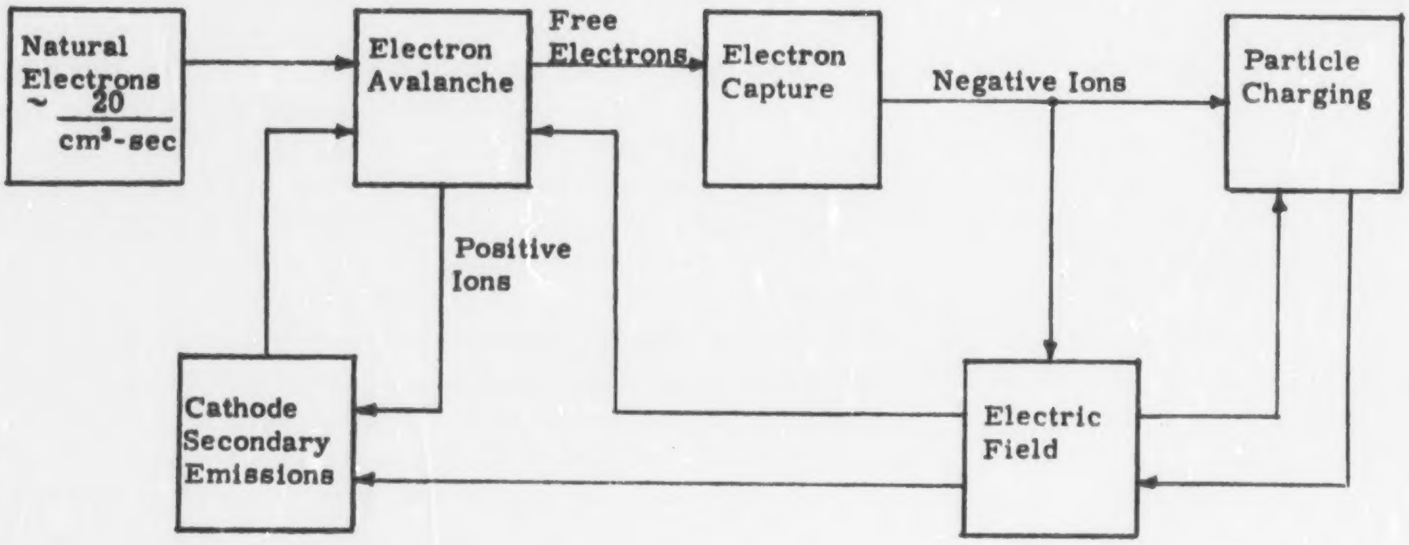

Figure 1.1 Diagram of the Feedback Nature of the Avalanche Process.

surface irregularities of the corona electrode. Points and other surface conditions lead to electric field enhancement, and when the field in one of these localized regions exceeds the breakdown potential at that point, the avalanche process is initiated. The region in which breakdown potential is exceeded is quite limited for voltages near breakdown. As the avalanche proceeds, the highly mobile free electrons are swept clear of the relatively sluggish positive ions. These ions build up a positive space charge of a sufficient value to quench the avalanche process by the attraction of, and recombination with, the secondary electrons, and by the repelling effect of the negative space charge. The avalanche process will remain inactive until a sufficient portion of the positive space charge drifts to the corona wire for the process to repeat. The net result of the above causes intermittent pulses of corona from the localized avalanche. This phenomenon, known as "Trichel Pulsing," is described in detail by Loeb.[4]

Increasing the applied voltage causes an increase in the space charge required to quench the corona at the initial breakdown point and also causes localized breakdown in additional regions. Further increases in applied voltages lead to increasing regions of ionization. The current flow is still intermittent as localized areas break down, build up a space charge, and are quenched.

The second stage in the development of the corona occurs when the applied voltage exceeds a certain value, and the character of the corona changes into a more stable configuration. This situation is commonly referred to as a glow discharge. The glow discharge is characterized by relatively steady regions where the positive space charge near the ions, the negative space charge in the interelectrode space, and the avalanche electrons are in electrical equilibrium with the applied voltage.

1.1 CURRENT VOLTAGE RELATIONSHIP

The current and voltage relationships in a concentric wire and cylinder electrode system are such that a relatively simple mathematical relationship can be derived from Poisson's equation, which governs all electrostatic phenomena. Poisson's equation, in the rationalized MKS system of units, is:

$$\Delta^2 V = -\frac{\rho}{\epsilon_0} \qquad (1.5)$$

which for cylindrical coordinates reduces to

$$\frac{d^2V}{dr^2} + \frac{1}{r}\frac{dV}{dr} + \frac{\rho}{\epsilon_0} = 0 \qquad (1.5a)$$

The space charge density, ρ, for the cylindrical corona is given by

$$\rho = \frac{i}{2\pi r E \mu} \qquad (1.6)$$

Since $\frac{dV}{dr} = -E$, substitution of 1.6 and 1.7 into 1.5 yields (1.7)

$$rE\frac{dE}{dr} + E^2 - \frac{i}{2\pi\epsilon_0\mu} = 0 \qquad (1.8)$$

which integrates to

$$E = -\frac{dV}{dr} = -\sqrt{\frac{i}{2\pi\epsilon_0\mu} + \frac{C^2}{r^2}} \qquad (1.9)$$

C is a constant of integration, and need only be constant with respect to r. In general, C will be dependent upon the physical dimensions of the corona wire and collection electrode, as well as the applied voltage. This constant of integration can be evaluated from the boundary condition that the electric field is very close to the breakdown potential at the boundary of the visible glow region ($r = r_0$) from which

$$C = r_0\sqrt{E_C^2 - \frac{i}{2\pi\epsilon_0\mu}}$$

Utilizing this value for C yields the following relationship between current and voltage for the cylindrical precipitator

$$V = r_0 E_C\left[\ln\frac{b}{a} - 1 + \sqrt{1 + \frac{i}{2\pi\epsilon_0\mu}\cdot\frac{b^2}{E_C^2 r_0^2}} - \ln\left(\frac{1 + \sqrt{1 + \frac{i}{2\pi\epsilon_0\mu}\cdot\frac{b^2}{E_C^2 r_0^2}}}{2}\right)\right] \qquad (1.10)$$

where

a = radius of the corona wire, m
b = radius of the collection electrode, m
i = current per unit length of the corona wire, amp/m,
μ = effective mobility of the charge carrier, m^2/v-sec,
E_c = breakdown field strength, kV/m,
r_0 = outer radius of the glow region, m,
V = applied voltage, kV, and
ϵ_0 = permittivity of free space.

The initial field strength required for breakdown for smooth, round wire and for air of relative density, d, as determined from Equation 1.3 is

$$E_c = (30d + 9\sqrt{d/a}) \text{ kV/cm}, \tag{1.11}$$

setting the current equal to zero and assuming that the radius of the corona glow region is equal to the radius of the discharge electrode wire in Equation 1.10, leads to a starting voltage of

$$V_0 = (30ad + 9\sqrt{ad}) \ln \frac{b}{a} \tag{1.12}$$

From Equation 1.12, it is clear that reducing the size of the corona wire will result in a decrease in the applied voltage necessary to initiate corona. As shown in Figure 1.2, for a given applied voltage, Equation 1.10 can be satisfied only if the current per unit length increases with a decrease in E_c, which leads to an increase in the corona current. Conversely, the current can be decreased by increasing the corona wire size.

The situation described above is specifically calculated for the cylindrical electrode configuration, but the parallel plate and wire electrode are similar. The equations are not as simple because the symmetry of the cylindrical precipitator simplifies the mathematics. However, the effects of wire size and electrode spacing will be governed by the relationship of voltage vs. current in the same manner.

The plate-type precipitator also has an additional degree of freedom—the corona wire spacing. Qualitatively, it is apparent that if the corona wires are spaced very close together, the system would approach the field configuration in a parallel plate capacitor, which yields

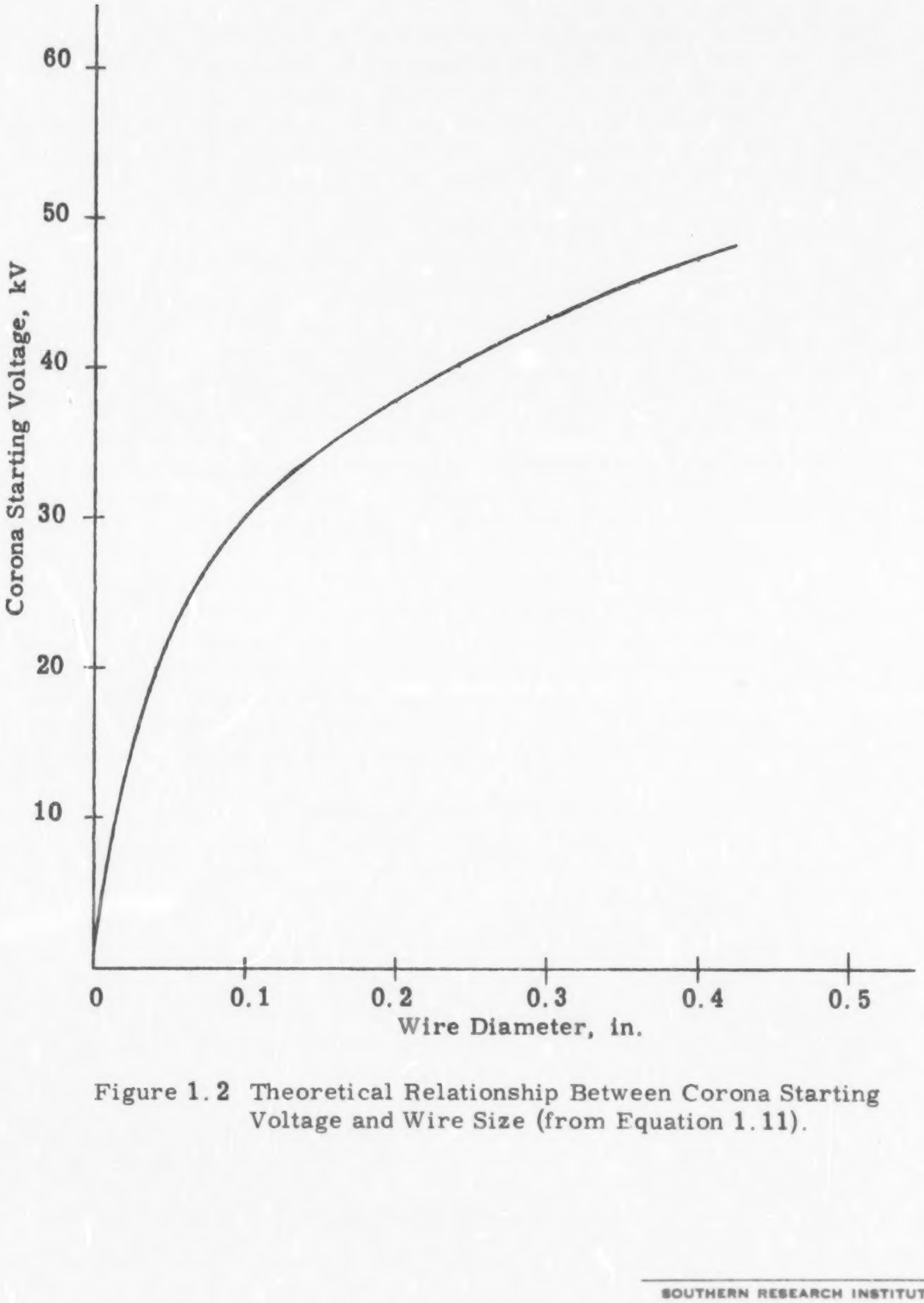

Figure 1.2 Theoretical Relationship Between Corona Starting Voltage and Wire Size (from Equation 1.11).

a constant field strength in the interelectrode space. For a given applied voltage, this reduces the electric field near the corona wire. Therefore, if it is desirable to increase the current density in a region, it may be accomplished by either using smaller wires or spacing the wires farther apart; see Figure 1.3. Similarly, the current density can be reduced by spacing the corona wires closer together, using larger wires, or both.

1.2 TEMPERATURE AND PRESSURE EFFECTS

For the most part, the discussion of precipitator fundamentals is concerned with operations at atmospheric pressure and temperatures between 100°F and 600°F. There is, however, current interest in the limitations placed on precipitator operation by high temperature and high pressure.

One effect of gas temperature on corona generation is a change in the relative number of ionized molecules. The gas in a precipitator is normally an insulating medium; however, as discussed earlier, it becomes conductive through ionization. In the electron avalanche process, the ionization energy is supplied by the applied electric field. However, any source of energy, such as thermal energy, can be utilized for ionization. The average energy of a molecule is related to the absolute temperature by the Boltzmann constant. But the energy of each individual molecule is statistically distributed on both sides of the average energy. Those molecules with energies greater than the ionization potential of the gas will be ionized, and therefore will provide charge carriers for conduction.

This mechanism has been reported by Saha.[10] The Saha equation, relating the number of thermally ionized molecules to the ionization potential of the gas, is described by Cobine.[11] This equation is given as:

$$\log_{10}\left(\frac{X^2 P}{1 - X^2}\right) = -\frac{5050\ V_i}{T} + 2.5 \log_{10} T - 6.5 \qquad (1.13)$$

which relates the fraction of the molecules ionized to the temperature, pressure, and ionization potential of the molecule.

The fraction ionized, X, can be calculated from the above equation where P is in atmospheres absolute, V_i is the ionization potential in volts, and T is absolute temperature, °Kelvin. For a temperature of 1500°F (1090°K) and at atmospheric pressure, the fraction of thermal ions fo

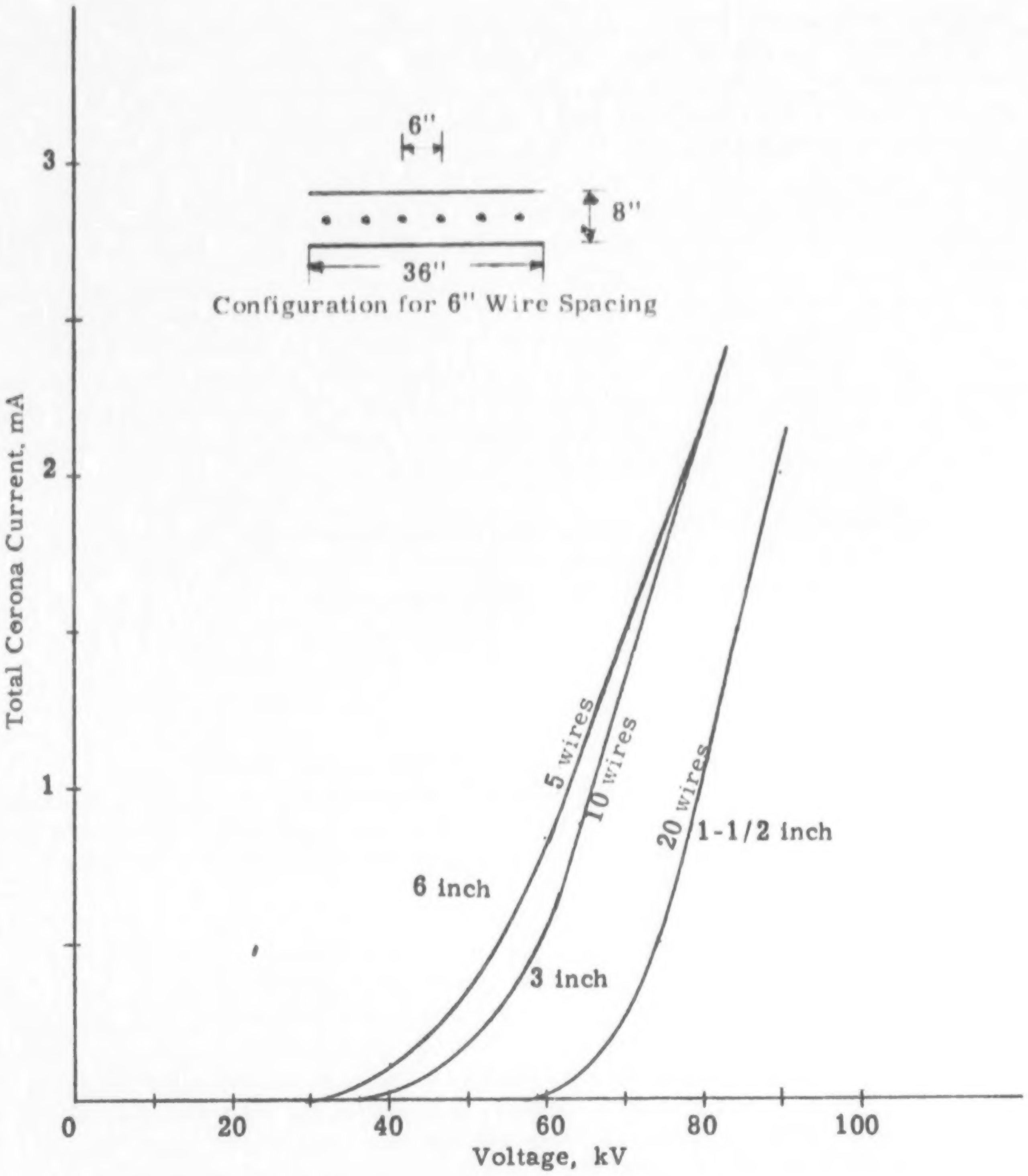

Figure 1.3 Effect of Wire-to-Wire Spacing on Clean Electrode Corona Current (Reference 5).

oxygen, with an ionization potential of 13.6 volts, is about 10^{-31}, which is less than the number of ions formed by naturally occurring radioactivity and cosmic rays. An increase in pressure reduces the ionized fraction still further. Therefore, thermal ionization can be completely neglected in precipitator operations up to 1500°F.

Temperature and pressure do modify corona starting and sparkover potentials. The avalanche process is brought about because the electron has sufficient time between inelastic collisions to be accelerated to a velocity sufficient to ionize the gas. Therefore, the potential necessary to start corona is related to the density of the host gas. If pressure, and hence density, is increased, the molecules are effectively moved closer together, resulting in a shortened mean free path and reduced mean free time. This reduced mean free time requires a greater electric field to accelerate the electron to the ionization velocity.

Both temperature and pressure modify the gas density. The gas density, d_0, at a given temperature, T_0, and pressure, P_0, is related to the density at other temperatures and pressures by:

$$d = d_0 \frac{T_0}{T} \cdot \frac{P}{P_0},$$

thus, an increase in pressure at a given temperature results in an increased density, while an increase in temperature at constant pressure results in a decreased density. The effect of gas pressure and density on corona starting potential has been experimentally determined by Shale[12], and is shown in Figure 1.4.

The electrical limits for operation of a precipitator are defined by the corona onset on the one hand, and sparking potential on the other. Shale points out that in negative corona, both corona starting voltage and sparkover voltage are influenced by gas temperature and pressure. Figure 1.5 shows the relationship between corona current and voltage for air at 1500°F at various pressures. It is apparent that for pressures between 0 and 20 psig, there is little change in voltage as current is increased. In such case, sparkover would occur at a voltage near the corona starting voltage, severely limiting the range of operation. The low operating voltage imposed by these conditions result in low values of electric field, which in turn limit precipitator performance. At higher

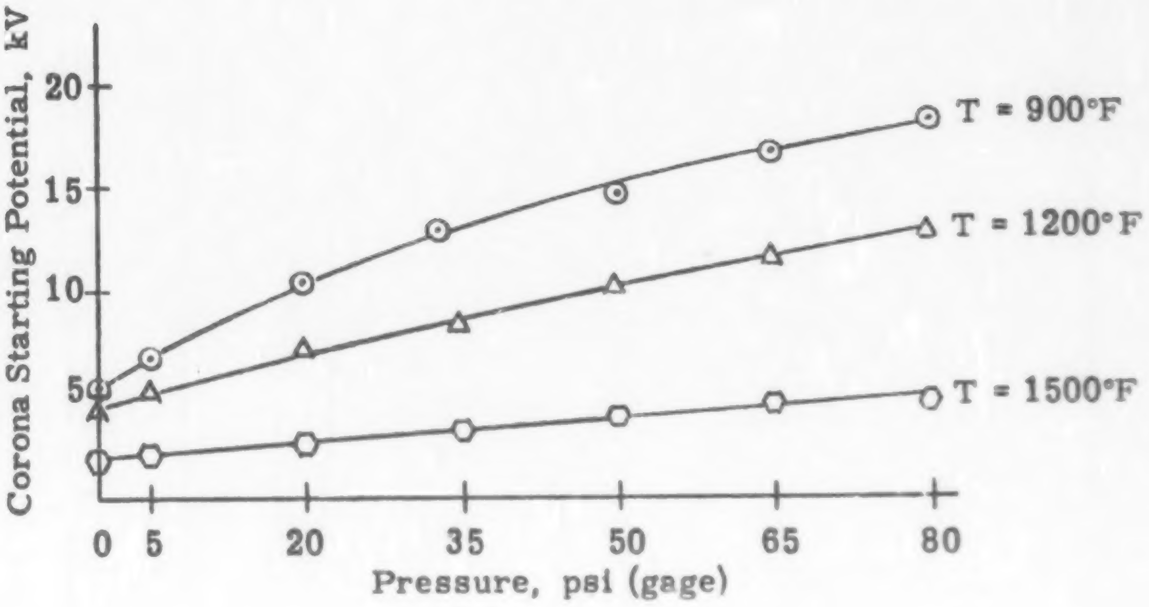

Figure 1.4 Variations in Clean Electrode Corona Starting Potential With Pressure and Temperature Negative Corona (Reference 12).

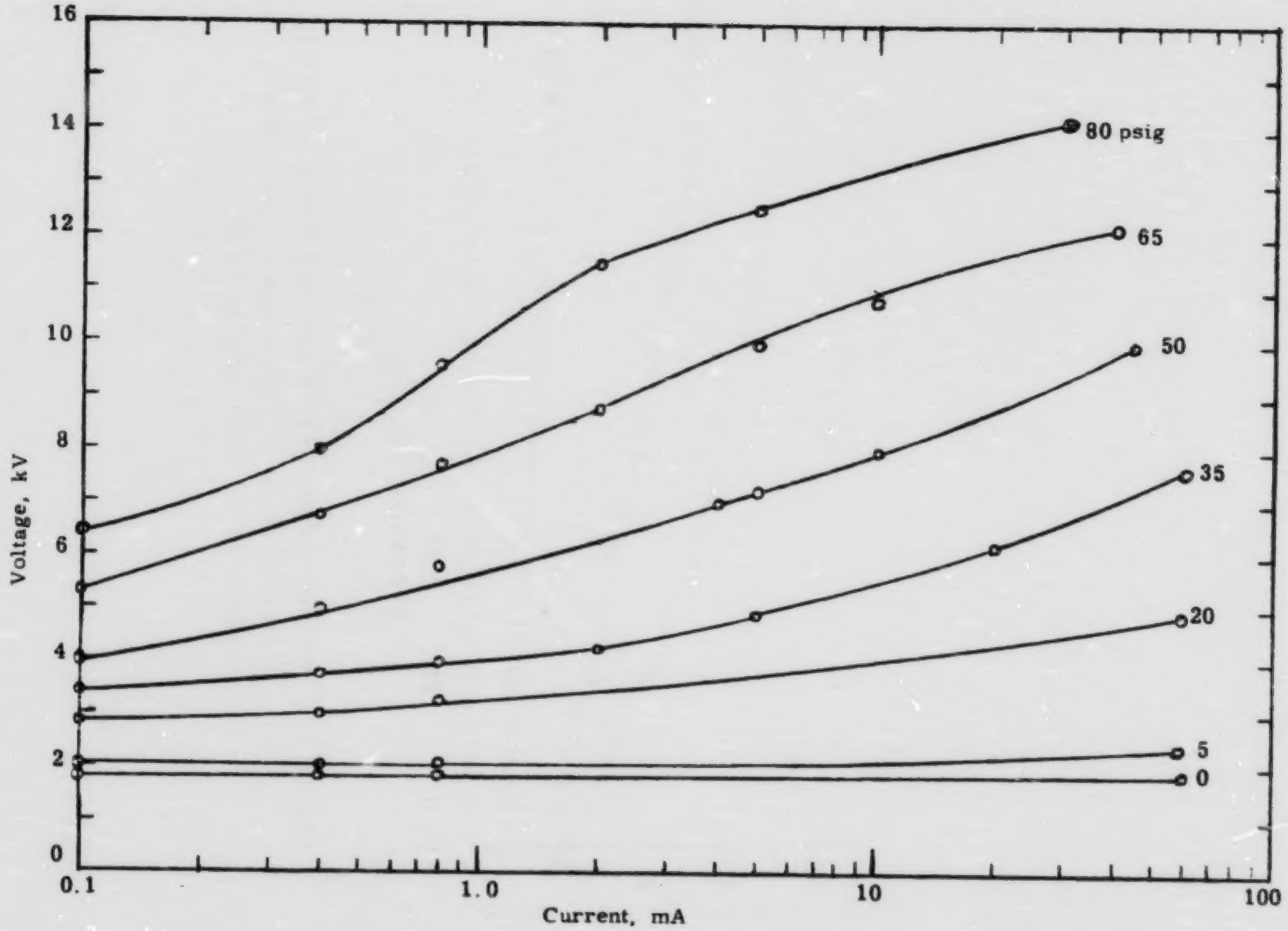

Figure 1.5 Electrical Characteristics of Air at 1500° F Negative Corona (Reference 12).

pressures, the effective range of operating voltages is increased so that reasonable electric fields can be maintained.

In negative corona, Shale has shown that effective ion mobilities increase due to the following factors:

(1) at constant gas temperature and field strength, ion mobility increases with decreasing gas density,

(2) at constant density and field strength, ion mobility increases with increasing temperature, and

(3) at constant temperature and gas density, ion mobility increases with increasing field strength.

The effect of factor 1 is that at lower gas densities, electrons travel further before they are attached to gas molecules to form ions. Thus, the average velocity of the current carriers is increased. The other factors (2 and 3) are reportedly due to the increase in the number of free electrons in the vicinity of the corona wire due to increased thermionic emission and to increased secondary emission from positive ion impaction on the corona wire. The availability of these additional electrons and the presence of a high field again result in their traveling further toward the collection plate before being captured by inelastic collision with an electronegative gas molecule. Since the current in the interelectrode space is the product of the charge, effective mobility, and field strength, the apparent increase in mobility results in increased current. Consequently, for negative corona, the voltage-current curves would be altered toward higher currents at lower voltage.

In negative corona, the presence of negative ions near the corona wire provides a space charge which limits the field near the wire and serves to stabilize the discharge. However, with low gas densities, the highly mobile, free electrons move rapidly away from the corona wire and are not effective in providing a stabilizing space charge until they are captured by an electronegative gas molecule. Since the electrons move a longer distance before capture at low gas densities, the space charge effect is reduced and the current rises more rapidly than at higher gas densities. Thus, sparkover occurs at reduced voltage.

In positive corona, the same effects would not occur since the current carriers are positive ions. Electrons from the avalanche process are attracted to the corona wire and do not travel to the collection electrode. Consequently, positive corona should have more favorable voltage-current relationships in the high temperature region with higher sparkover potentials.

The more favorable voltage-current characteristics of the positive corona discharge have been confirmed experimentally on a 15 foot long wire and pipe precipitator, as indicated in Figure 1.6.

1.3 PRACTICAL ASPECTS OF CORONA THEORY ON ELECTROSTATIC PRECIPITATION

The behavior of an electrostatic precipitator is strongly dependent upon the value of the electric field in the vicinity of the collection electrode and the value of the charge imparted to the particulate matter. The charge, in turn, is related to the electric field in the charging region; therefore, the voltage-current relationship for the precipitator is important. Gas temperature and composition modify the V-I characteristics for a given precipitator. As previously mentioned, the presence of an effective space charge is necessary in order to maintain a stable corona. This space charge for negative corona is dependent upon the presence of a sufficient quantity of electronegative gases such as oxygen or sulfur dioxide. Figures 1.7 and 1.8 show the V-I characteristics for nitrogen with various percentages of oxygen and sulfur dioxide, respectively, for a concentric cylinder type precipitator. It is clear from the graphs that increasing the percentage of electronegative gas increases the space charge, which exerts a current limiting effect on the system.

Since water vapor is a constituent of combustion products, the effect on the V-I characteristics of the corona is important. As shown in Figure 1.9, increasing the amount of water vapor in air results in an increase in sparkover voltage and a decrease in the corona current. The effect is more pronounced as quantities of water up to about 40 percent by volume are added.

Since the effect of the space charge is to limit the current, the addition of particulate matter, which represents a much more immobile charge (mobility of electrons >> mobility of ions >> mobility of charged particulate) reduces the current still further. The effect of this can be

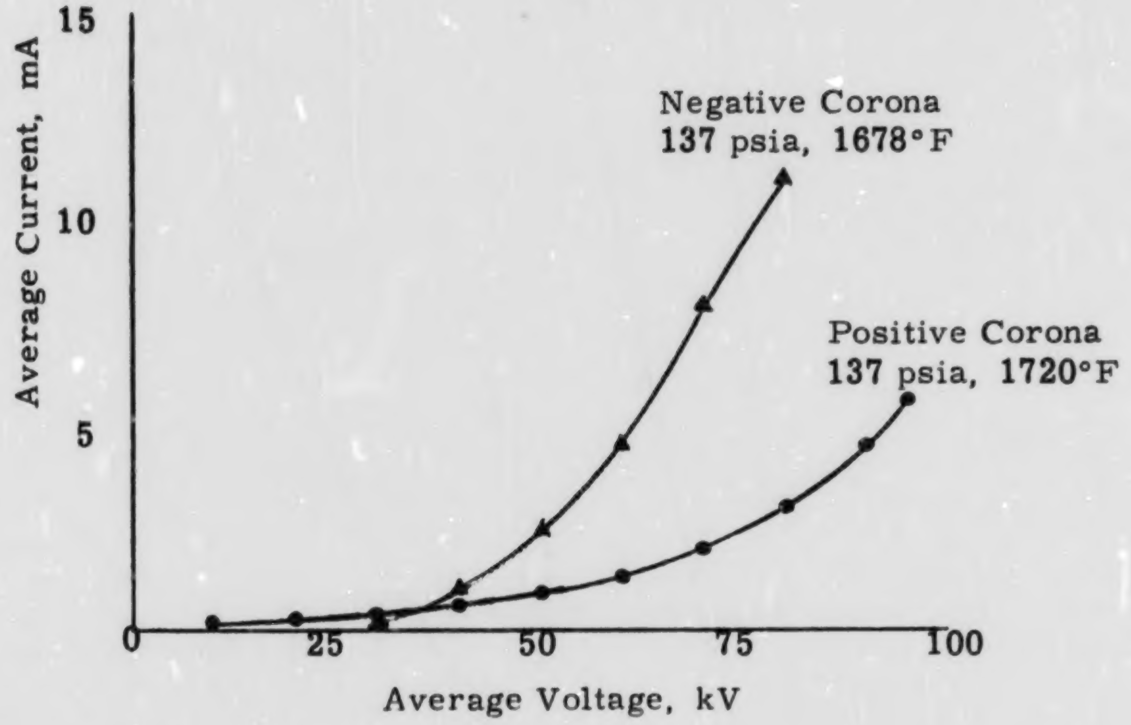

Figure 1.6 Current Voltage Relationships for 15-ft Wire and Pipe Precipitator at High Pressure and High Temperature (Reference 14).

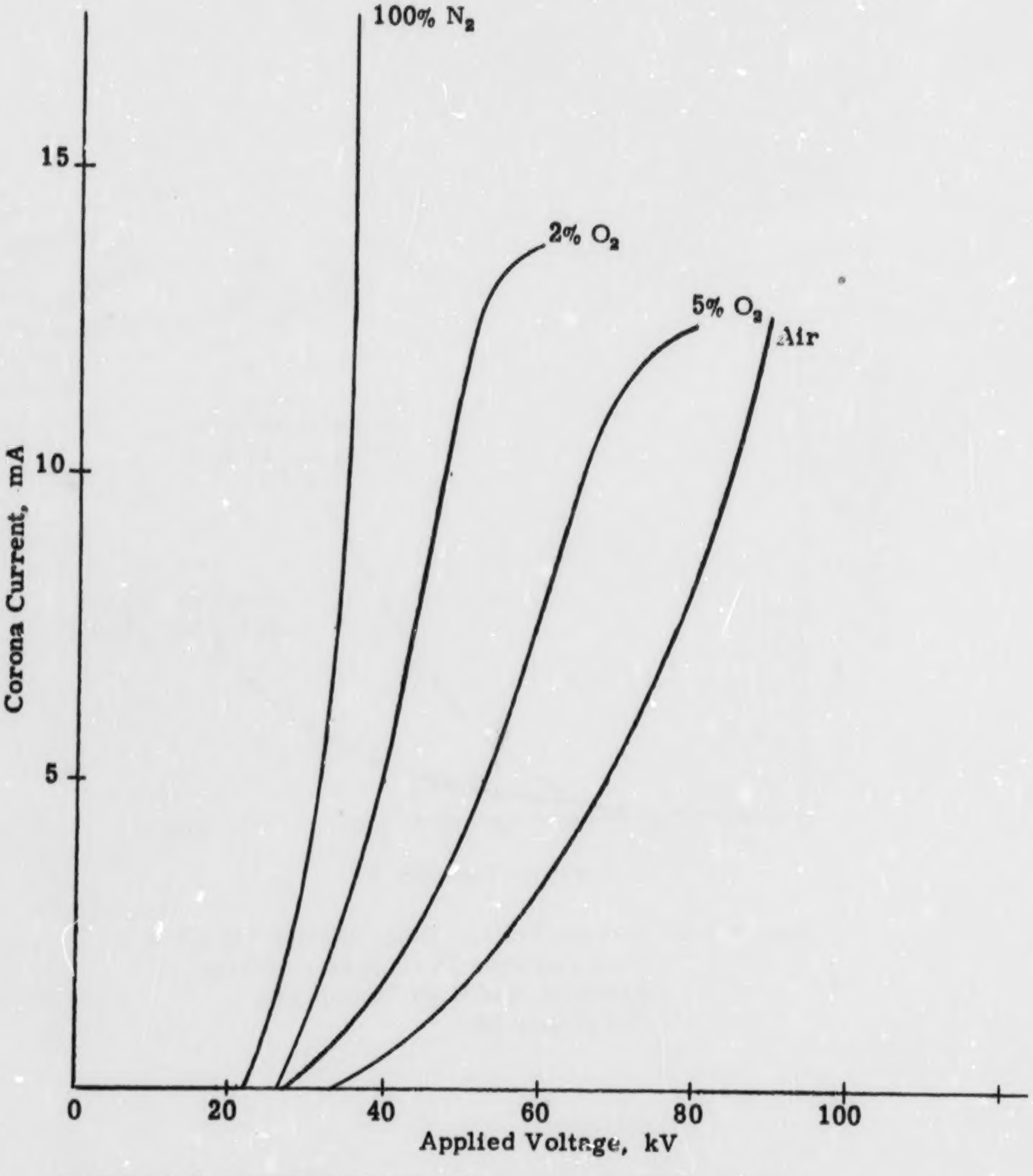

Figure 1.7 Negative Corona Characteristics for Nitrogen-Oxygen Mixtures With Clean Electrodes (Reference 5).

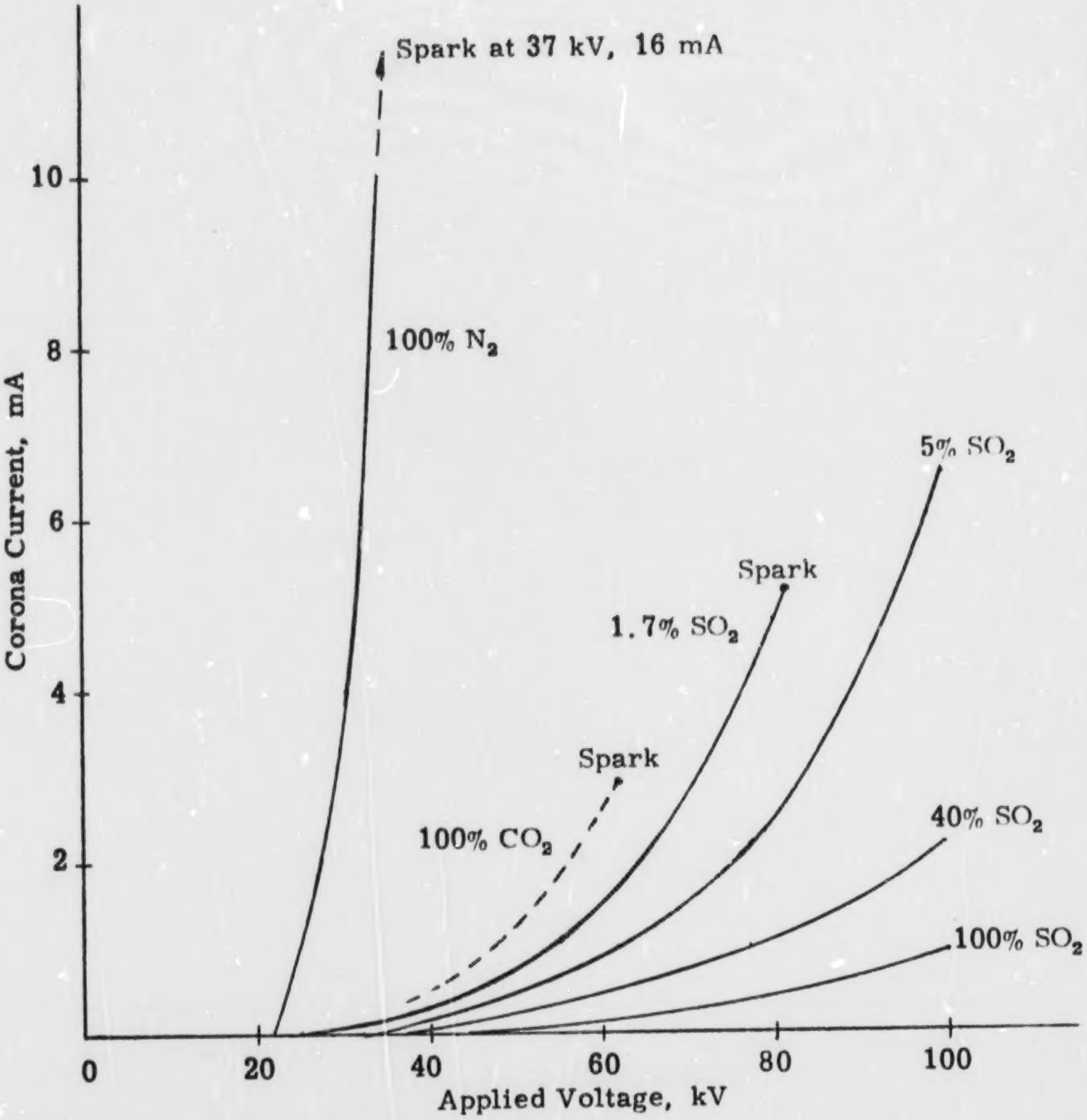

Figure 1.8 Variation of Negative Corona Current With Applied Voltage for Nitrogen-Sulfur Dioxide Mixtures (Reference 5 - Clean Electrodes).

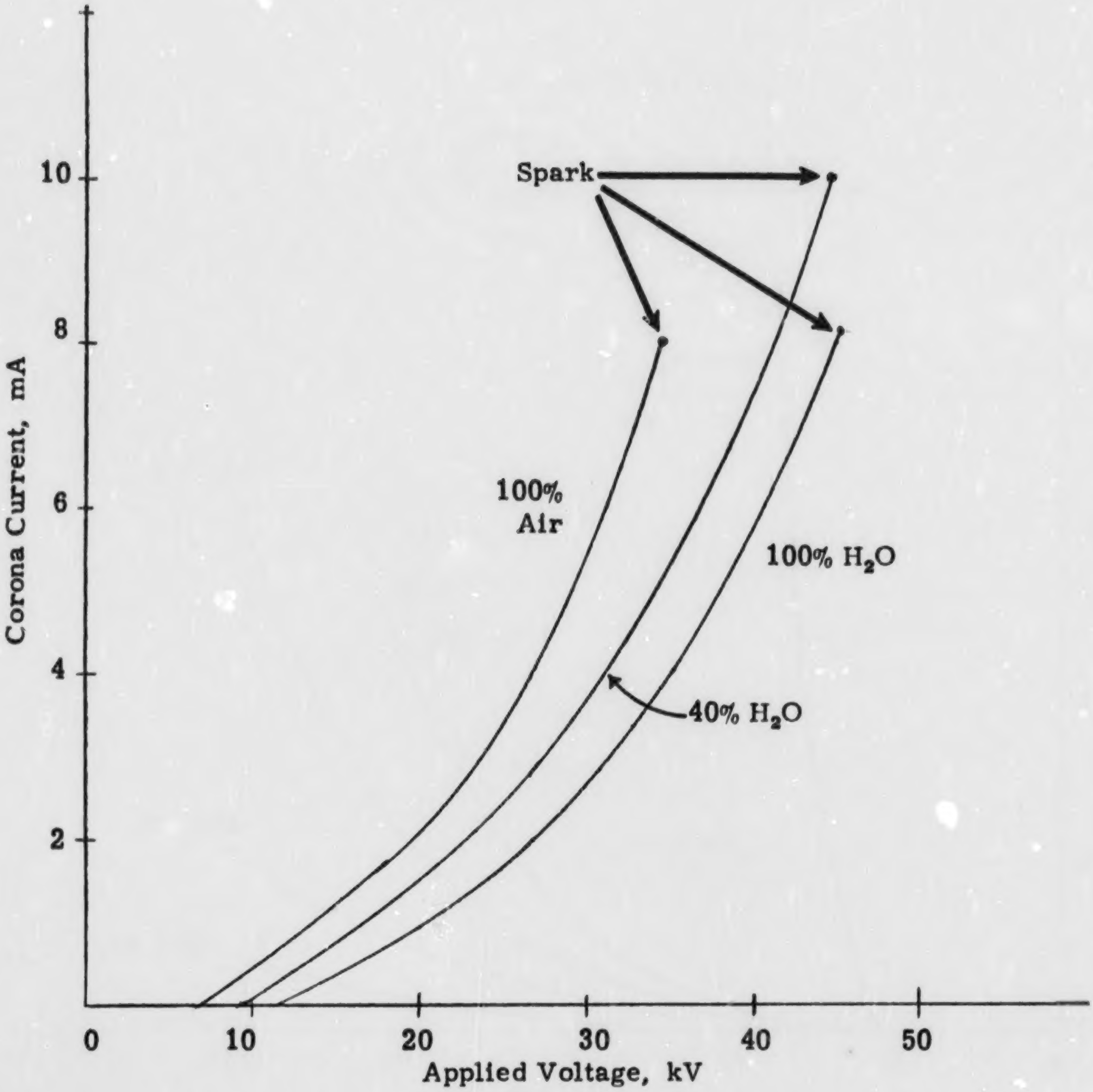

Figure 1.9 Variation in Negative Corona Current With Applied Voltage for Air-Water Vapor Mixtures at 400° F and Atmospheric Pressure (Reference 5 - Clean Electrodes).

seen by considering the relative amount of charge that appears as free electrons, negative ions, and negative charge on the particulate. In the following discussion, a concentric cylindrical precipitator with no particulate loading will be considered. Later (Chapter 2) the effect of particulate loading will be included.

The relative amount of charge carried by free electrons and negative ions can be determined from the relationship that the current at the corona wire must be equal to the current at the outer cylinder and, similarly, the charge transferred at both electrodes must be equal. The current per unit length of the corona wire must be equal to the current per unit length of the collection electrode under steady-state conditions. The current at the corona wire consists of the positive ion current to the wire, plus the free secondary electron current from the wire. This can be expressed as

$$i = n_e e + n_+ e \qquad (1.15)$$

where

n_e, n_+ = the number of electrons and ions per unit time crossing the wire surface,
e = the electronic charge, and
i = the current per unit length of the corona wire.

The number of electrons per unit time is related to the number of ions by the secondary emission coefficient γ of the corona material such that

$$n_e = \gamma n_+, \qquad (1.16)$$

so that the current per unit length becomes

$$i = n_+ e\,(1 + \gamma) \approx n_+ e \qquad (1.17)$$

because γ is a small number compared to 1.

The source of the positive ions which drift toward the corona wire is the ionization caused by the electron avalanche, since for every free electron there remains a positive ion. If we describe the ionization process as a mechanism by which every free electron generates a number of new electrons through ionization in unit distance, the rate of change of the number of electrons per unit distance can be expressed as

$$dn_e = n_e \alpha \, dr \tag{1.18}$$

where α is the ionization coefficient. The ionization coefficient is assumed to be independent of the electric field strength over the region of field and space normally encountered in precipitators. Strictly speaking, α is field dependent. Equation 1.18 can be integrated from the surface of the wire to the edge of the avalanche region to yield the relative increase in free electrons.

$$\frac{n_e}{n_{oe}} = \exp(\alpha r) \tag{1.19}$$

where n_{oe} is the number of electrons per second from the corona wire and natural processes. These electrons can be generated by irradiation, secondary emission or bombardment by metastables, but in the following discussion, all three effects are lumped in the secondary emission coefficient, γ.

For each positive ion, there must be a number of free electrons generated, equal to the secondary emission coefficient γ. Therefore, in the avalanche process, one free electron must generate $(\frac{1}{\gamma})$ electrons and positive ions, in order for the process to be continuous. The avalanche process generates an equal number of positive ions as electrons, so that

$$n_p = n_e - n_{oe} \tag{1.20}$$

For this quantity of positive ions, n_{oe} free electrons must be generated by secondary emission

$$n_{oe} = \gamma n_p = \gamma (n_e - n_{oe}). \tag{1.21}$$

Substituted into (1.19),

$$n_e = \gamma (n_e - n_{oe}) \exp \alpha r, \tag{1.21a}$$

from which

$$\exp(\alpha r) = \frac{n_e}{\gamma(n_e - n_{oe})} - \frac{1}{\gamma\left(1 - \frac{n_{oe}}{n_e}\right)} \approx \frac{1 + \frac{n_{oe}}{n_e}}{\gamma}$$

and

$$n_{oe} \approx \gamma n_e \tag{1.22}$$

$$\exp(\alpha r) \approx \frac{1}{\gamma}\left(1 + \frac{\gamma n_e}{n_e}\right) = 1 + \frac{1}{\gamma} = \frac{1+\gamma}{\gamma} \tag{1.22a}$$

or,

$$\alpha r = \ln \frac{1+\gamma}{\gamma} \tag{1.23}$$

from which

$$r = \frac{1}{\alpha} \ln \frac{1+\gamma}{\gamma} \; . \tag{1.24}$$

Equation 1.24 relates the radius of the glow region to the secondary emission coefficient (γ) and the avalanche coefficient (α).

At the collection electrode, there are three current-carriers—free electrons, negative ions, and negatively charged particulates. The total current per unit length at the collection electrode can be expressed as

$$i = n_e'e + n_-e + n_p q_p e \tag{1.25}$$

where n_e', n_-, and n_p are the number per unit time of electrons, negative ions, and particles, respectively, arriving at the collection electrode, and q_p is the number of electrons bound to the particulate matter. Equations 1.15 and 1.18 yield

$$n_+e\,(1+\gamma) = e\,(n_e' + n_- + n_p q_p)$$

Before any particulate is introduced, n_p will be zero. This is the case under current consideration; later, in the chapter on systems analysis, this term is included in the analysis of the precipitation mechanism.

Since they are equal, the current flow in the space just outside the corona wire can be equated to the current just inside the collection electrode. Current carried by free carriers under the influence of an electric field is well understood.[7] In the region near the corona wire, the electric field can be designated E_{co}, and at the collection electrode, E_p. The current density at the corona wire can be expressed as

$$j_{cor} = N_e e\mu_e E_{co} + N_+ e\mu_+ + E_{co} = eE_{co}(N_e\mu_e + N_+\mu_+). \qquad (1.26)$$

Where (N_e) and (N_+) are the number densities (number per unit volume) of the charge carriers in the region just outside the corona wire, and (j) is the current density (amps/m²). Similarly, at the collection electrode

$$j_{col} = N_e' e\mu_e E_p + N_- e\mu_- E_p + N_p q_p e\mu_p E_p. \qquad (1.27)$$

Where N_e', N_-, and N_p are the number densities of free electrons, negative ions and particulates near the collection electrode. N_p is again equal to zero in this example, but is included for completeness. Equating the total current at the corona wire to that at the collection electrode yields:

$$j_{cor} 2\pi R_1 = j_{col} 2\pi R_2, \text{ from which} \qquad (1.28)$$

$$R_1 e E_{co}(N_e\mu_e + N_+\mu_+) = R_2 e E_p (N_e'\mu_e + N_-\mu_- + N_p q_p), \text{ but} \qquad (1.28a)$$

since $N_p = 0$,

$$\frac{N_e\mu_e + N_+\mu_+}{N_e'\mu_e + N_-\mu_-} = \frac{R_2}{R_1}\frac{E_p}{E_{co}} \qquad (1.29)$$

The relative values of the above mobilities are known, and related as follows:

$\mu_+ \approx \mu_- \approx 10^{-3}\mu_e$, which yields, upon substitution

$$\frac{R_2}{R_1}\frac{E_p}{E_{co}} = \frac{10^3 N_e\mu_+ + N_+\mu_+}{10^3 N_e'\mu_+ + N_-\mu_+} = \frac{N_+}{10^3 N_e' + N_-} + \frac{N_e}{N_e' + N_- 10^{-3}} \qquad (1.30)$$

Next, relate N_+ and N_e at the corona

$$n_+ = 2\pi R_1 N_+ \mu_+ \qquad (1.31)$$

$$n_e = 2\pi R_1 N_e \mu_e E_{co} \tag{1.32}$$

$$n_e = \gamma n_+ \tag{1.33}$$

$$2\pi R_1 N_e \mu_e E_{co} = \gamma 2\pi R_1 N_+ \mu_+ E_{co} \tag{1.34}$$

$$N_e = \gamma N_+ \frac{\mu_+}{\mu_e} \tag{1.35}$$

or,

$$\frac{N_e}{N_+} = \gamma \frac{\mu_+}{\mu_e} \tag{1.35a}$$

Substitute into Equation 1.29

$$\frac{\gamma N_+ \dfrac{\mu_+ \mu_e}{\mu_e} + N_+ \mu_+}{N_e' \mu_e + N_- \mu_-} = \frac{R_2}{R_1} \frac{E_p}{E_{co}} \tag{1.36}$$

$$N_+ (1 + \gamma) = \frac{R_2}{R_1} \frac{E_p}{E_{co}} \frac{(N_e' \mu_e + N_- \mu_-)}{\mu_+} \tag{1.36a}$$

$$N_+ (1 + \gamma) = \frac{R_2}{R_1} \frac{E_p}{E_{co}} \left(N_- = N_e' \frac{\mu_e}{\mu_+} \right) \tag{1.37}$$

$$\frac{N_+ (1 + \gamma)}{N_-} = \frac{R_2 E_p}{R_1 E_{co}} \left(1 + \frac{N_e'}{N_-} \frac{\mu_e}{\mu_+} \right) \text{ and} \tag{1.37a}$$

$$\frac{N_+ R_1 E_{co} (1 + \gamma)}{N_- R_2 E_p} = 1 + \frac{N_e'}{N_+} \frac{\mu_e}{\mu_+} \tag{1.37b}$$

but $\dfrac{N_+ R_1 E_{co} (1 + \gamma)}{N_- R_2 E_p}$ can never be less than unity because the numerator represents the current to the corona wire, while the denominator represents the negative ion current to the collection electrode. This ratio must always be greater than or equal to 1. (See Equation 1.22.)

Therefore,

$$\frac{\gamma N_+ R_1 E_{co}}{N_- R_2 E_p} \approx \frac{N_e'}{N_-} \quad \frac{(\mu_e)}{\mu_+} \tag{1.38}$$

which yields after manipulation

$$\frac{N_e'}{N_+} = \frac{\gamma R_1 E_{co} \mu_+}{R_2 E_p (10^3) \mu_e} = \frac{R_1}{R_2} \cdot \frac{E_{co}}{E_p} \cdot \frac{\gamma(\mu_+)}{\mu_e} \cdot \frac{1}{10^3} \tag{1.38a}$$

Typical values for $\frac{R_1}{R_2}$, $\frac{E_{co}}{E_p}$, γ, and $\frac{\mu_+}{\mu_e}$ are, respectively, 10^{-3}, 10, 10^{-3}, and 10^{-3}, which yield for an order of magnitude estimate

$\frac{N_e'}{N_+} \approx 10^{-3}$ and is therefore negligible.

At the other extreme, if $N_- << N_e' \; \frac{\mu_e}{\mu_+}$, and

$\frac{\mu_e}{\mu_+} \approx \frac{\mu_e}{\mu_-} \approx 10^3$, then Equation 1.37 becomes

$$N_+ \; (1 + \gamma) \; R_1 E_{co} = R_2 E_p N_e' \; \frac{\mu_e}{\mu_+} \tag{1.39}$$

$$\frac{N_e'}{N_+} = \frac{(1 + \gamma) \; R_1 E_{co}}{R_2 E_p \quad \frac{\mu_e}{\mu_+}} \tag{1.40}$$

$$\frac{N_e'}{N_+} = 10^{-5}. \tag{1.40a}$$

Again, N_e' is negligible when compared with the number of positive ions per unit volume at the corona wire, and we can conclude from this that $N_- >> N_e'$, or that most of the negative charge is attached to molecules to form negative ions outside of the glow region. This is not to say that some current could not be carried by the free electrons because of their increased mobility. If only one free electron were present for every 10^4 negative ions, then about 10 percent of the current would be carried by electrons. But the majority of charge is bound to molecules as negative ions.

The spacial distribution of the various charged particles within the cylindrical precipitator is illustrated in Figure 1.10. The free electrons and positive ions result from avalanche; the negative ions result from electron attachment.

The space charge in the quiescent zone outside the glow region serves to limit the current flow by electrostatic repulsion. The level of current is a function of the characteristics of the host gas. For example, nitrogen does not readily form negative ions by electron attachment. Therefore, the electrons are free to move (high mobility) and are rapidly carried to the collection electrode. However, oxygen readily attaches an electron for decreased mobility with the associated sluggish space charge, which tends to limit the current.

This effect is readily seen with the introduction of dust particles into the precipitator. The large dust particles are charged by the negative ions, and since they are much more sluggish (still smaller mobility than ions), more significant space charge results, and the current flow immediately drops. This effect is explained theoretically by Gauss' law, which states that the integral of the normal component of the electric field over a closed surface is proportional to the enclosed charge.[6] Therefore, it is seen that the value of the original electric field near the corona wire in a precipitator is first modified (reduced) by the space charge caused by gaseous conduction, and still further reduced by the introduction of the charged particulate.

The physical laws governing negative corona also pertain to the positive corona. The naturally occurring free electrons are accelerated by the high electric field in the region of the corona wire, and in turn experience ionizing collision with the neutral molecules of the host gas. However, in this case, the electrons are driven to the collection electrode. The most probable source of primary electrons is photoionization by light quanta from the glow region, as well as from natural radiation.[13] Since the positive ions are captured in a low field region (E_p) in the positive corona situation, then fewer secondary electrons are produced, which leads to a reduced current compared to that which would result in the negative corona case. Also, positive corona does not depend upon the presence of

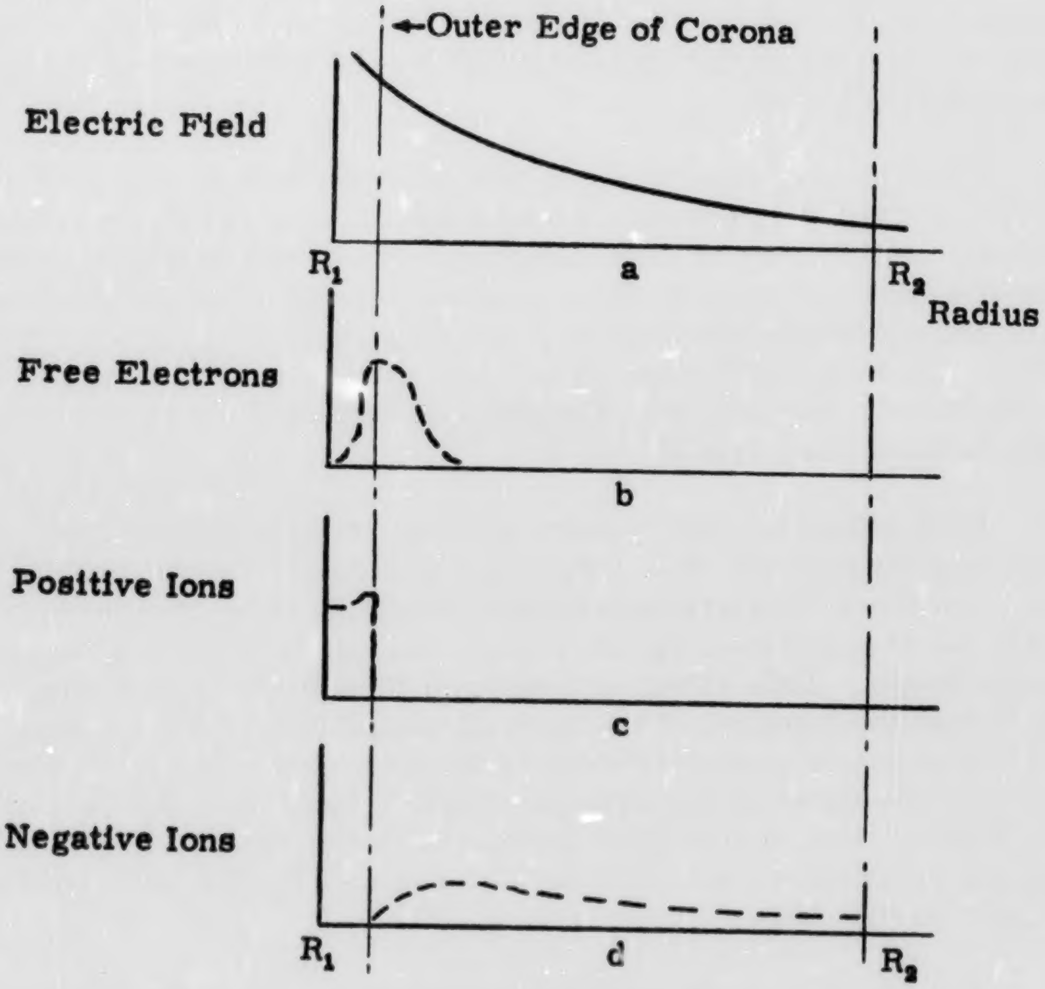

Figure 1.10 Electric Field and Charged Particle Distribution Within a Corona.

electronegative gases, as did the negative corona. The charge is carried in the quiescent zone exclusively by positive ions. Therefore, positive corona is stable in mixtures which do not contain electronegative gases.

1.4 PRACTICAL ASPECTS OF CORONA GENERATION

The discussions to this point have been for the highly idealized case of clean electrodes with atmospheric air. The basic mechanisms and principles described for this idealized case apply in general to the situations encountered in commercial electrostatic precipitators, even though the particular calculated values and specific boundary conditions may be altered by the presence of both a dust loaded gas and electrodes covered by a collected deposit.

In the practical precipitation process, dust particles will be deposited on the collection electrode and to varying degrees on the corona electrode. These deposits can lead to significant modifications in the behavior of the precipitator over that predicted for clean electrodes.

The modifications that occur due to dust deposits are dependent upon the thickness of the layer and the electrical properties of the dust.

Deposits on the corona wire are manifested as an apparent increase in the radius of the wire. An increase in corona wire radius causes a decrease in the corona current and an increase in the value of the corona initiation voltage.

These factors may be partially offset by the surface irregularities caused by the deposition of individual dust particles. Geometric variations on the surface of a conductor cause electric field enhancement in the region of the irregularity with a resultant localized increase in corona current. Thus, a compensation to some degree may be associated with the deposit buildup.

High resistivity dusts on the corona wire can either enhance or retard the formation of corona. The current density is greater at the corona wire than at the collection electrode by the ratio of their areas. Since the electric field in the collected dust layer is equal to the product of the current density and resistivity, this large value of current density, together with a rather high value of resistivity can lead to electric field values greater than the breakdown field strength of the gas in the interstitial regions of the deposit on the corona wire. Thus, corona currents can flow with a high resistivity deposit on the corona wire. In situations where the corona region does not extend past the deposit, a significant voltage drop can occur in the deposit. This voltage subtracts directly from the power supply voltage, and may cause a decrease in the performance of a precipitator.

Deposits on the collection electrode seem to cause no electrical difficulties except for high resistivity dusts. The literature typically lists high resistivity dusts as those deposits with resistivities exceeding about 2×10^{10} ohm-cm. Two detrimental factors are associated with a high resistivity deposit on the collection electrode. The first is that a voltage drop occurs across the dust layer that is proportional to the resistivity of the dust, the current density, and the thickness of the deposit. The power supply must have sufficient dynamic voltage range to compensate for the voltage drop or the behavior of the precipitator will be impaired.

A second factor that is covered in some detail in Chapter 8, Particle Collection, is back corona. Back corona is a condition where the electrical breakdown strength of the gas in the interstitial regions of the deposit is exceeded. The electric field in the deposit is proportional to the current density and the deposit resistivity. If this value of electric field exceeds some critical value, a corona glow is formed on the dust deposit that proves detrimental to precipitator operation.

The above factors must be considered when applying the principles of Chapter 2 to industrial electrostatic precipitators.

CHAPTER 1
BIBLIOGRAPHY

1. von Engel, A., Ionized Gases, Clarendon Press (1955).

2. Wannier, Bell System Technical Journal 32, p 170 (1953).

3. Loeb, L. B., "Fundamental Processes of Electrical Discharge in Gases," Gaseous Discharge, J. Wiley (1939).

4. Loeb, L. B., Electrical Coronas, Their Basic Physical Mechanisms, University of California Press, Berkeley (1965).

5. White, H. J., Industrial Electrostatic Precipitation, Addison-Wesley Publishing Co., Reading Mass. (1963).

6. Frank, N. H., Introduction to Electricity and Optics, McGraw-Hill, New York, p 38 (1950).

7. Allis, W. P. and Brown, S. C., "Basic Data of Electrical Discharges," Research Laboratory of Electronics Technical Report 283, Massachusetts Institute of Technology, Cambridge, Mass. (1958).

8. von Engel, A., Ionized Gases, p 100, Clarendon Press (1955).

9. Peek, F. W., Jr., Dielectric Phenomena in High Voltage Engineering, 3rd Ed., McGraw-Hill, New York (1929).

10. Saha, M. N., "Ionization in the Solar Chromosphere," Philosophical Magazine 40, Section 6, p 422 (July-December 1920).

11. Cobine, J. D., "Theory and Engineering Application," Gaseous Conductors, p 92, Dover Publishing, Inc., New York (1956).

12. Shale, C. C., et al., "Feasibility of Electrical Precipitation at High Temperatures and Pressures," U. S. Department of the Interior, Bureau of Mines (1963) T. N. 23. U7 6325 622.06173.

13. Penney, G. W. and Hammert, G. T., "Photoionization Measurements in Air, Oxygen, and Nitrogen," Journal of Applied Physics **41**, No. 2. pp 572-577 (Feb. 1970).

14. Brown, R. F., "An Experimental High Temperature, High Pressure Electrostatic Precipitator Module Design and Evaluation," Research-Cottrell, Inc. report,September 26, 1969, Subcontract No. PH 198-3, to the U.S. Public Health Service.

CHAPTER 2
THE ELECTRIC FIELD

A preliminary discussion of the establishment of the electric field was included in the preceding chapter as it related to corona generation. A second and equally important function of the electric field is to provide the force required to remove the charged particles from the gas stream.

The electric field in a precipitator is the result of two components:

1) electrostatic field related to applied voltage and electrode geometry, and

2) electric field related to the space charge caused by the presence of electrons, ions, and charged particulate in the inter-electrode space.

If one considers a wire and pipe precipitator, the field, before corona is initiated, is only the electrostatic component. The equation describing this electric field as a function of radial distance from the corona wire is:[1,2]

$$E(r) = \frac{V}{r \ln \frac{b}{a}} \qquad (2.1)$$

where

V = applied voltage

a = radius of corona wire

b = radius of collecting cylinder

r = radial distance

This equation is valid up to the point where corona is initiated.

2.1 SPACE CHARGE PHENOMENA

With the initiation of corona, current flows, in the form of ions and perhaps a few free electrons, through the inter-electrode space. Under this

---

[1] Refer to the bibliography for this chapter.

dynamic condition Poisson's equation can be used to determine the field and currents within the precipitator. For cylindrical coordinates this is:

$$\frac{d^2V}{dr^2} + \frac{1}{r}\ \frac{dV}{dr} + \frac{\rho}{\epsilon_0} = 0 \qquad (2.2)$$

where

V = applied voltage

ρ = space charge density

r = radius

ϵ_0 = permittivity of free space

The space charge for a single carrier species in the inter-electrode space is related to the current density and electric field by the following equation:

$$j = N_0 e \mu E \qquad (2.3)$$

where

j = current density (amp/m^2)

N_0 = number density of carriers (number/m^3)

e = electrical charge

μ = carrier mobility = ratio between field and particle velocity (m^2/volt-sec)

E = electric field = $-\frac{dV}{dr}$ (volts/m)

When multiple charge carriers are present, as in electrostatic precipitators, the current will result from three different carriers: electrons, ions, and charged particulate. For this case, the current density equation must be modified to

$$j = N_e e \mu_e E + N_i e \mu_i E + N_p q_p e E \tag{2.3a}$$

where

$N_e, N_i, N_p,$ = number densities of free electrons, ions, and particles, respectively.

$\mu_e, \mu_i, \mu_p,$ = respective carrier mobilities, and

$q_p e$ = electrical charge carried by each particle.

The space charge density ρ is defined as the quantity of charge per unit volume of the interelectrode space and is equal to the summation of the product of the number density of particles and the charge on each.

$$\rho = N_e e + N_i e + N_p q_p e \tag{2.4}$$

For gases normally encountered in electrostatic precipitators, sufficient quantities of electronegative gases are present to attach essentially all of the free electrons. Therefore, the terms involving free electrons can be neglected, resulting in:

$$j = N_i e \mu_i E + N_p q_p e \mu_p E, \text{ and} \tag{2.5}$$

$$\rho = N_i e + N_p q_p e \tag{2.6}$$

Equation 2.5 can be replaced by a simplified expression which includes the total space charge and an equivalent mobility. The expression for the equivalent mobility can be determined by the relation:

$$\rho \mu_{eq} E = N_i e \mu_i E + N_p q_p e \mu_p E = \rho_i \mu_i E + \rho_p \mu_p E \tag{2.7}$$

from which

$$\mu_{eq} = \frac{\rho_i \mu_i + \rho_p \mu_p}{\rho} = \left[\rho_i + \rho_p \frac{\mu_p}{\mu_i}\right] \frac{\mu_i}{\rho} \tag{2.8}$$

$$= \left[\rho_i + \rho_p - \rho_p \left(1 - \frac{\mu_p}{\mu_i}\right)\right] \frac{\mu_i}{\rho}$$

but since $\frac{\mu_p}{\mu_i} << 1$, Equation 2.8 can be approximated by

$$\mu_{eq} = \frac{\rho_i}{\rho} \mu_i \tag{2.8a}$$

where

μ_{eq} = equivalent mobility of the total space charge

ρ_i = ionic space charge density

ρ_p = particulate space charge density

$\rho = \rho_i + \rho_p$ = total space charge density.

Poisson's equation relates the electric field to the space charge. The space charge is related to the current density by

$$j = \frac{i}{2\pi r} = \rho \mu_{eq} E \tag{2.9}$$

from which

$$\rho = \frac{i}{2\pi r \mu_{eq} E} = \frac{\rho}{\rho_i} \cdot \frac{i}{2\pi r \mu_i E} \tag{2.10}$$

Even though the ratio ρ/ρ_i has some variation with radius, the average ratio of ionic space charge to total space charge can be approximated from the measured voltage-current characteristics of the particular installation. If the current corresponding to the applied voltage is known for a no-dust-load condition, the ratio of ionic space charge to total space charge is very nearly the ratio of current density at loaded conditions to no-load conditions for a fixed voltage. Expressed as an equation:

$$\frac{\rho_i}{\rho} \approx \frac{j_A}{j_{NL}} \Bigg|_{v\ =\ \text{constant applied voltage}} \qquad (2.11)$$

where

j_A = actual current density under loaded conditions, and

j_{NL} = current density under no load.

The electric field can be determined from Poisson's equation by substituting Equation 2.10 for the space charge.

$$\frac{d^2V}{dr^2} + \frac{1}{r}\frac{dV}{dr} + \frac{i\rho}{2\pi r\epsilon_0 E\mu_i\rho_i} = 0 \qquad (2.12)$$

But since $E = -\frac{dV}{dr}$, Equation 2.12 can be modified to

$$rE\frac{dE}{dr} + E^2 - \frac{i\rho}{2\pi\epsilon_0\mu_i\rho_i} = 0 \qquad (2.13)$$

The solution to 2.13 is

$$E = -\frac{dV}{dr} = -\left(\frac{i\rho}{2\pi\epsilon_0\mu_i\rho_i} + \frac{C^2}{r^2}\right)^{\frac{1}{2}} \qquad (2.14)$$

where C is a constant of integration and needs only to be independent of r.

If we designate the breakdown field strength of air as E_c and solve Equation 2.14 with the boundary condition that the electric field at the outer edge of the corona glow region is equal to E_c, we have

$$C = r_0\sqrt{E_c^2 - \frac{i\rho}{2\pi\epsilon_0\mu_i\rho_i}} \qquad (2.15)$$

where r_0 is the radius of the glow region, typically somewhat greater than the radius of the corona wire electrode. Substituting Equation 2.15 into 2.14 yields

$$E = -\left[\left(\frac{r_0 E_c}{r} \right)^2 - \left(\frac{r_0^2}{r^2} - 1 \right) \frac{i\rho}{2\pi\epsilon_0 \mu_i \rho_i} \right]^{\frac{1}{2}} \qquad (2.16)$$

The breakdown field strength, E_c, has been determined semi-empirically by Peek[3] to be:

$$E_c = 3\text{x}10^3 md\,(1 + 0.3\sqrt{d/a}\,)\ \text{kV/m} = 30md(1 + 0.3\sqrt{d/a}\,)\ \text{kV/cm} \qquad (2.17)$$

where

m = roughness factor for the corona wire (0.5 - 1.0),

d = relative air density = $\frac{T_0 P}{T\ P_0}$,

T, P = temperature (°K) and pressure (mmHg), respectively,

T_0, P_0 = 293°K and 760 mmHg, and

a = radius of corona wire (cm).

The voltage-current relations can be determined from Equation 2.8 by integrating the electric field from the surface of the wire to the collection electrode. If we designate a, b = radius of wire and pipe respectively we find

$$V = \int_a^b - E(r)\,dr = -\int_a^b \left[\left(\frac{r_0 E_c}{r} \right) - \frac{r_0}{r^2} - 1 \right) \frac{i\rho}{2\pi\epsilon_0 \mu_i \rho_i} \right]^{\frac{1}{2}} dr \qquad (2.18)$$

from which

$$V = r_0 E_c \left\{ \ln \frac{b}{r_0} - 1 - \ln \frac{1 + \sqrt{1 + \frac{i\rho}{2\epsilon_0 \mu_i \rho_i} \cdot \frac{b^2}{E_c^2 r_0^2}}}{2} + \sqrt{1 + \frac{i\rho}{2\epsilon_0 \mu_i \rho_i} \cdot \frac{b^2}{E_c^2 r_0^2}} \right\} \qquad (2.19)$$

The corona starting voltage, V_0, can be determined by applying the boundary conditions when $i = 0$, $r_0 = a$, which yields

$$V_0 = aE_c \left[\ln \frac{b}{a} - 1 - \log 1 + 1 \right] = aE_c \ln \frac{b}{a} \qquad (2.20)$$

Substituting Equation 2.17 for E_c, we find

$$V_0 = 30a\, md(1 + 0.3 \sqrt{d/a}) \ln \frac{b}{a} \text{ kV}$$

Equation 2.19 is strictly correct for the voltage-current relationship. Since r_0 is somewhat indefinite (radius of the glow region), an approximation to reduce Equation 2.19 to a more usable form is worthwhile. The substitution of (a) for (r_0) will not modify the value significantly, so that a more workable approximation for Equation 2.19 is

$$V = V_0 + aE_c \left[\sqrt{1 + \frac{i\rho}{2\epsilon_0 \mu_i \rho_i} \cdot \frac{b^2}{a^2 E_c^2}} - 1 - \ln \sqrt{\frac{1 + \frac{i\rho}{1 + 2\mu_i \epsilon_0 \rho_i} \cdot \frac{b^2}{a^2 E_c^2}}{2}} \right] \qquad (2.21)$$

For moderate and high currents, the log term will be small in comparison to the numerical term.

$$\ln \left[1 + \sqrt{\frac{1 + \frac{i\rho}{2\pi\epsilon_0 \mu_i \rho_i} \cdot \frac{b^2}{E_c^2 r_0^2}}{2}} \right] << 1 - \sqrt{1 + \frac{i\rho}{2\pi\epsilon_0 \mu_i \rho_i} \cdot \frac{b^2}{E_c^2 r_0^2}}$$

For this case, Equation 2.21 is approximately

$$V = V_0 + aE_c \left[\sqrt{1 + \frac{i\rho}{2\epsilon_0 \mu_i \rho_i} \cdot \frac{b^2}{a^2 E_c^2}} - 1 \right] \qquad (2.21a)$$

Equation 2.21 contains a term that is the ratio of total space charge to free ion space charge. This ratio changes significantly as a function of position in the precipitator. In the input section the heavy dust concentration is electrically charged. This large space charge tends to quench the current and bind the free ions to the point where the ratio of total charge to ion charge becomes very large, with the current flow drastically reduced. As the gas moves through the precipitator, the dust is collected to the point that the space charge contribution of the dust is reduced and the charge ratio in this region approaches a value of 1.

For detailed calculation it becomes important to determine the value of this space charge ratio. A general idea about the voltage-current characteristics can be determined by assuming that the dust does not contribute to the space charge. This assumption leads to large errors in the inlet section, but is reasonably accurate for the outlet section. The value for the electric field is valid, but this assumption leads to errors in the current, and therefore, the free ion density. When making detailed calculations, such as would be desirable for designing or analyzing precipitators, the value of this ratio must be known. It is interesting to note, that if ρ / ρ_i is set equal to one in Equation 2.21, the dust-free voltage-current characteristics will result. This equation then becomes identical to the one developed by White[4] neglecting dust space charge.

There are two techniques for obtaining an estimate of the ratio of the total to ionic space charge in an installation. If the particle size distribution, dust loading and electric field are known, then the total charge carried by the dust can be determined. Similarly, the dust charge density can be found if the surface area of the dust per gram, dust loading, and electric field are known.

In the first case, the dust concentration as a function of particle size is known, and the saturation charge for each size range is determinable. If the total charge per cm^3 is then multiplied by the volume flow rate of the system, the total current required to remove the dust is known. The ionic charge density can be determined from the current density-electric field data. The actual current carried by the particulate is only a small percentage of the total current in the precipitator. This can be verified as follows. The mobility of an object driven by an electric field is defined as the ratio of the velocity to the electric field.

$$\mu = \frac{v}{E} \qquad (2.22)$$

The mobility of negative ions, which are customarily present in commercial installations, is generally on the order of 2.2 cm^2/volt-sec.

The mobility of the dust will, in general, be a function of the specific particle size distribution in the precipitator. The value for each size range will be the ratio of migration velocity (w) to electric field (E).

As an estimate of the average mobility, the migration velocity for the mass median diameter (mmd) is a reasonable choice. The theoretical migration velocity for 10μ particle in an electric field of 3 kV/cm, with standard gas condition, is

$$w = \frac{qE}{6\pi a \eta} = \frac{2\epsilon_0 E_0 E_p a}{\eta} = 0.44 \text{ m/sec} = 44 \text{ cm/sec} \qquad (2.23)$$

and the mobility of the dust from Equation 2.22 becomes

$$\mu_d = \frac{44 \text{ cm/sec}}{3\text{x}10^3 \text{ V/cm}} = 1.46\text{x}10^{-2} \quad \frac{\text{cm}^2}{\text{V-sec}} \qquad (2.22a)$$

the ratio of the dust mobility to the ion mobility is

$$\frac{\mu_d}{\mu_i} = \frac{1.46\text{x}10^{-2}}{2.2} = 6.6\text{x}10^{-3} \text{ or less than 1 percent.} \qquad (2.24)$$

Therefore, the space charge due to the charged dust would have to be 100 times the space charge due to free ions in order for the two currents to be equal. In general, the current carried by the dust can be neglected in comparison to that carried by the free ions, even though the charge bound to the dust may be equal to, or perhaps even greater than, the charge appearing as free ions.

If the current carried by the dust is negligible, as is generally the case, then the ionic space charge can be determined from the current density-electric field equation given previously

$$j = N_0 e \mu E \qquad (2.3)$$

Substituting typical values for the parameters we find

$$N_0 e = \frac{j}{\mu E} = \frac{1.3\text{x}10^{-8} \text{ A/cm}^2}{2.2 \ \frac{\text{cm}^2}{\text{V-sec}} \text{ x } 3\text{x}10^3 \ \frac{\text{V}}{\text{cm}}} = 2\text{x}10^{-12} \text{ Coulombs/cm}^3 \qquad (2.25)$$

The ratio of total charge to ion charge can be stated as

$$\frac{\rho}{\rho_i} = \frac{\rho_d + \rho_i}{\rho_i} = \frac{5.8\text{x}10^{-12} + 2\text{x}10^{-12}}{2\text{x}10^{-12}} = \frac{7.8}{2} = 3.9 \quad (2.26)$$

Similarly, if the percentage of the current carried by the dust is known, then that portion of the current can be subtracted from the total current density, and only that component carried by the free ions need be substituted in Equation 2.25.

The ratio of total charge to ionic space charge can be determined as a function of position within the precipitator. If the collection efficiency per foot is known for each size range, then the percent of dust removed corresponds to the percent of space charge removed with the dust. Thus the dust space charge can be incrementally corrected as a function of position within the collector.

2.2 PRACTICAL ASPECTS OF THE ELECTRIC FIELD

The effect of the electric field is manifested in two ways in the precipitation process. First the charge on each dust particle is proportional to the peak value of the electric field for field charging; and second, the force acting on each particle is proportional to both the charge on the particle and the average value of the electric field in the vicinity of the dust.

The electric field at any point within a precipitator is caused by three factors. The applied voltage and the particular geometry of the unit results in an electrostatic type of field which is modified by the presence of a space charge. Both free ions and charged particulate contribute to this space charge.

The remaining concern is to provide an electric field of sufficient magnitude to move the particulate to the collection electrode. This field can be provided by any or all of the above methods.

In a single-stage precipitator, corona current flows throughout the entire precipitator. The electric field is a result of all three factors listed above.

In a two-stage precipitator, a large value of corona current flows in the first section to provide a region of relatively high concentration of free ions. No great concern is given to the collection efficiency in this region because the prime function is to charge the dust. The charged dust is then carried into the second stage for collection. This section is normally a uniform field produced by parallel plate electrodes, and no corona current flows. The electric field in this section is caused by the space charge of the dust and by the electrostatic field from a voltage applied between parallel collection plates.

The single-stage precipitator has a marked advantage for dusts that are easily reentrained. The corona current flow through the deposit establishes an electric field that tends to hold the deposit against the collection electrode. The magnitude of this force holding the deposit is proportional to the current density and the resistivity of the dust. In the absence of ion current flow, this component of the retaining force will be greatly reduced.

The situation is somewhat different for dusts with high resistivity. Large values of ion current may hold the dust so tenaciously that the rappers become ineffective. In this situation, either a two-stage collector or one with a greatly reduced current density in the primary collection zone may be required.

Another problem resulting from the collection of high resistivity dusts at high current densities is back corona. The electric field in regions of the deposit or on the surface may exceed the breakdown strength of the entrapped gas. Electron avalanche will be initiated on the collection electrode which can lead to either increased sparking or stable back corona glow spots distributed over the collection electrode. These factors are discussed more completely in the chapter on resistivity.

CHAPTER 2
BIBLIOGRAPHY

1. Frank, N. H., Introduction to Electricity and Optics, McGraw-Hill, 1950.
2. Stratton, J. A., Electromagnetic Theory, McGraw-Hill, 1941.
3. Peek, F. W., Dielectric Phenomena in High Voltage Engineering, 3rd ed., McGraw-Hill, New York, 1929.
4. White, H. J., Industrial Electrostatic Precipitation, Addison-Wesley Publ. Co., Reading, Massachusetts, 1963.

CHAPTER 3
PARTICLE CHARGING

One of the fundamental steps in the precipitation process is the application of an electric charge to the particulate matter. The dust must be charged for the electric field to impart a driving force toward the collection electrode. This force is the predominant factor in removal of the particulate from the gas, and is proportional to the magnitude of the particle charge and the electric field. The mechanism concerned with the removal of this particulate is normally referred to as electrostatic, even though there is significant current carried by both the charged ions and the charged particulate.

Particle charging is normally considered to take place in the region between the boundary of the corona glow and the collection electrode. As discussed in the chapter on corona generation, this region contains large quantities of negative ions and perhaps some free electrons. However, there are positive ions within the corona region, and some of the particles passing into it will be positively charged and tend to drift toward the corona wire under the influence of the electric field. However, most of the particles will be carried out of the corona region by the turbulent gas flow, and only those that are swept in close proximity to the corona electrode will be deposited. The particles that are charged positively and do not precipitate on the wire must first be neutralized and subsequently charged negatively to precipitate on the collection electrode. The bulk of the particles, however, pass between the boundary of the corona region and the collection electrode, and are charged by the negative ions which predominate in that region. It is the negatively charged particles that are of interest in the precipitation process, and the discussions of the charging process that follow will be with reference to the charging of particles by a negative corona.

There are two mechanisms responsible for the charging of particles in an electrostatic precipitator. These mechanisms are generally referred to as field and diffusion charging. Both mechanisms are active in the charging; however, each becomes more significant for particles in a particular size range. Field charging is the dominant mechanism for large particles with a radius greater than about 0.25μ, while diffusion charging predominates for small ones with a radius less than about 0.1μ. In the intermediate range both mechanisms contribute significant charge, and therefore must be considered simultaneously.

Field charging is related to the ordered motion of ions under the influence of an applied electric field. This ordered motion causes collisions between the ions and particles suspended in the gas stream. Diffusion charging results from ionic collisions with the particles brought about by the random thermal motion of the ions in the gas. If these ions are retained by the dust particles, the particles become electrically charged.

Much work has been done on the theory of particle charging. Field charging theory leads to a straightforward expression for the charge acquired in terms of the applied electric field, physical dimensions, and dielectric constant of the particles. Rohman[1] in 1923 was the first to derive a valid expression for field charging, and Pauthenier[2] rederived Rohman's equation in a slightly different form in 1932. White[3] also gives a theoretical analysis of field charging.

Theoretical analyses of diffusion charging have primarily been made with the assumption that this charging mechanism is independent of the applied electric field. While this is definitely not the case in an electrostatic precipitator, it leads to equations with an analytic solution. If the effect of the applied field is included, then the equations cannot be solved in closed form but must be solved in an iterative fashion requiring either a high-speed computer or an inordinate amount of time. Arendt and Kallman[4] published the first analysis of this mechanism in 1926. White[3] derived an expression that is similar to that of Arendt and Kallman.

Several approximate solutions have been determined for the diffusion charging mechanisms in the presence of an applied electric field. These techniques make use of the computer and match the experimental levels of charge with varying degrees of success. The results of several investigations, including Liu, et al.[5] and Murphy, et al.,[6] are discussed in this report. Liu utilizes Hewitt's[7] experimental data in verifying his theory.

3.1 FIELD CHARGING

The theoretical analysis of field charging is generally made with three simplifying assumptions. These simplifications are necessary to avoid obscuration of the physics of the mechanism by the mathematics of the analysis. These assumptions are:

---

[1] Refer to the bibliography for this chapter.

1. The particles are considered to be spherical.
2. The field from one particle does not modify the field in the vicinity of another particle.
3. The particles and ions are suspended in a region permeated by a constant electric field.

The presence of particles with a dielectric constant greater than unity will cause a localized deformation in the electric field as is illustrated in Figure 3.1. The negative ions move rapidly toward the collection electrode under the influence of the applied electric field. These ions tend to travel along electric field lines in the direction of maximum voltage gradient, and since the field lines intercept the particulate matter, the ions will collide with the particles and impart a charge to them. This charge will be maintained on the surface of the particles by what is generally termed an image charge force. The image charge, as described in electrostatic theory, is caused by the electric field associated with the ion. As an ion is brought into the region near a particle, the internal charges of the dust particles are displaced such that an attractive force exists between the ion and the particle; see Figure 3.2.

As the ions continue to impinge on the dust particles, the charge on them will increase until a sufficient electrostatic field is established in the vicinity of the particle by the retained charge to effectively repel additional ions flowing to the particle. This leads to a field configuration in the vicinity of the particles as illustrated in Figure 3.3.

Derivation of the field charging equation. If a conducting sphere of radius a with a net charge q is suspended in a uniform electric field E_0 in the presence of a unipolar ion concentration N_0, the electric field in the vicinity of the sphere will consist of two components: (1) the self-field caused by the charge on the particle and (2) the applied field as modified by the presence of the conducting particle. The expression describing this field can be derived from the principles of electrostatics.[8,9] Stated in MKS units:

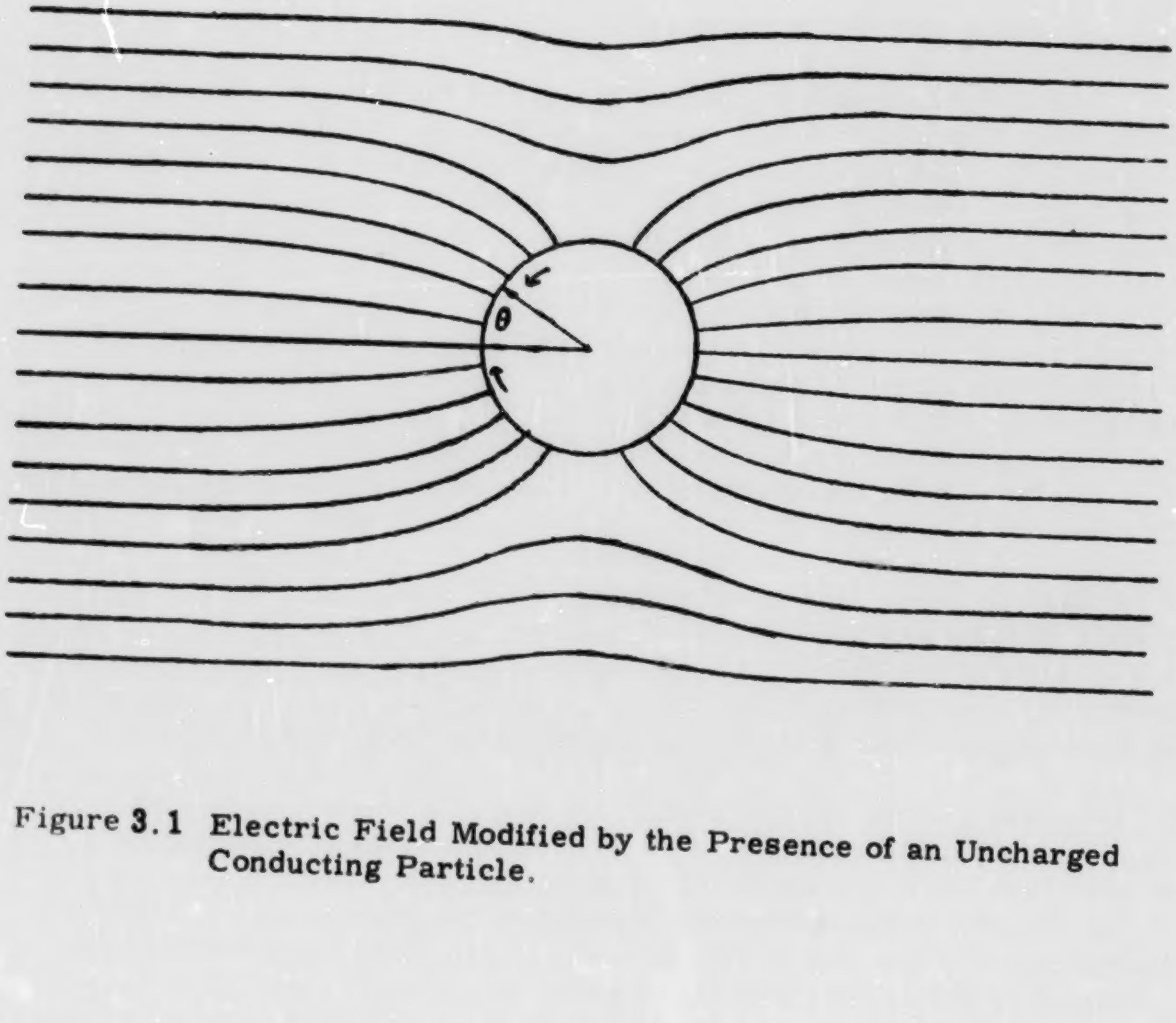

Figure 3.1 Electric Field Modified by the Presence of an Uncharged Conducting Particle.

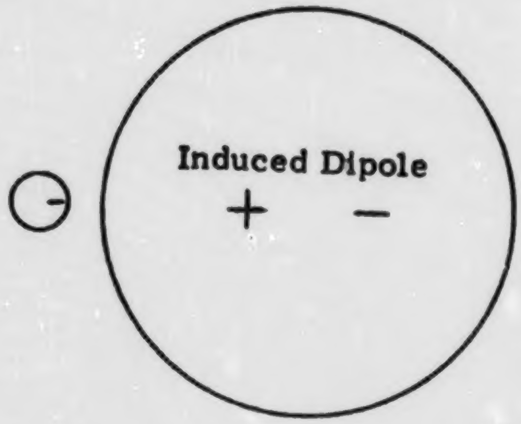

Figure 3.2 Induced Electrostatic Charge in Particulate Due to Proximity of Ion.

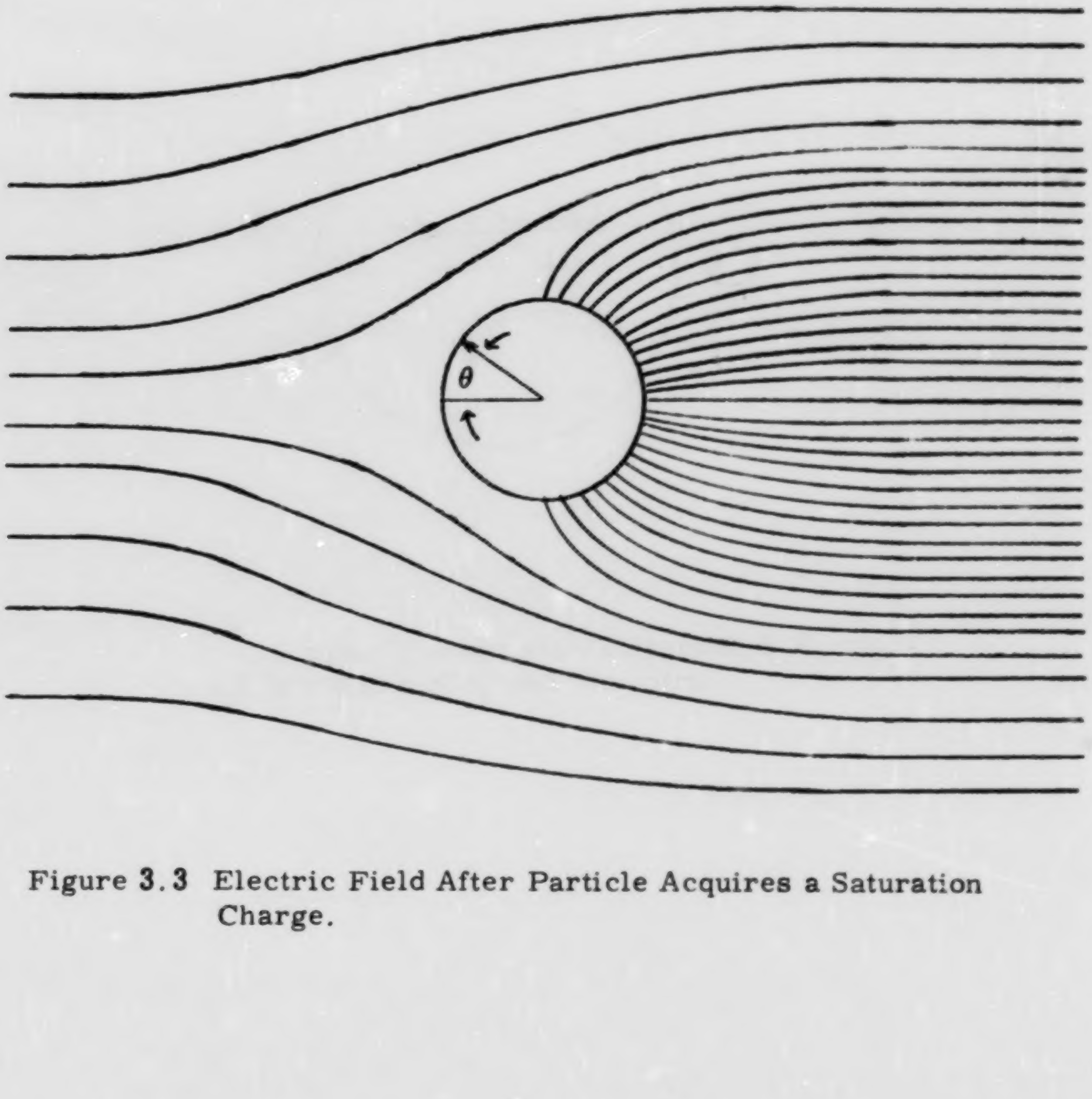

Figure 3.3 Electric Field After Particle Acquires a Saturation Charge.

$$E = 3E_0 \cos\theta - q/4\pi\epsilon_0 a^2 \tag{3.1}$$

where

E = the resultant electric field,
θ = the angle between a point on the sphere and electric field as shown in Figure 3.1, and
ϵ_0 = the permittivity of free space.

The term $3E_0 \cos\theta$ is the expression for the modified field due to the presence of a conducting sphere.

The rate of change of charge to the dust particle with respect to time is defined as the current. The ion current is equal to the integral of the current density times the differential active charging area:

$$\frac{dq}{dt} = \int_0^{\theta_0} j\,dA = \int_0^{\theta_0} (N_0 e\mu E)\,dA \tag{3.2}$$

$$= N_0 e\mu \int_0^{\theta_0} \left(3E_0 \cos\theta - \frac{q}{4\pi\epsilon_0 a^2}\right) dA$$

where

q = charge on the particle,
μ = mobility of the ion,
e = electronic charge,
j = current density = $N_0 e\mu E$
θ_0 = limiting angle for charge flow to the particle,
dA = element of area = $2\pi a^2 \sin\theta\, d\theta$, and
t = time.

Equation 3.2 shows that charge will continue to flow to the particle until the field from the charge just balances the applied external field, at which time a limiting charge is acquired. Since the electric field in the vicinity of the particle (E) is zero, this saturation charge, for a conducting particle, can be determined by setting Equation 3.1 to zero when $\cos\theta = 1$, or:

$$q_s = 12\pi a^2 \epsilon_0 E_0. \tag{3.3}$$

Cos θ is set to one for the saturation charge because θ approaches zero as the particle charge increases.

Similarly, the limiting angle θ_0 for charge flow to the sphere for any state of charge, can be determined by setting E equal to zero in Equation 3.1 and solving for Cos θ_0:

$$\text{Cos}\ \theta_0 = \frac{q}{12\ \pi a^2 \epsilon_0 E_0} = \frac{q}{q_s} \qquad (3.4)$$

The time behavior of the charge can be determined from Equation 3.2:

$$\frac{dq}{dt} = N_0 e \mu \int_0^{\theta_0} (3\ E_0\ \text{Cos}\ \theta - \frac{q}{4\ \pi a^2 \epsilon_0})\ 2\pi a^2\ \text{Sin}\ \theta\ d\theta$$

$$= 6\ \pi a^2\ E_0\ N_0 e\ \mu \left[\int_0^{\theta_0} \text{Cos}\ \theta\ \text{Sin}\ \theta\ d\ \theta - \frac{q}{12\pi a^2 \epsilon_0 E_0} \int_0^{\theta_0} \text{Sin}\ \theta\ d\ \theta \right],$$

and since the charge is independent of θ, Equation 3.2 can be integrated to yield (with $q_s = 12\pi a^2 \epsilon_0 E_0$)

$$\frac{dq}{dt} = 6\pi a^2\ E_0\ N_0 e\ \mu \left[\frac{\text{Sin}^2\ \theta}{2} \Bigg|_0^{\theta_0} + \frac{q}{q_s}\ \text{Cos}\ \theta \Bigg|_0^{\theta_0} \right]$$

$$\frac{dq}{dt} = 6\pi a^2\ E_0\ N_0 e\ \mu \left[\frac{\text{Sin}^2\ \theta_0}{2} - \frac{q}{q_s}\ (1 - \text{Cos}\ \theta_0) \right] \qquad (3.5)$$

$$\frac{dq}{dt} = 3\pi a^2\ E_0\ N_0 e\ \mu\ \ (1 - \frac{q}{q_s})^2 \quad \text{and rearranging} \qquad (3.6)$$

$$\frac{dq}{(1 - \frac{q}{q_s})^2} = 3\pi a^2 E_0 N_0 e \mu \, dt,$$ which can be readily

integrated to yield

$$\frac{q_s^2}{q_s - q} = 3\pi a^2 E_0 N_0 e \mu t + K_1, \tag{3.7}$$

and applying the boundary condition that at $t = o$ $q = o$

$K_1 = q_s$ which yields for Equation 3.7

$$\frac{q_s}{q_s - q} = \left(\frac{N_0 e \mu t}{4\epsilon_0} + 1 \right),$$ which yields after rearranging (3.8)

$$\frac{q}{q_s} = \frac{\frac{N_0 e \mu t}{4\epsilon_0}}{\frac{N_0 e \mu t}{4\epsilon_0} + 1} = \frac{t}{t + \frac{4\epsilon_0}{N_0 e \mu}}$$

and if we designate $\tau = \frac{4\epsilon_0}{N_0 e \mu}$ the charge as a function of time becomes

$$q(t) = q_s \frac{1}{1 + \frac{\tau}{t}} \tag{3.9}$$

which represents the charging characteristics of a conducting particle a precipitator.

The modification for nonconductive particles is to introduce a factor $\frac{\epsilon}{\epsilon + 2}$ into the equation for saturation charge (Equation 3.3) where ϵ = relative dielectric constant, which yields for the saturation charge for a general particle

$$q_s = 12 \frac{\epsilon}{\epsilon + 2} \pi\epsilon_0 a^2 E_0$$

This leads to an expression for the charge as a function of time

$$q(t) = 12 \frac{\epsilon}{\epsilon + 2} \pi\epsilon_0 a^2 E_0 \frac{t}{t + \tau} = q_s \frac{1}{1 + \frac{\tau}{t}} \tag{3.10}$$

The previous analysis for field charging was made with the system of units known as rationalized MKS. White[3] and Moreau-Hanot and Pauthenier[2] derived their equations in the electrostatic system of units (ESU) which leads to equations that are consistent with the MKS units. These equations are included for completeness.

$$q_s = N_s e = (1 + 2 \frac{\epsilon - 1}{\epsilon + 2}) E_0 a^2 = \frac{3\epsilon}{\epsilon + 2} E_0 a^2$$

$$q(t) = q_s \frac{t}{t + \tau} = q_s \frac{1}{1 + \frac{\tau}{t}}$$

$$\tau = \frac{1}{N_0 e \mu \pi}$$

3.2 DIFFUSION CHARGING

Under the assumption that diffusion charging is independent of the electric field, an equation can be derived relating particle charge to particle size, conductivity, etc. Collisions between ions and particles occur because of the random thermal motion of the ions. The ions collide with, and are retained by, an induced electric charge on the particle as illustrated in Figure 3.2.

The diffusion charging process can be described in terms of the kinetic theory of gases. If a particle of radius a, carrying n elementary charges, is located in a medium containing unipolar ions, the net current flow to the particle can be determined. The molecular density N of a gas in a potential field can be described by the following general equation:

$$N = N_0 \exp \frac{V}{KT}$$

where

N_0 = average number of molecules per unit volume (density),
V = potential,
k = Boltzmann's constant, and
T = temperature, °Kelvin.

If this general equation is applied to the case of a specific density of gas ions in the vicinity of a suspended charged particle, then

$$V = -\frac{qe}{r} \qquad (3.11)$$

$$N = N_0 \exp\left(-\frac{qe}{rkT}\right)$$

where

r = the distance from the center of the particle to a position in space.

Then, at the surface of a particle of radius a, the density of ions with various energies becomes:

$$N = N_0 \exp\left(-\frac{qe}{akT}\right)$$

from which the number of ions per second which collide with the particles becomes:

$$\frac{Nv}{4} \cdot (4\pi a^2) = \pi a^2 N v$$

where

v = rms thermal velocity of the ions.

If every ion that collides with the particle is retained, then the rate of change of charge with respect to time (ion current) becomes:

$$\frac{dq}{dt} = \pi a^2 e v N_0 \exp\left(- \frac{qe}{akT}\right) \tag{3.13}$$

and for a Maxwellian distribution, the rms velocity is related to the temperature of the gas by the equation:

$$v = \sqrt{\frac{8kT}{\pi m}}$$

$$\frac{dq}{dt} = a^2 e \left(\frac{8kT\pi}{m} \right)^{\frac{1}{2}} N_0 \exp\left(- \frac{qe}{akT} \right) \tag{3.13a}$$

and m is the mass of the particle

$m = (4/3)\pi a^3 d$

d = the mass density of the ions.

Integration of Equation 3.13 with respect to time yields the charge on the particle as expressed by the following equation:

$$q(t) = \frac{akT}{e} \ln\left(1 + \frac{\pi a v N_0 e^2 t}{kT}\right). \tag{3.14}$$

It is worthwhile to point out that no saturation charge exists for the diffusion charging process as derived herein. This is due to the fact that the range of thermal velocities does not have an upper boundary limit. The expression for the probability of finding an ion with a given velocity is a monotonically decreasing function, but this probability distribution does not go to zero. Therefore, regardless of what electrostatic potential the particle has, there is a nonzero probability of finding an ion with sufficient energy to overcome that potential and impact with the particle. However, as the potential of the particle increases, the probability of impact decreases until the diffusion charging rate decreases significantly.

A similar expression was cited by White, previously developed by Arendt and Kallman,[4] which had for the rate of change of charge with time the following equation:

$$\frac{dq}{dt}\left(1+\frac{a^2 v}{4nke}\right) = \pi a^2 v N_0 \exp\left(-\frac{ne^2}{akT}\right),$$

which yields essentially the same charge as a function of time that White's (Equation 3.14) does.

Field charging is more significant in the majority of precipitator applications than diffusion charging because, typically, the great majority of the material to be collected consists of particles greater than 0.25μ radius. For example, the mass of a 25μ particle compared with a 0.25 one of the same density is greater by a factor of 10^6, or stated more simply, it takes one million 0.25μ particles to equal the mass of a 25μ one. However, as precipitator design approaches 100% collection efficiency, the collection of the very small particles becomes more significant and the consideration of the diffusion charging mechanism becomes more important.

3.3 COMBINATION OF FIELD AND DIFFUSION CHARGING

In the intermediate range of particle sizes both charging mechanisms contribute significant charges. Since the previous analyses neglected one of the charging mechanisms in the derivation of the charge, it would be erroneous to merely add the net charge of the two mechanisms. In this analysis, it is more nearly correct to sum the rates of charging from the two mechanisms and then solve for the charge. Utilizing the charge rate for field charging from Equation 3.6 and for diffusion charging from Equation 3.13 leads to an expression for the charge rate of

$$\frac{dq}{dt} = \frac{q_s}{\tau}\left(1-\frac{q}{q_s}\right)^2 + a^2 e N_0 \sqrt{\frac{8kT\pi}{m}}\,\exp\left(-\frac{qe}{akT}\right)$$

$$\frac{dq}{dt} = \frac{q_s}{\tau} - \frac{2q}{\tau} + \frac{q^2}{q_s\,\tau} + a^2 e N_0 \sqrt{\frac{8kT\pi}{m}}\,\exp\left(-\frac{qe}{akT}\right). \tag{3.15}$$

Equation 3.15 is a nonlinear differential equation with no analytic solution. Approximate solutions to the above equation can be determined by the use of iterative integration methods.

However, the above equation was derived with the assumption that diffusion charging was independent of applied electric field. The justification for this assumption was that when considering diffusion charging in the absence of field charging, it led to a solvable equation. In the above analysis, this justification is no longer valid and computer techniques would be required for a solution. Since a computer is required in the solution to the above equation, several investigators have attempted to extend the theory to include the charging characteristics in the presence of an applied electric field. These investigations have led to expressions that more nearly match experimental data. These investigators include Murphy, Adler, and Penney[6] and Liu and Yeh.[5]

Murphy derived a formula for the charging of small particles in the presence of an applied electric field. The results of this work are shown in Figures 3.4 and 3.5, where two computer solutions to the differential equation for charge rate are compared with the previous theories of White and Kallman and with experimental data. The technique provides a much better agreement with experimental data indicating that the electric field does have significance in the diffusion charging process.

The theory described in this paper takes into account the modification in ion distribution around the particle and the velocity distribution in a particular direction caused by the applied electric field. This leads to a differential equation for charge rates that can be approximately solved by a finite difference method of iterative integration.

Liu reviews the previous diffusion and field charging theories. He then develops a unified charging equation where the effects of both field and diffusion charging are combined. The charge rate is derived from the electric potential field caused by both the charge on the particle and the modified external field. The charging mechanism is divided into two regions such that both field and diffusion charging are simultaneously active until the saturation field charge is acquired by the particle. At this point, the electric field caused by the charge on the particle exceeds the applied field and field charging stops.

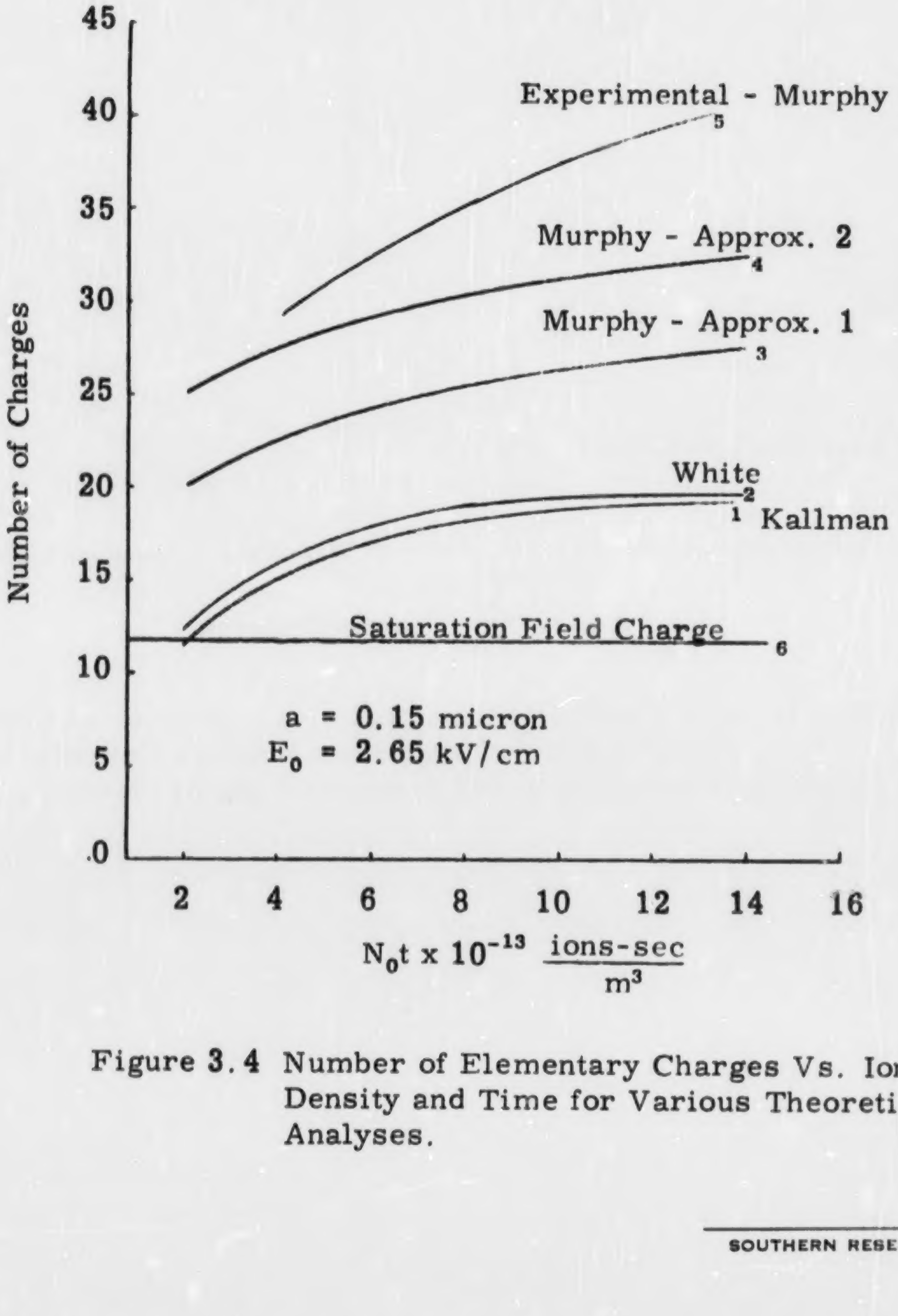

Figure 3.4 Number of Elementary Charges Vs. Ion Density and Time for Various Theoretical Analyses.

1. Field Charge Saturation, 10.8 and 0.6 kV/cm, respectively.
4. Diffusion Charging (Neglecting Electric Field) $N_0t = 10^7$ ions sec/cm^3.
2, 6. Liu Diffusion Charging, $E_0 = 10.8$ and 0.6 kV/cm, respectively.
3, 5. Hewitt Experimental $N_0t = 10^7$ ions sec/cm^3, $E_0 = 10.8$ and 0.6 kV/cm, respectively.
7. Penney, $N_0t = 6.4 \times 10^7$ ions sec/cm^3, $E_0 = 2.3$ kV/cm.

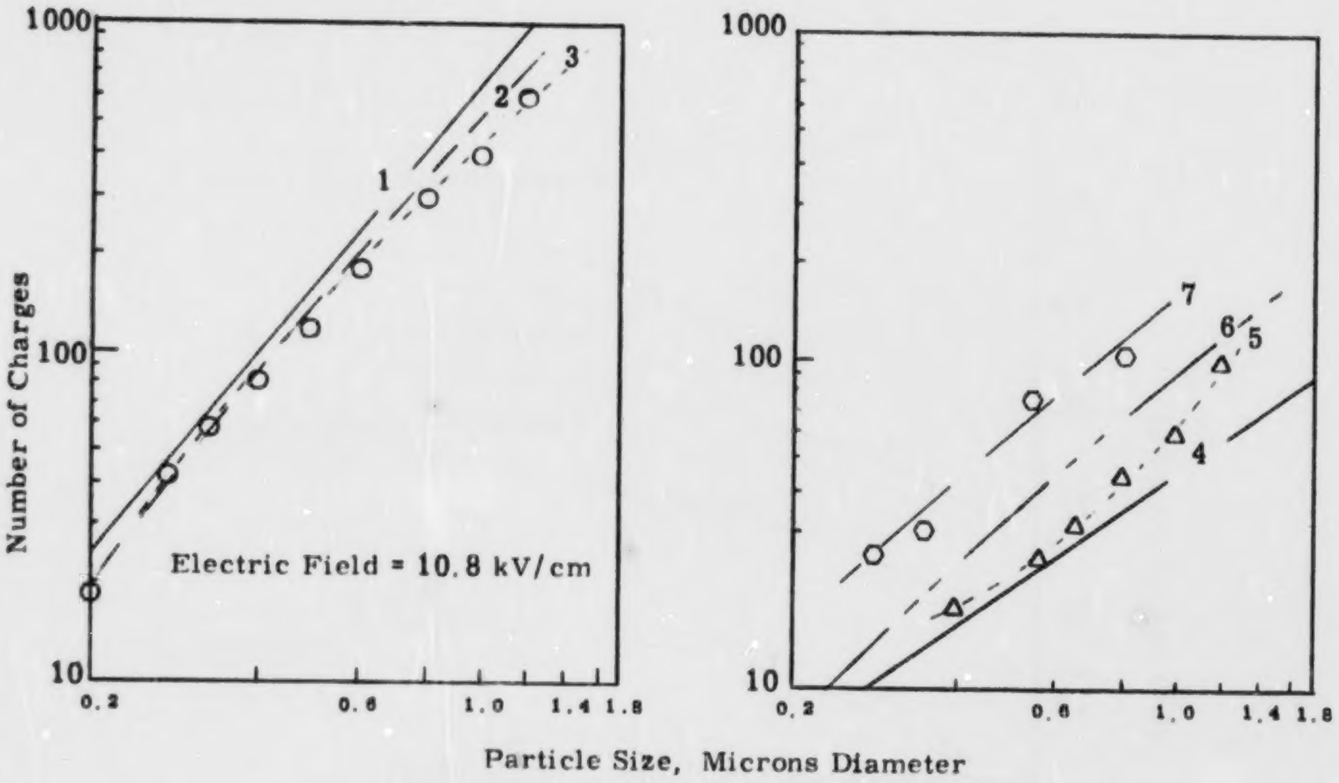

Figure 3.5. Particle Charging Characteristics - Number of Charges Vs. Particle Size. Comparison between Hewitt's Experimental Data and Various Charging Theories.

In the second regime, only diffusion charging is active. The ion density adjacent to the particle is approximated, and this, together with the thermal velocity distributions, leads to a modified diffusion term in the presence of an applied electric field.

This theory provides an expression for charge as a function of time for all sizes of particles. When compared with experimental data, the agreement is very good. Liu's approximation predicts charges somewhat higher than experimental data. This may be due to the fact that the ion density was determined along the directions of the applied electric field and assumed to be independent of relative position around the particle. There is a possibility that the point where the ion concentration was determined is higher than the average concentration around the particle. This would lead to a constant error in the diffusion charge rate as shown. Liu's theoretical results are compared with Hewitt's experimental data in Figures 3.5 and 3.6.

3.4 PRACTICAL ASPECTS OF PARTICLE CHARGING

The development of the theory of particle charging was based on assumptions for a highly idealized case. The idealizations include such things as uniform and constant applied electric field and free ion density in the vicinity of a single particle. The conditions in an operating commercial installation are considerably different from this idealized situation.

The first significant difference is in the applied voltage. The power supply typically derives a direct voltage from the alternating voltage of the commercial electric power by either full-wave or, half-wave rectification. The output from the power supply is typically supplied to the precipitator in an unfiltered condition, although the distributed capacitances and effective resistances of the collector system act as a filter. The voltage on the unit swings through a range of values during each cycle of input power to the unit. Sketches of the type of variation expected in an installation operating from half-wave rectification systems are shown in Figures 3.7a and 3.7b.

The variation in applied voltage causes a corresponding change in the corona current. Since the voltage-current characteristics of a precipitator system are of the form

$$I = KV^n \qquad (3.16)$$

Hewitt's experimental data corresponding to the different field strengths are shown adjacent to Liu's theoretical plot. The standard field charge for each field strength is also shown.

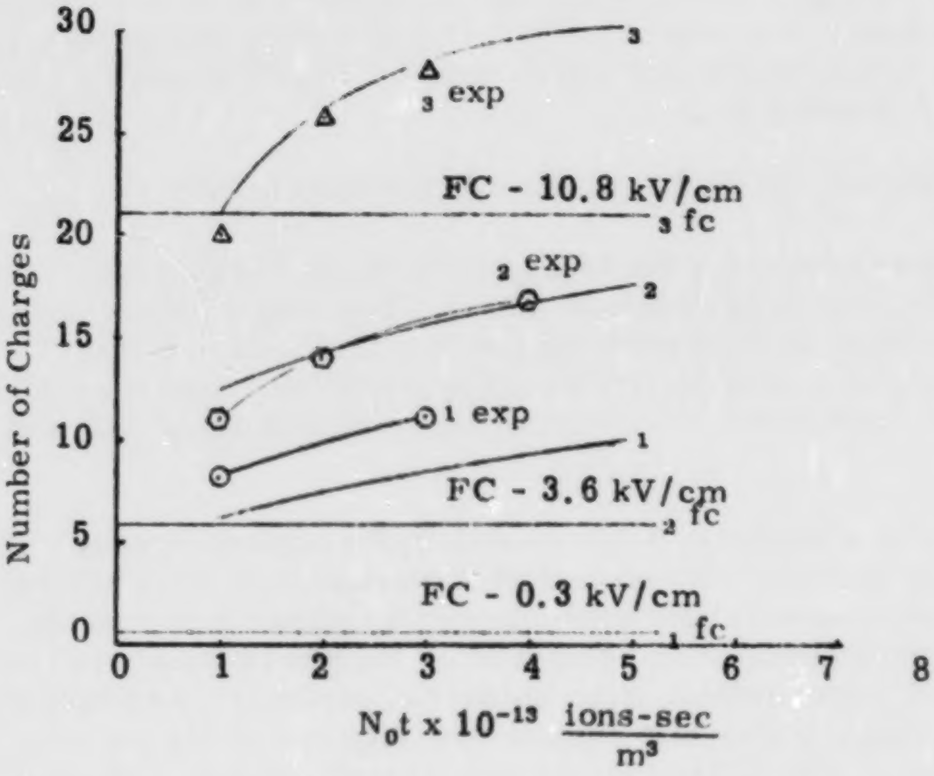

Figure 3.6. Number of Elementary Charges Vs. Charge Density - Time Product for 0.06 Micron Radius.

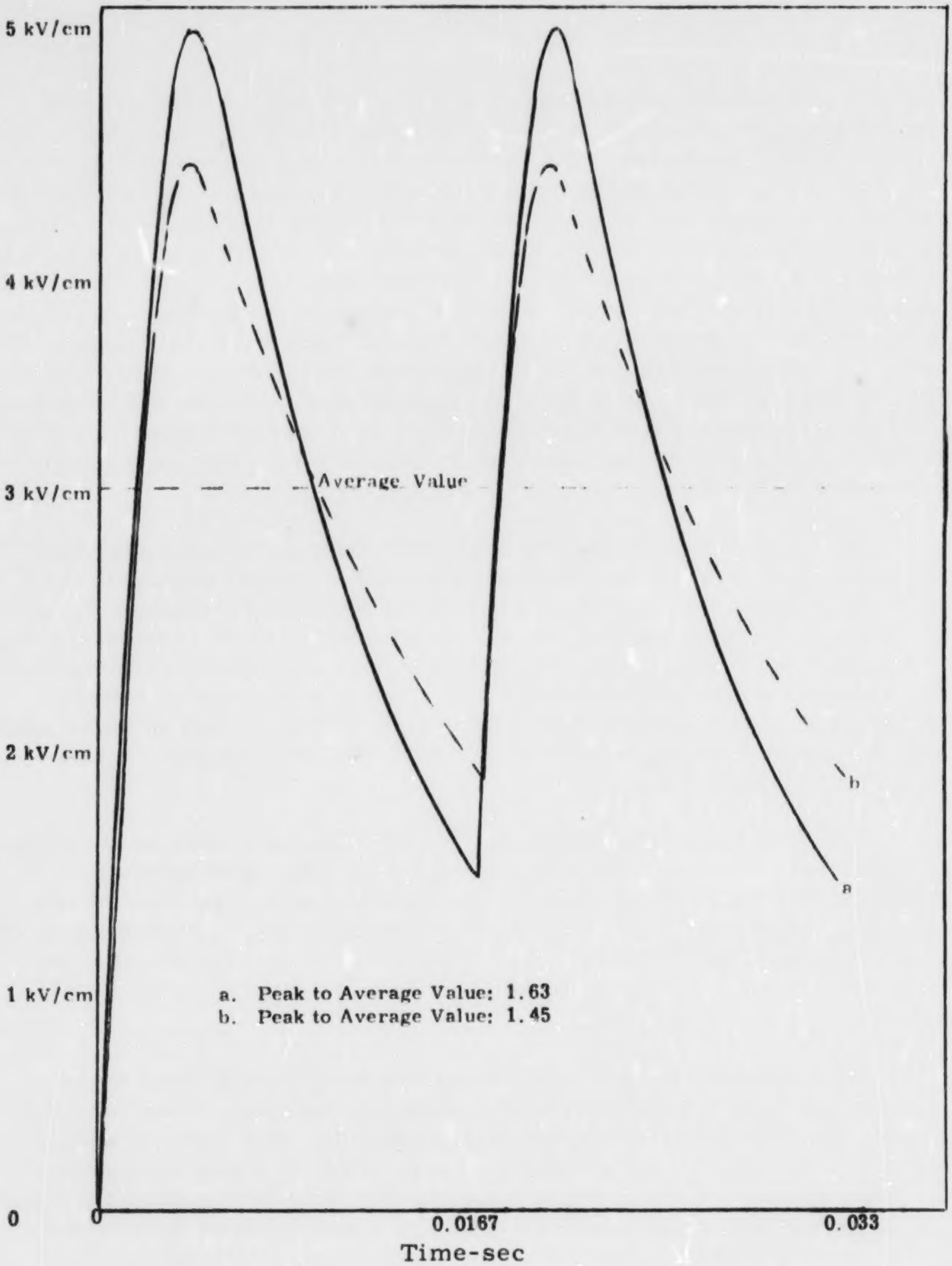

Figure 3.7 Electric Field Variations as a Function of Time at a Particular Point in Space Caused by the Variation in the Applied Voltage from the Power Supply.

where n is a number greater than 1 and K is a linear coefficient, the percentage current change is greater than the percentage voltage change in the installation. The variation in voltage and current causes a two-fold change in the charging characteristics of the dust particles. The charge on a particle is directly proportional to the electric field, which is related to the applied voltage. The particle will tend to acquire a saturation charge dictated by the peak value of the applied electric field. The particle will accept charge during the interval of time that the applied electric field in the vicinity of the particle exceeds the self-field from the charged particle. When the applied field drops below that from the charge on the dust, charging ceases until the next cycle of input from the power supply.[10] This charging time constant is effectively increased by the reciprocal of the percentage of the time that ions flow to the particle. This percentage decreases as the particle attains a near saturation charge.

The charge rate is proportional to the free ion density near the particle. The free ion density is related to the current density in the interelectrode space. As the voltage drops between the conduction periods of the power supply, the current and current density are reduced according to Equation 3.16 above. This reduction in free ion density causes a further increase in the charging time constant. The single factor of voltage variation with time is reflected in two related effects, both of which cause an increase in the time required for a dust particle to acquire a near saturation charge.

A second significant variation from the idealized case is the variability of electrical conditions within the precipitator. The dust particles are transported through the unit by the gas stream. At the inlet of the precipitator, large quantities of uncharged dust are introduced into the interelectrode space for charging. As the particulate acquires charge, the free ions become attached, resulting in a rapid decrease in the free ion density.

This cloud of charged dust represents a significant increase in space charge which tends to quench the corona current. Since the free ion density is proportional to the current density, this factor causes a further reduction in the ionic space charge in the charging section of the preceipitator. The charging time constant will be significantly greater for an industrial precipitator than would be expected from an analysis where the incremental behavior of the process was neglected.

The significance of the above factors can be illustrated by estimating their effect on the behavior of a typical installation, with values for pertinent parameters as follows:

Collection efficiency	90%
Dust load	3.4 grains/acf
Volume flow rate	1.7×10^6 acfm
Collection electrode area	1.06×10^5 ft^2
Gas velocity in collector	7.5 ft/sec
Average electric field	3 kV/cm
Average current density	30×10^{-9} amp/cm^2 = 28 μA/ft^2
Length of precipitator	12 ft

If average conditions are assumed to exist throughout the precipitator, the charging time constant is computed from the average current density and charging field. The free ion density is computed as follows:

$$N_0 = \frac{30 \times 10^{-9}\ \text{A/cm}^2}{1.6 \times 10^{-19}\text{Cou} \times \dfrac{2.2\ \text{cm}^2}{\text{V-sec}} \times 3 \times 10^3\ \text{V/cm}} = 2.85 \times 10^7\ \text{ions/cm}^3$$

$$= 2.85 \times 10^{13}\text{ions/m}^3.$$

The charging time constant from Equation 3.8 (MKS units) is:

$$\tau_2 = \frac{4\epsilon_0}{N_0 e\,\mu} = \frac{4 \times 8.85 \times 10^{-12}\ \text{F/m}}{2.85 \times 10^{13}\ \dfrac{\text{ions}}{\text{m}^3} \times 1.6 \times 10^{-19}\text{Cou} \times 2.2 \times 10^{-4}\ \dfrac{\text{m}^2}{\text{V-sec}}} = 35\ \text{ms.}$$

About ten time constants are required for the particle to acquire 90% saturation charge; thus the particle is considered to be charged within about 350 milliseconds, or a little over 1/3 second. This corresponds to a travel of about 2.6 ft through the unit.

Next, consider the time required for the particles to charge to a 90% saturation charge when the electric field varies as shown in Figure 3.7a and 3.7b. These plots represent the effect of half-wave operation of the rectifier system with precipitator discharge characteristics approximated by a simple R-C filter network. Figure 3.7a and 3.7b represent the voltage vs. time for a unit with an effective discharge time constant of 10 milliseconds and 15 milliseconds, respectively. Both examples are based on an average value of the electric field of 3.0 kV/cm.

Figure 3.8 illustrates the variation in charge as a function of time for dust with a charging time constant of 35 milliseconds. The 90% saturation charge for the 4.9 kV peak is attained after about 1.35 seconds, whereas it is attained after 1.17 seconds in the 4.35 kV peak case. This should be compared to the time required for the pure direct current case, where a saturation charge occurs after ten time constants or 0.35 seconds. Therefore, the dust acquires a 90% saturation charge after traveling distances of 10.2 and 8.75 feet through the precipitator, rather than the 2.6 feet originally expected.

It is evident that the actual charge on the dust is greater for the variational case than for the steady case because the particle charges toward the peak value of the field. If comparisons are made between waveforms with the same average value, the particle charges toward a higher final value for the high peak-to-average-value waveforms. The actual gain in using high peak-to-average-value waveforms is not as great as would be expected from a cursory examination. The effective charging time constant increases for the high peak-to-average situation. A tradeoff must be made between charging time and peak value in order to arrive at the best collection efficiency. This will be covered in greater detail in the chapter on precipitator systems analysis.

The next variation to consider is the effect of the introduction of the uncharged dust into the inlet section. Equations relating the electric field in the interelectrode space to the current density and space charge, and the current density to the applied voltage are given in the chapter on the electric field. These equations show that for a fixed voltage, the electric field is almost independent of dust space charge to total space charge density. Therefore, the addition of dust in the interelectrode space results in a decrease in the current in the inlet section with a similar reduction in the free ion density.

This reduction in free ion density increases the charging time constant proportionally. Qualitatively, the current is carried almost exclusively by the free ions. Since current quenching is normally observed

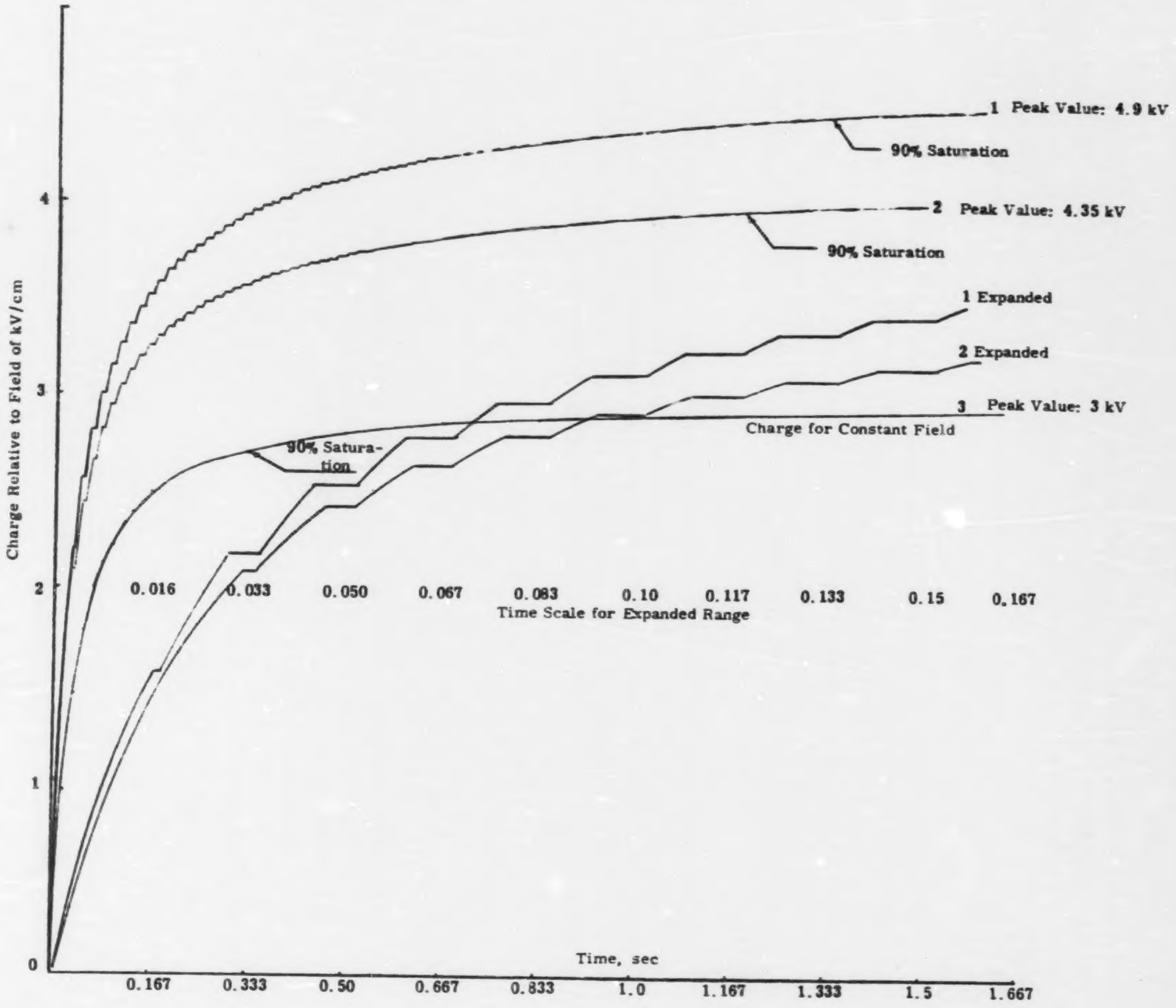

Figure 3.8 Charging Characteristics for Various Waveforms With 3 kV/cm Average Values.

in the inlet sections of operating installations, the charging time constant will be expected to increase in this section. The magnitude of this increase can be estimated from the knowledge that the precipitator collection efficiency equation is an exponentially decaying function of distance through the precipitator. An estimate of the modification to the space charge caused by the dust can be made from this.

If an installation is operating at a collection efficiency of 90%, then the dust concentration at the outlet section is 10% of that in the inlet. Thus, the space charge at the inlet section caused by the dust will approach a factor of 10 greater than that at the outlet. From this, the current density in the first foot of the unit could be expected to be significantly less than that at the outlet, with the result that the charging time constant would be greater.

If the charging time constant for the installation based on average current densities were about 35 milliseconds, then the charging time constant vs. position within the unit would be an exponentially decreasing function, with an average value over the 12 ft length of 35 milliseconds. This corresponds to a charging time constant vs. position as given by

$$\tau(x) = \tau_0 \exp\left(-\frac{\alpha x}{L}\right) \tag{3.17}$$

where

τ_0 = the charging time constant at inlet = 90 milliseconds,
x = the distance through the precipitators, ft,
L = the length of precipitator = 12 ft, and
α = numerical coefficient.

These factors yield

$$\tau(x) = 90 \exp\left(-\frac{2.3x}{12}\right) \text{ milliseconds.} \tag{3.17a}$$

Thus, the charging time constant at the inlet is approximately 90 milliseconds, whereas at the outlet it approaches 9 milliseconds if the average value is 35 milliseconds.

The effect of the above factors is to increase the time required for the dust to acquire a saturation charge. If one were to assume that the dust is charged to saturation instantaneously, then the Deutsch-Anderson efficiency equation in the simplified form would apply. However, when the delay in particle charge is considered, the efficiency per foot of precipitator is reduced by a factor of the ratio of actual charge to saturation charge. This factor leads to situations where the quantity of material removed in the first foot of the unit can be reduced by as much as a factor of 10 from that which would be expected when charging time is neglected.

The variation in charge vs. time for a system operating with a time constant of 350 ms rather than the 35 ms average for the installation is shown in Figure 3.9. In practice, the time constant would gradually change from the low charge rate at the inlet to the higher values as the individual particle traverses the installation. These and other dynamic effects are discussed in detail in the chapter on precipitator systems analysis.

The charging of nonspherical particles was investigated by Smith and Penney.[10] They show that the nonsphericity is in general not a problem when the charge is given in terms of the charge per unit area of the individual particles. Thus, for irregular particles, the surface area per unit volume of particle would suffice as a charge parameter. This factor will lead to a somewhat greater charge on the particles than would result from the spherical assumption.

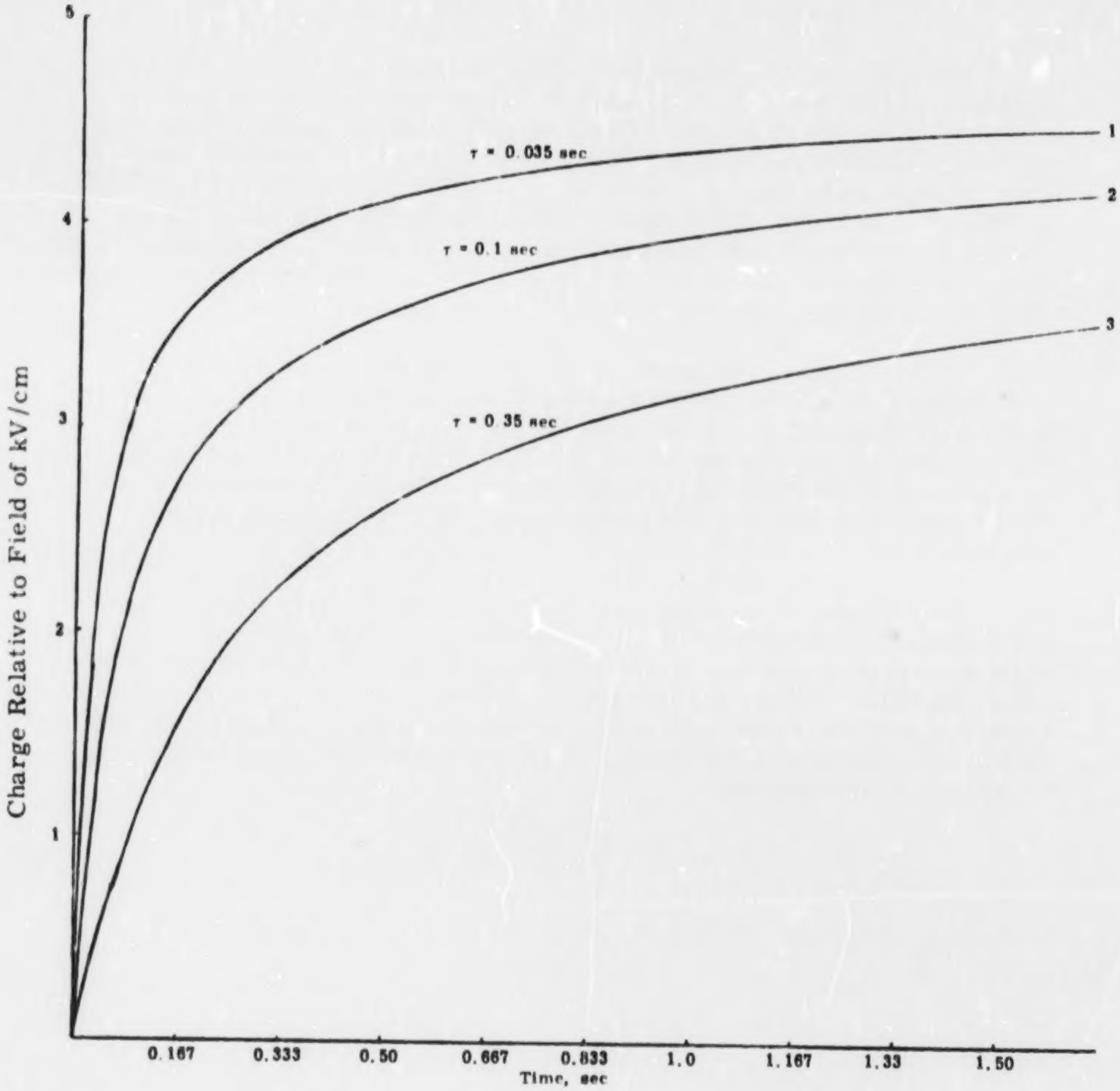

Figure 3.9 Charge Vs. Time in a Field of 3 kV Average, With Charging Time Constant as a Parameter, Peak/Average = 1.63.

CHAPTER 3
BIBLIOGRAPHY

1. Rohman, H., "Messung der Grösse von Schwebeteilchen," Z. Phys. 17, 253 (1923).

2. Pauthenier, M. M. and Moreau-Hanot, M., "La Charge des Particules Sphériques Dans un Champ Ionisé," Journal de Physique et le Radium 3, 590 (1932).

3. White, H. J., Industrial Electrostatic Precipitation, Addison-Wesley (1963).

4. Arendt, P. and Kallman, H., "The Mechanism of Charging Mist Particles," Z. Phys. 35, 421 (1926).

5. Liu, Benjamin Y. H. and Hsu-Chi, Yeh, "On the Theory of Charging of Aerosol Particles in an Electric Field," J. Appl. Phys. 39, No. 3, 1396 (1968).

6. Murphy, A. T., Adler, F. T., and Penney, G. W., "Theoretical Analysis of the Effects of an Electric Field on the Charging of Fine Particles, "Paper 59 - 102, AIEE Winter General Meeting, New York, February 1959. Published in Communications and Electronics, September 1959.

7. Hewitt, G. W., AIEE Trans. 76, 300 (1957).

8. Stratton, J. A., Electromagnetic Theory, McGraw-Hill (1941).

9. Frank, N. H., Introduction to Electricity and Optics, McGraw-Hill (1950).

10. Smith, P. L. and Penney, G. W., "Charging of Nonspherical Particles in a Corona Discharge," AIEE Trans. 80, Pt. 1, p 340 (1961).

BLANK PAGE

CHAPTER 4
PARTICLE COLLECTION

Fundamental electrostatic theory establishes that a force will act on a charged particle under the influence of an electric field. The magnitude of this force is dependent upon the charge on the particle and the strength of the electric field. The direction of the force depends upon the polarity of the particle charge and the direction of the electric field.

Simplified concepts of particle collection often consider that the electrostatic forces predominate, and that motion of the particle toward the collection plate is governed primarily by the electrostatic forces. However, in a full size precipitator, the aerodynamic forces associated with highly turbulent gas flow predominate, so that for particles smaller than about 10μ dia, the motion of the gas stream almost completely determines the particle trajectory through the precipitator. Near the collection plate, gas turbulence is reduced, and electrostatic forces predominate. The collection of an individual particle therefore depends on the probability that it will enter the region where the electrostatic forces result in its deposition on the collection surface.

In addition to the domination of the particle motion by the gas flow in the central regions of the precipitator, other factors influence particle collection. Once a dust layer is formed on the collection electrode, impingement of a particle being precipitated can reentrain those previously collected. Scouring of the dust layer, reentrainment of dust during rapping, and unusual electrical conditions, including sparking and back corona, can also alter the basic collection process. In developing a fundamental theory of particle collection, these factors are neglected in order to simplify the derivation and facilitate understanding of the collection process. Effects of these factors on collection are discussed following derivation of the basic collection theory.

4.1 PARTICLE KINETICS

The motion of a charged particle suspended in a gas and under the influence of an electric field is governed by Newton's laws of classical mechanics. One technique used to formulate equations for the solution of problems in kinetics is d'Alembert's principle, which states that the summation of all forces acting on a body is equal to zero.

The four principal forces acting on a particle in a precipitator are:

(1) gravitational force

$$F_g = mg,$$

(2) electrical force

$$F_e = qE,$$

(3) viscous force

$$F_\eta = 6\pi a \eta w, \text{ and finally}$$

(4) inertia force

$$F_i = m\,dw/dt$$

where

E = electric field,
q = charge on the particle,
η = viscosity of the medium,
a = particle radius,
w = velocity of the particle,
m = mass of the particle,
g = acceleration of gravity.

A free body diagram of the above forces acting on a particle is shown in Figure 4.1.

If we consider a particle suspended in a stationary gas with a coordinate system as shown in Figure 4.1, then according to the laws of mechanics we have:

$$\Sigma F_x = F_e - F_\eta - F_{i(x)} = 0$$

$$\Sigma F_y = F_g - F_{i(y)} = 0$$

$$\Sigma F_z = 0$$

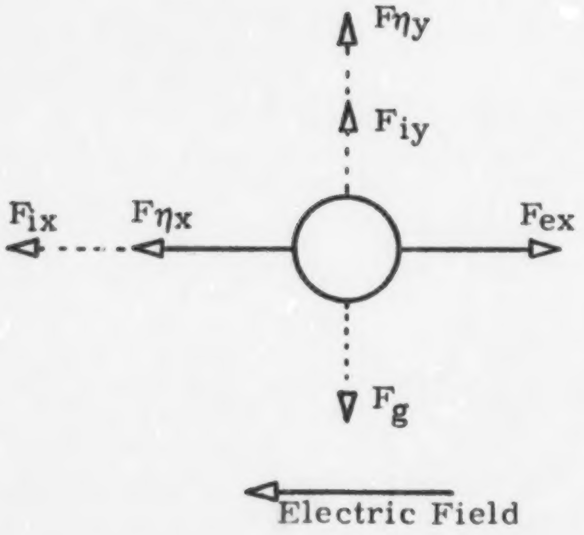

Figure 4.1. Free Body Diagram of Forces Acting on a Negatively Charged Particle in an Electrostatic Precipitator. The Significant Forces - Electrical (F_e) and Viscous ($F_{\eta x}$) - Are Shown in Solid Lines. Gravitational (F_g) and Inertial Force (F_i) Are in General Negligible.

The resultant motion of the particle can be determined by solving the above set of equations.

The coordinate system was chosen so that no forces exist in the z direction, therefore, there will be no particle motion in that direction. The gravitational force for particles encountered in gas streams is, in general, very small in comparison to the electrical and viscous forces, and can be neglected. Typically, the gravitational force is at least two decimal orders of magnitude smaller than the electrical force.

The only remaining equation of any consequence is that for the x direction

$$F_e - F_\eta - F_i = 0 \tag{4.1}$$

which upon substitution yields

$$qE - 6\pi a\eta w - m \frac{dw}{dt} = 0 \tag{4.1a}$$

rearranging

$$\frac{dw}{dt} + \frac{6\pi a\eta w}{m} = (q/m)E \tag{4.1b}$$

Equation 4.1b is a linear differential equation with constant coefficients, the general solution of which is the sum of the homogeneous solution and a particular solution. Solving for w gives:

$$w = \frac{qE}{6\pi a\eta}\left[1 - \exp\left(-\frac{6\pi a\eta t}{m}\right)\right] \tag{4.2}$$

The term, $m/6\pi a\eta$, denotes the time constant τ of the motion. The velocity w essentially reaches its terminal value within five (5) time constants. Thus, the relative residence times necessary for various particle sizes to acquire a terminal velocity can be determined.

For example, consider the particles to be unit density ($d = 1\ \text{gm/cm}^3 = 10^3\ \text{kg/m}^3$) spheres for which the mass is

$$m = 4/3\ \pi a^3 d$$

The exponent factor of Equation 4.2 becomes

$$\tau = \frac{m}{6\pi a \eta} = \frac{4/3\,\pi a^3 d}{6\pi a \eta} \doteq \frac{2a^2 d}{9\eta} \text{ sec}$$

For MKS units with a particle density of 10^3 kg/m^3

$$\tau = \frac{2 \times 10^3 a^2}{9\eta}$$

Since for atmospheric air, the viscosity is about 1.8×10^{-4} poise = 1.8×10^{-5} kg/meter-sec, the equation for the time constant as a function of particle radius becomes

$$\tau = 1.23 \times 10^7 a^2$$

where a is given in meters or

$$\tau = 1.23 \times 10^{-5} a^2 \text{ sec}$$

where a is the particle radius in microns. A plot of the time constant (τ) for unit density particles suspended in atmospheric air is shown in Figure 4.2

Residence time for dust in a precipitator typically ranges from 2 to 5 seconds. Thus, for particles up to about 50μ diameter, the acceleration time is short compared to the residence time in the collector. The larger particles (50μ and above) are generally collected entirely, and the residence time for smaller particles is long compared to the acceleration time; therefore, the exponential part of Equation 4.2 can normally be neglected. The neglect of the exponential term is equivalent to ignoring the Newtonian acceleration force. Thus Equation 4.2 becomes

$$w \approx qEp/6\pi a\eta \tag{4.2a}$$

Equation 4.2a is a valid expression for the migration velocity of all particles normally encountered in electrostatic gas cleaning, where q represents the charge on the particles. As discussed in Chapter 3, there are two charging mechanisms active in electrostatic precipitators. It is customary to derive migration velocities in terms of field charging alone.

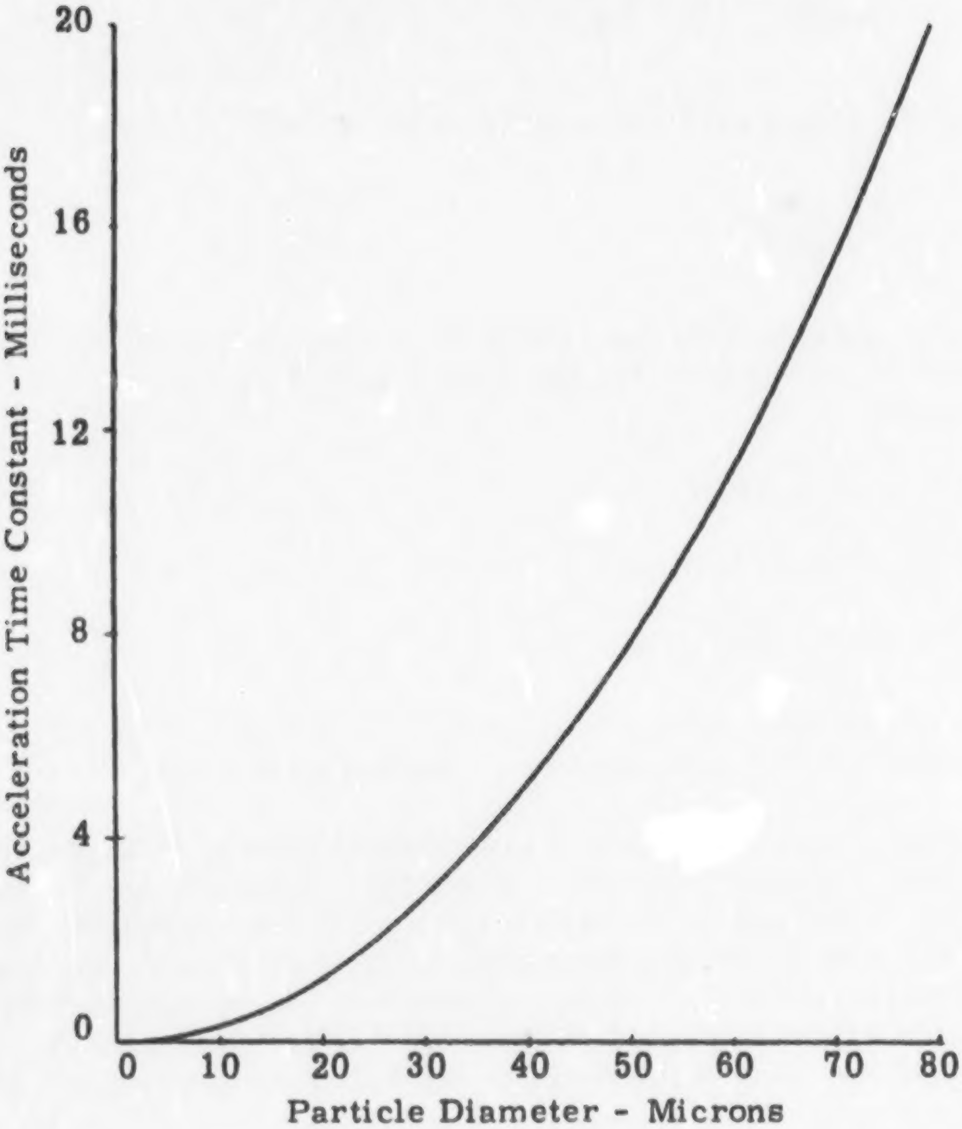

Figure 4.2. Acceleration Time Constant (τ) as a Function of Particle Diameter.

Since a particular charging mechanism may dominate for a certain size range of particles, we will derive migration velocity expressions utilizing each charging mechanism. The field charging expression applies to particle sizes greater than 0.5μ diameter, while the diffusion charging expression applies to those particles smaller than about 0.2μ.

Substituting Equation 3.10 for q in Equation 4.2a

$$w = 12 \frac{\epsilon}{\epsilon + 2} \pi \epsilon_0 a^2 E_0 \frac{1}{1 + \tau / t} \frac{E_p}{6 \pi a \eta} \qquad (4.3)$$

where after simplification yields

$$w = \frac{2\epsilon \ \epsilon_0 E_0 E_p a}{(\epsilon + 2)\eta} \frac{1}{(1 + \tau / t)} \qquad (4.3a)$$

For particles with a high dielectric constant which have attained a saturation charge, the factor $\frac{\epsilon}{\epsilon + 2}$ approaches unity and τ / t approaches zero, which gives a steady-state migration velocity for field dependent charging of

$$w = \frac{2 \epsilon_0 E_0 E_p a}{\eta} \qquad (4.4)$$

where w is given in meters/sec, E_0 and E_p are stated in volts/meter, a in meters, $\eta = 1.8 \times 10^{-5}$ kg/m-sec, and ϵ_0 = Farad/meter. Many texts and papers derive equations in electrostatic units (ESU). The expression for migration velocity in ESU for Equation 4.5 is

$$w = \frac{E_0 E_p a}{2 \pi \eta} \text{ (ESU)} \qquad (4.5)$$

where w is given in cm/sec, E_0 and E_p are in stat-volt/cm, and η in poise.

The expression for charge as a function of time for diffusion charging shows that no saturation charge, as such, exists. Therefore, the migration velocity for very small particles continues to increase throughout the time that the dust is retained in the precipitator. The expression for migration velocity for diffusion charging is obtained by substituting Equation 3.14 for q which yields

$$w = \frac{E_p}{6 \pi \eta} \frac{kT}{e} \ln \frac{(1 + \pi a v N_0 e^2 t)}{kT} \qquad (4.6)$$

In the size region between about 0.2 and 0.5μ, both diffusion and field charging are significant, and hence the migration velocity would be that associated with the combined charge resulting from the two charging regimes.

The migration velocity related to field charging is useful for most types of dusts. However, one should realize the limitations under which the equations were derived, and that they do not apply to very fine dusts and fumes.

Another modification to the previous migration velocity equations is necessary for very small particles. The equation as stated applies to particles where Stokes' law governs the equation of motion. For smaller particles, the Cunningham correction factor is applied to the equation for migration velocity. Under these conditions, the expression for migration velocity as given in Equations 4.4, 4.5, and 4.6 must be multiplied by a factor $(1 + A \frac{\lambda}{a})$, where

λ = mean free path of gas molecules,
a = radius of the dust particles, and
A = a numerical factor.

Note that the Cunningham correction factor is significant for small particles in the size region where diffusion charging is important.

4.2 PARTICLE COLLECTION WITH LAMINAR GAS FLOW

Although laminar flow is only obtained in some laboratory models, and approached in only a small percentage of the commercial two-stage precipitators, it is informative to begin the discussion of the theory of particle collection with the laminar flow model. In this model, the maximum velocity point is generally associated with the center of the pipe, and reduces with increasing radius. If we neglect the variation of velocity with radius, and assume a "plug" type flow, we can assign a velocity, V_g, to both the gas stream and the dust through the pipe (see Figure 4.3 for a sketch of this flow system).

Charged dust particles in an electric field will attain a velocity (w) towards the collection electrode. Since there are only two velocity components related to the dust motion, the net velocity is the vector sum of these two components. Since all dust particles will flow in this same resultant direction, a dust-free zone will develop in the center of the pipe

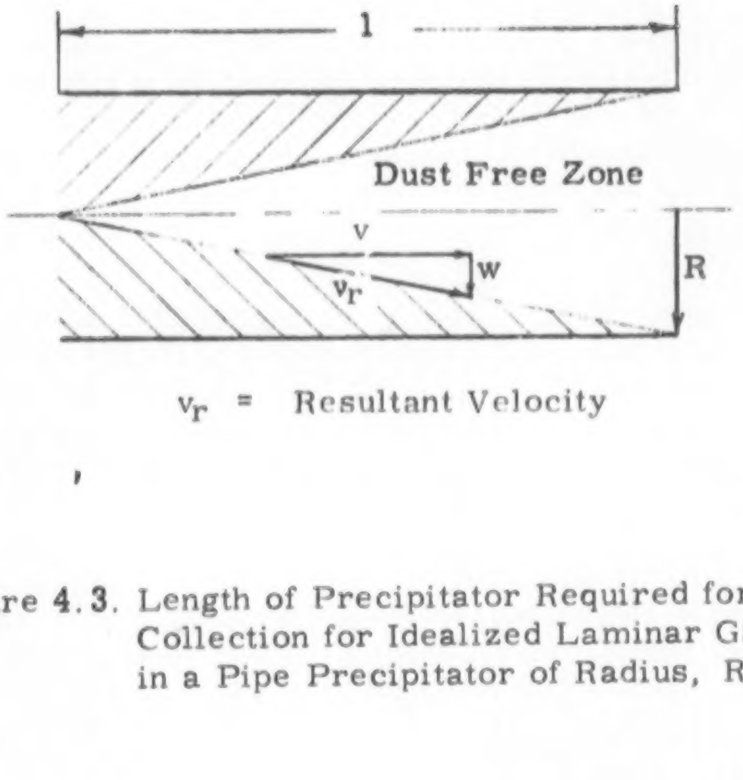

Figure 4.3. Length of Precipitator Required for 100% Collection for Idealized Laminar Gas Flow in a Pipe Precipitator of Radius, R.

and grow to fill the entire pipe as the gas flows through a distance (L) that is determined by the pipe radius **R**, gas velocity v and migration velocity w. The equation relating these quantities to the length required for 100 percent collection efficiency is:

$$L = \frac{Rv}{w} \qquad (4.7)$$

This assumes that there is no erosion or other reentrainment losses within the precipitator. Since migration velocity is proportional to particle radius (field charging), it becomes necessary to size the precipitator for the smallest particles expected in the dust.

This idealized case occurs so infrequently that it is almost of academic interest alone.

4.3 PARTICLE COLLECTION WITH TURBULENT GAS FLOW

In all practical precipitators, the gas flow is turbulent and the motion of a dust particle will be primarily the result of the turbulent gas flow, gas motion caused by collision between neutral gas molecules and the ions driven by the electric field (electric wind) as well as the migration velocity. Therefore, the specific trajectory for any one particle cannot be completely predicted for this case.

The equation for the collection efficiency of an electrostatic precipitator was discovered experimentally based on field tests by Anderson in 1919. Deutsch[1] derived a similar equation based on theoretical considerations in 1922. In the early 1950's, White[2] derived an identical expression based on the probability of collection for a single particle. Both derivations lead to collection efficiency equations of the form

$$\eta = 1 - \exp\left(-\frac{A}{v_g} w\right)$$

where

η = collection efficiency,
A/v_g = specific collection electrode area,
w = particle migration velocity.

---

[1] Refer to the bibliography for this chapter.

The exponential collection equation has also been verified by laboratory experiment, and is generally accepted as describing precipitator performance. Since Deutsch is credited with the initial development of the theory of collection, equations of the above form which relate to precipitator operation are known as Deutsch-Anderson efficiency equations.

The development of the original Deutsch-Anderson equation was based on several simplifying assumptions. These were:

(1) The particles are considered to be fully charged immediately on introduction into the collection system.

(2) Turbulent and diffusive forces cause the particles to be distributed uniformly in any cross section. (This assumption is more restrictive than necessary in actual practice.)

(3) The velocity of the gas stream does not affect the migration velocity of the particle.

(4) Particle motion is governed by viscous drag where Stokes' law applies.

(5) The particle always moves at its electrical terminal velocity.

(6) Dust particles are sufficiently separated so that their mutual repulsion can be neglected.

(7) The effect of collision between ions and neutral gas molecules can be neglected.

(8) There are no disturbing effects such as erosion, reentrainment, uneven gas flow distribution or back corona present.

As a review of the original derivation, consider a single charged particle in a wire and pipe precipitator suspended in a gas stream under the influence of an electric field. The particle will acquire a velocity (w) in a direction toward the collection electrode as described by Equation 4.2a. In the central turbulent region of a precipitator, the electrical migration velocity is small in comparison to that component due to the gas flow. But, in a boundary zone of thickness (δ), the gas flow will be laminar because of the friction between the gas stream and the wall. An example of the velocity distribution as a function of radius is shown in Figure 4.4. In this boundary layer, since the gas flow is laminar, the resultant velocity for a dust particle will be the vector sum of the gas velocity and the drift velocity. Therefore, in an increment of time Δt, all the dust particles present within the boundary layer (δ) will be driven to the collection electrode if

$$\delta = w\Delta t$$

During this same interval of time, the gas stream will have moved through the precipitator a distance

$$\Delta L = v\Delta t$$

where v is the average gas velocity.

From these conditions, the incremental equation for particle removal can be established

$$\frac{\Delta N}{N} = \frac{S\delta}{A_d} = -\frac{Sw\Delta t}{A_d} = -\frac{Sw\Delta L}{A_d v} = -\frac{w\Delta A_c}{A_d v} \qquad (4.8)$$

where

ΔN = particle concentration removed,
N = particle concentration in the gas stream,
ΔA_c = incremental collection area = $S\Delta L$
S = circumference of pipe
v_g = volume flow rate of gas = $A_d v$
A_d = cross sectional area
v = gas velocity

Passing to the limit with Equation 4.8, we find

$$\frac{dN}{N} = -\frac{Sw}{A_d v}\,dL = -\frac{w\,dA_c}{v_g} \qquad (4.9)$$

Integration of Equation 4.9 yields an expression for the particle concentration at the precipitator outlet.

$$N = N_0 \exp\left(-\frac{A_c w}{v_g}\right)$$

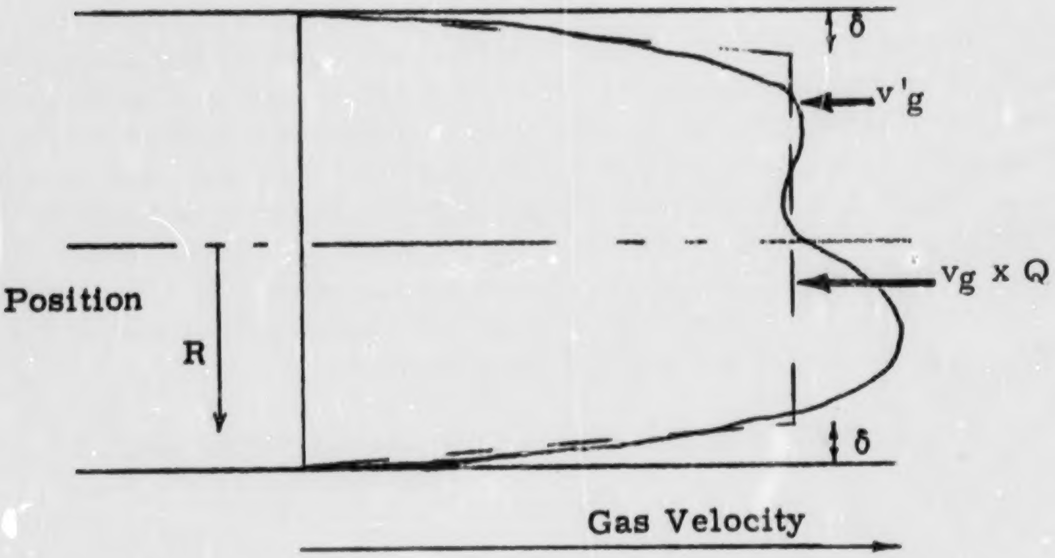

v'_g = actual gas velocity distribution,
$v_g \times Q$ = average gas velocity outside boundary layer x quality factor, and
δ = boundary layer.

Figure 4.4. Possible Gas Distribution in a Precipitator Duct.

where N_0 is the particle concentration at the inlet. The collection efficiency can be stated as the ratio of particles removed to the inlet concentration.

$$\eta = \frac{N_0 - N}{N_0} = 1 - \exp\left(- \frac{A_c w}{v_g} \right) \qquad (4.10)$$

White derived an identical equation based on the probability of a particle being collected in a circular wire and pipe precipitator during an interval of time, Δt. If the particle is within a distance, $w\Delta t$, of the collection electrode, it will be trapped by the electric field and will be collected. Then the probability of collection within a given interval of time is the probability of the particle being located within the outer annulus. Since the particle has equal probability of being located at any point within the cross section, then the probability of collection, P_c, is the ratio of the area of the annulus to the cross-sectional area of the precipitator.

The probability of escape within each section ΔL, is

$$P'_{es} = 1 - P_c = 1 - \frac{2w\,\Delta t}{R},$$

and the probability of escape through the complete precipitator is the probability of escape in one section raised to the power of the number of sections in the unit

$$P_{es} = (1 - P_c)^{\frac{L}{\Delta L}} = \left(1 - \frac{2wt}{Rn}\right)^n \qquad (4.11)$$

where

Δt = total time divided by the number of sections considered on the precipitator.

Algebraic manipulation yields an equation identical to that previously derived in Equation **4.10**.

A somewhat more general expression of the same form will result if the original assumptions are somewhat modified.

(1) The dust particle concentration, N_δ, in the collection layer, δ, is proportional (but not necessarily equal) to the average particle concentration, N_0, in any cross section.

(2) The effective gas flow through the precipitator can be described as the product of the average gas velocity, v_g, times a quality factor, Q.

(3) The collection layer thickness, δ, is defined as the distance away from the collection electrode to the point where the migration velocity, w, is equal to the linear velocity of the gas stream down the precipitator in the laminar flow region.

In the central region of the precipitator where the gas velocity and turbulent velocity components are large compared with the migration velocity, the dust trajectory will be random. In this region the effect of the migration velocity will be negligible. But, in the region near the wall, in the collection zone, the longitudinal velocity is limited by the frictional forces of the wall. The translational velocities are effectively reduced, while the migration velocity component towards the collection electrode remains constant. In this collection layer, δ, the migration velocity dominates and all particles within δ will be removed within an incremental time, Δt, which is defined by the relation

$$\Delta t = \delta / w$$

In the collection layer, the migration velocity causes all particles within the distance, δ, from the wall to be collected within a time, Δt. During this time the gas moves a distance $\Delta L = v_g Q \Delta t$. The number of particles in a particular size range removed will be the product of the number density of particles in the boundary layer and the volume of this region cleared, or

$$\Delta N = -N_\delta S w \Delta t \Delta L \tag{4.12}$$

The number of particles within the volume of the precipitator defined by the length, ΔL, and the cross section of the pipe is

$$N = N_0 A_d \Delta L \tag{4.13}$$

which yields an equation for the increment of particles removed

$$\frac{\Delta N}{N} = -\frac{N_\delta S w \Delta t \Delta L}{N_0 A_d \Delta L} = -\frac{N_\delta S w}{N_0 A_d} \Delta t = \frac{N_\delta}{N_0} \frac{S w}{A_d} \frac{\Delta L}{v Q}$$

where

N_δ = particle concentration in the boundary layer,
v = average gas velocity, and
Q = quality factor for the gas flow.

Passing to the limit we have

$$\frac{dN}{N} = -\frac{N_\delta}{N_0} \cdot \frac{S}{A_d} \cdot \frac{w}{v\,Q}\, dL \tag{4.15}$$

Integration of Equation 4.10 yields an expression for the particles collected or removed

$$N = N_0 \exp\left(-\frac{N_\delta}{N_0} \cdot \frac{Sw}{A_d\, v\, Q} L\right). \tag{4.16}$$

The efficiency can be determined from

$$\eta = \frac{N_0 - N}{N_0} = 1 - \exp\left(-\frac{N_\delta}{N_0} \cdot \frac{SL}{A_d\, v\, Q} \cdot w\right)$$

which can be expressed as

$$\eta = 1 - \exp\left(-\frac{N_\delta}{N} \cdot \frac{A_c}{v_g\, Q} \cdot w\right) \tag{4.17}$$

The derivation for the collection efficiency given above relates the collection efficiency of an installation to the migration velocity of the dust particles. Since the migration velocity of dust particles is dependent upon the particle size as well as other factors, the equation as stated applies specifically to a particular particle size for which the migration velocity is given. Thus in the strict sense, the Deutsch-Anderson equation applies only to a group of particles for which the migration velocity is known. If the performance for a typical dust is desired, it is necessary to separate the specific particle size distribution into several discrete size ranges, compute the migration velocity and collection efficiency for each size range, and then determine the overall efficiency. This is discussed in more detail in Chapter 8, Systems Analysis.

Equation 4.17 differs from the previously described Deutsch-Anderson equation in two respects: the particle concentration in any cross section, and a quality factor, Q, can be used to modify the average gas flow rate through the precipitator.

The quality factor, Q, is included to provide a means to modify the efficiency equation for installations with a highly uneven gas flow. The Deutsch-Anderson equation utilizes an average gas velocity, v. In the above derivation, the average gas velocity is multiplied by Q to yield an effective gas velocity. The factor, Q, could be different for each precipitator installation and must be determined individually. For installations with a relatively even gas flow the numerical value of the factor would approach unity, while in some extreme cases, it could approach a value of 2. A numerical example will show some insight into the manner in which the uneven gas distribution could cause a variation in the overall efficiency of an installation.

For this example, consider a simplified precipitator where a uniform gas flow exists in each of four identical areas of the unit, as depicted in Figure 4.5. The average gas velocity for this example is determined by summing the products of the velocity and the area, which yields an average gas velocity of 2.5 v where v is an arbitrary value. If the expected collection efficiency for this unit with a uniform gas flow of 2.5 v is 99%, the Deutsch equation can be used to determine the value of the exponent,

$$\eta = 99\% = 1 - \exp\left(-\frac{Aw}{2.5\,v_g}\right),$$

from which

$$Aw/2.5v_g = \ln\frac{100}{100-\eta} = \ln 100 = 4.6.$$

The example can be analyzed as if the simple precipitator in Figure 4.5 were really four individual precipitators with different gas flow rates. The percent of material not removed in each precipitator could be expressed as Δ_1, Δ_2, Δ_3, Δ_4, as follows:

$$\Delta_1 = \exp\left(-\frac{Aw}{v_g}\right) = \exp(-11.75) = 0.000007$$

$$\Delta_2 = \Delta_3 = \exp\left(-\frac{Aw}{2\,v_g}\right) = \exp(-5.875) = 0.0029$$

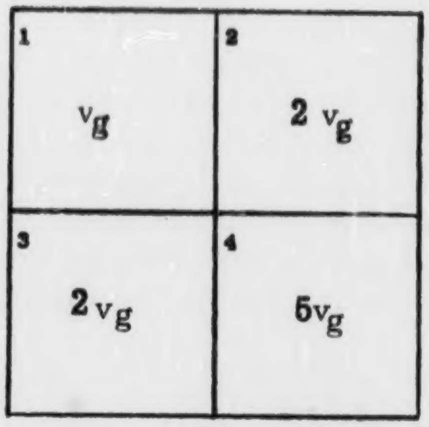

Figure 4.5. Assumed Gas Flow Distribution for Quality Factor Example. Average Velocity Proportional to Average Volume Flow Rate = $2.5\,v_g$.

$$\Delta_4 = \exp\left(- \frac{Aw}{5\,v_g}\right) \simeq \exp(-2.35) = 0.0954$$

The total material escaping is then the weighted sum of that lost in each section, or

$$\Delta_{\text{Total}} = 0.4887$$

for constant loading per cu ft. From this, the overall efficiency can be expressed as

$$\eta = \frac{9 - 0.4887}{9} \approx \frac{8.5}{9} = 94.4\%.$$

The efficiency for the actual case is about 4.6% less than expected for one with the average flow.

The numerical value for the quality factor can be determined from the relation

$$Q = \ln \frac{100}{100-\eta_1} \div \ln \frac{100}{100-\eta_2} = \frac{\ln 100}{\ln 18} = \frac{4.6}{2.9}$$

$$Q = 1.6$$

Therefore for this example, the effective velocity is 1.6 times the average velocity.

4.4 FACTORS MODIFYING THE PARTICLE COLLECTION IN A PRECIPITATOR

Several factors can lead to a significant change in the collection efficiency of the idealized precipitator as described in the section on particle collection theory. These factors include particle agglomeration, back corona, uneven gas flow, and erosion and rapping reentrainment, among others. Most of these factors tend to decrease collection efficiency. However, agglomeration would result in a larger effective particle size and would tend to increase collection efficiency.

The migration velocity of a particle is proportional to the radius of the dust, as seen from Equation 4.3. As the particles agglomerate, the ratio of electrostatic force to aerodynamic drag increases, with a resultant increase in migration velocity. Thus as the particles agglomerate, the collection efficiency of the precipitator tends to increase.

Electrical sparkover and back corona are two related phenomena that tend to decrease the collection efficiency of electrostatic precipitators. Electrical sparkover results when a localized gas breakdown occurs across the interelectrode space.

The phenomena of spark initiation have been studied extensively by Loeb[3], Penney[4] and others. In terms of electrostatic precipitator performance, the following factors are significant.

(1) Spark initiation occurs at the anode.

(2) Spark initiation is influenced by the magnitude of the electric field near the anode.

(3) Propagation of a spark depends on the magnitude of the applied voltage.

For a negative corona, the magnitude of the electric field near the collection electrode is related to the resistivity of the dust and the current density according to the equation

$$E = j\rho$$

where

ρ = electrical resistivity, ohm-cm.

The influence of the electric field on sparking can best be explained in terms of the voltage-current curve, Figure 4.6. The voltage impressed across the electrode of a precipitator will result in a current flow, the magnitude of which will depend upon the gas composition, temperature, pressure, and precipitator electrode dimensions. If the electrodes are clean, the voltage can be increased until sparking occurs. If the collection electrode has a dust layer with a resistivity of around 10^{10} ohm-cm, a current density of 10^{-6} amp/cm^2 will result in a field in the deposit of around 10 kV/cm (indicated by Point A in Figure 4.6).

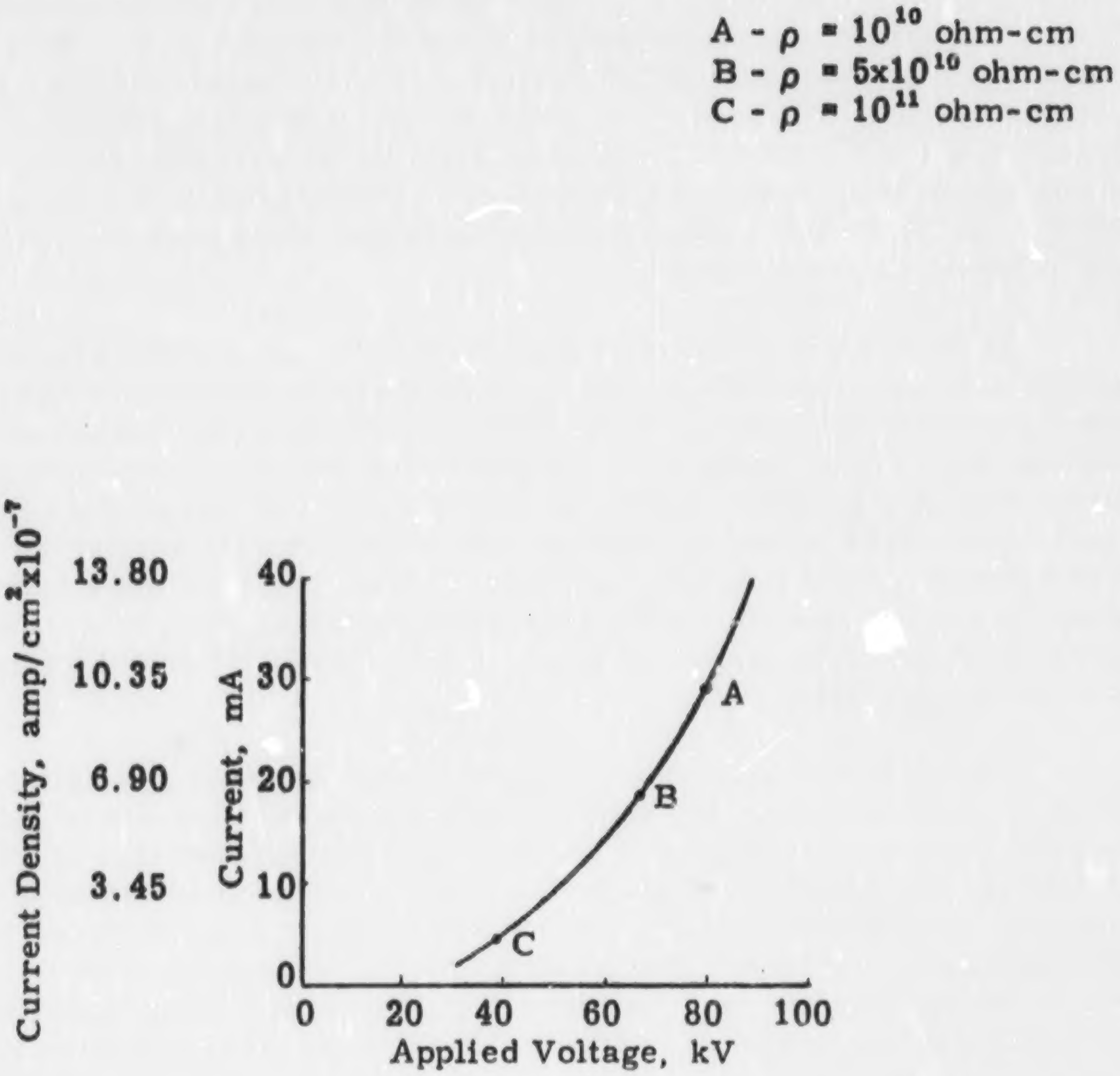

Figure 4.6. Negative Corona Voltage Current Characteristics in Air for a 15-Foot Pipe, 20-cm Diameter, 0.277-cm Wire Diameter.

A further increase in the resistivity to 5×10^{10} ohm-cm causes the electric field in the deposit to reach 10 kV/cm at a current density of about 7×10^{-7} amp/cm^2 corresponding to Point B on Figure 4.6. Since spark initiation will occur at a lower voltage due to the higher field at the anode, the precipitator will operate at Point B. If the dust resistivity is further increased to 10^{11} ohm-cm, the same field in the dust deposit will result from a current density of only 10^{-8} amp/cm^2. Consequently, the voltage and current at which the precipitator operates will be further reduced and operate at Point C on the curve.

As resistivity of the dust layer is increased, a point will be reached at which the applied voltage will be inadequate to propagate a spark across the interelectrode space. Under these conditions, the current and resistivity will be such that breakdown of the gas in the interstitial regions of the dust layer will occur. This condition results in the formation of a corona in the dust layer. The resulting positive ions formed travel across the interelectrode space toward the discharge electrode. These ions will impact upon dust particles in the interelectrode region and neutralize or reduce the charge present on the dust due to the negative ions flowing from the region of the discharge electrode.

The effects of sparking and back corona influence precipitator operation in several ways. Within the range of resistivities where sparking occurs, operating voltage and current are reduced over that of a clean electrode precipitator. The electric field is reduced by virtue of the reduced voltage and current, and the charging time is increased by virtue of the reduced current. In a sparking mode, the precipitator is momentarily deenergized during the interval of the spark. Consequently, the efficiency is influenced in proportion to the total deenergization time.

The effects of uneven gas flow, erosion, and rapping reentrainment were discussed previously and need not be repeated here.

4.5 PRACTICAL ASPECTS OF PARTICLE COLLECTION

The Deutsch-Anderson equation, $\eta = 1 - \exp\left(-\frac{A}{v_g} w\right)$, is widely used to describe the performance of precipitators. Because of this wide acceptance, a general term, effective migration velocity (EMV) or precipitation rate parameter, is customarily associated with the collection efficiency of installed units. The value of the EMV can be determined when values are known for the collection area (A), volume flow rate (v_g), and efficiency η.

$$w = \frac{v_g}{A} \ln \frac{100}{100-\eta} \qquad (4.19)$$

This w is not the velocity with which particles move toward the collection electrode as given in the previous section, rather it is the net average migration velocity for an average particle which would result in the measured efficiency for a particular installation, and therefore is, in effect, a performance parameter.

Several factors contribute to the fact that the precipitation rate parameter is different from the theoretical migration velocity. These factors include reentrainment, uneven gas flow, particle size distribution, and back corona, and have been discussed individually in other sections of the report. Collectively, the result is a net flow of particles from the wall back into the precipitator such that the effective flow toward the collection electrode is reduced.

Thus, while the precipitation rate parameter is useful for describing the actual performance of a precipitator, care should be exercised in order to insure that the value of this number is understood to be related only to the performance of a precipitator, and not to any real measurable velocity of particles toward the collection electrode.

4.6 RECENT MODIFICATIONS TO THE DEUTSCH EQUATION

It is generally recognized that the basic Deutsch-Anderson equation has a number of limitations principally associated with the assumptions made in the derivation. Several investigators have attempted to modify the basic Deutsch equation so that it would more nearly describe precipitator performance.

Cooperman[3] states that the Deutsch equation neglects the role of diffusional forces in the precipitator which can account for the variation between observed and theoretical migration velocities and the apparent increase in the precipitation rate parameter with increasing gas velocity. Cooperman postulates that the difference in particle concentration along the precipitator length gives rise to a diffusional force which results in a particle velocity through the precipitator that is greater than the gas velocity. At low gas velocities, the effect is pronounced, but is masked at higher velocities.

In addition to the linear diffusion, Copperman suggests that a difference in particle concentration would result in a back diffusion if the particle concentration at the collection surface were higher than that within the central sector, and hence result in a lower migration velocity.

Cooperman suggests an equation of the form

$$\eta = 1 - \exp\left[-\beta/\alpha\left(1 - \frac{1}{2\alpha^2}\right)\frac{L}{B}\right] \qquad (4.20)$$

where

$$\beta = (1-f)\frac{bw}{2D_1}$$

$$\alpha = \frac{bv}{2D_1}$$

b = half width of the precipitator duct (comparable to radius),
L = precipitator length,
f = ratio of particle transport away from the collecting electrode to the migration velocity towards it,
w = electrical migration velocity (theoretical),
D_1 = particle diffusion coefficient in the direction of the gas flow, and
v = mean gas transport velocity.

If we perform a few algebraic manipulations the exponential term can be made to appear more like the Deutsch terms. This is desirable because of the widespread use of the Deutsch equations.

$$\beta/\alpha = \frac{(1-f)\frac{(bw)}{2D_1}}{\frac{bv}{2D_1}} = (1-f)\left(\frac{bw}{2D_1}\right)\left(\frac{2D_1}{bv}\right) = (1-f)\frac{w}{v} \qquad (4.21)$$

Now let us add a factor (h) = height of the collection electrode from which

$$\frac{L}{b} \times \frac{h}{h} = \frac{A_c}{A_d} \qquad (4.22)$$

where

A_c = collection electrode area, and
A_d = cross-sectional area of the duct.

Thus the product of β/α and $\frac{L}{b}$ becomes

$$\beta/\alpha \times \frac{L}{b} = (1-f)\,\frac{w}{v_g}\,\cdot\,\frac{A_c}{A_d} \tag{4.23}$$

and $v \times A_d$ = the cross-sectional area of the duct times the mean gas velocity which is the volume flow rate (v_g) of the precipitator. Therefore, Equation **4.24** becomes

$$(1-f)\,w\,\cdot\,\frac{A_c}{v_g}$$

Equation **4.20** can be rewritten with more familiar terms so that

$$\eta = 1 - \exp\left[-(1-f)\left(1 - \frac{1}{2\alpha^2}\right)\frac{A}{v_g}\,w\right] \tag{4.24}$$

One way of viewing Equation **4.24** is that two modifying factors have been added to the original Deutsch equation. It appears to be reasonable to assume that the factor (1-f) is a modifier for the migration velocity (w), while the factor $\frac{1}{1-2\alpha^2}$ is a factor related to diffusion transport in the direction of gas flow that modifies the gas velocity and therefore the volume flow rate.

If we postulate a reentrainment velocity (w_r), and an electrical migration velocity (w_e), then the factor (1-f) becomes

$$1-f = 1 - \frac{w_r}{w_e} = \frac{w_r - w_e}{w_e} \tag{4.25}$$

Upon substitution of Equation **4.25** into Equation **4.24** we have

$$\eta = 1 - \exp\left\{-\left[\frac{w_e - w_r}{w_e}\right]\left[1 - \frac{1}{2\alpha^2}\right]\frac{A}{v_g}\,w_e\right\} \tag{4.24a}$$

$$= 1 - \exp\left[-\left(1 - \frac{1}{2\alpha^2}\right)\frac{(w_e - w_r)}{v_g}\,A\right] \tag{4.24b}$$

but $(w_e - w_r)$ is merely the net particle velocity towards the collection electrode (w_n) so that Equation 4.24a becomes

$$\eta = 1 - \exp\left[- \left(1 - \frac{1}{2\alpha^2}\right)\left(\frac{w_n A}{v_g}\right)\right] \tag{4.24c}$$

Therefore, the new theory developed by Cooperman is closely related to the original theory developed by Deutsch, and takes into account two factors which can significantly modify the electrical and convective parameters used in the original derivation. These factors can bring theory and practice into better agreement.

No experimental verification of this theory was included.

Robinson derived an equation for collection efficiency[4] which also offers an explanation for the wide disparity between the precipitation rate parameter and the theoretical migration velocity. In this analysis, two erosion terms are introduced. The first erosion term is proportional to the density of dust particles in the boundary layer. Erosion of this type is based on the concept that the greater number of impacts between dust particles and the deposit layer, the greater the quantity of dust that will be reentrained. The second erosion term is a constant term such as one would expect to find with a constant velocity gas stream flowing near a collected layer of dust, which for a fixed velocity should give a constant erosion rate. These two factors are combined to yield an efficiency equation which is a modified Deutsch equation.

$$\eta = 1 - \left(1 - \frac{\beta}{1 - \alpha}\right) \exp\left[- (1 - \alpha)\, \chi\, w\, A/v_g - \frac{\beta}{1 - \alpha}\right] \tag{4.26}$$

where

α = coefficient of the variable erosion,
β = coefficient of the constant erosion,
χ = ratio of dust concentration near the wall to the average concentration in the cross section, and
w, A, v_g = standard precipitation parameters.

Equation 4.26 can be algebraically manipulated to become

$$\eta = (1 - \frac{\beta}{1 - \alpha}) \left\{1 - \exp\left[- (1 - \alpha) \chi \, w \, A/v_g \right]\right\} \qquad (4.26a)$$

which corresponds to modifying the Deutsch equation in three respects:

(1) The entire equation is multiplied by an erosion sensitive term, $1 - \beta (1 - \alpha)$.

(2) The particle concentration near the wall can be different from the average particle concentration (χ).

(3) The migration velocity is modified by the variable erosion effect, $w_{eff} = (1 - \alpha) w$.

The two papers discussed above represent the more significant attempts to bring the theoretical and experimental aspects of precipitation phenomena into closer agreement. Experimental verification of one of the above models appears to be necessary to resolve the differences, if in fact differences exist.

CHAPTER 4
BIBLIOGRAPHY

1. Deutsch, W., Ann. der Physik 68, p 335 (1922).

2. White, H. J., Industrial Electrostatic Precipitation, Addison-Wesley (1963).

3. Cooperman, P., "A New Theory of Precipitator Efficiency," Paper No. 69-4, APCA Meeting, New York City (1969).

4. Robinson, Myron, "A Modified Deutsch Efficiency Equation for Electrostatic Precipitation," Atmospheric Environ 1, No. 3, pp 193-204 (May 1967).

CHAPTER 5
GAS FLOW

5.1 INTRODUCTION

Gas flow is important in the precipitation process for a variety of reasons. First, the gas volumes handled can be large so that the cost of equipment can be high if high pressure drops are involved. The power costs also will be excessively high if large losses occur in the duct. An even more important consideration, however, is the uniformity of the gas flow entering the precipitator. Severe nonuniformity causes erosion of the collected dust from hoppers and collecting electrode and causes variable gas treatment times in the precipitator. The combined effects can cause marked reduction in precipitator performance, often as much as 20-30 percent. Poor gas flow can also result in excessive deposits of dust on ducts, turning vanes, elbows, and distribution plates. These deposits can further alter the flow pattern and result in further nonuniformity of flow.

The fundamentals of fluid flow are covered in many standard texts on fluid mechanics. Basic types of flow are defined depending upon the gas velocity, duct size, and gas properties. One of the most important dimensionless parameters in fluid flow is the Reynolds number which is defined as

$$R_e = \rho \frac{vD}{\mu},$$

where

ρ = gas density,
v = velocity of gas,
μ = viscosity, and
D = equivalent diameter based on wetted perimeter

$$(D = 4 \frac{\text{area}}{\text{perimeter}}).$$

If the Reynolds number is less than critical (about 2000 to 2600 in a duct), the flow will be laminar and the velocity profile across the duct will be parabolic as illustrated below. In this type flow, the maximum velocity is twice the average for a cylindrical pipe.

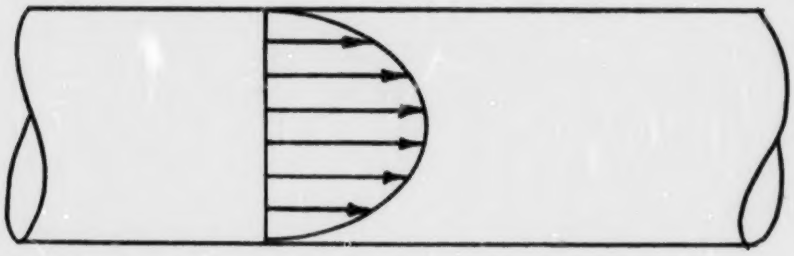

When the Reynolds number is greater than critical, any small disturbance will not die out but will continue to grow until the gas flow has fully developed turbulence. The flow profile will have a boundary layer that increases in velocity from zero at the wall up to the mean velocity of the core of the flow. With reasonably constant average velocity and turbulent flow, the maximum velocity will be about 110% of the average velocity. The velocity profile will be nearly parabolic in the boundary layer and nearly flat, but fluctuating, in the core:

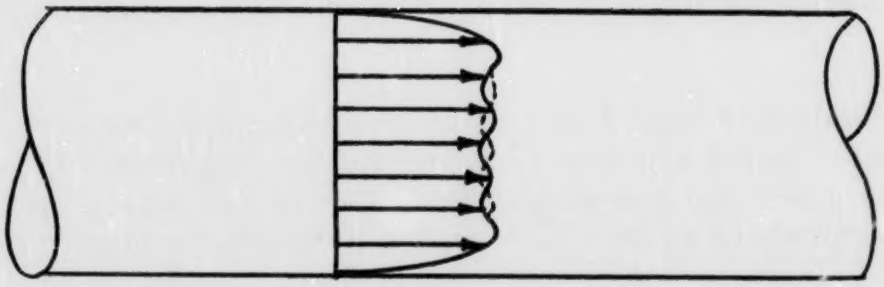

With an uneven velocity distribution, the maximum velocity can be much higher than the average velocity and the profile can be almost any shape.

All large size precipitators operate well into the turbulent region. Typical values for Reynolds numbers for electric precipitators are 10,000 and higher. The gas flow in all practical sizes of duct work is also in the turbulent region. Gas flow in duct work is subject to wide variations in velocity distribution.

When a duct changes cross section, the velocity profile changes. In a converging transformation, the velocity vectors must increase to compensate for the smaller area of cross section. If the profile is reasonably constant, the magnitude of the vectors change with little variation between maximum and average velocity. However, with a diverging transformation, the entering air tends to maintain its velocity distribution because of inertia. The flow separates from the wall, and eddies form which tend to grow to the full size of the duct because of the large Reynolds number (see sketch below). The stream tends to spread out slightly, but separation will occur for diverging angles greater than about 7° included angle.

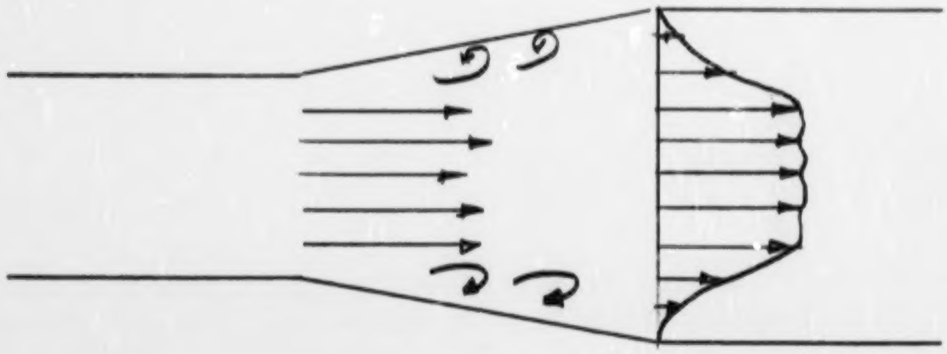

Separation will also occur on one side of a turn, as illustrated below.

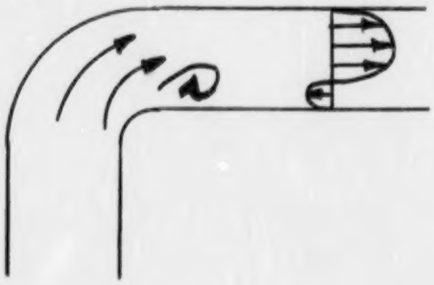

Reverse flow in the separation zone as indicated above is common in flue systems unless special precautions are taken to prevent it.

As illustration of the effect of a sudden transformation in cross section of a duct, let us consider the kinetic energy of the moving gas:

At a point (1) upstream of a transformation: $(KE)_1 = 1/2\ mv_1^2$

At a point (2) downstream of the transformation: $(KE)_2 = 1/2\ mv_2^2$.

The continuity equation for a square duct of side S would be:

$$v_g \qquad \rho m = Av = S^2 v;$$

then

$$\frac{v_1}{v_2} = \left(\frac{S_2}{S_1} \right)^2,$$

and

$$\frac{(KE)_1}{(KE)_2} = \frac{1/2\ mv_1^2}{1/2\ mv_2^2} = \left(\frac{v_1}{v_2} \right)^2 = \left(\frac{S_2}{S_1} \right)^4,$$

or the kinetic energies vary inversely as the fourth power of the side of the duct; thus doubling the side of a square duct reduces the average kinetic energy far downstream to 1/16 of what it was upstream. The other 15/16 of the energy must be dissipated in turbulence and viscous losses.

The relationship of velocity to pressure, or "head" is based on kinetic energy. The velocity head equals the kinetic energy:

$$h = \frac{1}{2} mv^2 = \frac{1}{2} \frac{\rho}{g} v^2$$

or

$$v = \sqrt{\frac{2gh}{\rho}} .$$

In English units, we have

p = pressure in inches water gage,

w = pounds per cubic foot, and

v = feet per minute.

$$v = \sqrt{\frac{p}{w}} .$$

For standard air, 70°F at 29.92 inches Hg barometer,

$$v = 4005\sqrt{p}\ .$$

Now, a loss due to friction in any part of duct system is a loss in energy. Therefore, the loss can be expressed as a function of the "Velocity Pressure":

$$p = w\left(\frac{v}{1096.5}\right)^2$$

Losses in elbows, wyes, transformations, and so on, are often expressed as "percent of velocity pressure". Some texts convert this to "equivalent feet of duct". Either kind of data can be used in the calculation of friction losses in ductwork.

There is also friction in the boundary layer. This "wall friction" depends on the Reynolds number and on the roughness parameter of the wall construction. The roughness parameter is the variation in the wall divided by the duct equivalent diameter, $D = (4 \times \frac{\text{area}}{\text{perimeter}})$. In the large sizes of ducts used in precipitator work, the roughness would generally be considered "smooth", unless there were structural protuberances, rough welds, extreme corrosion, or severe dust deposits. Numerical values of friction factors can be found in textbooks and handbooks such as the ASHRAE Handbook[1] (see Figure 5.1).

The method of calculating frictional losses in gas handling systems is straightforward and well developed. The most common form of expressing frictional losses in straight runs of duct is that described by the Fanning equation:

$$\Delta p = \frac{fL\rho v^2}{M2g}$$

where

Δp = static pressure loss,

f = friction of factor,

---

[1] Refer to the bibliography for this chapter.

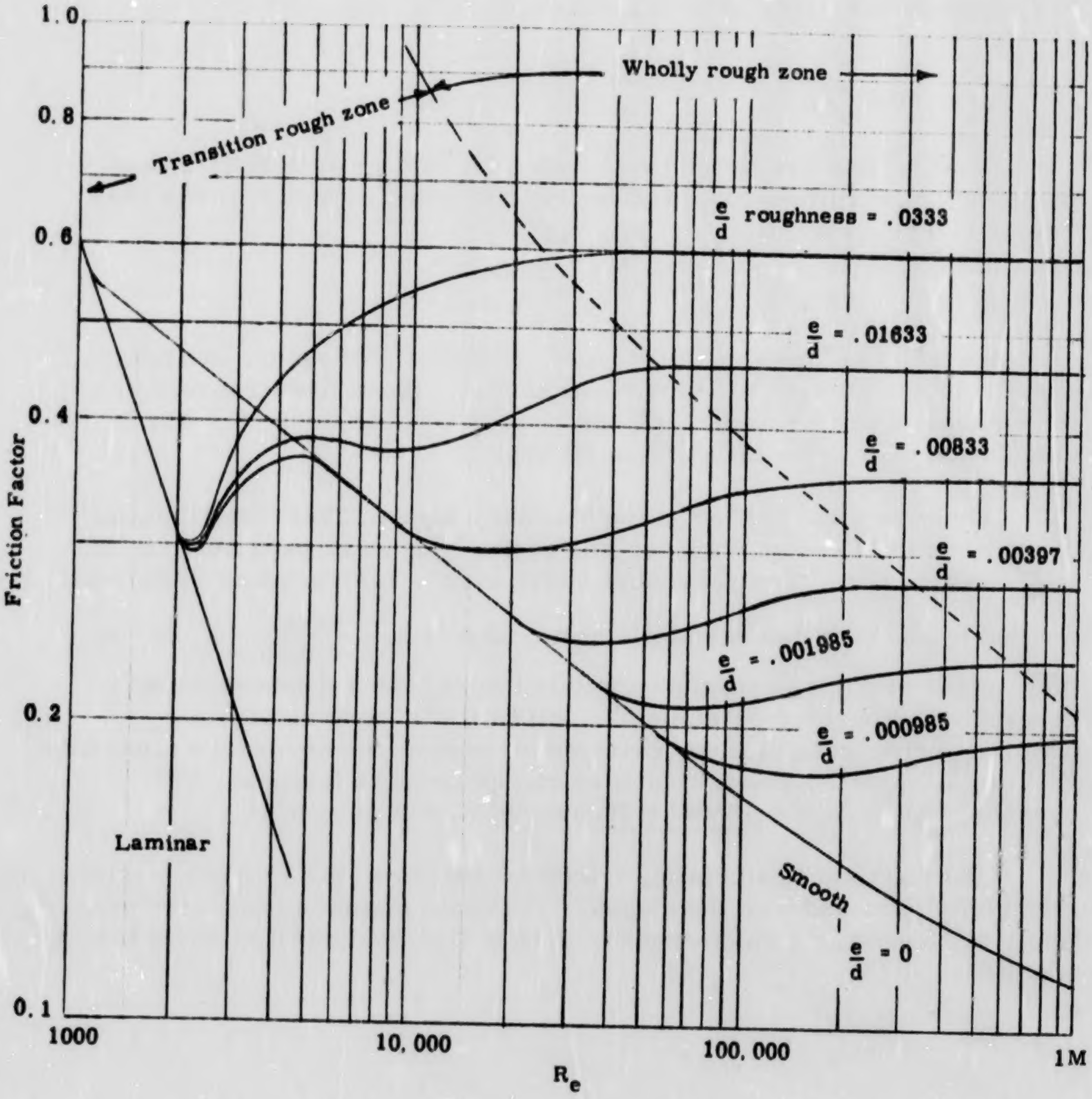

Figure 5.1 Air Friction Vs. Reynolds Number and Roughness.

L = length of duct,

ρ = density of gas,

v = velocity,

g = gravity, and

M = hydraulic radius.

Let

v_g = Av = volume rate of gas flow, and

$M = \frac{A}{P}$ = area/perimeter;

then

$$\Delta p = \frac{fL\rho v_g}{2g} \quad \left(\frac{v_g/A}{A/P}\right)^2$$

$$\Delta p = \frac{fL\rho v_g^2}{2g} \times \left(\frac{P}{A^3}\right).$$

Combining the constants:

$$\Delta p = k \frac{P}{A^3}$$

or pressure loss for odd-shaped ducts varies with $\frac{P}{A^3}$.

If $\frac{P}{A^3}$ or $\frac{A^3}{P}$ is held constant, an approximate equivalent diameter can be calculated for any odd-shaped duct. It will be approximate because the velocity used in the derivation is an average velocity calculated from volume flow rate and cross-section area, but the real friction will be the sum of the friction due to the actual velocity distribution, which is never known exactly. Therefore, any form of equivalent diameter calculation is approximate. For example, let us compare the above with another form of equivalent diameter:[2]

$$D_1 \approx \frac{2ab}{a + b}$$

where a and b are dimensions of a rectangular duct.

$$\frac{A_1^3}{P_1} = \frac{A_2^3}{P_2}$$

$$\frac{\left(\frac{\pi}{4}\right) D_2^2}{\pi D} = \frac{(ab)^3}{2\,(a + b)}$$

$$\frac{\pi^2 D_2^5}{64} = \frac{a^3 b^3}{2\,(a + b)} .$$

Let b = Ka in both formulas

$$D_2^5 = \frac{16}{\pi^2} \; \frac{K^3 a^5}{k+1}$$

$$D_2 = \sqrt[5]{\frac{16}{\pi^2} \; \frac{K^3}{K + 1}} ,$$

and

$$D_1 = \frac{2Ka^2}{a\,(K + 1)} = a\,\frac{2K}{K + 1}$$

when

$$K = 2, \qquad D_1 = 1.33\ a$$

$$D_2 = 1.34\ a.$$

So the two formulae are almost the same if the aspect ratio, K, of the duct cross section is not too high:

when

$$K = 10, \qquad D_1 = 1.82\ a$$

$$D_2 = 2.72\ a.$$

The friction loss with such an extreme aspect ratio should be checked by a model if possible.

Friction, however, is only part of the problem. If sharp bends, sudden transformations and rough walls in the system generate severe turbulence and nonuniform velocity profiles, there will be trouble in any equipment sensitive to air flow. Because fans, dust collectors, and similar equipment are designed on the basis of some average velocity, any extreme variation from that average may degrade the operation. For example, the standard fan test code calls for a straight inlet duct 10 diameters long with a straightener 6 diameters from the fan. If in the field, a sharp bend is located at the fan inlet so that most of the air is thrown to one side by inertia, then part of the fan is operating unloaded and the volume handled will be less than design by 10 to 15%.

The best operating condition for an electrostatic precipitator will occur when the velocity distribution is uniform. Because of the logarithmic nature of the efficiency formula, an increased velocity in one plate section will decrease the efficiency of that section more than the decreased velocity in a parallel section would increase the efficiency of that section. As a consequence, for a precipitator with nonuniform gas velocity, the total plate area required to achieve a given efficiency will be greater than that for a precipitator with uniform gas velocity.

Figure 5.2 illustrates the adverse effect of uneven gas flow on overall precipitator efficiency.[3] Efficiencies are plotted for each unit of a 3-unit precipitator with 1/2, 1, and 1-1/2 meters per second gas flow in the three units respectively. Although the collection efficiency for the average velocity is 97.3%, the average collection efficiency for the three units is only 94.5%. In practice, for dry collection the actual loss in efficiency would very likely be far worse because of reentrainment of collected particles in the high velocity zones.

In order to describe nonuniformity of gas flow, some easily understood means must be employed, either qualitative, or quantitative. The readings of each row or column of a velocity traverse can be plotted to arrive at a series of velocity profiles such as shown in Figure 5.3. Alternatively, an isopleth, or contour plot, of the lines of constant velocity can be constructed as shown in Figure 5.4. These methods of plotting are useful in visualizing the velocity distribution

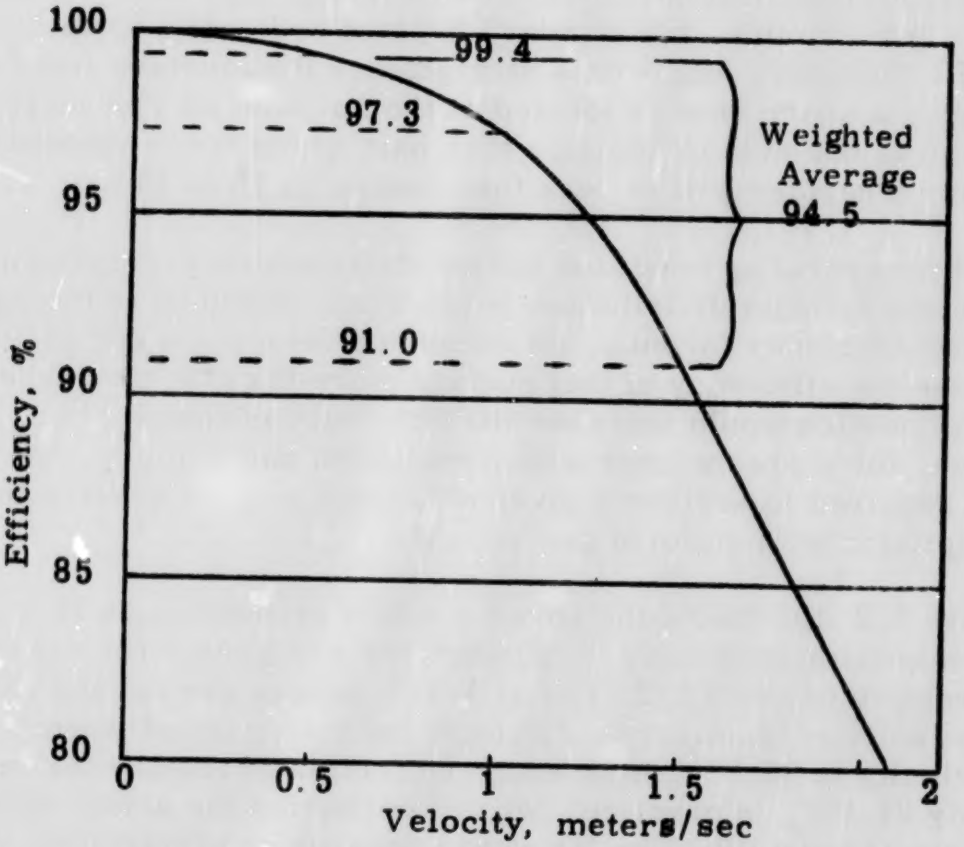

Figure 5.2. Collection Efficiency as a Function of Flow Velocity.

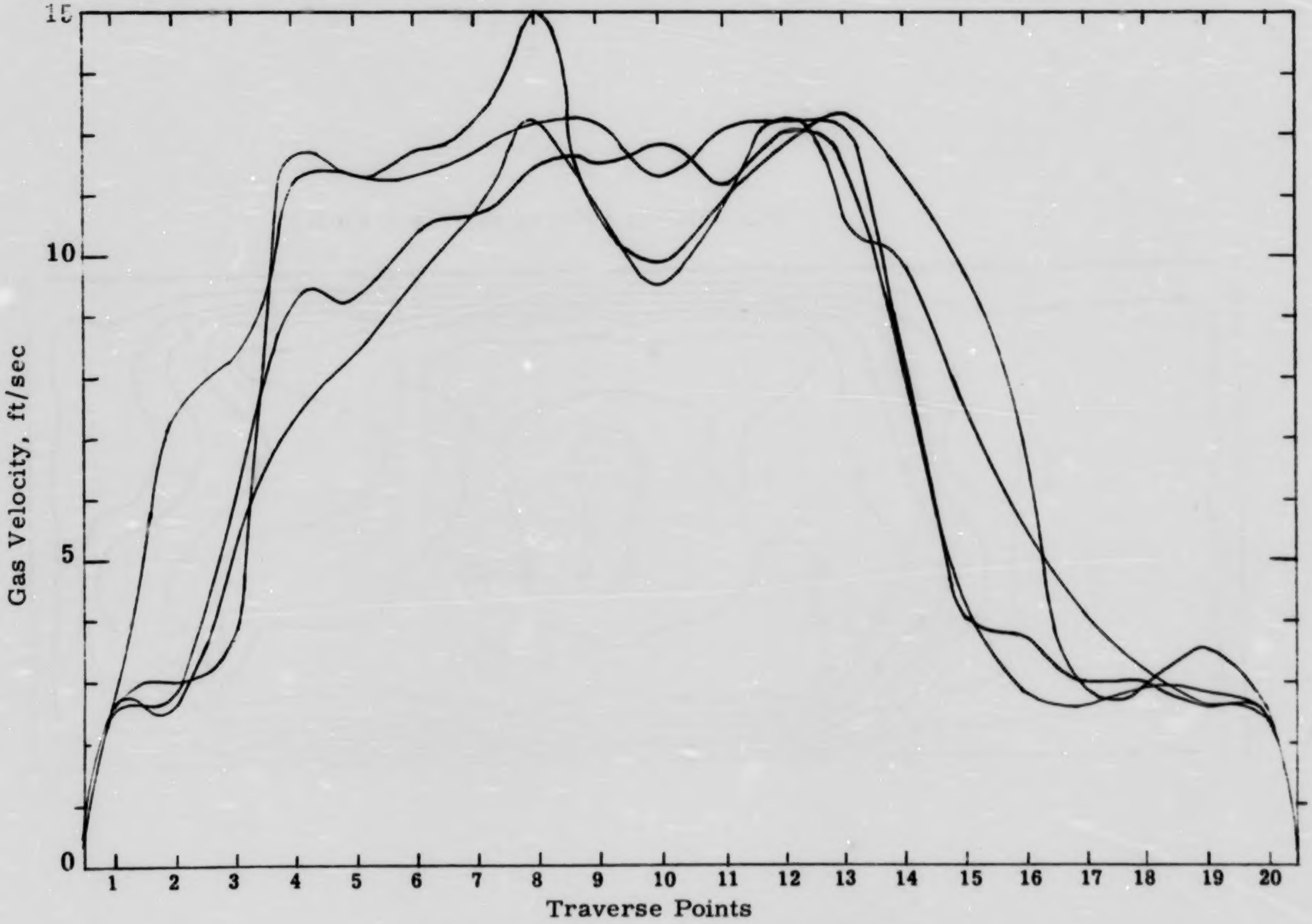

Figure 5.3. Gas Velocity Profiles.

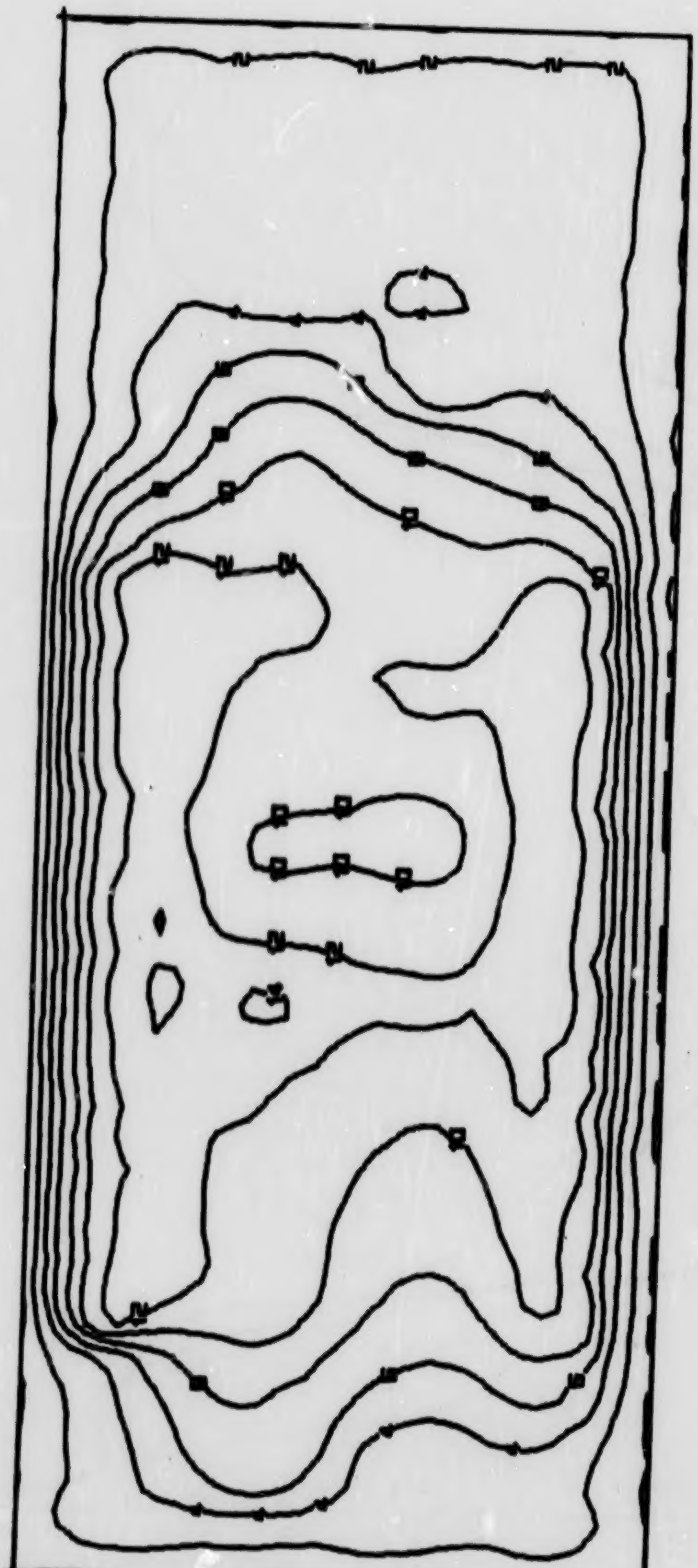

Figure 5.4. Gas Velocity Contour Plot.

and in determining the location and type of corrective measures to be taken. Note that the velocity at the walls in both these plots is zero.

In order to reduce the nonuniformity of the data on gas velocity to a single quantitative measure, statistical calculations can be made, or the ratio of the maximum velocity to the average velocity can be determined. Because the average velocity enters the electrostatic precipitation formula, the ratio of maximum velocity-to-average-velocity will give some measure of the degradation of efficiency due to nonuniform air flow. Alternatively, the ratio of the root-mean-square of the readings to the arithmetic average can be calculated. Both ratios would be 1.00 for perfectly uniform flow, but the maximum velocity-to-average-velocity ratio would be the larger of the two when the velocities are nonuniform.

The frequency of occurrence of velocities falling into a series of intervals can also be plotted, and thus a histogram showing the statistical velocity distribution can be constructed as shown in Figure 5.5. This curve and the data for the profiles and contour plots were taken from a particularly poor velocity distribution cited by White in Industrial Electrostatic Precipitation.[4] The two peaks indicate extremely bad distribution. A good distribution should approximate a Gaussian or normal distribution in the core of the gas flow, with a tendency to skew somewhat toward zero because of the wall friction. The narrower the spread of the distribution, the better the uniformity. Statistically, the spread is measured by the standard deviation, the root-mean-square of the sum of the deviations from the average. The standard deviation of the example shown is about 50% of the average velocity. No references were found giving examples of the standard deviation to be expected for good distribution, but the Industrial Gas Cleaning Institute recommends 85% of local velocities within ±25% of the mean, and no single reading more than ±40% from the mean as an acceptable criteria. This set of conditions corresponds to a standard deviation of about 23% of the average velocity.

Note that it is impossible to achieve a completely uniform velocity distribution in a practical duct system. There will be zero velocity at the wall of the ducts and there will be random variations due to turbulence in the core of the flow. A practical goal, then, must be to achieve a nearly uniform gas flow using the best duct design procedures in the present state-of-the-art plus field corrective measures as required. Present practice is to use models constructed of plastic or hardboard from 1/4 to 1/6 scale of the full-size plant to determine a practical design. Field corrections are used as a last resort.

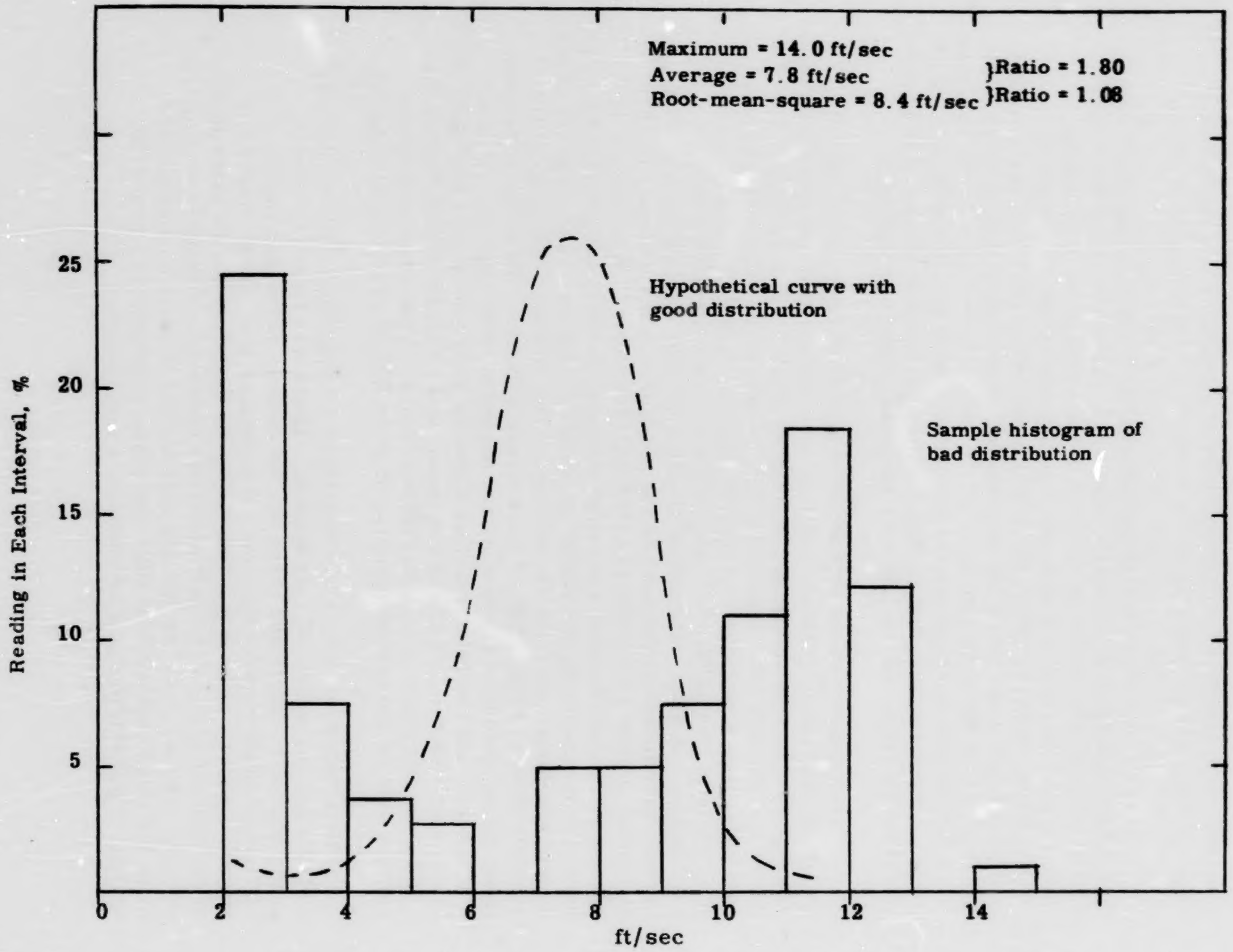

Figure 5.5. Histogram Showing Statistical Velocity Distribution.

To achieve uniform flow in a duct according to ASME test procedures, one should have at least ten diameters of duct before and after any disturbance such as the elbow, expansion or contraction. In practice, such conditions cannot always be economically realized because of space limitations and the high cost of ducts in the sizes involved. However, given a reasonable space, it is possible to approach an acceptable quality of flow at the precipitator inlet by the use of straighteners, splitters, vanes, and diffusion plates.

5.2 STRAIGHTENERS

Partitions in a straight section of duct for the purpose of eliminating swirl are called straighteners. They may be "egg crate" dividers or nested tubes as shown below:

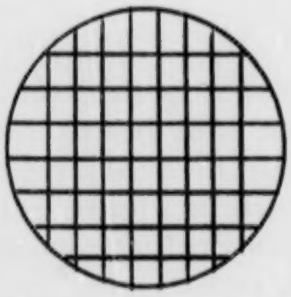

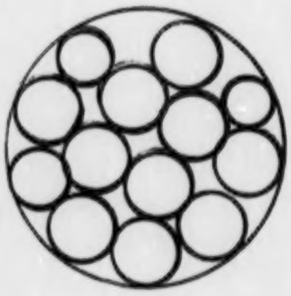

A straightener will reduce the angle of a helical flow path to some angle less than that defined by arc tan $= \frac{\text{length}}{\text{spacing}}$. The nonuniformity in the velocity in the axial direction will not be reduced. The scale of turbulence, or eddy diameter, will be temporarily reduced to the same size as the spacing of the straighteners, but because the Reynolds number is usually well above critical, the eddies will not die out, but will grow until they again reach the order of magnitude of the full duct. It is theoretically possible to make the spacing of straighteners small enough to obtain a Reynolds number less than critical and to obtain laminar flow through the straighteners, and to obtain nearly absolute uniformity. Unfortunately, such spacing would only be about the size of soda straws and the straightener would be expected to plug up with dust almost immediately.

A recommended straightener, according to AMCA Bulletin 210,[5] is an egg crate with a spacing of 7-1/2 to 15% of the diameter of a round duct or the average side of a rectangular duct, and with a length equal to three times the spacing. This reduces the swirl angle to arc tan 1/3 = 18-1/2°. An alternate straightener is a simple criss-cross at least one and a half diameters long. The loss in these straighteners is equal to the loss in four plain duct diameters. If it is necessary to reduce the swirl angle to smaller values, the ratio of length to spacing must be increased, and the resulting friction will be higher.

5.3 SPLITTERS

A duct section that changes size or direction may be divided into smaller ducts over the full length of the change by partitions called splitters. Splitters may be used in elbows where direction is changed, or in transformations where velocity is changed. Splitters add wall friction, but can reduce total friction by optimizing velocity pressure losses.

Losses in elbows depend in part on how sharp the bend is. A square, or mitered, elbow will have a loss of 1.25 times the velocity pressure, but an elbow of optimum configuration could have a loss of only 0.11 to 0.14 velocity pressure. As shown in Figure 5.6, the optimum configuration is an elbow with a ratio of inside radius to outside radius of about 0.66 for a square duct, or 0.7 for a round duct.[2]

To design a splitter elbow, therefore, it is only necessary to divide the given elbow into segments all having a radius ratio of about 2/3.

5.4 TRANSFORMATION SPLITTERS

Splitters may also be used in a diverging duct transformation to divide the flow into nearly equal parts and then distribute the flow to the larger section:

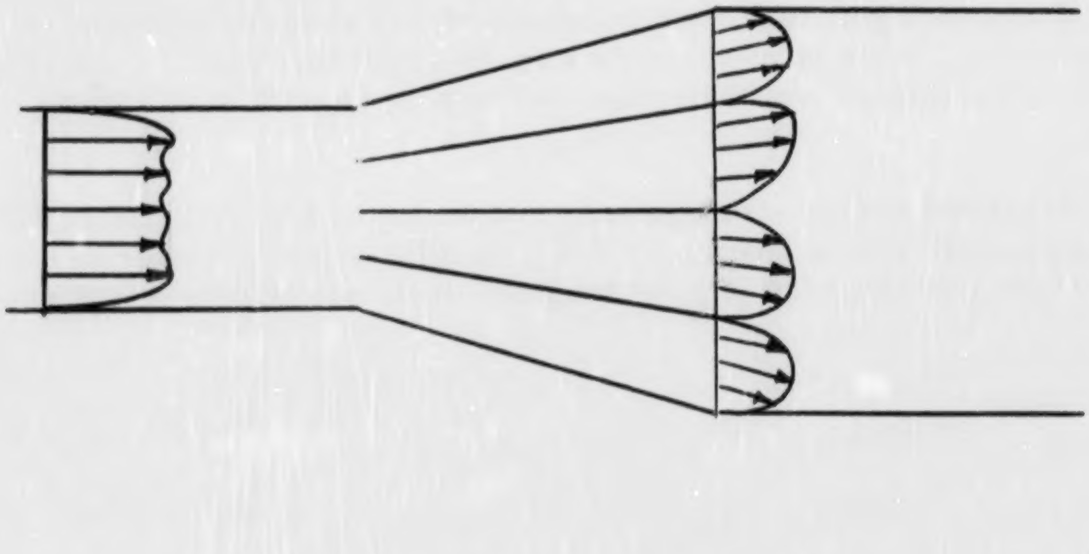

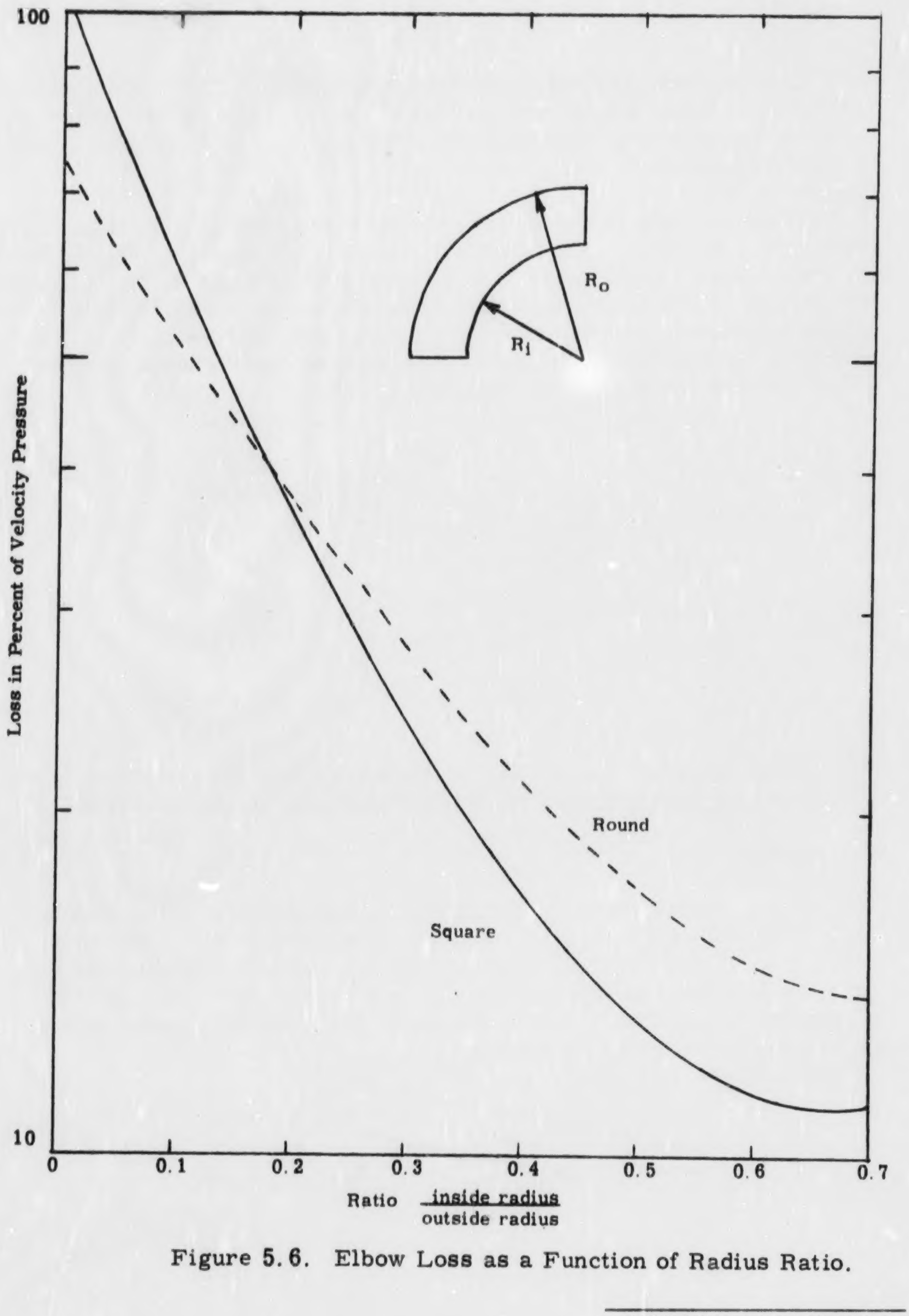

Figure 5.6. Elbow Loss as a Function of Radius Ratio.

The gas flow will not be uniform within each segment of the transformation section, but the volume through every segment can be made equal to that in every other segment if the splitters are manufactured to be field adjustable.

A sharp angle in the transformation causes the gas to separate from the walls of the duct, introducing turbulence and nonuniform flow. The maximum angle of divergence for no separation is about 7° included angle. Therefore, splitters in a transformation should be selected to have 7° to 10° included angle between successive splitters. For example, a transformation with 60° included angle could be split into 8 channels with 7-1/2° spread, or 6 channels with 10° spread:

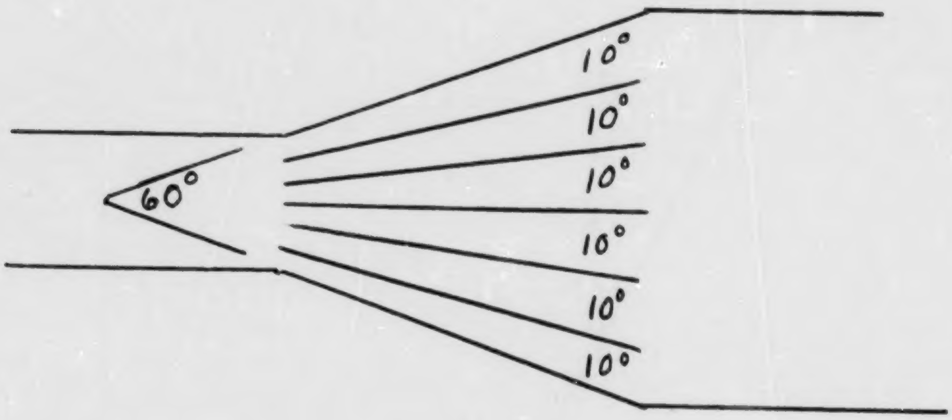

Note that a transformation in one direction is the simpler. Transforming in two directions would require pyramidal splitters.

5.5 VANES

Another kind of deflector for redirecting gas flow is the turning vane. Turning vanes are flat, bent, or curved plates which are short relative to the duct section in which they are installed, as opposed to splitters which extend the full length. A plain flat plate vane used to deflect the air stream is partly effective, but it tends to increase turbulence as shown in the sketch:

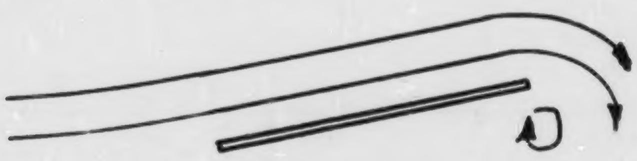

The low pressure area behind the plate also tends to pull the gas flow back toward its original path.

Curved turning vanes in an elbow can be quite effective if they are spaced to give about a 6:1 aspect ratio and a 2/3 radius ratio, and are streamlined to give constant cross section through the turn.

The streamlined turning vanes shown in Figure 5.7 will preserve the flow pattern and will have a loss of about 10% of the velocity pressure. A set of single thickness turning vanes will also preserve the flow pattern, but will have about 35% velocity pressure loss and may introduce some turbulence because of the unequal cross sections between them. Single thickness vanes should have a straight extension downstream with length about twice the spacing. In practice, single thickness turning vanes are generally used because of cost considerations.

For rectangular elbows, one parameter is the aspect ratio, or the ratio of the depth of the elbow measured parallel to the axis of the bend to the width of the elbow measured in the plane of the bend:

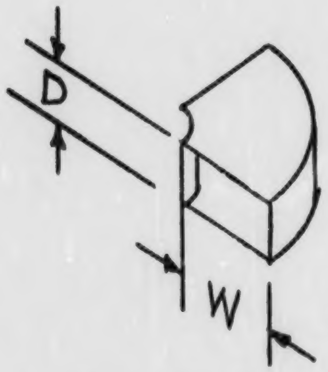

"Hard" Bend

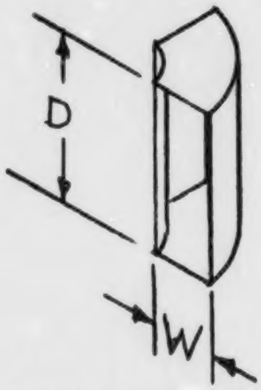

"Easy" Bend

It is intuitively obvious from the sketches that a low aspect ratio elbow is a "hard" bend with high pressure loss which has very nonuniform flow caused by inertial forces. Any aspect ratio greater than unity will make a fair elbow, but aspect ratios from 4 to 6 are recommended.

Turning vanes are also used in transformation elbows; that is, elbows that change cross section between inlet and outlet. Although the combination of elbow and transformation is relatively poor design practice, severe space limitations may force it upon the designer. If a transformation elbow must be used, then turning vanes are essential,

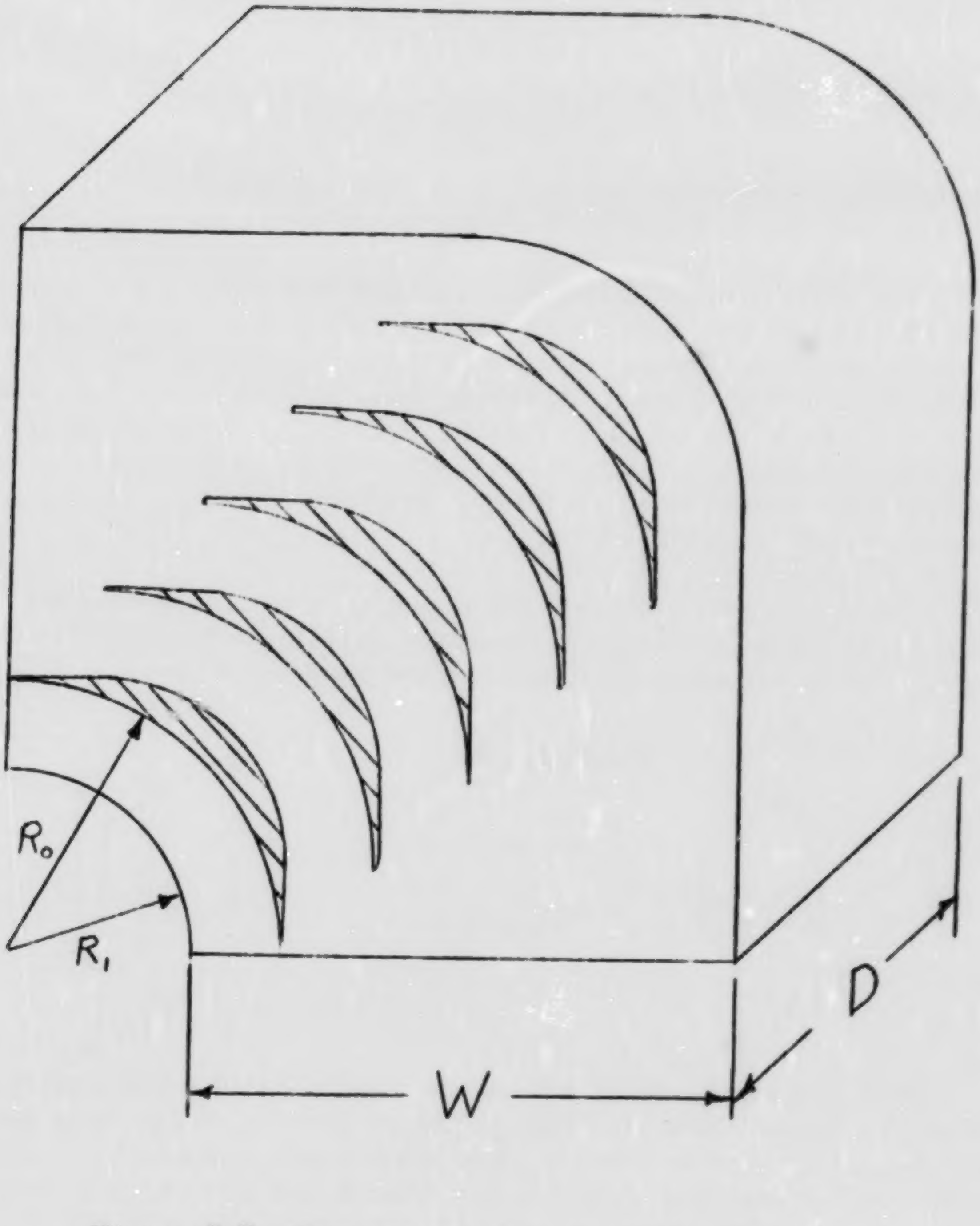

Figure 5.7. Streamlined Turning Vane Elbow.

and they must be closely spaced to about the same spacing as the precipitator plates. They must also be followed by additional flow rectification means such as diffusion plates.

5.6 DIFFUSION PLATES

Diffusion plates, or screens, are simply perforated plates or wire screens which improve the uniformity of air flow by a combination of effects. First, they reduce the scale of turbulence from the order of magnitude of the duct to the order of magnitude of the holes. Of course, the kinetic energy that existed in the large scale eddies will reappear in the small scale eddies, but the large differences in velocity will be reduced. Second, there is a pressure drop across the screen and a reduction in area. The pressure drop will partly reappear as a velocity vector perpendicular to the plate. This vector added to the original velocity vector will give a resultant velocity always more nearly perpendicular to the plate:

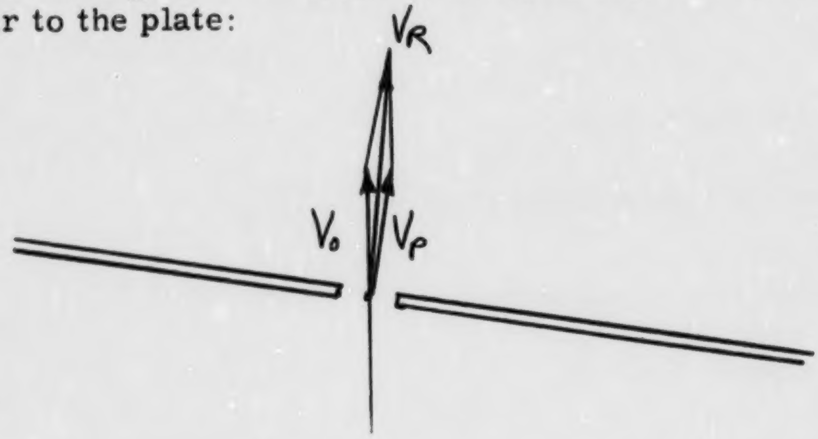

Thus, it might be possible to design a diffuser plate to turn the gas stream through a precise small angle. However, in practice, it is usually simpler and less costly to use two or more diffusion screens in series to achieve a fair degree of uniformity.

Perforated plate screens break the gas stream up into a multiplicity of small jets with high turbulent intensity and small scale of turbulence. These jets eventually coalesce downstream. The turbulent intensity reaches a peak at 2 to 3 mesh lengths (center to center of holes) downstream and declines exponentially thereafter. The scale of turbulence is of the order of the hole size at the screen and increases until it reaches the size of the duct. There is a critical parameter of 50%

open area for diffusion screens. When the percentage of open area is less than 50%, the jets seem to be too far apart to coalesce uniformly and the screen introduces nonuniformity. When the percentage of open area is between 50% and 65%, the jets appear to coalesce within 5 to 10 mesh lengths (center to center of holes) with improvement in uniformity.[6]

Screens may be used in series to provide greater uniformity at the cost of larger pressure drops. Dryden and Schubauer[7] developed the following relationship for the reduction in turbulent intensity:

$$r = (1 + k)^{-\frac{1}{2}n},$$

where

r = reduction factor

k = pressure drop coefficient = $\frac{\Delta p}{\rho v_o^2/2}$

n = number of screens in series

Δp = pressure drop

ρ = density

v_o = average velocity.

All of the preceding ductwork design techniques are available to the designer. None of the criteria are rigid, so there is considerable freedom in design. It is the designer's choice as to whether to use splitters, turning vanes, or screens to control the air distribution. On the inlet side of a precipitator, there may be a heavy dust loading of particle sizes large enough to settle out. Horizontal splitters or vanes form convenient shelves for the deposition of disastrous quantities of dust. Therefore, horizontal splitters and vanes are generally used only when the velocity is higher than the erosion velocity of deposited dust. Dust will collect by impaction on the diffusion screens, so some means of cleaning then is required, such as regular rapping or soot blowing.

The pressure drop through a screen at large Reynolds numbers depends on the coefficient of contraction of the jets formed by the gas flow through the openings:

$$k = \frac{\Delta p}{\rho v_o^2/2} = \left(\frac{1}{C_c(1 - s)} - 1\right)^2$$

C_c = coefficient of contraction

s = solidity ratio

(1 - s) 100 = percent open area.

The coefficient of contraction depends on whether the holes are sharp edged, or round edged, whether the screen is made of non-coplanar bars, on the thickness of the plate, and on the accuracy of manufacture. The best procedure is to measure the pressure drop for the actual screen to be used. Alternatively, use values of the coefficient of contraction as reported in the literature:

For sharp edges, C_c is about 0.62.
For round edges, C_c equals unity.
For thick plates (more than 2-1/2 times hole diameter), C_c is unity.

Other values lie between 0.6 and 1.0.

The design criteria for diffusion screens are summarized below:

(1) Open percent area should be between 50% and 65%.

(2) Screens in series must not be closer than 5 to 10 mesh lengths apart.

(3) Hole size must be large enough to be unlikely to become plugged with dust, but small enough to reduce the scale of turbulence as much as possible. Sizes from 1 to 2 inches in diameter are reported.[4]

(4) Screens should be oriented to refract the gas stream toward the desired direction.

5.7 MODELLING

Because of the difficulties in the design of ducts for large size precipitation installations, the use of models for air flow studies is almost universally practiced. The models usually consist of sheet acrylic plastic or pressed hardwood constructed to be geometrically similar to the full scale system. The models are used to obtain a visual pattern of the gas flow by the injection of smoke streamers or by the placement of yarn tufts in the air stream. Quantitative measurements are made with pitot tube traverses or thermoanemometers. A visual evaluation of the particulate drop-out characteristics of the system can be made by the introduction of dust into the gas stream. An evaluation of the erosion of deposited dust can be made by placing a layer of ground cork on the bottom of the duct before starting the blower.

Information from model studies can be presented in the form of photographs of smoke streamers, yarn tuft deflections, and cork erosion patterns. Data on nonuniformity of gas flow can be presented in the form of plots of velocity profiles or velocity contour diagrams.

Modelling has been practiced for many years in designing air flow systems. Early work was done at scales of 1/4 or 3/8 size with the Reynolds number held substantially constant. Because of the increasing size of modern installations, the trend has been toward the use of models constructed to 1/16 scale. Whereas models can give a considerable amount of valuable information on velocity distribution, dust fallout patterns, and static pressure loss, they do not necessarily accurately reflect the actual velocity distribution in a full size unit, and a small scale model may be less accurate than a larger scale model. The results of models in part depend on such factors as the fidelity of the model and the skill of the investigator.

In the theory of modelling fluid systems, certain dimensionless parameters should be made equal in the full size system and in the model. There are as many dimensionless numbers as there are fundamental dimensions in the physical system. Therefore, if some of the physical parameters are arbitrarily chosen or fixed by the nature of the fluid, it becomes impossible to hold all the dimensionless numbers constant. The dimensionless numbers in fluid flow depend on the ratio between the important physical parameters as follows:

$$(1) \quad \frac{\text{Inertial force}}{\text{Viscous force}} = \frac{\rho v L}{\mu} = \text{Reynolds Number}$$

$$(2) \quad \frac{\text{Inertial force}}{\text{Gravity force}} = \frac{v^2}{Lg} = \text{(Froude's Number)}$$

(3) $$\frac{\text{Inertial force}}{\text{Pressure force}} = \frac{v^2}{v_c^2} = (\text{Mach's Number})^2$$

(4) $$\frac{\text{Acceleration force}}{\text{Inertial force}} = \frac{\Delta p}{\frac{1}{2} v^2} \quad (\text{Euler's Number})^2$$

Note that within the electric field of the precipitator an "electrical" Froude's Number can be defined:[8]

$$\frac{\text{Inertial force}}{\text{Body force}} = \frac{\rho v^2}{6 \pi N a \mu w L}$$

Symbols in the above are as follows, in consistent units:

ρ = density

v = velocity

L = linear characteristic dimension

μ = viscosity

g = gravity

v_c = velocity of sound in the fluid

N = number of dust particles per unit volume

a = radius of dust particles

w = migration velocity

Δp = pressure gradient.

In equipment the size of industrial electrostatic precipitators, the flow nearly always has a high Reynolds number and is in the turbulent regime. Theoretically, for testing in a model, the Reynolds number in the model should be exactly the same as in the full scale unit. Unfortunately, this is usually impractical. For example, to make a $\frac{1}{16}$ scale model of a system having air at 300°F in a duct with a characteristic dimension of 16 feet, and using room air for the model fluid, the Reynolds number for the system must be equated to the Reynolds number for the model:

$$R_e = \frac{\rho_0 \, v_0 \, L_0}{\mu_0} = \frac{\rho_0 \left(\frac{460 + 70}{460 + 300} \right) v_1 \frac{L_0}{16}}{\mu_0 \, (1.33)}$$

Note that the density and viscosity at 70°F have been replaced by a temperature correction factor times the values.

Simplify

$$v_0 = \frac{530 \times v_1}{760 + 1.33 \times 16} = \frac{v_1}{30.515}$$

Solve:

$$v_1 = 30.5 \, v_0 .$$

Therefore, to maintain the Reynolds number constant, the velocity in the model should be 30.5 times as high as in the system. If the system were to be run at 10 ft/sec, then 305 ft/sec would be required in the model, or about 27% of the speed of sound. Thus, the model would have a Mach number of 0.27 where the system would have Mach number about a tenth as much and the model would not be dynamically similar. Similarly, if the actual system velocity were 50 ft/sec, the model flow would be supersonic. If the scale ratio were to be 1/4 instead of 1/16, the situation would be better by a factor of 4, even if still theoretically incorrect.

Because the main problem in ductwork design for electrostatic precipitators is to achieve uniform gas distribution, unrealistically high velocities in the model are not recommended. Also, the actual velocity distribution from the upstream equipment cannot be fully known or duplicated because of the effects of temperature and density variations and of the effects of the presence of dust. Dust changes the density and viscosity of the gas slightly; dust tends to deposit on the walls, splitters, and vanes by settling or impaction and changes the roughness parameter or even the size and shape of the ductwork. The only system that perfectly models a given system is the system itself. This is the one reason why field engineering may be required to rectify the gas flow distribution if the system was modelled.

This is not to say that models should not, or need not, be used. In fact, models are essential for difficult duct configurations. A more important reason to conduct model studies is to investigate the gas flow pattern expected in the commercial installation. Poor gas flow conditions may cause severe dust reentrainment that can result in the precipitator performance falling far short of design expectations.

The calculation of the pressure losses of a complicated system with nonuniform gas flow may be impossible. A model will give a conservative estimate of the pressure loss provided the roughness parameter and the Reynolds number are properly duplicated. Note on Figure 5.1, which plots friction against Reynolds number for various roughness numbers, that in the "wholly rough zone", the friction is essentially constant. Therefore, the friction will be correct if the Reynolds number is high enough, even though it is not correct for theoretical similarity.

In those cases where severe space limitations force the designer to violate all the criteria for good air flow, it would be highly desirable to use a model to make the air flow distribution as good as possible under the circumstances. Note, however, that the scale of turbulence in any duct is of the order of magnitude of the scale of the duct, so that the size of eddies in the model will be much smaller than the size of eddies in the full size system. It can be expected, and it has been shown,[8] that the gas flow distribution in the full size system will be worse than in the model, and the smaller the scale of the model, the greater the deviation.

In the cited reference, an air flow distribution with the ratio of maximum velocity to average velocity of about 1.20 was obtained in the model, but the full scale unit had the maximum velocity about 1.40 times the average. Experience built up over a long period of time is required before one would have any real confidence in scaling up from models having a very small scale factor such as $\frac{1}{16}$ to 1 and smaller. An example of successful modelling with this scale factor is reported by Burton et. al.[9]

In general, the recommended plan would be to design good duct work with field adjustable vanes and splitters whenever possible. When poor duct work is required because of space limitations, a model study is absolutely essential, with a safety factor included as determined by experience. Careful field adjustments by competent people will then provide a reasonable probability of acceptable operation.

CHAPTER 5
BIBLIOGRAPHY

1. ASHRAE Handbook of Fundamentals, American Society of Heating, Refrigerating, and Air Conditioning Engineers, Inc. (1967).

2. Fan Engineering, Sixth Edition (1961) Buffalo Forge Company.

3. Remmers, Karl and Bingel, Rolf, "The Importance of Gas Distribution in Electrostatic Precipitators," Staub **19**, 422 (Dec. 1959).

4. White, H. J., Industrial Electrostatic Precipitation, Addison-Wesley Publ. Co., Reading, Massachusetts (1963).

5. AMCA Bulletin 210, "Standard Test Code for Air Moving Devices," Air Moving and Conditioning Association, Detroit, Michigan (1960).

6. Baines, W. D. and Peterson, E. G., "An Investigation of Flow Through Screens," ASME Trans. (July 1961).

7. Dryden and Schubauer, "The Use of Damping Screens for the Reduction of Turbulence," J. of Aero. Science **14**, No. 4 (1947).

8. Opfell, J. B. and Sproull, W. T., "Limitations of Model Studies in Predicting Gas Velocity Distribution in Cottrell Precipitators," I and EC Proc. Des. and Dev. **4**, No. 2 (April 1965).

9. Burton, C. L., et al., "Application of Model Studies to Industrial Gas Flow Systems," Am. Soc. Mech. Engrs. Ann. Mtg., Atlantic City, New Jersey, Nov.-Dec. 1959, Paper 59-A-280, 9P (1959).

CHAPTER 6
RAPPING AND REENTRAINMENT

6.1 RAPPING

After collection of the dust on the collection electrode, it must be removed from the system. This is accomplished by washing or flushing the plates in the case of a wet collection electrode, or by impacting or rapping in the case of a dry collection system.

The successful removal of dust from a precipitator by rapping depends upon the formation of a coherent dust so that on removal, it falls in sheets and large agglomerates into the hoppers. The adhesive and cohesive forces acting on the dust layer are electrical, mechanical, and molecular in nature, and influence the difficulty of dislodging the dust from the electrode, as well as reentrainment of the dust during the rapping process.

Within the collected dust layer, the forces acting on the particles are the cohesive forces due to adsorbed gases on the surface, mechanical forces due to interlocking of the particles and interparticle friction, Van der Waal's forces due to proximity of adjacent particles, and electrical forces.

One component of the electrical force is generated by the ion current flow to the dust layer. The magnitude of the net electrical force is given by Lowe and Lucas[1] as:

$$P_{el} \approx d^2 \left[k_1 E j \rho - \frac{E^2}{32} \right]$$

where

P_{el} = electrical adhesive force,
d = particle diameter,
E = electrical field strength,
j = current density,
ρ = specific electrical resistance,
k_1 = constant,
$k_1 E d^2 j \rho$ = proportion of Coulomb force due to ion current, and
$\frac{d^2 E^2}{32}$ = share of Coulomb repelling force caused by influence effects.

---

[1] Refer to the bibliography for this chapter.

If the dust resistivity is high, as in the case of fly ash, cement dust, etc., the net force will tend to cause the dust layer to adhere more tenaciously to the collection electrode, thereby increasing the rapping intensity required to dislodge it. Highly conductive dust, such as carbon black, tends to reduce the net electrical force.

A second component of the electrical retentive force is electrostatic in nature. If the particles are collected under the influence of an electric field as is the case here, the dipole moments of the individual particles will tend to align in such a manner that adjacent particles will be attracted by a coulombic force.

Fundamental studies of the adhesive forces on dust particles have been made by Davies,[2] Penney,[3] and others. In terms of practical precipitator operation, the forces will vary with the type, size, and condition of the dust, as well as its electrical properties.

Temperature of the gas and gas composition also influence the adhesive forces. When operating at temperatures below the dew point, the dust layer can become moist and extremely difficult to dislodge.

In practical precipitators, rapping is usually required on both the collection and discharge electrodes, although the problems of reentrainment are of no consequence in the case of the discharge electrode, due to the small quantities of dust involved. The considerations for dust removal are the same as those for the collecting electrode, since deposits can form on the discharge wire. However, the current density through the dust layer is larger than that through the dust layer on the collecting electrode by the ratio of the collecting surface area to the area of the discharge wire. Consequently, the electrical forces would tend to hold the dust more tenaciously to the discharge electrode than to the collection plate. These deposits can reach the point of serious impairment to precipitator efficiency if the discharge electrode rapping is inadequate.

Rapping systems for both collection and discharge electrodes can be of the impact or vibrator type. Impact rappers are normally actuated pneumatically, electrically, or by gravity, and can vary from a single blow to a rapid succession of impacts. The rapping cycle can be varied over a wide range depending upon the requirements of the precipitator. Vibrator types are generally motor-driven vibrators that shake the electrode support structure, and are often used on the discharge electrode in conjunction with an impact rapper on the collection plate.

The principal consideration in any rapping system is the magnitude of the forces required to dislodge the dust without mechanical damage to the electrodes or support structure, or causing excessive reentrainment. It is a general rule to rap just hard enough to dislodge the dust and keep the collected dust layer at an acceptable thickness. It is impractical to maintain the collecting electrode completely clean, since successful rapping is accomplished by removal of the dust in clumps or sheets. Dust thicknesses of $\frac{1}{2}$ to 1 inch prior to dislodging are usual. Figure 6.1 shows the results of several tests reported by the British Central Electricity Generating Board relating the acceleration required to dislodge dusts remaining on the collection electrode to a given thickness.

Some investigations have been made of the magnitude of the rapping blow required to achieve the desired rapping efficiency. Brandt and Heinrich[4] attribute the dust removal from the electrodes to the peak value of acceleration normal to the plane of the surface. Sproull[5] reports that the determining factor in dust removal is the acceleration imparted to the electrodes and that it varies with type of dust, whether the electrode is rapped in the plane of the electrode (shear) or perpendicular to the plane (normal). Figures 6.2 and 6.3 show the accelerations required for shear and normal rapping for several dusts and various temperatures. As shown on the curves, acceleration of the order of 100g's may be required for 90% removal of the collecting electrode dust for rapping normal to the plate, and 200g's for rapping in the plane of the electrode for difficult-to-remove dust. For fly ash and easier-to-remove dusts, the accelerations required are considerably less — of the order of 10-30 g's.

The efficiency of rapping, measured in terms of residual dust, is in general improved if the power is removed during the rap as indicated in Figure 6.2. This is due to the removal of the corona current and the reduction of the force holding the dust layer to the plate. Since this force is dependent on resistivity, its magnitude will vary for different types of dust and the requirement for power-off rapping will depend on the dust characteristics. Power-off rapping is usually resorted to in the event normal rapping practice is inadequate. It is to be recognized that the portion of the precipitator that is in operation during rapping will not be collecting material and stack puffs may result.

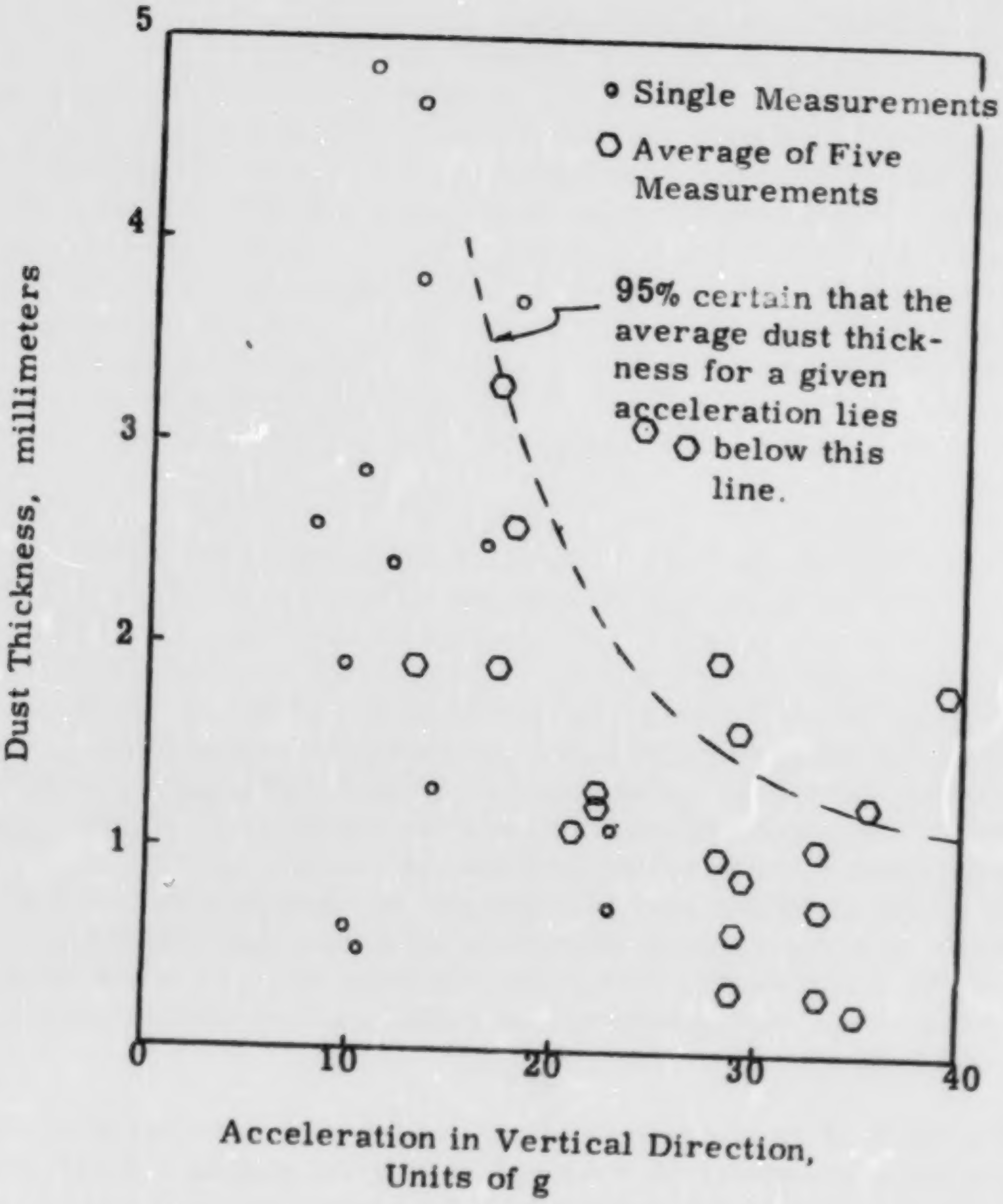

Figure 6.1. Acceleration to Remove Dust Down to a Given Remaining Thickness for Fly Ash in British Installations.

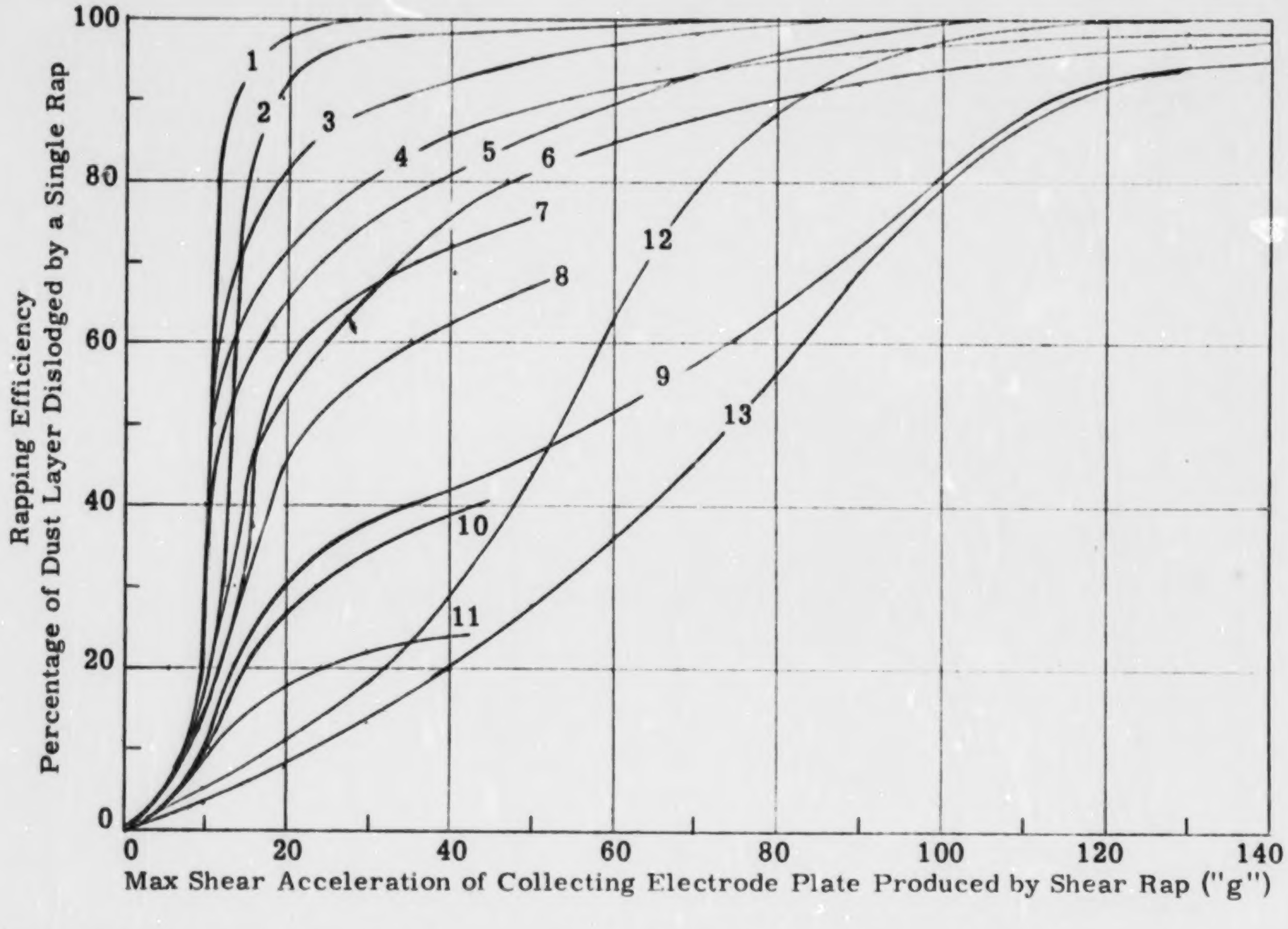

Figure 6.2. Shear (parallel) rapping efficiency for various precipitated dust layers having about 0.2 gram of dust per square inch, as a function of maximum acceleration in multiples of "g." Curve 1, fly ash, 70 to 300°F, power off. Curve 2, fly ash, 300°F, power on. Curve 3, fly ash, 200°F, power on. Curve 4, cement kiln feed, 70°F, power off. Curve 5, same as 4, except at 300°F. Curve 6, same as 4 and 5, except at 200°F. Curve 7, cement dust, 300°F, power off. Curve 8, same as 7, except at 200°F. Curve 9, cement kiln feed, 200 or 300°F, power on. Curve 10, cement dust, 300°F, power on. Curve 11, same as 10, except at 200°F. Curve 12, fly ash, 70°F, power on. Curve 13, cement kiln feed, 70°F, power on.

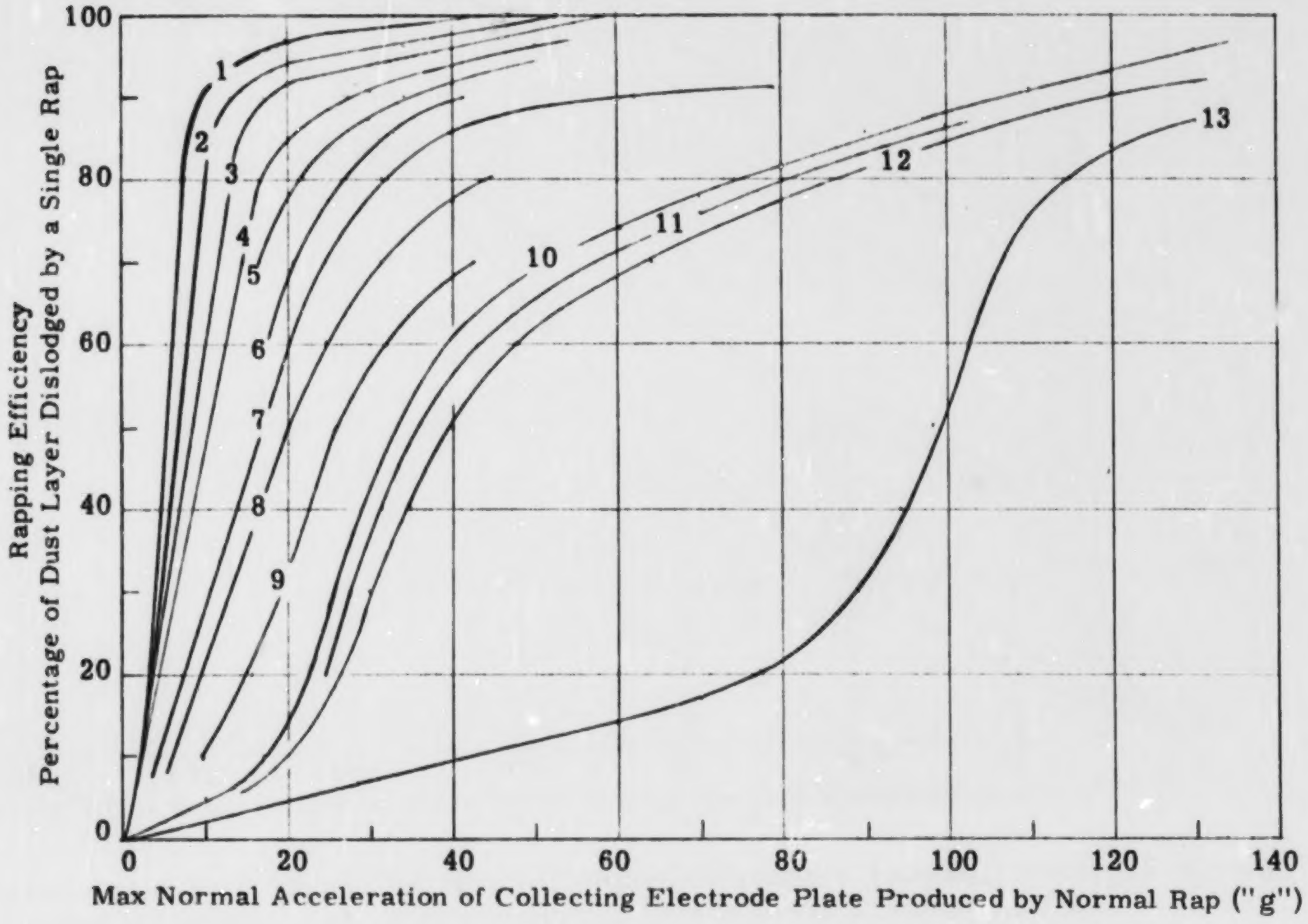

Figure 6.3. Normal (perpendicular) rapping efficiency for various precipitated dust layers having about 0.2 gram of dust per square inch, as a function of maximum acceleration in multiples of "g." Curve 1, fly ash, 200 or 300°F, power off. Curve 2, fly ash, 70°F, power off; also 200 or 300°F, power on. Curve 3, fly ash, 70°F, power on. Curve 4, cement kiln feed, 300°F, power off. Curve 5, cement dust, 300°F, power off. Curve 6, same as 5, except power on. Curve 7, cement kiln feed, 300°F, power on. Curve 8, cement dust, 200°F, power off. Curve 9, same as 8, except power on. Curve 10, cement kiln feed, 200° F, power off. Curve 11, same as 10, except at 70° F. Curve 12, cement kiln feed, 200° F, power on. Curve 13, cement kiln feed, 70° F, power on.

One problem encountered in dry dust removal is reentrainment of the dust during rapping. Because of the height of the plates is often 30 ft or more, it is apparent that some dust will be reentrained as it falls through the passage to the hoppers. This gives rise to a rapping "puff," which is often visible in the plume during the rap. To minimize this effect, rapping is done in stages with only a portion of the plates rapped at one time. Various collecting electrode shapes are also used in an effort to shield the falling dust from the gas stream, thereby minimizing reentrainment.

There are many variations possible in rapping practice depending on the particular installation and process. If parallel units are used, the gas flow can be directed by dampers during rapping so that there is no gas flow through the unit. Where the dust load is intermittent, as in the case of a basic oxygen furnace, it is possible to eliminate rapping of the plates. Following the oxygen blow, when the dust load is reduced, the draft fan can be shut off and the plates rapped.

The accelerations required to maintain a given rapping efficiency are those at the plate itself and the design of the rapping system should include consideration of the rigidity of the supporting members and the electrode, and their ability to transmit the impact to all areas of the electrode. Recent studies of operating precipitators in Europe have shown that accelerations measured on the collection electrode are as low as 5 g's, whereas minor changes in the method of applying the blow could yield accelerations of 30-50 g's. The latter range appears adequate for most fly ash precipitators.

Although it has been recognized that rapping is more than just a minor adjunct to precipitator operation, there is a conspicuous lack of experimental data that defines the conditions required to effectively remove the types of dusts encountered. There are reports of inability to dislodge high resistivity dust by rapping, and there is no experimental verification of the rapping requirements as a function of dust resistivity. Also, there should be some measure of the reentrainment tendency for various dusts as related to particle size, specific gravity, particle configuration, and quality of gas flow.

6.2 REENTRAINMENT

Particles on a dust surface at the boundary of a gas stream are transported by suspension, by saltation (repeated rebounding), or by "creep."

A compact layer of settled dust will not move until the least secure surface particle is dislodged by the drag force of the gas velocity, by impaction by another particle, or by the explosive impact of electric sparkover, which also results in momentary disruption of power. When this particle again strikes the surface of the dust, it dislodges more particles and initiates a cascade of saltating particles. If an impacted particle is not ejected into the gas stream, it may be displaced a small distance downstream which is the motion described by Bagnold[6] for dust held by gravitational forces. If the force due to gravity is replaced by the electrical force, the equation can be written as:

$$U^* = k_1 \frac{S_p - S}{S} \alpha a$$

where

U^* = threshold drag velocity,
k_1 = experimental coefficient,
S_p = density of particle,
S = density of gas,
α = acceleration on deposit (electrical force divided by mass), and
a = particle size.

Bagnold found the coefficient "k_1" to be constant for particles larger than 200 microns. Chepil[7] obtained the curve shown in Figure 6.4 for threshold drag velocity versus particle size. Note that the minimum drag velocity occurs around 60-100 microns and that the threshold is very high for very small particles such as might be found in electrostatic precipitator installations.

The initiation of erosion is strongly related to the adhesion of the dust layer. Adhesion depends in part on the history of the accumulation of the dust. If the dust layer accumulates essentially one particle at a time with sufficient freedom of motion and sufficient time for each particle to orient itself to the randomly situated positive and negatively charged areas on the dust layer and on itself, then the dust layer will have an adhesive strength an order of magnitude higher than the same dust piled in bulk.[8] The requirement for the formation of a layer thus held together by Coulomb forces is met by electrostatic precipitation and by sedimentation in low velocity zones in the ductwork. On the collection plate, however, additional forces due to

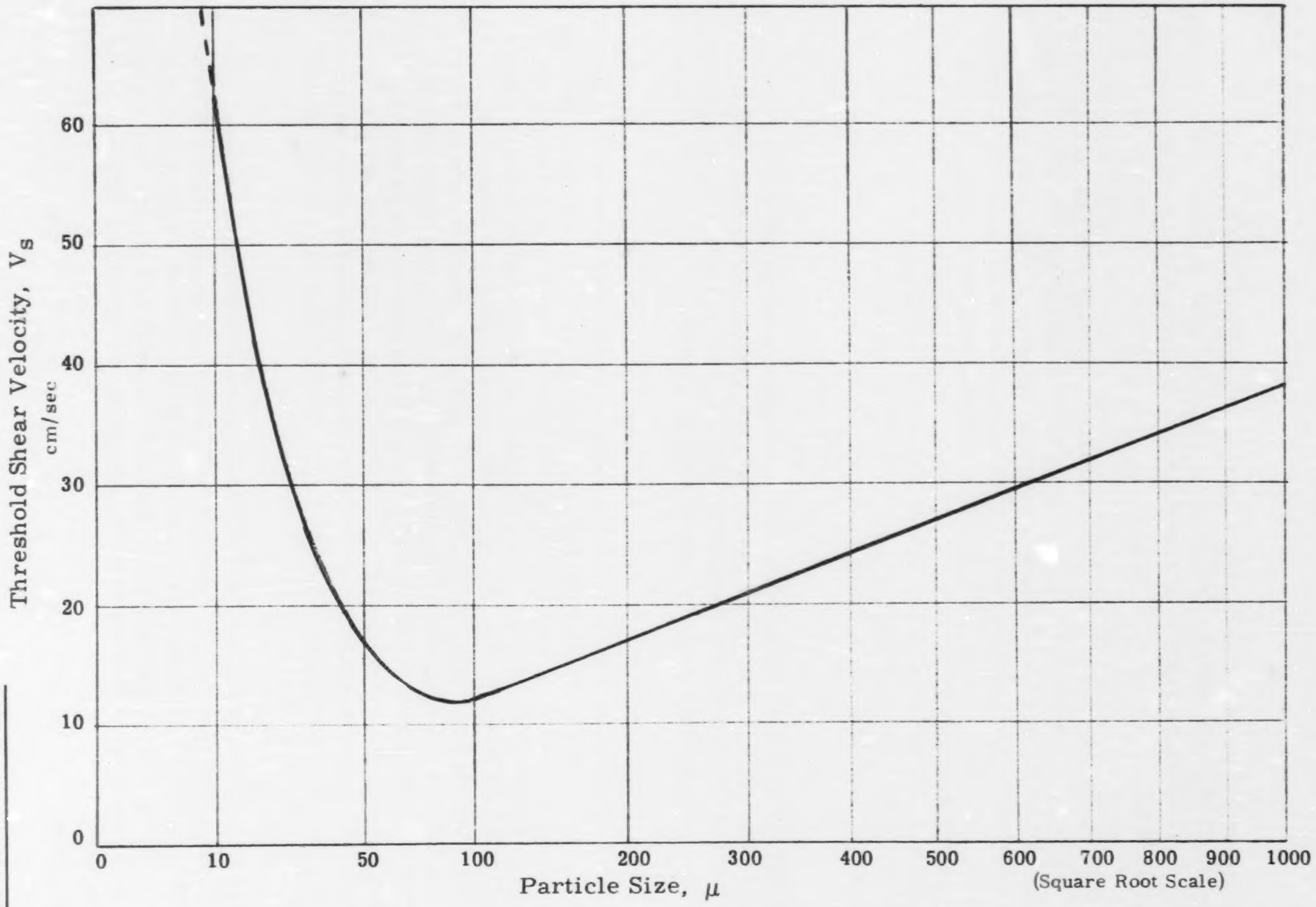

Figure 6.4. Threshold Shear Velocity Vs. Particle Size.

the ion current act on the dust layer. Loosely piled dust that results from rapping of plates, electrodes or diffusion screens does not meet the requirements for an adhesive layer, so a much lower velocity will erode such piles in the hoppers.

With particles larger than 100 microns, initiation of erosion can occur when the drag on one particle is enough to start a saltation cascade. A random gust of turbulence can initiate a cascade, so it is apparent that a uniform gas velocity with the least amount of turbulent intensity is highly desirable. With particles smaller than 100 microns, erosion will be initiated when the velocity exerts enough drag force on the edge of a discontinuity. Such discontinuities will exist as the results of slabs of dust falling off the plates through the action of rapping and gravity. As the slabs break up, agglomerates larger than 100 microns may occur, which can permit saltation to begin.

Erosion may also be initiated by the impact of large particles on the collected dust layer. The large particles have greater electrical migration velocities and therefore impact the deposit with greater momentum. The impact energy may be sufficient to initiate erosion.

Erosion can occur at any place that dust accumulates. Dust accumulation in the inlet ductwork does not necessarily result in carryover of dust from the precipitator, but it does result in alteration of the gas flow pattern, usually in the direction of greater nonuniformity of velocity and lower collection efficiency. Therefore, it is desirable to have a velocity in the ductwork high enough to prevent settling or high enough to erode away dust deposits. Dust accumulation in the hoppers is a required function of precipitators, so gas velocity in the hopper area must be below some critical velocity for loose unconsolidated dust. It is also important to prevent inleaks through the collection hopper discharge gates because the erosion velocity in this case is equal to the terminal settling velocity of the particles. Air in-leak through conveyors should be less than the critical velocity for loosely piled dust.

Erosion in the precipitator itself is important because it results in a direct loss of collected dust, and a direct reduction in collection efficiency. Sharp edges on the dust layer always exist because of rapping and gravity, and erosion can always occur if the local velocity is high enough. Control of uniformity of velocity and of the intensity of turbulence can hardly be overemphasized.

When the dust slab falls off the collection plate, some of the slab breaks up, and the dust becomes reentrained. It is a usual practice to limit the local gas velocity in the area of the falling dust by the use of pockets in the plate or baffles on the plate, perpendicular to the gas flow.

In addition to erosion due to wind velocity, there is some reentrainment of particles in a precipitator which can be called "electrostatic reentrainment". Particles which have a low resistivity can discharge their acquired electrical charge when they reach the collector plate. With no electrical force holding the particle to the plate, the particle may simply fall off, or be eroded by the wind or saltating particles. The particles may also acquire an induced positive charge and migrate toward the negative discharge wire. Reentrainment can also occur during sparking when a precipitator section is momentarily out of service.

The opposite problem to reentrainment can exist in some cases where the adhesion of the dust is extremely high. The dust cakes on the collector plates or the corona wires and even severe rapping may not dislodge all the dust.

Table 6.1 summarizes the different erosion situations that can exist in a system using electrostatic precipitation.

Note that there are many critical velocities for erosion:

(1) Threshold velocity for particles greater than 100 microns.
(2) Threshold velocity for sharp edged discontinuity on a compact dust layer.
(3) Threshold velocity for undisturbed compact dust layer.
(4) Threshold velocity for mechanically compacted dust.
(5) Threshold velocity for loose dust.

Furthermore, each of the above velocities will be different for every possible particle size distribution, as well as for different adhesion strengths induced by chemical, mechanical, and thermal conditions. Thus, no simple analytical method has been developed to predict erosion and reentrainment.

The cascade effect of saltating particles cannot increase without limit. Eventually, the number of particles ejected by impaction will equal the number of particles that become reembedded in the dust layer and do not bounce

Table 6.1

Erosion Situations

Location	Adhesion	Desired Velocity
Precipitated dust on corona wires	High	More than critical for compact dust
Precipitated dust on collector plates	High	Less than critical for compact dust
Settled dust in ductwork	High	Greater than critical for compact dust
Dislodged dust in hoppers	Low	Less than critical for loose dust
Dislodged dust in ductwork	Low	Greater than critical for loose dust
Dust in conveyors and air locks	Low	Less than critical for loose dust
Falling dislodged dust	Zero	Minimum practical

out again. The rate of erosion will therefore eventually reach a saturation value. The saturation point will be reached in a precipitator at some point downstream from the inlet. At the inlet, the erosion rate is necessarily zero, because there is no material collected at zero length.

Eroded material from one area of the collector will normally be recaptured downstream. The last section of the precipitator has no downstream collector, so that a constant erosion rate will result in a net loss of dust and a reduction in efficiency of collection. Robinson[9] has derived a modification of the usual efficiency equation

$$\eta = 1 - \exp\left(-\frac{A}{v_g} w\right)$$

to include the effect of erosion

$$\eta = 1 - \left(1 - \frac{\beta}{1-\alpha}\right) \exp\left[-(1-\alpha)\frac{A}{v_g} \chi w - \frac{\beta}{1-\alpha}\right]$$

where

α = mass of dust eroded per unit mass precipitated for normal dust,

β = mass of dust eroded per unit mass precipitated for "problem" dust (i.e., low resistivity dust that is repeatedly precipitated and reentrained with no change in concentration in the length of the precipitator),

χ = concentration uniformity factor, the ratio of the dust concentration near the wall to the average dust concentration over the cross section between precipitator plates,

A = collection area,

v_g = volume gas flow rate, and

w = migration velocity.

When $\chi = 1$ for uniform distribution and $\alpha = 0$, and $\beta = 0$, the modified equation reduces to the usual form. If $\beta = 0$, $\chi = 0$, and $\alpha = 0$, the equation reduces to an exponential form which could be expressed using an equivalent migration velocity.

CHAPTER 6
BIBLIOGRAPHY

1. Lowe, H. J. and Lucas, D. H., "The Physics of Electrostatic Precipitation," Brit. J. Appl. Phys. **24**, No. **2**, pp **40-47 (1953)**.

2. Davies, C. N., Aerosol Science, Academic Press, London-New York **(1966)**.

3. Penney, G. W. and Klingler, E. H., "Contact Potentials and the Adhesion of Dust," Communications and Electronics (July **1962**).

4. Heinrich, D. O., "The Cleaning of Collection Electrodes in Electrostatic Precipitators," Staub **22**, No. **9**, pp **360-364 (1962)**.

5. Sproull, W. T., "Fundamentals of Electrode Rapping in Industrial Electrical Precipitators," JAPCA **15**, No. **2**, pp **50-55** (Feb. **1965**).

6. Bagnold, R. A., The Physics of Blown Sand and Desert Dunes, Wm. Morrow and Co., New York City, pp **322-334 (1943)**.

7. Chepil, W. S., "Dynamics of Wind Erosion: II - Initiation of Soil Movement," Soil Science **60**, pp **397-441 (1945)**.

8. Niedra, J. M. and Penney, G. W., "Orientation and Adhesion of Particles," IEEE Trans. IECI **12**, No. **2**, p **46 (1965)**.

9. Robinson, Myron, "A Modified Deutsch Efficiency Equation for Electrostatic Precipitation," Atmospheric Environment, Pergamon Press I, pp **193-204 (1967)**.

CHAPTER 7
RESISTIVITY AND CONDITIONING

Resistivity of the collected particulate layer has a dominant influence on the operation of electrostatic precipitators. If the resistivity is greater than about 2×10^{10} ohm-cm, the electric field in the dust layer resulting from normal current densities will exceed the breakdown strength in localized areas, and excessive sparking and back corona may occur. Consequently, the high tension voltage and resulting corona current must be reduced, adversely affecting precipitator performance. If the resistivity is less than about 10^7 ohm-cm, the electrical force holding the dust deposit will be low, and excessive reentrainment can occur for certain types of dust.

There are two conduction mechanisms which determine the resistivity of the collected dust layer in an electrostatic precipitator. These mechanisms are termed volume conduction, which is related to the bulk composition of the material, and surface conduction, which depends on an adsorbed film on the particle surface and which is related to the composition of the gas and dust surface.

7.1 VOLUME CONDUCTION

In volume conduction, electric charge is transferred through the bulk material that comprises the collected dust layer. In most materials of interest in electrostatic precipitator applications, volume conduction occurs by means of electron carriers within the materials and is dependent upon the thermal excitation of the electrons in the molecular structure of the materials. It has been shown that for most industrial dusts and fumes, the relationship of volume conductivity and volume resistivity to temperature may be approximated by

$$\rho = C \exp\left(\frac{E_a}{kT}\right)$$

where

ρ = resistivity,
C = constant,
k = Boltzmann's constant,
T = temperature, and
E_a = Activation energy.

White[1] has shown that resistivities of dusts as measured in the laboratory follow the theoretical relationship between volume conduction and activation energies above about 250°F. Figure 7.1 shows the experimental relationship between resistivity and the factor $\frac{1}{kT}$ for a variety of types of materials. Figure 7.2 shows the quantitative relationship between resistivity and electron activation energies.

The influence of temperature on resistivity of collected dusts is shown in Figure 7.3. In the absence of moisture, the resistivity would continue to increase with decreasing temperatures due to the decreased electron excitation. Conversely, increases in temperature increase the thermal electron excitation resulting in decreased resistivity.

This decrease in resistivity at elevated temperatures is significant in many electrostatic precipitator applications which operate in the temperature range in which volume conduction is predominant.

7.2 SURFACE CONDUCTION

At gas temperatures below 300-400°F, surface conduction becomes the increasingly important mode provided ample moisture and other conditioning materials are present in the gas. Surface conduction depends on the presence of a conductive film of adsorbed material on the surface of the particulate which provides for transfer of the electric charge along the surface. If ample moisture is present in the flue gas, it will be adsorbed on the surface of the particles following the basic laws of adsorption. It has been calculated that the existence of a film 5 to 10 molecules thick on the

---

[1] Refer to the bibliography for this chapter.

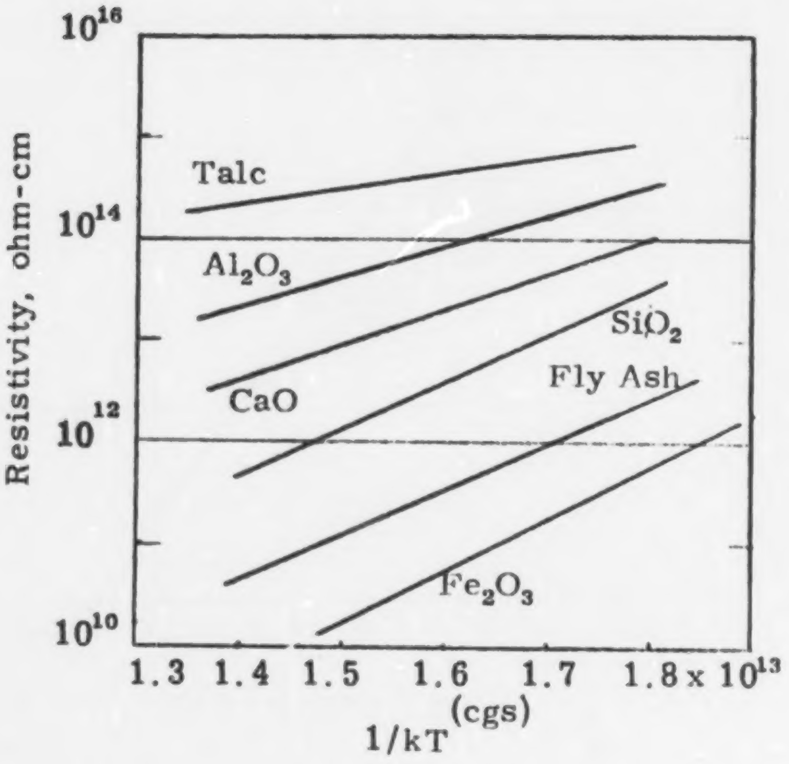

Figure 7.1 Plots of Resistivity Vs. 1/kT.

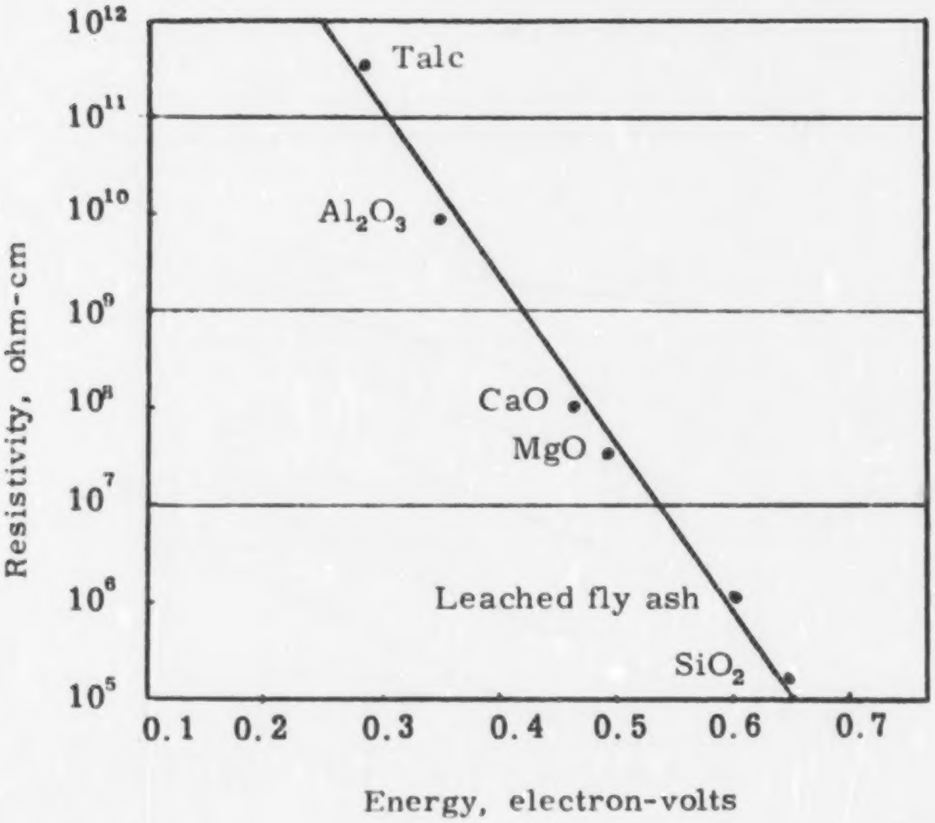

Figure 7.2 Experimental Values of Electron Activation Energy. (Reference 1)

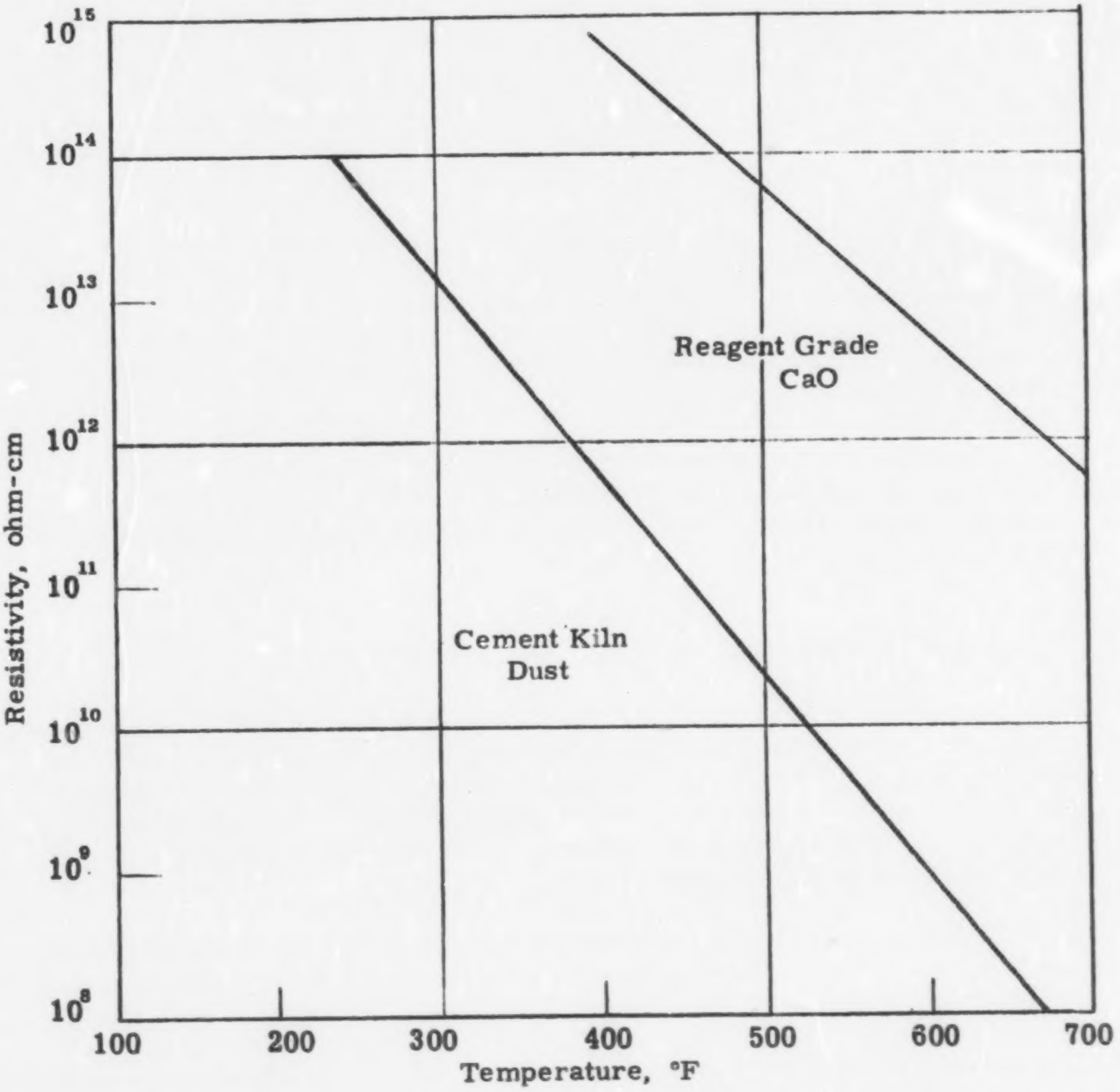

Figure 7.3 Resistivity of Bone-Dry Dusts at Elevated Temperatures.

surface is sufficient to explain the observed decrease in apparent resistivity of collected layers of particulate with increased moisture content. The effect of adsorbed moisture on resistivity is illustrated in Figure 7.4. If moisture is present in the gas, the resistivity departs from the bone dry resistivity curve at temperatures where significant adsorption occurs.

In processes where sufficient moisture is present in the gas, either from the process itself or as a result of evaporative water cooling, the resistivity of the dust is usually sufficiently low to be readily accommodated by electrostatic precipitators.

Many processes that emit dust do not have sufficient moisture in the flue gas for adequate conditioning in the absence of other conditioning agents. If such substances are present, however, as they are in many combustion processes, they may interact to alter the surface conduction properties and reduce the resistivities beyond the values indicated by the moisture content alone.

Because of the dominant role of moisture in the conditioning process, it is termed the primary conditioning agent. Other materials, either naturally occurring or added to the flue gas, are termed secondary conditioning agents.

7.3 MECHANISMS OF SURFACE CONDITIONING

The role of secondary conditioning agents has received considerable study to determine how naturally occurring constituents of the gases, as well as chemical additions to the gases, act to alter the dust resistivity. The extent of the use of electrostatic precipitators in the collection of fly ash from low sulfur coals has resulted in more work on the resistivity of fly ash than on any other type of dust.

Research carried out by Chittum and others[2] in the early 1940's on the fundamentals of conditioning led to the advancement of a theory of conditioning by alteration of the moisture adsorption properties of dust surfaces. Chittum proposed that an intermediate chemical adsorption film, which was strongly bound to the particle and which in turn strongly adsorbed water, would be an effective conditioner. For example, he postulated and later showed qualitatively, that a weak basic particle such as ZnO would

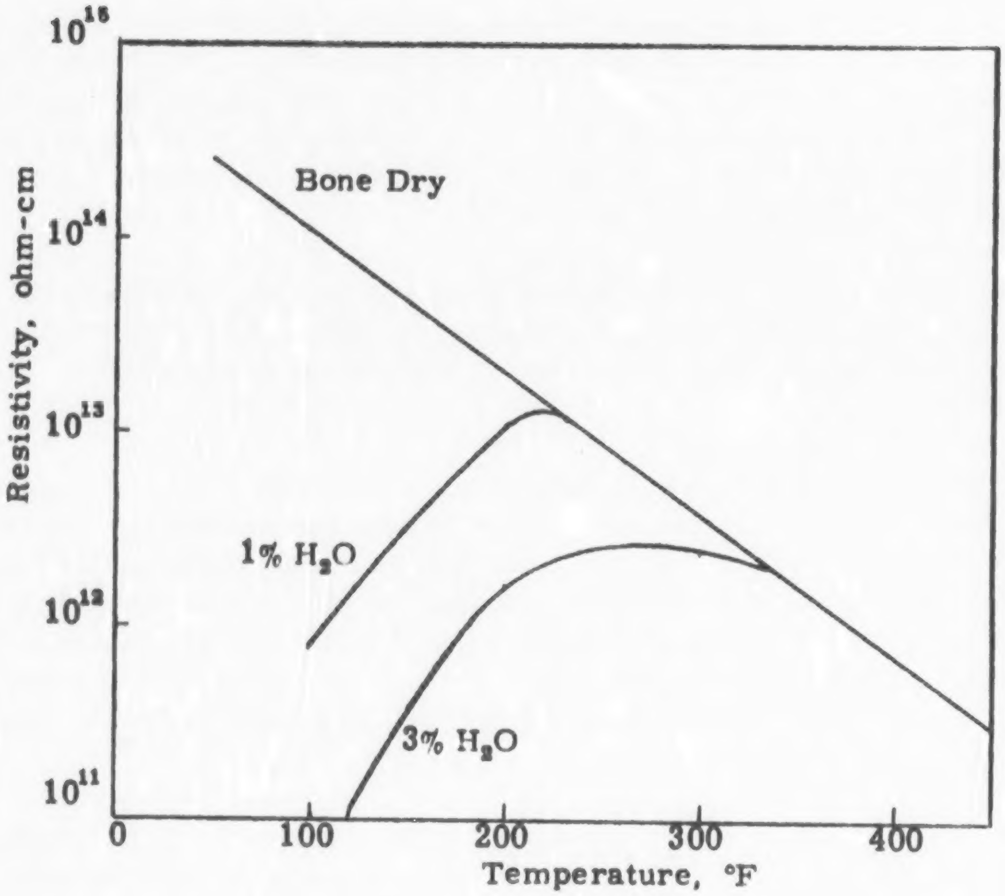

Figure 7.4 Effect of Humidity on Particle Resistivity.

exhibit improved adsorption capacity with prior additions of HCl or H_2SO_4. Similarly, weak acidic particles such as Al_2O_3, when exposed to ammonia, showed improved water adsorption characteristics.

In fly ash precipitators, the influence of sulfur content of the fuel has been recognized as a highly significant factor in precipitator performance. The sulfur appears in the flue gas principally as SO_2. However, approximately 1 to 2% of the sulfur is oxidized to SO_3, and it is sulfur in this form that is active in the conditioning process. The quantity of SO_3 present depends upon the sulfur content of the fuel, the operating conditions in the boiler, and the composition of the fly ash.

At the temperatures that exist downstream of the air heaters, the SO_3 probably combines with moisture to form adsorbed H_2SO_4 on the fly ash. The H_2SO_4 is highly hygroscopic and attracts free moisture to further enhance the conduction.

The rate at which H_2SO_4 is adsorbed is dependent on the composition of the fly ash surface. If the particulate surface is acidic or neutral, adsorption occurs only by van der Waal's forces or physical adsorption, which involves nonspecific, relatively weak attractive forces between the solid particle surface and the gas molecule. On the other hand, if the particulate surface is basic, strong chemical attractive forces of the same nature and magnitude as those involved in chemical bonds are present, resulting in much higher adsorption rates.

This mechanism of the formation of the conductive film appears to be substantiated by experience with specific fly ash which indicates that ash high in basic constituents is conditioned much more readily by SO_3 than is ash high in acidic constituents. Conversely, acidic particles appear to be more readily conditioned by a basic conditioning agent.

Darby and Heinrich[4] reported apparent physical differences in fly ash which has been conditioned by the addition of SO_3. Electron microscope photographs of nonconditioned dust showed completely smooth surfaces, while conditioned dust exhibited a surface film. They postulated that as a result of this film or layer, a more conductive path was provided. Figure 7.5 is a photograph provided by the Central Electricity Generating Board illustrating a "conditioned" fly ash. It is proposed that SO_3 tended to be

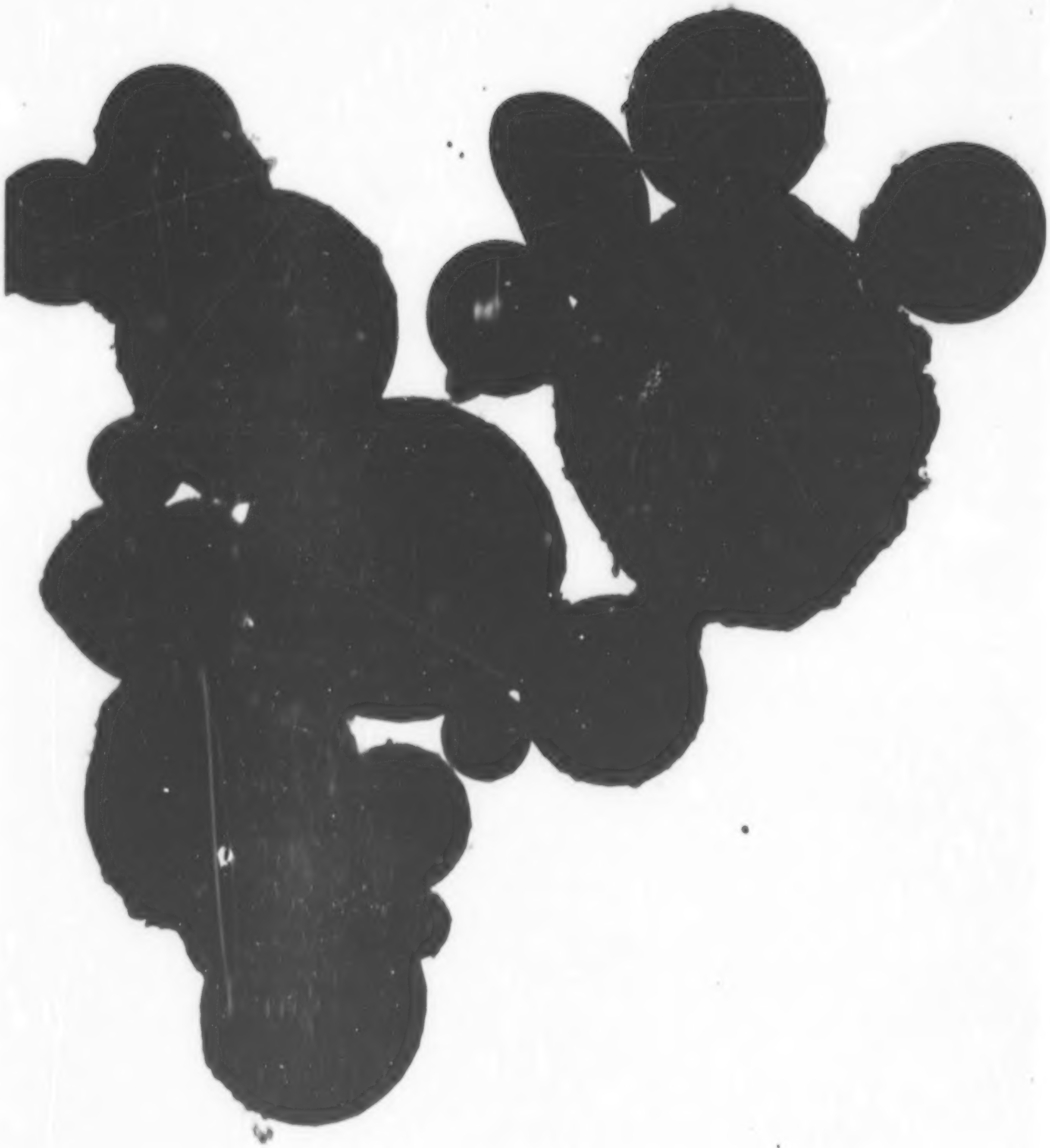

Figure 7.5. Conditioned Fly Ash Particle - CERL, England (20,000X)

adsorbed on the particle surface at temperatures up to 400°C, and upon cooling, the adsorbed SO_3 brought down water vapors to form liquid/semi-plastic nodules as shown. These nodules, in turn, resulted in lower resistivity and stronger mechanical bonds between adjacent particles. Diameter of the particles shown is in the range of from 0.3-3 microns. No photograph of nonconditioned particles was available for comparison.

A sample of fly ash from a power plant in Alabama burning low sulfur (approximately 0.5%) coal was obtained for comparison by Southern Research Institute. According to observations mentioned previously, the fly ash should have a high resistivity and be difficult to precipitate.

Figure 7.6 is an electron microscope photograph taken at Southern Research Institute of one of the typical particles enlarged approximately 80,000 X. Clearly visible on the surface are aggregates similar to the "nodules" shown on the conditioned fly ash. This observation leaves some question as to the significance of these surface characteristics with respect to resistivity.

A review of much of the literature available on the fundamentals of electrostatic precipitation reveals that very little recent experimental work, and no recent theoretical work, has been reported in the field of gas conditioning and resistivity of dusts. This is particularly surprising in view of the relatively important role of resistivity in precipitation.

A fundamental investigation with modern instrumental methods now available should provide a much needed quantitative model of conductivity and conditioning mechanisms.

There is some evidence that the resistivity of collected dust may not be a static property. Cohen[3] reports that the resistivity of fly ash collected in a cyclone separator varies by two orders of magnitude in a period of 15 to 20 minutes. It is postulated that the increase in resistivity is due to a loss of the absorbed film due either to physical or chemical interaction with the bulk of the dust particle. If similar changes occur in the collected dust layer, a resistivity gradient could occur with the freshly collected dust having a lower resistivity than that deposited earlier.

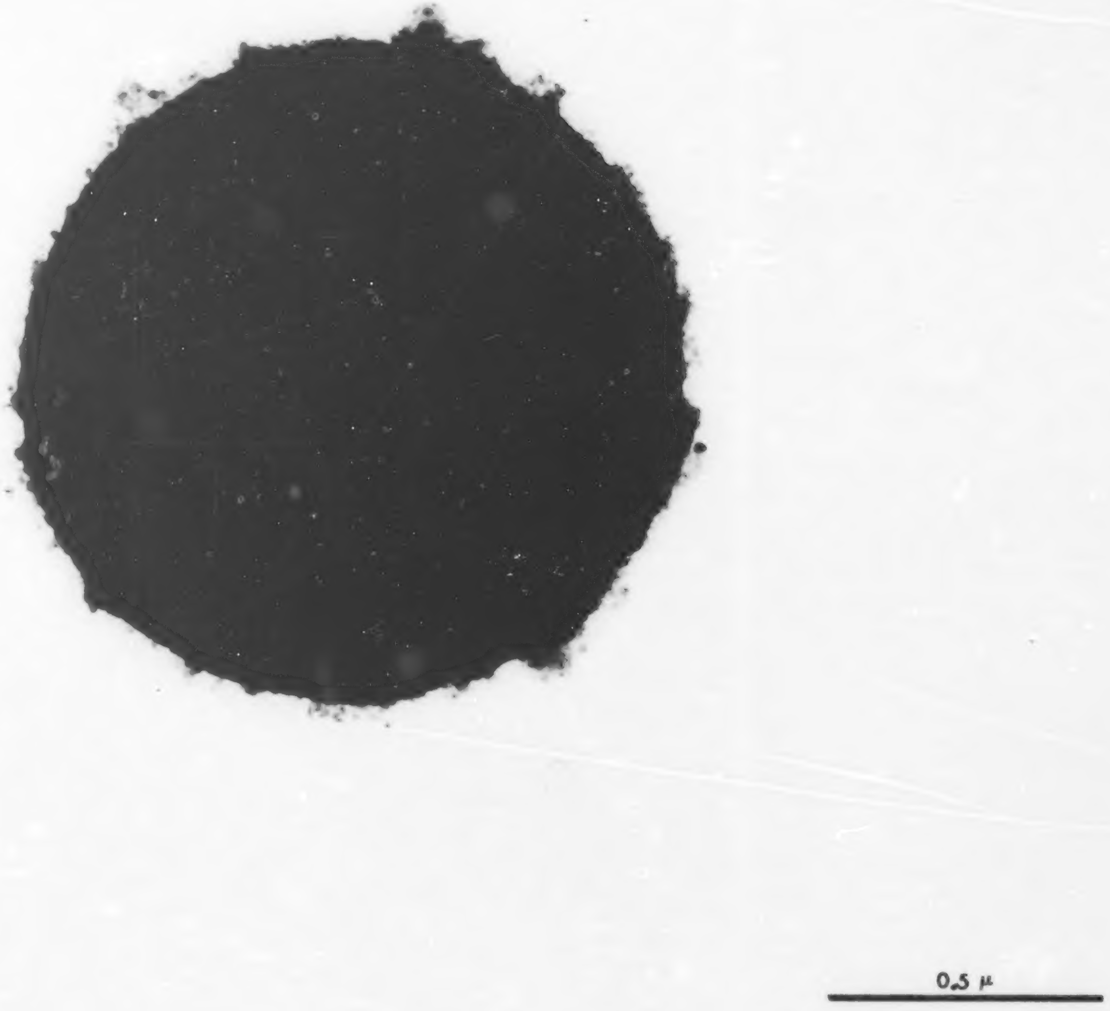

Figure 7.6. Unconditioned Fly Ash Particle - Low Sulfur Coal (80, 000X)

7.4 FIELD CONDITIONING STUDIES

In the precipitation of high resistivity dusts, the addition of conditioning agents to the gas stream is an option in improving precipitator performance. The choice of whether to meet the requirements by additional precipitator capacity or by the use of conditioning agents is largely one of economics.

The types of conditioning agents used in dust conditioning are moisture, sulfur trioxide, and ammonia. Other agents, such as sulfuric acid, ammonium sulfate, and ammonium bisulfite, have been tried experimentally, but no operating plants utilize these agents on a continuous basis.

7.5 MOISTURE CONDITIONING

Moisture can be used as a conditioning agent in processes in which gases exit at temperatures in the range of 1500-2500° F. Normal practice is to cool the gases to temperatures that can be handled by the precipitator by the injection and subsequent evaporation of water. The process of cooling raises the humidity of the gases entering the precipitator and can result in resistivities in a suitable range for precipitation.

The effect of gas cooling by water spray can be seen from the high temperature psychrometric chart as shown in Figure 7.7. If gases from the process enter the cooling chamber at, say, 1300° F with a moisture content $\frac{(\text{wt. moisture})}{(\text{wt. dry air})}$ of 3% and are cooled by evaporation of water to 300° F, the resulting moisture content will be approximately 24%. Under these conditions, the resistivity of the collected dust should be reasonably low. On the other hand, if the starting temperature is only 700° F, cooling to 300° F would result in a moisture content of only about 11%.

On processes in which heat recovery is used, the gas temperature is normally too low to evaporate the amount of water necessary to provide adequate conditioning. An example is the flue gas from steam electric generating plants which leaves the air preheater at temperatures of from 250-400° F.

Field tests on water conditioning were carried out at the Pyrmont Station of the Electricity Commission of New South Wales using steam from

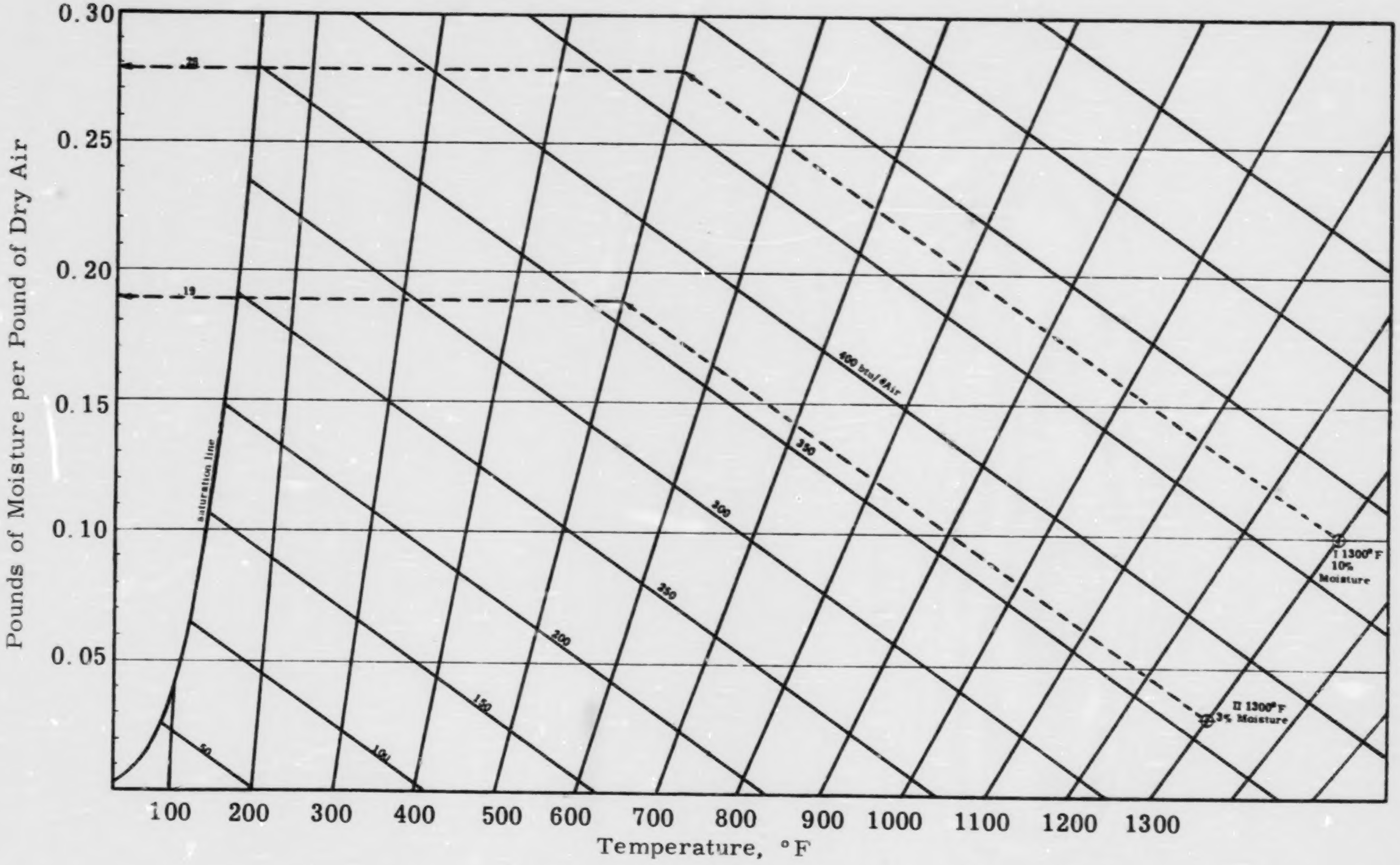

Figure 7.7. High-Temperature Psychrometric Chart.

the soot blowers, water sprays in the combustion chamber, and water sprays in the flue following the air heater. It was found that spray water injection in the duct following the air heater did not result in complete evaporation of the water, and carryover to the precipitator caused excessive dust buildup on the electrodes.

As steam, injections of 12,000 lb/hr were found to be required on the plant at Pyrmont, which was considered uneconomical as compared with other conditioning agents.

Moisture conditioning in the form of steam injection is used on intermittent processes, such as BOF furnaces, to provide moisture during the interval between the start of oxygen lancing and the beginning of water spray cooling. Water sprays in the cooling tower are normally thermostatically controlled to start at a preset gas temperature to ensure complete evaporation of the water. In the absence of the steam conditioning, high stack emissions known as lance puffs will occur, until such time as the temperature reaches the point that resistivity is in the proper range.

7.6 CHEMICAL CONDITIONING

Extensive pilot and full trials with sulfur trioxide conditioning have been carried out in this country, the United Kingdom, and Australia. An operating plant at the Kincardine, Scotland station of the South of Scotland Electricity Generating Board utilizes SO_3 injection as a regular operating practice. Tests on the plant show improvements from collection efficiencies from 60-65% to somewhat over 90% with additions of around 10 ppm SO_3. Results at Kincardine have led to the design of SO_3 conditioning plants for the Central Electricity Generating Board plant at Rugeley and another in South Africa in which sulfur is to be burned on site and the SO_2 catalytically oxidized to SO_3.

The SO_3 injection facilities are generally rather simple in concept. The sulfur trioxide used is a stabilized form to prevent polymerization, and is supplied to the plant from a temperature controlled railroad tank car or truck. It is generally stored in a heated insulated tank with the temperature being 20-30°C (68-86°F).

From the storage tank, the liquid SO_3 is piped to a metering flow controller and than to an evaporator to convert the liquid SO_3 to a gas. The SO_3 gas can be mixed with dry air for transport through heated pipes to the distribution manifold. From the manifold it is distributed in the flue gas duct through a series of pipes fitted with teflon nozzles.

The major problems with SO_3 additions are the cost of process, the requirements for temperature and moisture control, and the safety aspects associated with handling of SO_3. Temperature control is required in the system because liquid SO_3 solidifies at temperatures below around 20°C, and boils at around 44°C. Both extremes must be avoided during storage and transport. Moisture must also be excluded from storage, metering, and piping to prevent the formation of sulfuric acid and subsequent corrosive attack on the system.

There is some reluctance on the part of plant personnel to the use of SO_3 conditioning due to the safety problems. In either liquid or gaseous form, SO_3 is an effective oxidizer and strongly attacks tissue. Leaks from the system form dense acid fumes as SO_3 reacts with atmospheric moisture, and safety precautions must be considered. The problems, however, are not unlike those associated with many chemical plants and difficulties can be avoided by proper design of the system, especially selection of valves, seals, etc., to prevent leakage.

Figure 7.8 is a schematic diagram of an SO_3 conditioning plant used in pilot scale studies in tests at the Creil station of Electricite de France.

Experience with SO_3 conditioning of fly ash has been varied, ranging from substantial improvements with additions of 10-20 ppm to requirements of over 100 ppm without striking improvement. The difference in effectiveness appears to be in the nature of the fly ash. Tests conducted on the Tallawarra plant of the Electricity Commission of New South Wales showed that SO_3 was effective in reducing the resistivity, but quantities were about 600% greater than estimated from prior experience with low sulfur coals. Subsequent tests showed the ash to be acid (pH 3-5.5) and perhaps account for the relative ineffectiveness of the SO_3 additions. Baxter[5] reports similar experience with SO_3 conditioning of acidic fly ash.

BLANK PAGE

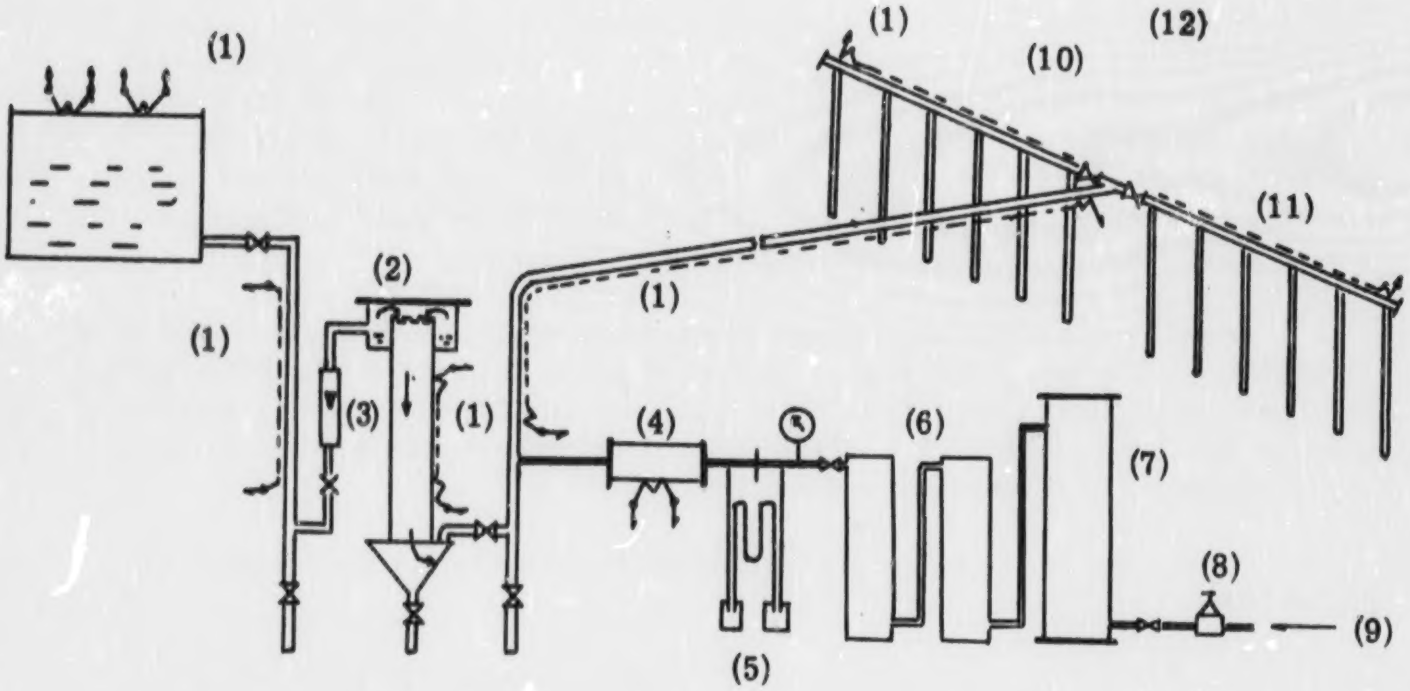

1. Heating Filaments
2. SO_3 Evaporator
3. Flow-Controller
4. Air Reheater
5. Condensation Pots
6. Air Tanks
7. Air Dryer
8. Pressure Regulator
9. Air
10. Duct, No. 1
11. Duct, No. 2
12. Injection Manifold

Figure 7.8 Schematic Diagram of SO_3 Conditioning Plant.

Ammonia has been used extensively as a conditioning agent to reduce the normally high resistivity of aluminum silicate catalyst dust from petroleum cracking processes used in the production of high-octane gasoline. The dust resistivity from the cracking operation is normally high (about 5×10^{11} ohm-cm). It was found that additions of about 20 ppm of ammonia reduced the resistivity to around 10^{10} ohm-cm and minimized sparking and back corona problems associated with the higher resistivity material. Ammonia additions were utilized as a standard procedure on such plants, since the cost of conditioning proved to be low in relation to improved precipitator performance and recovery of the valuable catalyst.

Conditioning of fly ash by ammonia addition to the flue gas is not so straightforward as SO_3 addition. Baxter reports that ammonia addition to the flue gas of power plants must be made ahead of the air heater at temperatures of around 700° F. Injections downstream of the air heater at lower temperatures showed no conditioning effect.[5]

The formation of ammonium bisulfate in the temperature range of 570-670° F

$$\underset{\text{(gas)}}{SO_3} + \underset{\text{(gas)}}{NH_3} + \underset{\text{(gas)}}{H_2O} = \underset{\text{(liquid)}}{NH_4\ HSO_4}$$

was suggested as a possible reaction.

Consideration of this product as a conditioning agent is consistent with the experience and theory advanced by Dalmon and Tidy[6] who investigated the use of sulfamic acid and ammonium sulfate conditioning of fly ash in a laboratory precipitator. Both compounds were believed to be converted in this temperature range to a mist of ammonium bisulfate droplets which were subsequently attached to fly ash particles with a resultant improvement in precipitability.

Baxter reports associated problems with ammonia conditioning due to the fouling of heat exchanger surfaces by solid ammonium bisulfate at temperatures below 300° F.

Full scale experience with ammonia conditioning has been somewhat varied. Tests on the acidic ash of the Tallawarra station of the Electricity

Commission of NSW showed an increase in efficiency from 85-99% from additions of 15-20 ppm of ammonia. This is contrasted to the requirements of SO_3 in excess of 100 ppm with the same ash. Figure 7.9 shows the effect of ammonia additions on the electrical readings. The increase in voltage and decrease in current are indicative of the decrease in resistivity accompanying ammonia additions.

The major reason for addition of conditioning agents is to reduce the resistivity of a normally high resistivity ash. However, it has been reported that difficulties arising from the operation of precipitators below the acid dew point can be corrected by conditioning additives. Tests on full scale plants at the Tennessee Valley Authority's Widow's Creek Plant have shown increases in efficiency of from 50% to 95% with additions of around 15 ppm of ammonia.

Reese and Greco[7] have shown that increases in efficiency of the same order can be achieved by increasing the precipitator inlet gas temperature, which would tend to result in an increase rather than a decrease in resistivity. This evidence would indicate that increases in efficiency with ammonia injection are associated with an increase in resistivity by effectively removing some of the SO_3 or H_2SO_4. This would be in contrast to the usual procedure of adding conditioning agents to reduce resistivity.

Full scale SO_3 injection operations have been carried out in Australia, England, Scotland, France, and South Africa.

Darby and Heinrich[8] present some economic considerations for a full scale SO_3 injection system similar to the installation at Kincardine, Scotland. The equipment for a 300 MW plant consisting primarily of SO_3 storage tanks, an evaporator, and an injector manifold, was estimated to cost approximately $63,000 (1966). At an injection rate of 10 ppm SO_3 for 8000 hrs, annual operating costs were estimated at $25,000 based on the 1966 price of SO_3 in England, and $5000 for heating costs.

Coutaller and Richard[9] describe a similar installation in France and estimate investment costs for a 125 MW to 250 MW plant at $60,000 to $80,000 (1967). Operating costs for SO_3 at about 17 ppm (v/v) were estimated at about $11,000 to $12,000 per year (125 MW).

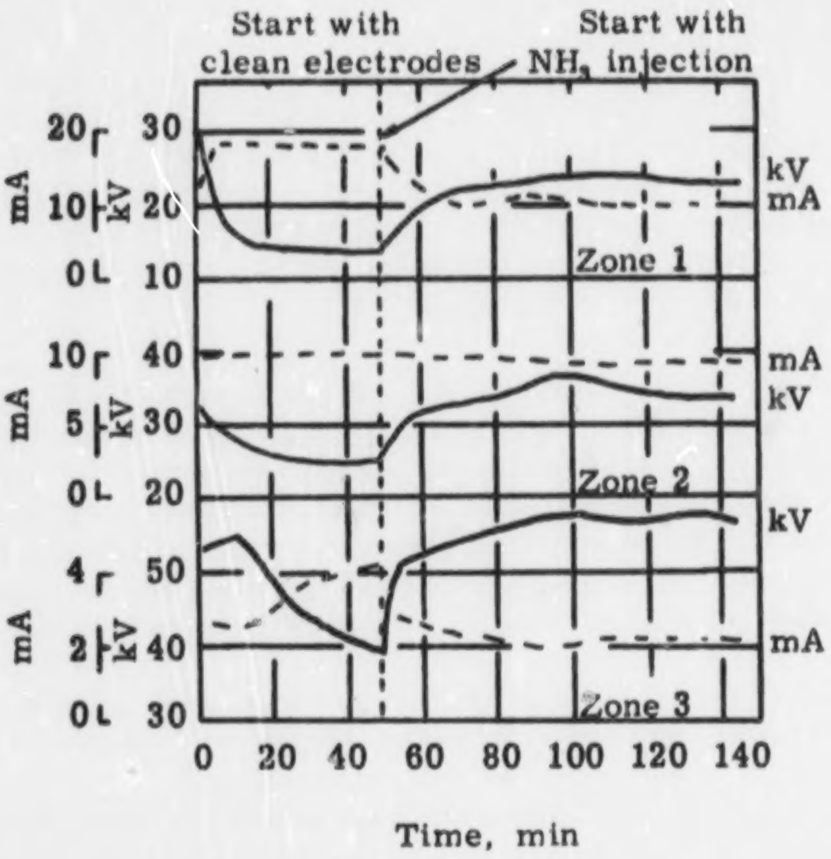

Figure 7.9. Effect of Ammonia Conditioning on Southern N.S.W. Fly Ash. Specific Collecting Area, 300 ft^2/1000 ft^3 per min; Mean Gas Temperature, 280° F.

Alternatives for the use of stabilized liquid SO_3, a source of chemical conditioning, may affect the economics. For example, sulfuric acid injections have been tried with some success, although quantitative data on cost and effectiveness as compared with SO_3 are not substantiated.

CHAPTER 7
BIBLIOGRAPHY

1. White, H. J., Industrial Electrostatic Precipitation, Addison-Wesley (1963).

2. Schmidt, W. A., "Electrical Precipitation and Mechanical Dust Collection", I. & E. C. Proc., **41**, No. 11, 2428 (1949).

3. Cohen, L. and Dickinson, R. W., "The Measurement of the Resistivity of Power Station Flue Dust", J. Sci. Instrum., **40**, 72 (1963).

4. Darby, K. H. and Heinrich, D. O., "Conditioning of Boiler Flue Gases for Improving Efficiency of Electrofilters", Staub **26**, No. 11, 12 (1966).

5. Baxter, W. A., "Recent Experience with Ammonia Conditioning of Power Boiler Flue Gases", JAPCA **18**, No. 12, 817 (Dec. 1968)

6. Dalmon, J. and Tidy, D., "Effect of Ammonium Sulphate and Related Compounds on the Performance of an Experimental Electrostatic Precipitator", CERL Laboratory Note, Central Electricity Generating Board, England, (1968).

7. Reese, J. T. and Greco, J., "Experience with Electrostatic Fly-Ash Collection Equipment Serving Steam-Electric Generating Plants", JAPCA **18**, No. 8, 523 (1968).

8. Darby, K. and Heinrich, D. O., "Conditioning of Boiler Flue Gases for Improving Efficiency of Electrofilters", Staub, **26**, No. 11, 12 (Nov. 1966), Engl. Transl.

9. Coutaller, J. and Richard, C., "Improvement of Electrostatic Dust-Filtering by SO_3 Injection", Pollution Atmospherique (Paris) **9**, No. 33, (Mar. 1967), Fr.

CHAPTER 8
ELECTROSTATIC PRECIPITATOR SYSTEMS ANALYSIS

Systems analysis is the term applied to the analytical study of a complete process. This technique is particularly useful for analyzing the behavior of processes that are characterized by strong interdependencies between the system subfunctions. The significant subsystem functions of an electrostatic precipitator were described in the preceding chapters of this document. These fundamental relations have been available either qualitatively or quantitatively for many years; however, the comprehensive behavior of the entire system has not been presented in a form that is useful for either the design or analysis of complete installations. The purpose of this chapter is to report on the progress in the development of the application of this systems analysis technique to the electrostatic precipitator.

The benefits of a complete systems analysis of electrostatic precipitation are threefold. First, it permits a systematic review of the parameters that influence precipitator performance. A review of this nature points out the significance of the relationships that are known and also pinpoints those areas where quantitative relationships are not available. Second, it may permit the design of precipitators from theoretical relationships rather than empirical ones. Finally, utilizing this approach, there is a possibility for optimizing the performance of a precipitator for a given set of dust and gas properties.

Present design methodology utilizes empirical data accumulated from past experience. The relationships that are used do in fact contain information that could be derived from theoretical considerations. There is a possibility of improving the design techniques by replacing the empirical relationships with theoretical ones. Experience has shown that the performance of fly ash collectors is, in general, related to the particle size distribution of the dust. The overall systems analysis should be able to provide information to go one step further and explain how and why this is so.

The electrostatic precipitator is actually a single subsystem in the overall operation of an installation. The input parameters to this subsystem are dictated by the overall behavior of the entire installation. For example, if the dust collector is installed in a coal-fired steam electric generating plant, the input conditions are established by the boiler load and other operating parameters of the installation. The primary input parameters of the installation are:

dust load,
particle size,
resistivity,
gas volume flow rate,
temperature, and
composition.

These input parameters may be adjusted by the plant operator on the basis of overall system optimization, but in general are beyond the control of the precipitator manufacturer. These parameters do dictate the operational constraints on the electrostatic precipitator unit.

A second constraint on the system is the particulate emission limit established for the output gas conditions. These constraints determine the required behavior of the precipitator. For the systems analysis approach, the above factors constitute the independent input and output constraints for the precipitator system.

8.1 GENERALIZED PRECIPITATOR MODEL

The unit subfunctions required for electrostatic precipitation have been discussed elsewhere in this report. These subfunctions, namely,

source of unipolar ions,
formation of an electric field,
particle charging,
particle collection, and
dust removal,

together with their interdependent relationships can be described in a functional block diagram. One possible system block diagram is shown in Figure 8.1.

The behavior of each unit subfunction has been discussed in previous chapters. However, in the fundamental theory section, the functional behavior of the subsystem was stressed. In systems analysis, a description of

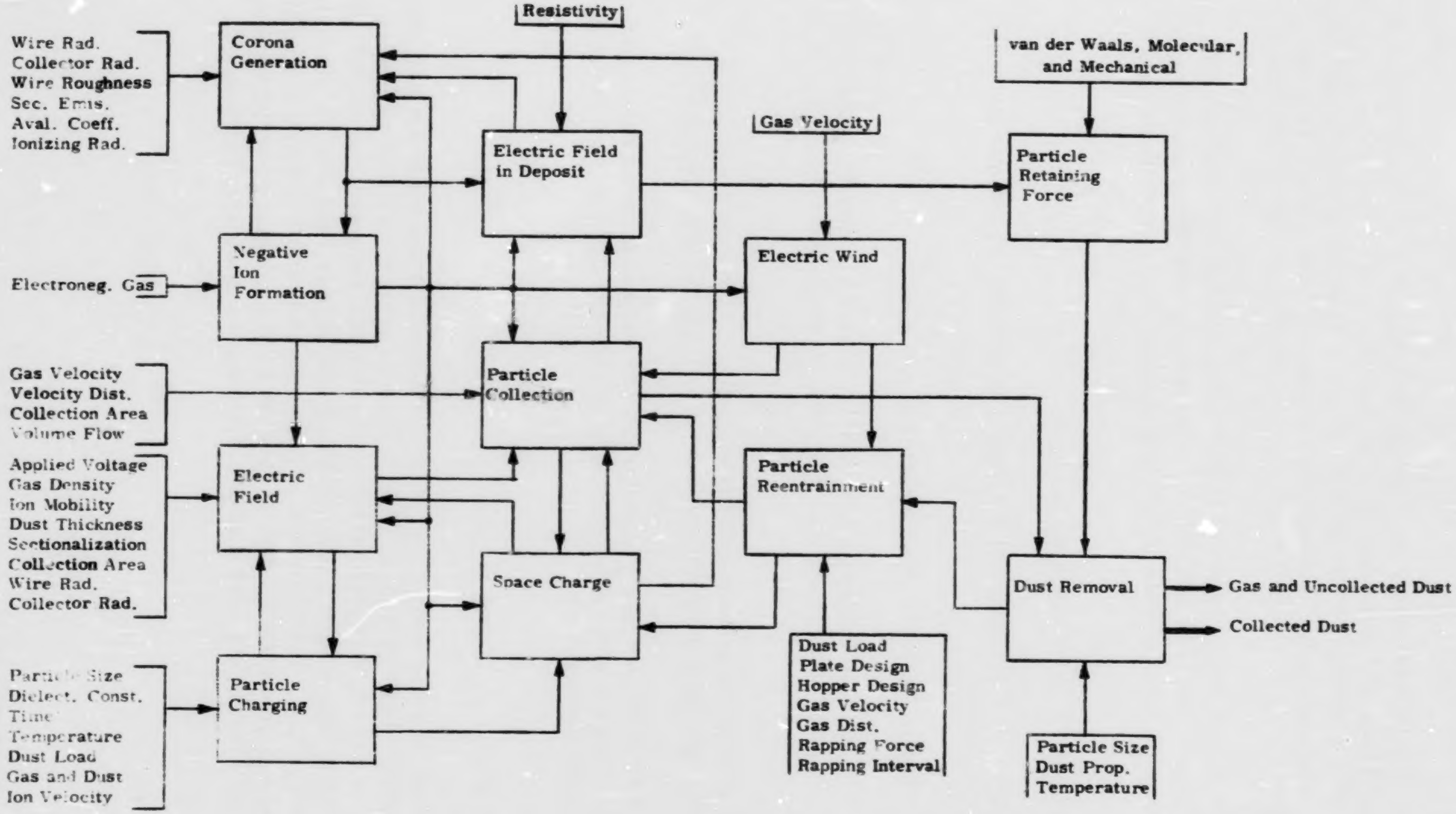

Figure 8.1. Electrostatic Precipitator System Model.

the strong interdependencies among these subsystems is necessary to provide a description of the entire system function. The complexity evident from Figure 8.1 points to the necessity for a high speed computer to allow definitive computations. Without the computer, the system flow diagram will only serve to point out the strong interrelationships in the system.

There are several system subfunctions where the detailed quantitative relationships are not yet available. The qualitative effects are known, but further research is required to complete the definition of the system behavior.

Examples of these factors include:

(1) specific relationship between the electric wind and particle collection,

(2) specific particle reentrainment factors,

(3) relationship between resistivity, current density, and sparking conditions as a function of position within the precipitator, and

(4) detailed relationship between particulate and ionic space charge as a function of position within the precipitator.

These factors are known to modify the behavior of an electrostatic precipitator, but the specific relationships necessary for detailed calculations must be determined.

8.2 SIMPLIFIED SYSTEM MODEL

A simplified system model was developed as the first step in the detailed model. In this model, the unknown factors listed above were neglected. A second simplification was possible because the model was used for evaluation of operating installations rather than for the design of new installations. Voltage and current measurements were available, thus eliminating the need for the inclusion of the corona generation subsystem. The simplified model block diagram is shown in Figure 8.2.

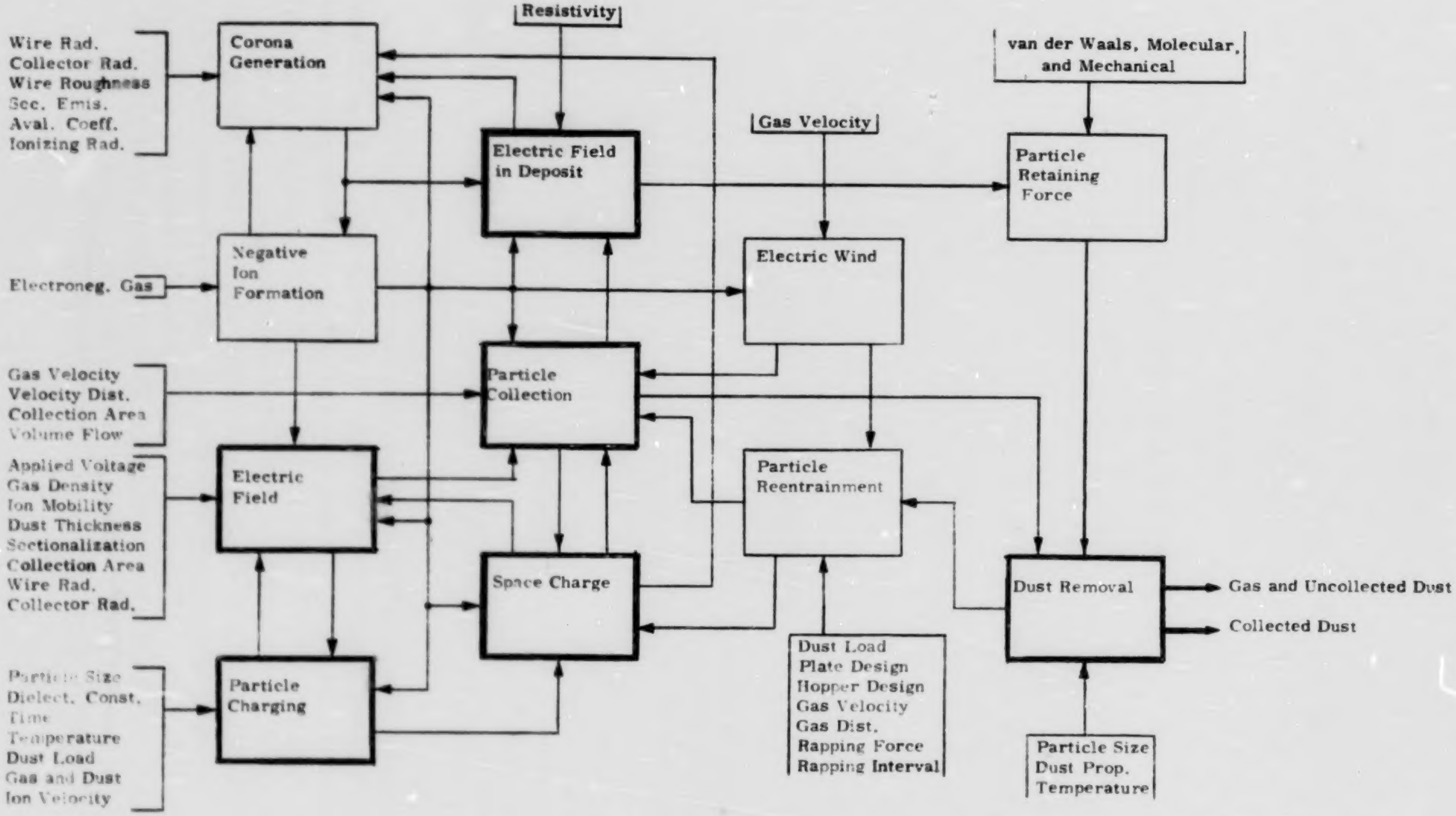

Figure 8.2. Electrostatic Precipitator System Model - Parts Simulated in Computer Program in Heavy Line.

The inputs to the model are listed in Tables 8.1 and 8.2

Table 8.1

Input Parameters from Boiler

Dust Load, D	grains/ft^3
Gas Volume Flow, v_g	ft^3/min
Particle Size Distribution	
Dust Resistivity, ρ	ohm-cm
Gas Temperature, T	°F
Particle Dielectric Constant, ϵ	F/meter

Table 8.2

Precipitator Parameters

Collection Electrode Area, A	ft^2
Corona Electrode Length, L_w	ft
Corona Electrode Radius, a	in.
Collection Electrode Radius, b	in.
Corona Current, I	amps
Applied Voltage, V_i	kilovolts
Corona Wire Roughness Factor, f	
Relative Air Density, d	
Ion Mobility, μ	cm^2/ESU (volt) sec

The present model is used to compute the incremental collection efficiency of the installation as a function of particle size. The collection efficiency per unit distance through the precipitator is determined from the particle charge and collection electric field. Calculations are based on wire and pipe equations utilizing the electrostatic system of units. The computation begins with a determination of the electric field within the first foot of the unit, and proceeds to the collection efficiency for each particle size. The inlet particle size distribution is modified by the amount of material removed in each size range. This computation is iteratively carried through the dust collector until the outlet dust concentration is determined. A list of the derived quantities is given in Table 8.3. A system flow chart with the equations associated with each function is shown in Figure 8.3

Table 8.3

Derived Quantities

Breakdown Field Strength, E_0	ESU/cm
Breakdown Voltage, V_0	ESU (volts)
Corona Current per Unit Length, I_1	ESU (amp/cm)
Dust Surface Area per cm³, S	cm²/cm³
Current Density at Collection Electrode, j_{col}	ESU (amp/cm²)
Average Electric Field, E_c	ESU/cm
Saturation and Actual Charge, q_s, q_i	ESU (Coulomb)
Migration Velocity for Each Size, w_i	cm/sec
Gas Velocity (average)	cm/sec

8.3 EXAMPLE UTILIZING EXISTING SIMPLIFIED SYSTEM MODEL

Electric field. The equation used for the electric field in this particular model is given below*

$$E(r) = \left\{ \left[\left(\frac{aE_0}{r} \right)^2 + \frac{i}{\mu S^2 r^2} \right] \exp 6Sr - \frac{i}{\mu} \left(\frac{2}{3Sr} + \frac{1}{\rho S^2 r^2} \right) \right\}^{\frac{1}{2}} \qquad (8.1)$$

This equation is valid where the contribution to the space charge is primarily from the charged dust.

E_0 is the breakdown field strength as shown in Chapter 1. The equation relating E_0 to applied voltage and geometry is:

$$E_0 = \left[30\, f\, d\, (1 + 0.3\sqrt{d/a}\,) \right] \times 3.3 \text{ ESU/cm} \qquad (8.2)$$

Current required to charge the dust. The total amount of current required to charge the dust can be computed if the quantity of dust in each size range per unit time and the saturation charge for each particle is known. The equation for saturation charge due to field charging developed

---

* See list of symbols on Figure 8.3.

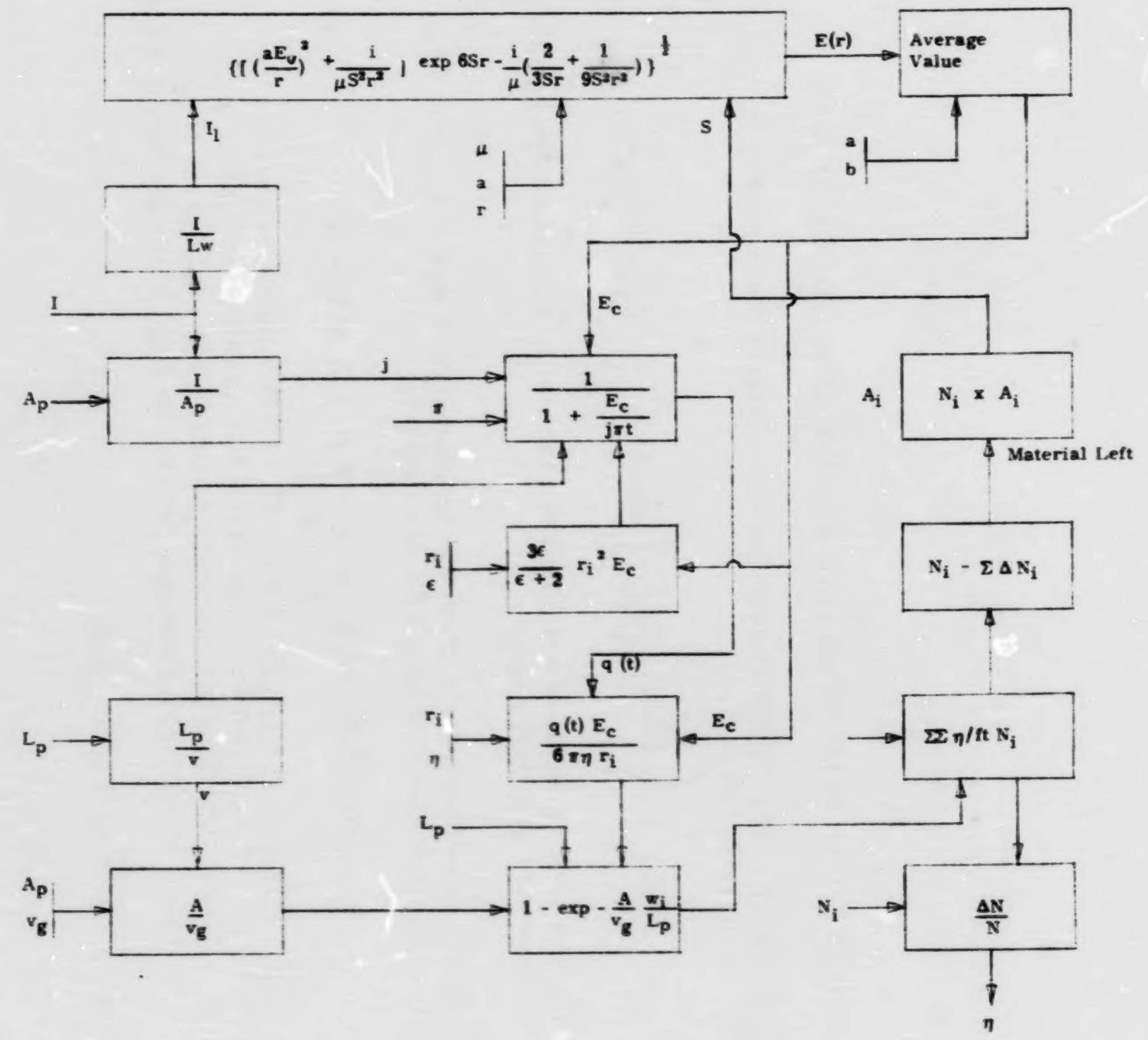
$\{[(\frac{aE_v}{r})^2 + \frac{i}{\mu S^2 r^2}]\ \exp 6Sr - \frac{i}{\mu}(\frac{2}{3Sr} + \frac{1}{9S^2r^2})\}^{\frac{1}{2}}$
E(r)
Average Value
I_1
μ
a
r
S
a
b
$\frac{I}{Lw}$
I
E_c
A_p
$\frac{I}{A_p}$
j
π
$\frac{1}{1 + \frac{E_c}{j\pi t}}$
A_i
$N_i \times A_i$
Material Left
r_i
ϵ
$\frac{3\epsilon}{\epsilon + 2} r_i^2 E_c$
$N_i - \Sigma \Delta N_i$
q (t)
L_p
$\frac{L_p}{v}$
v
r_i
η
$\frac{q(t) E_c}{6\pi\eta r_i}$
E_c
$\Sigma\Sigma \eta/ft N_i$
L_p
A_p
v_g
$\frac{A}{v_g}$
$1 - \exp - \frac{A}{v_g} \frac{w_i}{L_p}$
N_i
$\frac{\Delta N}{N}$
η

a = Wire Radius
b = Collector Radius
f = Roughness Factor
d = Relative Air Density
E_o = Breakdown Field Strength
V_o = Breakdown Voltage
I = Total Current
Lw = Corona Wire Length
i = Current/Length
μ = Ion Mobility
S = Surface Area of Dust per cm^3 of Gas
A_p = Area of Plate
j = Current Density of Plate
E_c = Average Electric Field
$q_s q_i$ = Saturation and Present Charge
ϵ = Dielectric Strength Relative
r_i = Radius of Particulate
v_g = Volume Flow Rate
t = Time Lapsed in Collector
w_i = Migration Velocity
N_i = Number of Particles
L_p = Precipitator Length
v = Gas Velocity
η = Efficiency
Δ = Increment
Σ = Summation

Figure 8.3. Computer System Flow Diagram.

in Chapter 3 converted to ESU is:

$$q_s = \frac{3\epsilon}{\epsilon + 2} r^2 E_c \qquad (8.3)$$

where E_c is the charging field. Therefore, the only remaining requirement is determination of the number of particle charges in each particle size range that is introduced into the precipitator per unit time.

Particle size distributions are generally available for dusts that are to be collected. The particle size continuum given for a given installation can be approximated by an equivalent set of discrete particle sizes that approaches the specific distribution, as shown in Figure 8.4. The continuum was replaced by a set of particle sizes where all the material in each size range interval can be considered to be made up of identical spheres.

The total weight of dust introduced per unit time is obtained from the product of the dust concentration (D) and the gas volume flow rate

$$W = v_g\left(\frac{ft^3}{sec}\right) \times D \left(\frac{grain}{ft^3}\right) \times \left(\frac{gram}{grains}\right) \qquad (8.4)$$

where the total weight of dust per second (W) is given in units of grams/sec. The total weight of dust in each size range is given by the product of the total weight of dust per second and the discrete mass size distribution. The total number of particles in each size range is determined by dividing the total weight of material in each size range by the weight (volume x density) of one particle. This yields a number distribution of particles per unit time into the precipitator.

The total current required to charge the particles (C_p) is obtained by summing the products of the saturation charge per particle (q_{is}) and the number of particles per second in each size range (N_i).

$$C_p = \sum_{i=1}^{n} q_{is} N_i \qquad (8.5)$$

The percentage of the total current required to charge the dust to saturation is

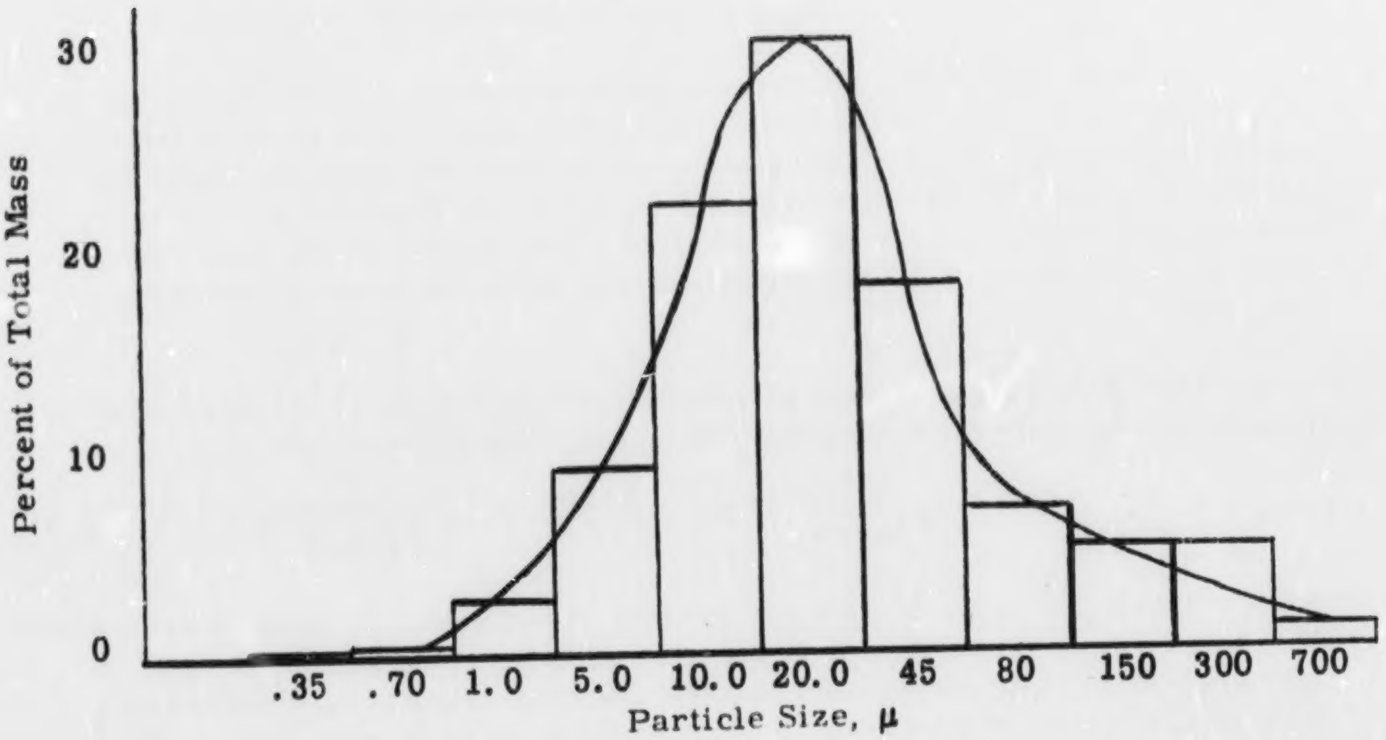

Figure 8.4. Input Particle Size Distribution and Discrete Approximation.

$$\frac{C_p}{I_T} \times 100 \qquad (8.6)$$

The surface area of the dust per unit volume of gas is determined from the particle size distribution and the dust load. The number of particles in each size range times the surface area of one particle (A_i) summed over all size intervals yields this quantity

$$S_i = \sum_{i=0}^{n} N_i \; A_i \qquad (8.7)$$

Particle charge as a function of position. The charge on each particle as a function of time is related to the free ion density in the vicinity of the particle. The charging rate is independent of particle size for field charging. Thus a general expression relating charge to saturation charge as derived in Chapter 3 is

$$\frac{q(t)}{q_s} = \frac{1}{1 + \tau / t} \qquad (8.8)$$

where τ = charging time constant = $\frac{1}{N_0 \; e \; \mu \; \pi} = \frac{Ec}{j \; \pi}$

The free ion charge density (N_0 e) is related to the current density (j) in the interelectrode space. The current density can be determined from either the known voltage-current characteristics of the unit, or from measured current when working with operating installations. In this model, measured currents were used.

Since only average values of current were known for individual installations, estimates of current density as a function of position within the precipitator were used. The variation of current with position can probably be determined by an iterative calculation of charge vs. time (distance) in the computer, but an approximation to this was used in this demonstration model. For lack of a more definitive value, the assumption made for this current distribution was that the amount of current that went to apply charge in each foot of the precipitator was that amount of charge required to charge to saturation the quantity of material expected to be removed within that foot of the unit. This is a conservative estimate of the amount of charge bound to particulate in the inlet section. The actual bound charge is expected to be somewhat greater in practice.

The amount of material removed per foot, used for a gross estimate of bound particulate charge, is calculated from the Deutsch-Anderson equation using the expected efficiency.

$$\eta_{ft} = 1 - \exp\left(- \frac{A}{v_g} \quad \frac{w}{L}\right) \tag{8.9}$$

The free ion density is then estimated by multiplying the average free ion density in that section of the precipitator by the ratio of the free ion charge to total space charge within each foot of the precipitator. This free ion density is used to compute the charging time constants within that increment of the precipitator. The charge on each particle is computed from Equation 8.3. The time used is the distance through the precipitator divided by the velocity

$$t = \frac{L}{v} \quad \text{and} \tag{8.10}$$

$$\tau = \frac{E_c}{j \; \pi} \quad \text{from which} \tag{8.11}$$

$$q/q_s = \frac{1}{1 + \frac{E_c L}{j \; \pi \; v}} \tag{8.12}$$

Collection efficiency. At this point, values are available for the electric field, saturation charge for each size range, and percent of saturation charge. Thus, the collection efficiency for each size range within this increment can be computed. The equation for this efficiency for each size range is

$$\eta_i = 1 - \exp\left(- \frac{A}{L} \quad \frac{w_i}{v_g}\right) \tag{8.13}$$

Values are computed for each size range and stored.

The amount of material removed within each size range is determined by multiplying the efficiency per foot by the particle count. This quantity of material is subtracted from the incoming particles to yield a new particle size distribution as the input to the second foot of the precipitator. The process is repeated for each foot of the collector until an output particle size and overall efficiency is computed.

8.4 LIMITATIONS OF EXISTING MODEL

As indicated previously, the simplified precipitator model neglects several factors that significantly influence precipitator performance. These factors were omitted primarily because data were not available or because analytical relationships had not been developed.

A review of the factors that were omitted shows that some of them tend to increase the predicted efficiency, whereas others would tend to decrease the efficiency. The equations for electric field strength used in the model include the electrostatic component and the contribution of charged particles. The contribution of the free ions to the electric field is considerable. However, equations relating field strength to both free ion density and charged particle density were not available. Consequently, the field predicted by the simplified computer model will be low. The particle charge and collecting field will be greater than predicted by the model. The effect of neglecting the ion density contribution to the electric field would be especially significant in installations preceded by a mechanical collector.

The computer model also does not include diffusion charging. For most fly ash applications, the particle size distribution is sufficiently large that diffusion charging is not too significant. However, for small size dusts, such as metallurgical fumes, diffusion is significant and the effect of neglecting it will result in lower predicted efficiencies.

The effect of particle reentrainment reduces overall collection efficiency. The amount of dust lost from each section during rapping must be small, otherwise overall collection efficiencies would be low. Since quantitative data relating dust loss to rapping conditions were not available, they were not included in the model.

Since the total corona current was used as the basis for determining electric field, resistivity of the dust layer did not influence the predicted efficiency. High dust resistivity would serve to limit corona current and operating voltage. For arriving at a precipitator design, effect of dust resistivity in determining current-voltage characteristics must be included. This necessitates a knowledge of the current-voltage characteristics of the gas and the sparking limitations as determined by precipitator geometry and dust resistivity.

8.5 MODEL VERIFICATION

The simplified model was used to predict the collection efficiency of a few installations for which test data were available. The purpose of the verification was to determine how closely the simplified theory could come to predicting efficiency, and to indicate the influence of some of the operating variables.

Within the constraints of the factors that were omitted in the simplified model, predicted efficiencies agreed reasonably well with measured efficiencies, except where excessive reentrainment was suspected.

Table 8.4 lists the input data to the model and the predicted and measured efficiencies. In Cases 1, 2, and 3, predicted and measured values were quite close. These installations have reasonably normal conditions and the neglect of rapping losses is probably balanced by the neglect of field contribution to ion current and diffusion charging.

Figure 8.5 shows the predicted collection efficiencies for various particle sizes for the five cases. The effect of the neglect of ion contribution to the field is apparent in Case 4, which has a mechanical collector preceding the precipitator. Consequently, the space charge due to charged particles is low and the space charge due to ions would be proportionately higher for Case 4 than for the other installations.

Cases 4 and 5 are operated under conditions where excessive reentrainment is suspected. Also, gas flow quality has not been determined. In view of the neglect of these factors in the model, it is not surprising that variations between measured and predicted efficiencies occur in the two cases.

Table 8.4

Comparison Between the Measured and Computed Collection Efficiency for Five Fly Ash Precipitators

Unit No.	Computed Efficiency, %	Measured Efficiency, %
1	97.8	99.1
2	98.9	96.5
3	98.5	98.4
4	96.5	84.1
5	96.0	55.0

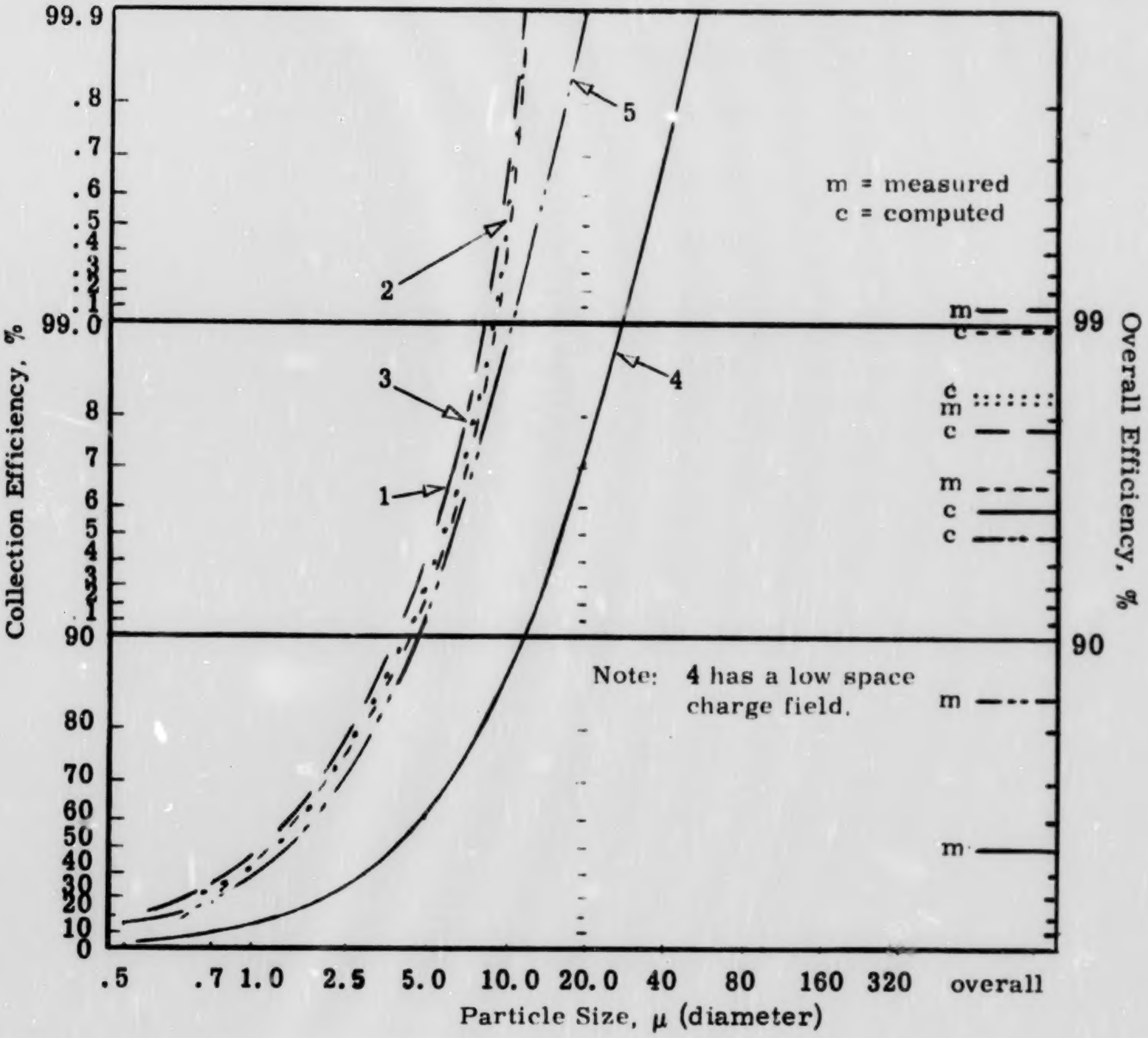

Figure 8.5. Computed Efficiency Vs. Particle Size for Five Installations, Fly Ash from Electric Utilities. Overall Computed and Measured Efficiencies Are Compared on Right Margin.

CHAPTER 9
DESIGN METHODOLOGY

The design of an electrostatic precipitator for a particular installation involves many parameters that can influence both cost and performance. The more significant variables involved in the design are:

(1) Area and type of collection electrodes,
(2) Dimensions of the precipitator shell,
(3) Size, spacing, and type of discharge electrodes,
(4) Size and type of power supply units,
(5) Degree of sectionalization,
(6) Layout of the precipitator in accordance with physical space limitations,
(7) Design of the gas handling system,
(8) Size and shape of hoppers,
(9) Type and number of electrode rappers, and
(10) Type of dust removal equipment.

There are several methods used for the selection of suitable values for these variables and each manufacturer may utilize slightly different methods in arriving at a particular design.

The following discussions are intended to point out the methods that can be used in the design or the assessment of the adequacy of a design rather than in presenting a detailed design handbook.

Two approaches to the selection of precipitator size will be presented. One approach, Method I, is based on the conventional Deutsch-Anderson efficiency equation and the other, Method II, approaches the design from the standpoint of the electrical requirements. These methods must obviously give compatible results. They differ mainly in the fundamental way in which design is approached.

9.1 DESIGN METHOD I

A common approach to the selection of the area of collecting plate required is to utilize the Deutsch-Anderson equation

$$\eta = 1 - \exp\left(-\frac{A}{v_g} w\right)$$

where

A = area of collecting surface,
v_g = gas flow rate,
w = precipitation rate parameter,
η = efficiency, %, and
exp = base of natural logarithms.

The critical parameter in this equation is the precipitation rate w. This parameter varies with each installation depending upon resistivity and particle size of the dust, quality of gas flow, reentrainment losses, and sectionalization, among other factors. The values of w are selected by the equipment manufacturers on the basis of past experience with a particular dust, or from the composition of the dust that can be related to past experience. Each precipitator manufacturer therefore has a file of experience from which a precipitation rate parameter can be selected, and this file of information is kept as proprietary data.

The values of the precipitation rate parameter w vary with the application as a result of variations in dust properties. Variations also occur within each application area. Table 9.1 lists the average values of precipitation rate parameters for various applications, and the range of values that might be expected within each application. From this table, it is apparent that the spread in the values of the precipitation rate parameter is large in some instances such as fly ash precipitators, and within a reasonably narrow range within others. For the pulp and paper industry, a precipitator designed for recovery boilers would have an uncertainty of around 15-20% in precipitation rate parameter. For a precipitator designed for a 98% collection efficiency, the measured efficiency would range from 97 to 99.4% based on the range of design precipitation rate parameters.

For fly ash precipitators, on the other hand, the variation in precipitation rate parameters is quite large, so that a precipitator designed on the basis of a w of 0.43 for 98% efficiency would give an efficiency of only around 75% if the precipitation rate parameter were 0.13 ft/sec.

The major problem in the design of precipitators based on this approach is in the selection of the precipitation rate parameter for the specific application. Several techniques can be used to narrow

Table 9.1

Representative Precipitation Rates for Various Applications

Application	Precipitation Rate w ft/sec Average	Range
Utility Fly Ash	0.43	0.13-0.67
Pulp & Paper	0.25	0.21-0.31
Sulfuric Acid	0.24	0.20-0.28
Cement (wet)	0.35	0.30-0.40
Smelter	0.06	-
Open Hearth	0.16	-
Cupola	0.10	-
Blast Furnace	0.36	0.20-0.46

the uncertainty of the value of w to be used. If the in-situ resistivity of the dust is known, the precipitation rate parameter can be determined for some applications. Figure 9.1 shows the variation in w with resistivity for fly ash precipitators. If the precipitator being designed is a replacement for, or an addition to an existing unit, resistivity can be measured, and the uncertainty in the value of w can be reduced. Alternatively, if a similar installation burning the same fuel is available, measurements of resistivity can be made and the value of w selected with some confidence.

The data from Figure 9.1 only apply to fly ash or to a dust with similar properties. If the particle size differs significantly, the absolute values of w will change, although the general character of the curves would be similar.

In-situ resistivity data have not been determined to the same degree in applications other than fly ash, so that statistically reliable data relating w and resistivity are not generally available.

If it is impractical to select w on the basis of resistivity, other factors can often be used. In fly ash precipitators, resistivity is influenced by the sulfur content of the fuel, and relationships have been developed between precipitation rate parameter w and percent sulfur. Figure 9.2 shows a curve developed by Ramsdell[1] for a group of fly ash precipitators burning coals of varying sulfur contents. On a statistical basis, the precipitation rate can be predicted within reasonable accuracy. However, on an individual installation, the variations are too great to predict w with acceptable precision based upon sulfur content alone. In many instances, the only information available is the sulfur content of the coal, and designs are sometimes based solely upon this parameter.

Particle size of the dust is a very important consideration in determining the value of w for design purposes. Referring to Table 9.1, the variations in w between the various application areas are due largely to particle size variations. In cement kilns, the alkali content of the raw material alters the size distribution of the dust. Metallurgical operations characteristically produce smaller size dusts from high temperature melting operations. Size of dusts from recovery boilers in pulp and paper mills can change with temperature. These factors result in variations in precipitation rate parameters between the various applications, and within the same application area.

---

[1] Refer to the bibliography for this chapter.

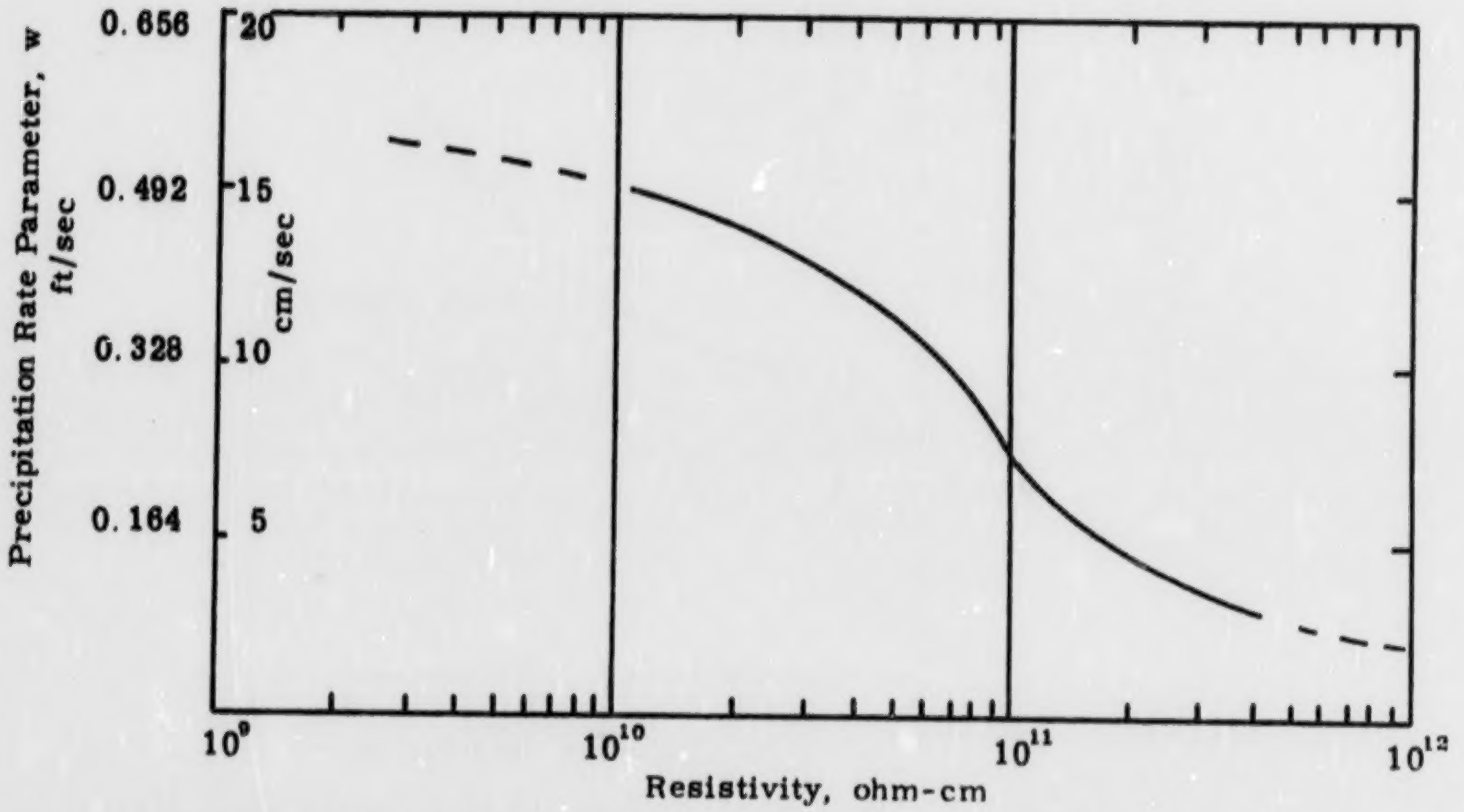

Figure 9.1. Relationship between Precipitation Rate Parameter and Resistivity. (Reference 2)

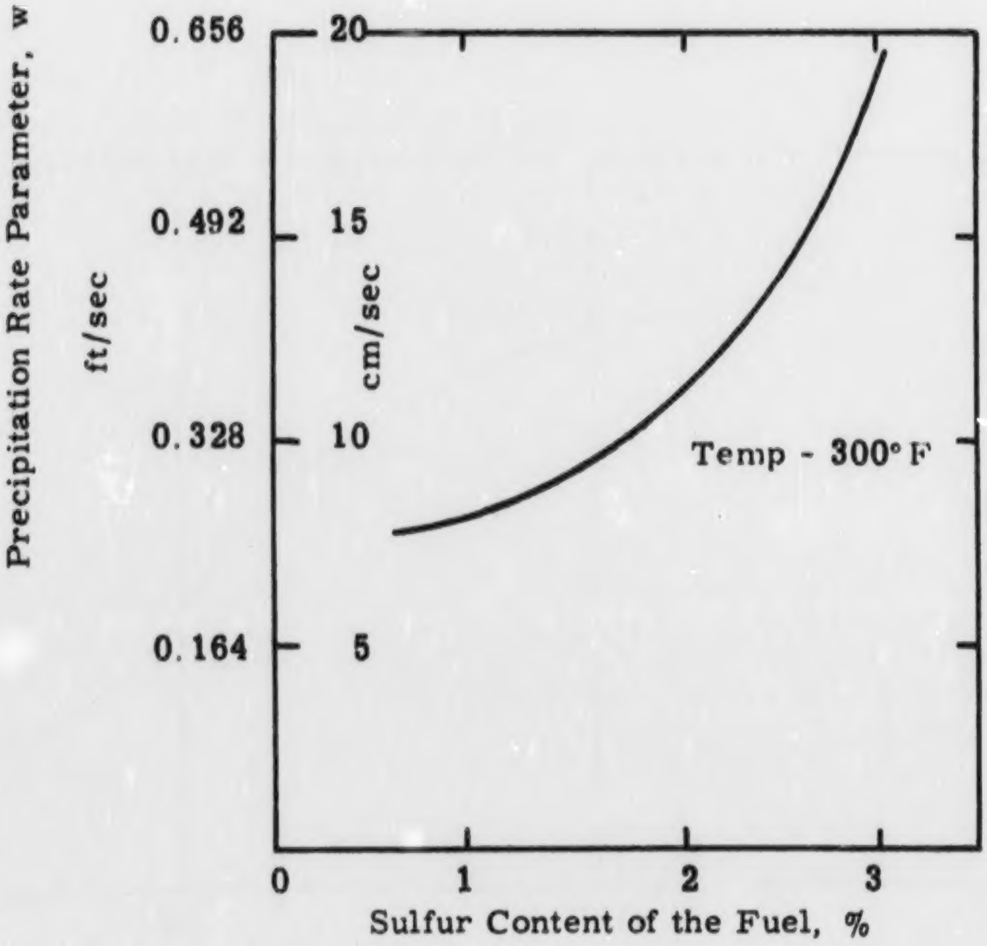

Figure 9.2. Relationship between Precipitation Rate Parameter and Sulfur Content for Electric Utility Installations at a Temperature of 300°F (Reference 1).

The sections covering the specific application areas in Part II describe the emissions from each process in greater detail, and also present data showing the range of design and test precipitation rate parameters where they are available. Reference should be made to each section for a more detailed analysis of the range of precipitation rate parameters.

When the selection of precipitation rate parameter has been made, the area of collecting surface required to achieve a given efficiency when handling a given gas volume can be determined.

The power required for a particular application is determined on an empirical basis. The power requirements for a given application are related to the efficiency and the gas volume handled. Figure 9.3 is a curve showing the power requirements per unit of gas volume for two applications; fly ash and pulp and paper mill recovery boilers. Similar curves can be developed for other applications. The second step in design, therefore, is to determine the total power requirements based on efficiency and gas flow. Note that the recovery boiler precipitators require greater power per unit of gas flow to achieve the same efficiency as a fly ash precipitator. This is primarily due to differences in particle size of the dust, and is related to the precipitation rate parameter.

Figure 9.4 shows the variation in collection efficiency with the number of independently powered bus sections. The number of sections required to reach a given efficiency can be determined from curves for the specific application. The curves shown in Figure 9.4 are for fly ash precipitators, and were developed from empirical relationships from a large number of tests.

The above procedure will provide a rational basis for arriving at plate area, total power, and degree of sectionalization required. It should be recognized that the selection of the value of w and the curves relating power and sectionalization requirements are all interrelated. If inadequate sectionalization is used, a lower value of w would result, the precipitator could not be operated at the required power level, and the efficiency would be reduced. Consequently, curves relating the design parameter should be internally consistent.

The type and number of rappers for the collecting and discharge electrodes depend upon the properties of the dust, gas properties, current

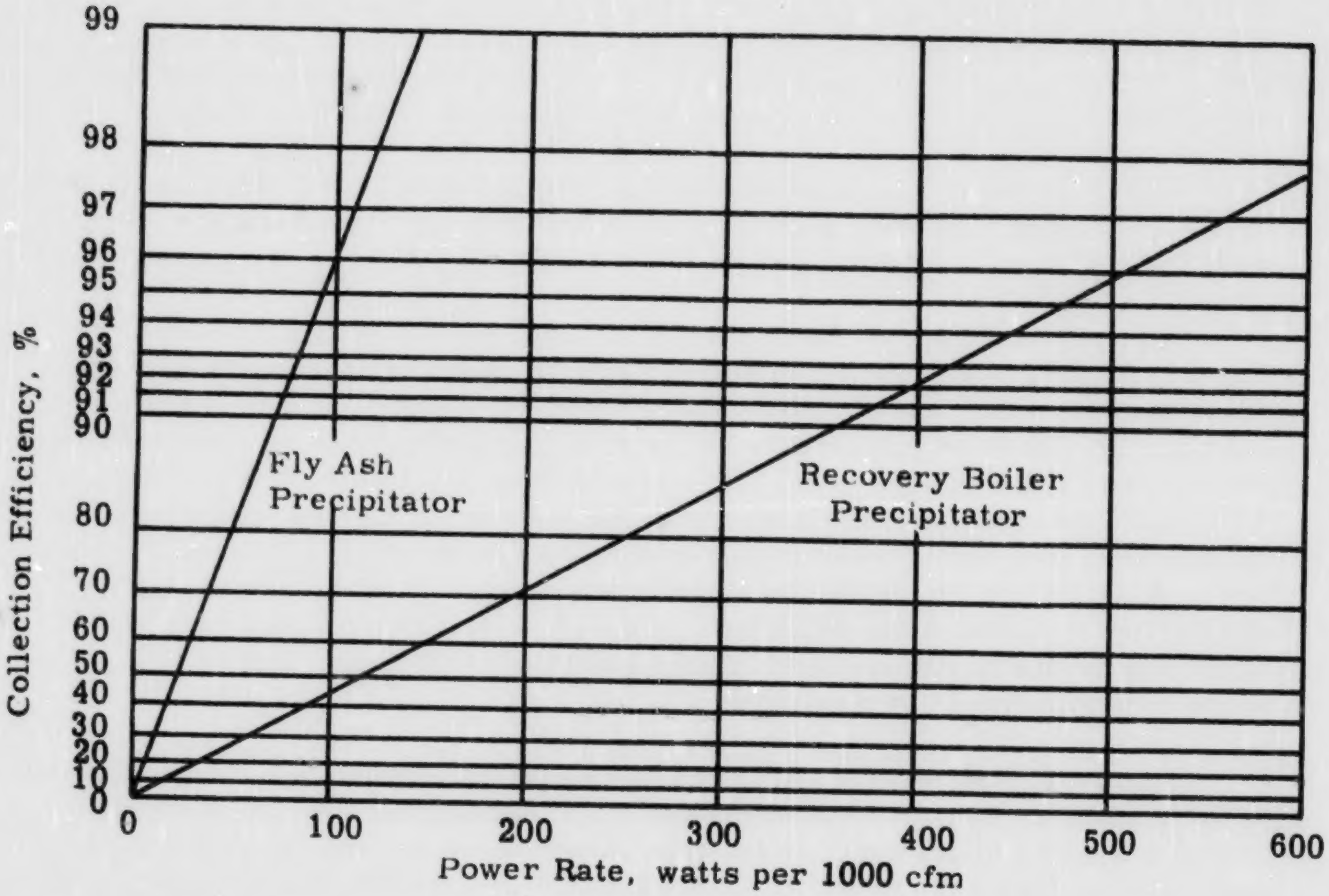

Figure 9.3. Collection Efficiency Vs. Power Rate.

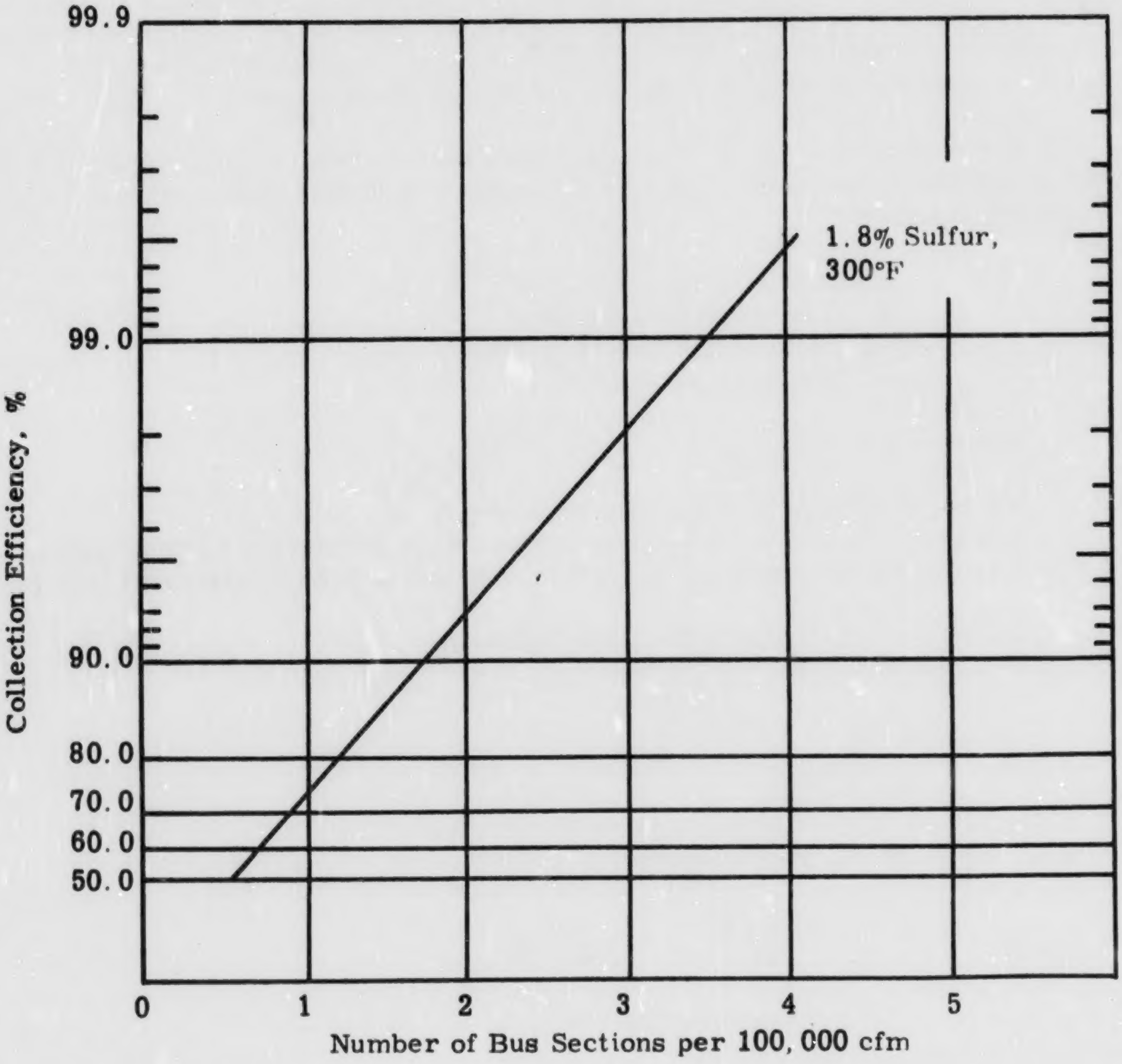

Figure 9.4. Relationship between Collection Efficiency and Sectionalization (Reference 2).

densities, and the configuration of the electrodes and electrode support structures. High resistivity dust is usually harder to remove because of the increased force holding it to the plate. Low temperature operation also tends to give a moist dust that is more difficult to remove. Table 9.2 shows the number of rappers per unit area of collecting electrode and the number per unit length of discharge wire for a group of installations.

The following example will serve to illustrate this design approach. Design an electrostatic precipitator for a pulverized fuel boiler with the following given conditions:

(1) Dust resistivity 7×10^{10} ohm-cm
(2) Gas temperature 300°F
(3) Gas volume 750,000 acfm
(4) Sulfur content 1.8%

Example 1

(a) Select a precipitation rate parameter.
From Figure 9.1, the precipitation rate parameter corresponding to a dust resistivity of 7×10^{10} ohm-cm is 0.35 ft/sec or 21 ft/min.

(b) From the Deutsch-Anderson equation

$$\eta = 1 - \exp\left(\frac{A}{v_g} w\right)$$

or rearranging

$$A = \frac{v_g}{w} \ln \frac{100}{100 - \eta}$$

$$= \frac{750,000}{21} \ln \frac{100}{100 - 99}$$

$$= 35,600 \ln 100$$

$$= 164,000 \text{ sq ft}$$

(c) Compute total power requirements.
From Figure 9.3, power required for 99% efficiency is 140 watts/1000 cfm. For 750,000 cfm, total power = 750 x 140 = 105,000 watts.

(d) Determine number of bus sections.
From Figure 9.4, number of bus sections required is 3.5 per 1000 cfm. 7.5 x 3.5 = about 26 bus sections.

Table 9.2

Rapping Practices

Application	Collection Electrode Rappers/1000 ft^2	Corona Electrode Rappers/1000 ft
Utilities	0.25 - 0.90	0.09 - 0.66
Pulp and Paper	0.25 - 0.99	0.21 - 0.32
Metals	0.11 - 0.82	0.28 - 0.50
Cement	0.33 - 0.52	0.19 - 0.33

9.2 DESIGN METHOD II

A second approach to the sizing of precipitators is to determine the electrical characteristics first and develop relationships that relate efficiency and power requirements to the required collection surface area. The concept of the electrical approach is based on the theoretical factors that influence the precipitation rate parameter, that is, the current required to charge the particles and provide the space charge field, and the voltage required to establish the electrostatic collection field.

In this design method, the curves relating efficiency and corona power density are developed on an empirical basis. The curves are the same as that for Design Method I, and are given for fly ash and recovery boiler precipitators in Figure 9.3. Figure 9.5 is an empirically developed curve showing relationship between precipitation rate parameter w and corona power density. Since the total power has been determined previously, the collecting surface area can be computed from the data read from Figure 9.5. The number of independent bus sections can be determined in the same manner as in method I. The following example will serve to illustrate the design procedure based on this method.

Example 2

(a) Select a precipitation rate parameter.
From experience with this coal, the precipitation rate parameter is selected to be 0.35 ft/sec.

(b) Compute corona power.
From Figure 9.3, power per unit volume corresponding to a collection efficiency of 99% is 141 watts/1000 cfm. The total power is then computed:

$$P \quad \frac{141 \text{ watts}}{1000 \text{ cfm}} \times 750,000 \text{ cfm} = 105,000 \text{ watts}$$

(c) Determine collection electrode area
From Figure 9.4, for w = 0.35 ft/sec, power density = 0.64 watts/ft^2. area = power total power density = 105,000 watts x $\frac{1 \text{ ft}^2}{0.64 \text{ watt}}$ = 164,000 ft^2

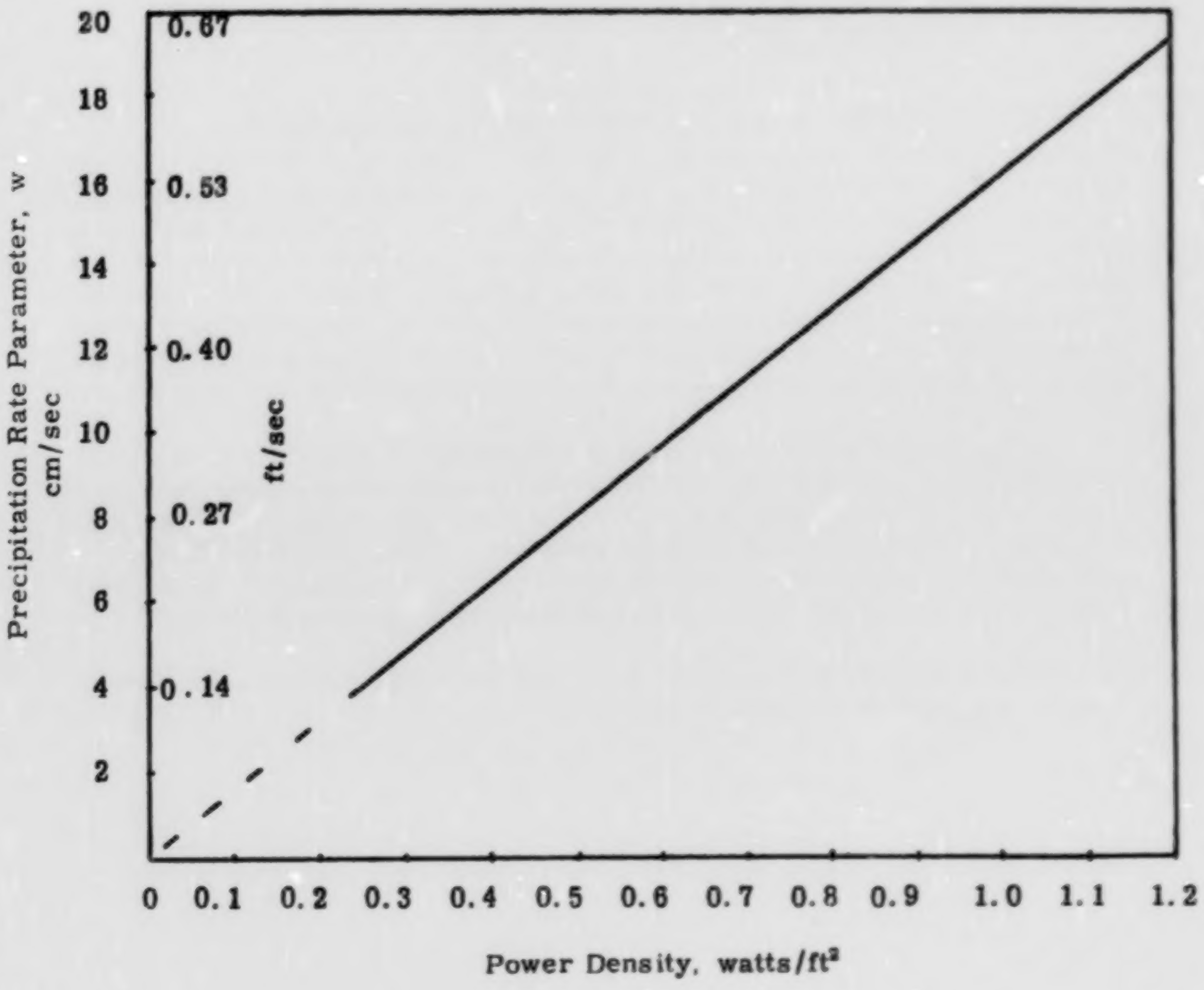

Figure 9.5. Linear Relationship between Precipitation Rate Parameter and Power Density for Fly Ash Collectors.

(d) Number of electrical sections
From Figure 9.5 the number of sections per 100,000 cfm at 99% efficiency = 3.5
Number of sections $2.8 \times \dfrac{750,000}{100,000} = 26$

It should be noted that the curves relating the various factors in method II must also be mutually compatible. The major difference between these two design methods is that the empirical data are used to arrive at the collecting surface area as opposed to the use of the Deutsch-Anderson equation. In the examples shown, the precipitation rate parameter w was used in both instances. However, it is possible to develop other relationships that would eliminate the necessity for arriving at a value of w altogether. Such relationships would be empirical and be subject to the same degree of uncertainty as the selection of the precipitation rate parameter.

A more fundamental approach to precipitator design would be based upon theoretical factors such as particle size, gas composition, dust resistivity, precipitator dimensions, and other input conditions. This method is discussed in the chapter on systems analysis. However, at this time, techniques for design based only on theoretical relationships have not been developed to the extent that they can be used on a commercial basis.

Consideration in the design of the gas handling equipment and ash removal systems is covered in other sections.

CHAPTER 9
DESIGN METHODOLOGY

1. Ramsdell, R. G., "Design Criteria for Precipitators for Modern Control Station Power Plants," Proc. Am. Power Conf. **30**, (April, **1968**) Abstr. Combustion **39**.

2. White, H. J., Industrial Electrostatic Precipitation, Addison-Wesley, Reading, Massachusetts (**1963**).

BLANK PAGE

CHAPTER 10
MECHANICAL COMPONENTS

The mechanical construction of an electrostatic precipitator varies according to the particular process to which it is applied and according to the design philosophy of the precipitator manufacturer. Broadly classified, precipitators are of the tubular or plate type depending on the collection electrode geometry. Precipitators are further classified as horizontal or vertical-flow types depending on the direction of gas flow through the precipitator.

10.1 TUBULAR TYPE PRECIPITATORS

Tubular type precipitators are composed of cylindrical collection electrodes with discharge electrodes passing through the axis of the cylinders. A typical arrangement of a commerical tubular precipitator is shown in Figure 10.1. Gas to be cleaned flows around the outside of the cylindrical electrodes and up through the inside of the cylinders where precipitation takes place. The collected dust or liquid is removed from the bottom of the chamber.

Hexagonal tubes are also used in tubular type precipitators to increase the amount of collecting surface available in a given volume since closer packing is possible with a hexagonal configuration.

Tubular type precipitators are frequently used where the gas flow is low, where mists or fogs are being precipitated, or where water flushing is used to remove collected material. When water flushing is used, the tubes do not have to withstand the rapping forces and can be made of lighter-weight materials. Tube diameters vary from 6 to 12 inches, and lengths of the tubes are typically between 6 and 15 feet.

10.2 PLATE TYPE PRECIPITATORS

The great majority of electrostatic precipitators in service are of the plate type. Collection plates are spaced 8 to 12 inches apart with a series of discharge electrodes spaced along the centerline of adjacent plates. A typical arrangement is shown in Figure 10.2. The gas to

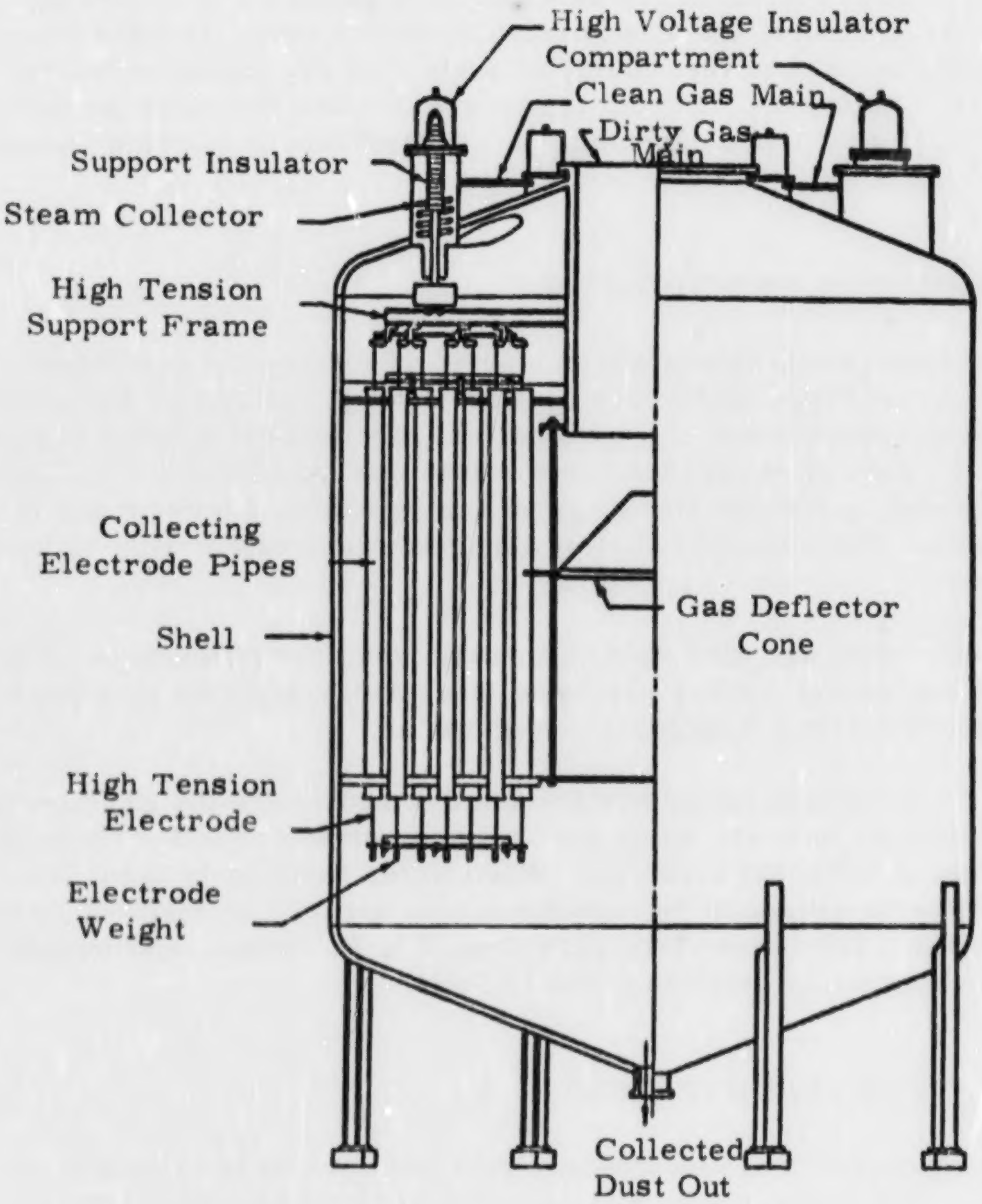

Figure 10.1. A Single-Stage Vertical Wire and Pipe Unit.

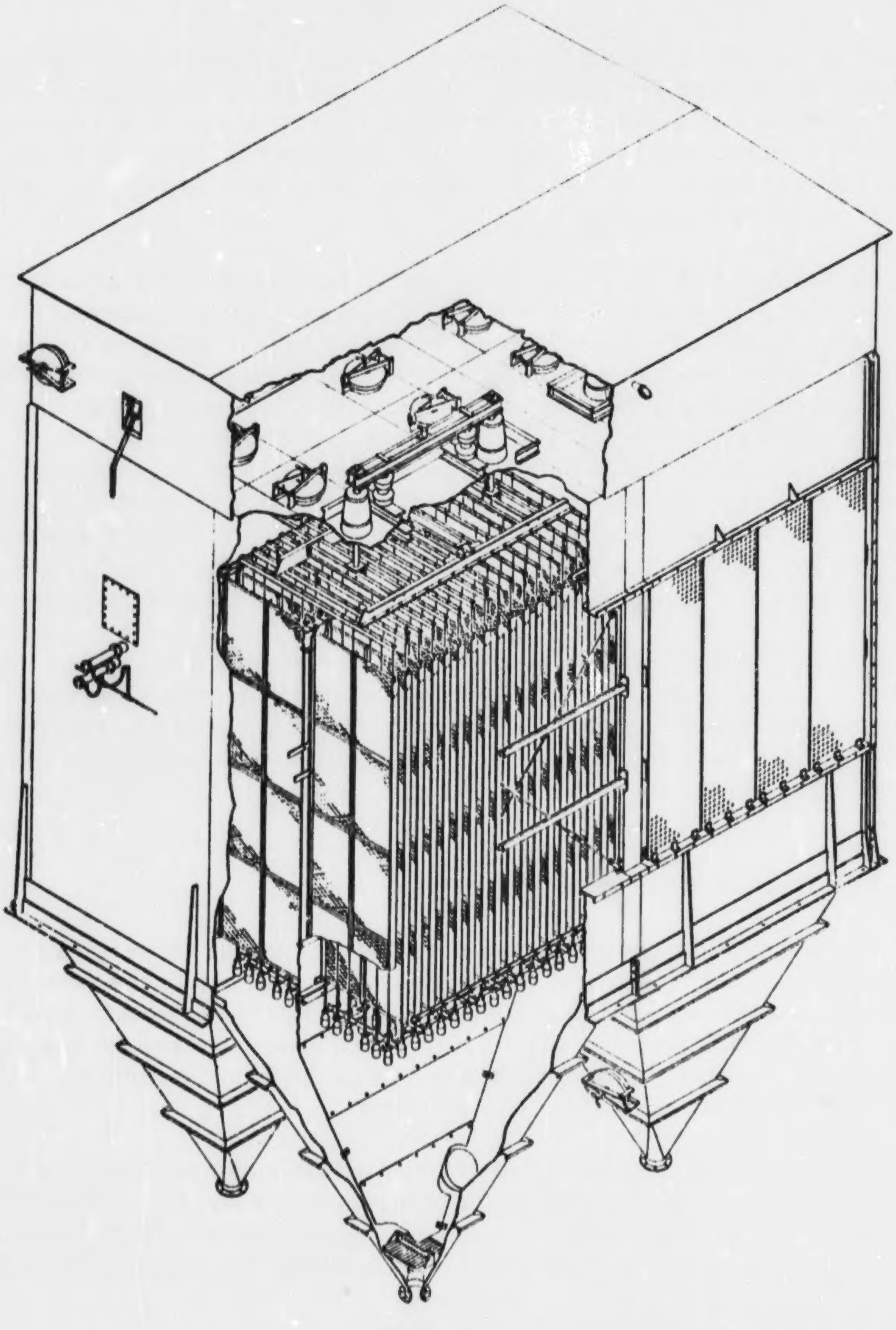

Figure 10.2. Parallel Plate Precipitator.

be cleaned passes horizontally between the plates (horizontal flow type) or vertically up through the plates (vertical flow type). Material collected by the precipitators is generally deposited in bins or hoppers at the base of the precipitator in the dry bottom type, and in a liquid in the case of the wet bottom precipitators. The collected material is then removed by appropriate dust handling equipment.

The purpose of the shell is to confine the gas flow for proper exposure to the electrodes, to avoid excess heat loss, and provide structural support for the electrodes and rapping equipment. The shell is normally rectangular, where plate electrodes are used, or cylindrical if tube electrodes are used. Cylindrical shells may also be used with plate type electrode precipitators where relatively high or low gas pressures are encountered.[1] Shell material is usually steel; but because of particular corrosion problems, it may be made or lined with tile, brick, concrete, or special corrosion-resistant steels. Insulation is usually required to maintain the shell at a temperature above the dew point if the gases contain corrosive materials.[2] Access doors and stairways and safety provisions are provided as auxiliary equipment.

Gas diffuser plates can be provided as a part of the shell to improve gas flow. These plates are usually of the order of $\frac{1}{4}$ inch thick with holes to equalize gas flow. Design of diffuser plates is covered in more detail in the section on gas flow. Roof and wall baffles are used to minimize the amount of gas which may by-pass the electrodes.

10.3 DISCHARGE ELECTRODES

Discharge electrodes can be of a wide variety of types. Practice differs between American and European manufacturers in the method of supporting the discharge electrodes. Typical European practice is to provide a frame or tubular support for the electrodes, whereas most American manufacturers suspend the electrodes from a support and maintain them in position by weights and guides at the bottom.

The shape and size of the discharge electrodes are governed by the corona current and mechanical requirements of the system. Where high concentrations of fine dusts are encountered, space charge limits the current flow, especially in the inlet sections. In such cases, special electrodes that give higher currents may be used to achieve a high power density within the inlet sections. Variation in the current flow and electric field within limits is possible by controlling the type and size of discharge electrode.

---

[1] Refer to the bibliography for this chapter.

Weighted wire. Weighted wire discharge electrodes consist of vertically hung wires spanning the full height of the collecting electrodes as illustrated in Figure 10.3. They are typically from 0.100 to 0.150 inch in diameter. In practice, they are suspended from a support frame at the top and held taut by a weight at the bottom. The wires are kept in place by a steadying frame, equipped with guides at the bottom.

There is considerable variation among manufacturers in the method of supporting the discharge wire from the support frame. The principal concern with the support is to minimize wire breakage due to mechanical fatigue. The discharge wires move under the influence of both aerodynamic and electrical forces, and under severe conditions, mechanical fatigue failure can occur. Various methods of allowing some movement of the support have been attempted to minimize the fatigue problem.

Wires are also subjected to localized sparking in regions of high field strength and shrouds are sometimes used to give a larger diameter, and hence low field strength in critical regions near the ends of the electrodes.

Weighted twisted squares. Weighted bar discharge electrodes consist of vertically hung square bars spanning the full height of the collecting electrodes. They are usually $\frac{3}{16}$ inch or $\frac{1}{4}$ inch square and are twisted longitudinally. The twisting helps straighten the rods and increases the length of sharp edge, which increases the corona current. In practice, they are suspended from a support frame at the top and held taut by a weight at the bottom. The wires are kept in place by a steadying frame equipped with guides at the bottom.

Spiral wires. Spiral wires are formed as a spring and then pulled out. The ends are attached to a formed frame. The spring tension developed keeps the wires taut. A complete frame containing a multiplicity of wires is then installed between the collecting plates as a discharge electrode. The wire used is on the order of No. 12 gauge.

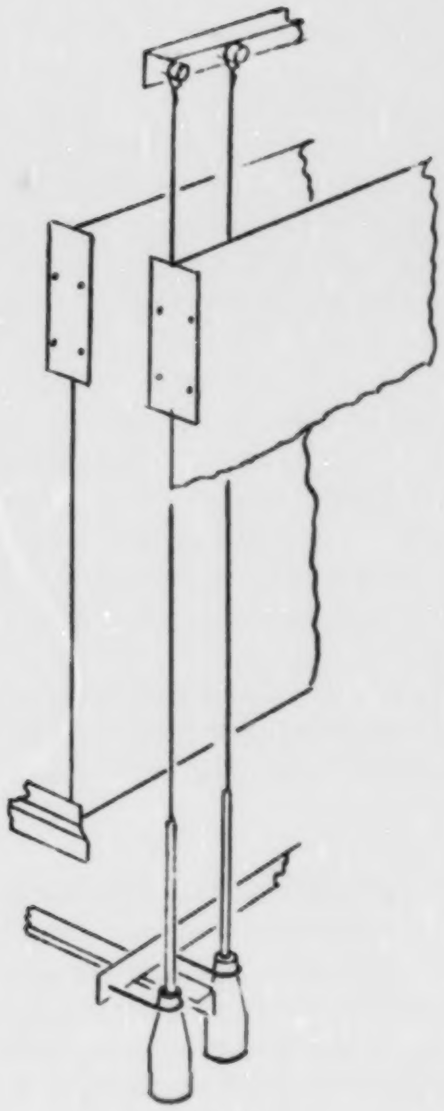

Figure 10.3. Weighted Wire Corona Electrodes.

Barbed wire. Barbed wire is also employed for discharge electrode service. These wires are hung vertically and weighted at the bottom to hold them taut. The wires span the full height of the collecting plates. Commercial grade barbed wire has been used for this application. The wires are supported at the top and are guided and kept in place at the bottom by a steadying frame.

Stiff electrodes. Stiff electrodes consist of formed sheet or structural members rigidly fastened to a support frame at the top. The length can span the height of the collecting plates or be supported from frames. For the longer spans, the electrodes are kept in place at the bottom by an alignment frame. The thickness of the base material is on the order of $\frac{3}{16}$ inch. In order to enhance corona generation, the sheets are formed with sharp edges or with prongs pierced out of the base metal. Figure 10.4 shows typical shapes of stiff discharge electrodes.

Supported wires. As indicated previously, European practice generally is to utilize a stiff structural member for the support of the discharge electrodes. The support members (usually tubes) are fastened rigidly to a top support frame. The electrodes themselves can be of a variety of shapes ranging from circular, square twisted, or formed sheets to other special shapes to give the desired current-voltage relations. The electrodes are strung through crossarms fastened to the central support member or from sections of a rigid frame. The distance between supports is around 2 to 4 feet.

The supported wire electrode system has the advantage of minimizing the wire breakage problem since the electrodes are supported by rigid members and remain in position and energized even if breakage of the electrode occurs. Figure 10.5 illustrates two types of support frames.

Horizontal rods. Horizontal rod type discharge electrodes are used in vertical flow applications. Small diameter rods (order of $\frac{1}{8}$ inch) or twisted square rods ($\frac{3}{16}$ to $\frac{1}{4}$ inch) are placed horizontally in a metal frame. The rods are fastened at one end only. The remaining end is allowed to float freely in the frame to prevent rod bowing due to expansion. The rods are extended beyond the frame and capped with a contoured knob to reduce end arcing. The frame assembly is installed between the collecting plates and suspended from a support frame above.

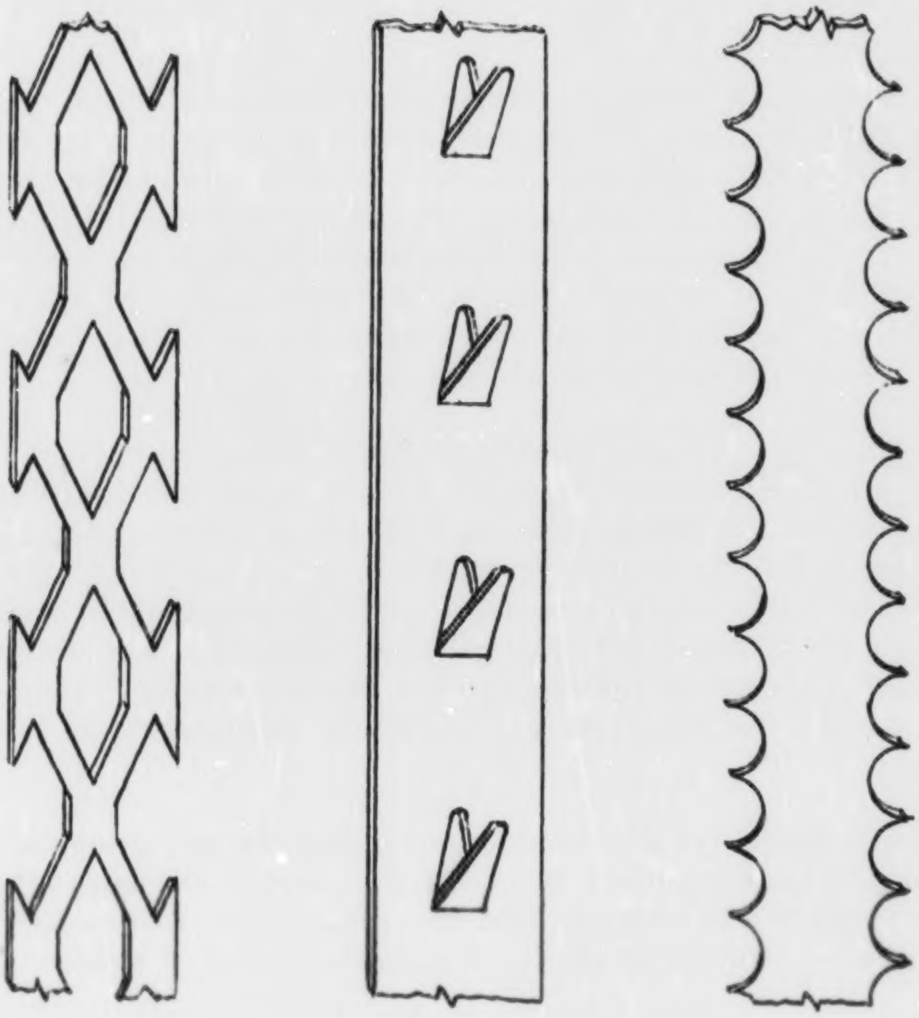

Figure 10.4. Typical Shapes of Stiff Discharge Electrodes (Reference 3).

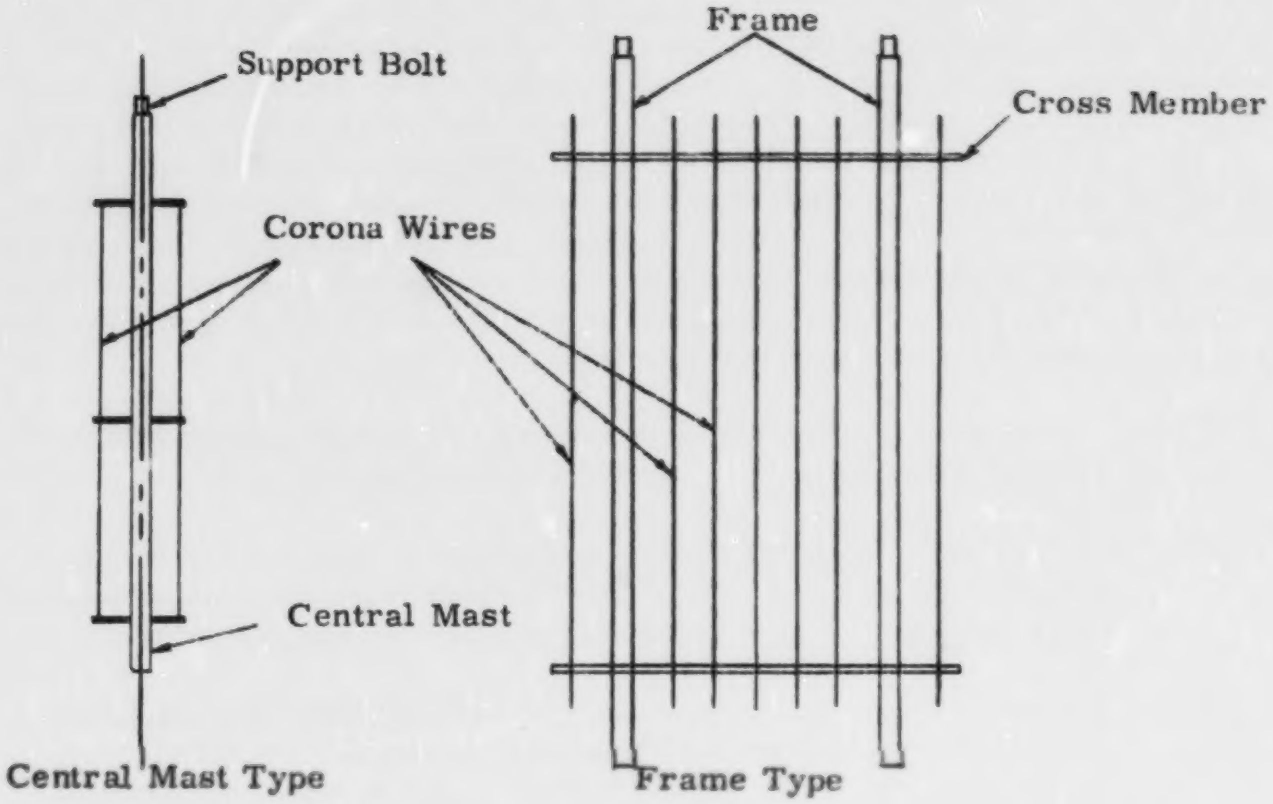

Figure 10.5. Two Types of Support Structures for Corona Wires.

10.4 DISCHARGE ELECTRODE SUPPORT

The main functions of the discharge electrode support are to provide the necessary high voltage electrical insulation and to give mechanical support to the discharge electrode frame.

There are several types of support systems currently used in precipitator design. One type is a support insulator with bushings as illustrated in Figure 10.6. In this design, the high voltage insulators are located on the roof of the precipitator. A bus beam is mounted on top of the insulators and the discharge electrode assembly is suspended from the bus beam by hanger rods. Porcelain pin-type insulators support the mechanical load of the internal framework and are located in a relatively low temperature zone comparatively free of contaminants. The entrance bushings, commonly called flower pots, are made of a clay refractory and cemented in place with a refractory cement. These bushings are not gas tight, and it is common practice to provide a flow of air into the insulator compartment to prevent entrance of dust laden air from the precipitator. This type of arrangement has several inherent disadvantages.

1. The refractory bushing is porous and therefore adsorbs moisture during low temperature operation.

2. It is made in separate pieces and must be cemented in place. Heat is required to dry the joints before it becomes an acceptable insulator, which results in a slow startup procedure.

3. If a positive pressure exists in the precipitator, the insulator compartment must be pressurized to maintain a positive pressure in excess of the precipitator pressure at all times. This means that there is a flow of air through the open space between the hanger support rod and the bushing.

4. In many instances the introduction of air into the treating zone of the precipitator can cause disturbance of the electrical field with the result that sparking will exist in the colder areas.

5. The surfaces of the refractory are generally rough and difficult to clean. In many instances, fly ash precipitators

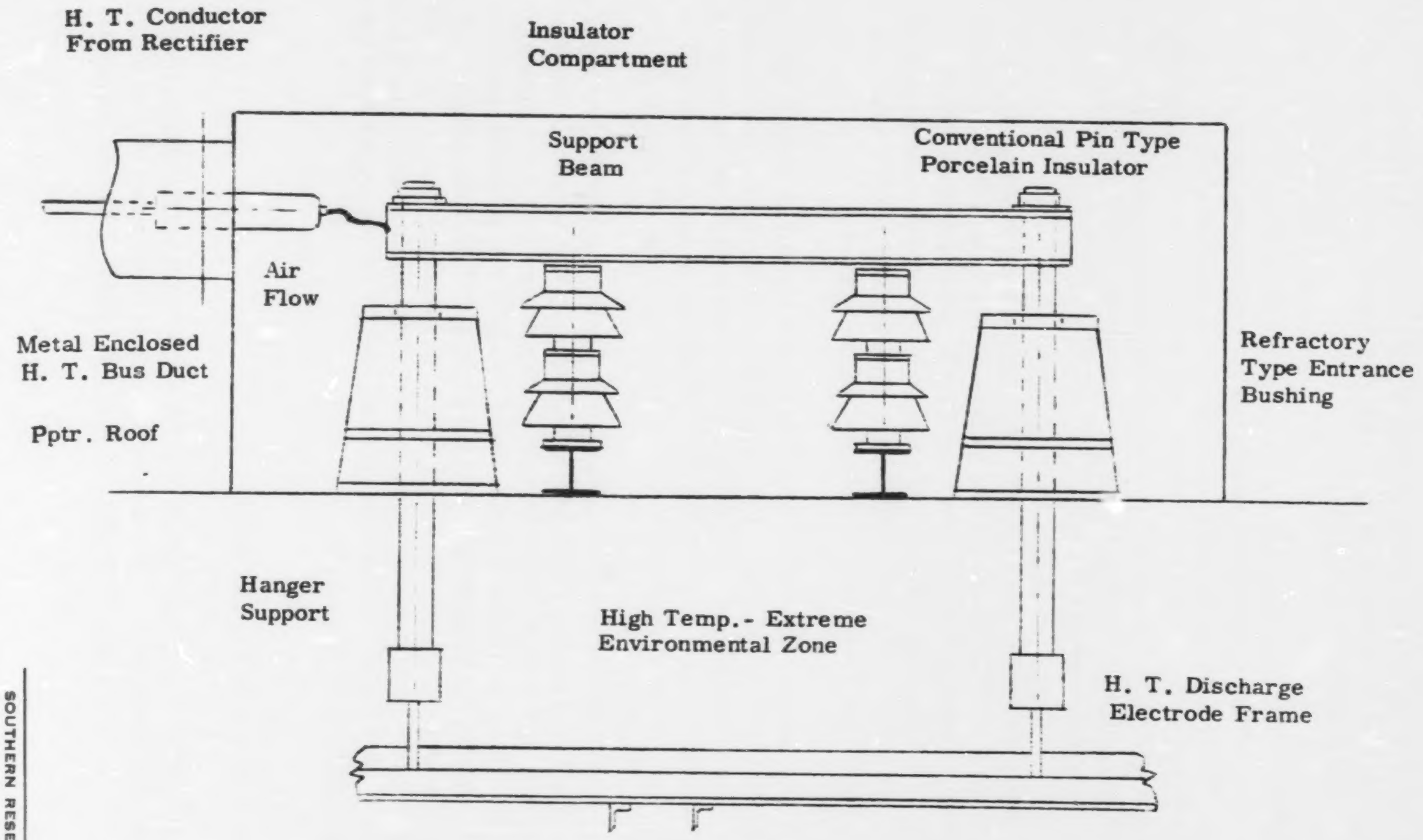

Figure 10.6. High Temperature Support Bushings, Style 1.

are subject to fume from oil firing. This fume condenses on the inside of the bushing with moisture and sulfur compounds, most of which are relatively conductive and practically impossible to remove.

6. Another disadvantage of the arrangement in Figure 10.6 is that in many instances the internal operating temperature in the insulator compartment is above the safe operating temperature of conventional porcelain insulators. This condition is, as a rule, relieved by introducing additional air or by adding thermal insulation to the floor of the compartment.

7. In many processes there are periods during startup when a large quantity of moisture exists in the gas. During these phases, the refractory bushing is wet and becomes conductive. To alleviate this condition, electric or steam heaters are installed in the compartment to keep the temperature of the bushings above the dew point of the gases.

Figure 10.7 illustrates a support bushing arrangement in which the discharge electrode assembly is suspended by hanger rods which are supported directly by bushings. In this case, the bushings are constructed of alumina or Pyroceram and have higher mechanical strength and better thermal shock resistance, permitting a much simpler electrode support design.

The low porosity of the insulation materials and better gas seal provided by the gasket minimize the gas inleakage to the insulator compartment. However, for some applications the bushings are continuously purged with air, either induced when the precipitator is under suction or forced by blowers. The bushings are housed in either individual roof tunnels or in a common housing on top of the precipitator. There are other types of electrode support structures in use, and each manufacturer will use a different type based upon experience. Most of the types will be some variation of these basic concepts.

10.5 COLLECTING ELECTRODES

Various types of collecting electrode structures have been used in the plate type precipitator. The desirable properties are: (1) that the plate act as a shield to provide protection of the collected dust and minimize

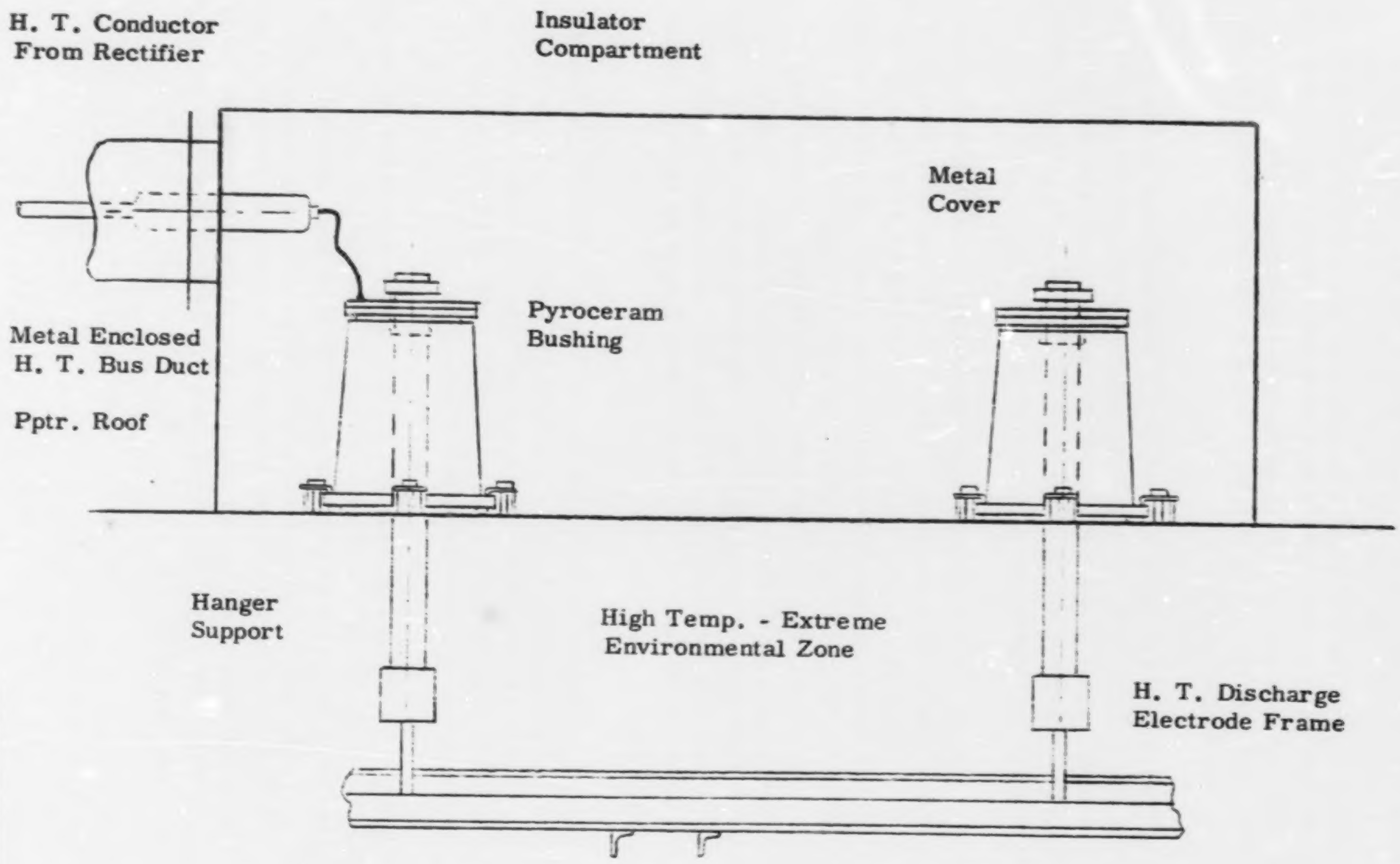

Figure 10.7. High Temperature Support Bushings, Style 2.

reentrainment by scouring from the gas stream, (2) should be free of points or sharp edges that may cause sparking and reduction in the operating voltage, and (3) that the design provide mechanical rigidity. The latter is also important from the standpoint of transmitting the rapping accelerations to all parts of the collecting plate.

Various types of collecting electrodes are illustrated in Figure 10.8. This list is by no means exhaustive. The patent literature contains numerous other electrode types which have been prepared to shield the collected dust and minimize reentrainment. Many of these are unacceptable because of excessive weight or cost.

Shielded flat plates. This type of collecting electrode is the most popular in present day use in this country. The electrode is used chiefly in horizontal flow, duct type precipitators. The plate proper consists of either solid sheet, expanded metal,or perforated sheet. In order to shield the precipitated dust from the gas passing across the plate, baffles are mounted along the plate. The baffles are fabricated as formed shapes, and welded to the ends and surfaces of the collecting plate. Baffle shapes vary from flat strips perpendicular to the collecting surface to aerodynamic designs to minimize gas turbulence. The size of the collecting electrodes ranges from 10 feet to 40 feet in height and from 3 feet to 12 feet in the direction of gas flow.

Offset plates. These collecting plates are made by bending a flat sheet into a square or angular zig-zag or a corrugated pattern. The dust precipitated in the troughs is shielded from the main gas stream, minimizing reentrainment. The plates are usually from 10 feet to 30 feet in height, and from 3 feet to 9 feet in the direction of gas flow.

Pocket plates. As the name implies, these plates are made up by fabricating pockets or louvers out of the base sheet. The plates are arranged so that the pockets face into the gas stream. Two plates, spaced about 1-½ inches back-to-back, are employed to make up a collecting electrode assembly. The hollow space between the plates is used as a chute wherein the dust collected on the plate can fall down to the hopper out of contact with the gas stream. Plates are from 18 feet to 24 feet high and 6 feet in the direction of the gas flow.

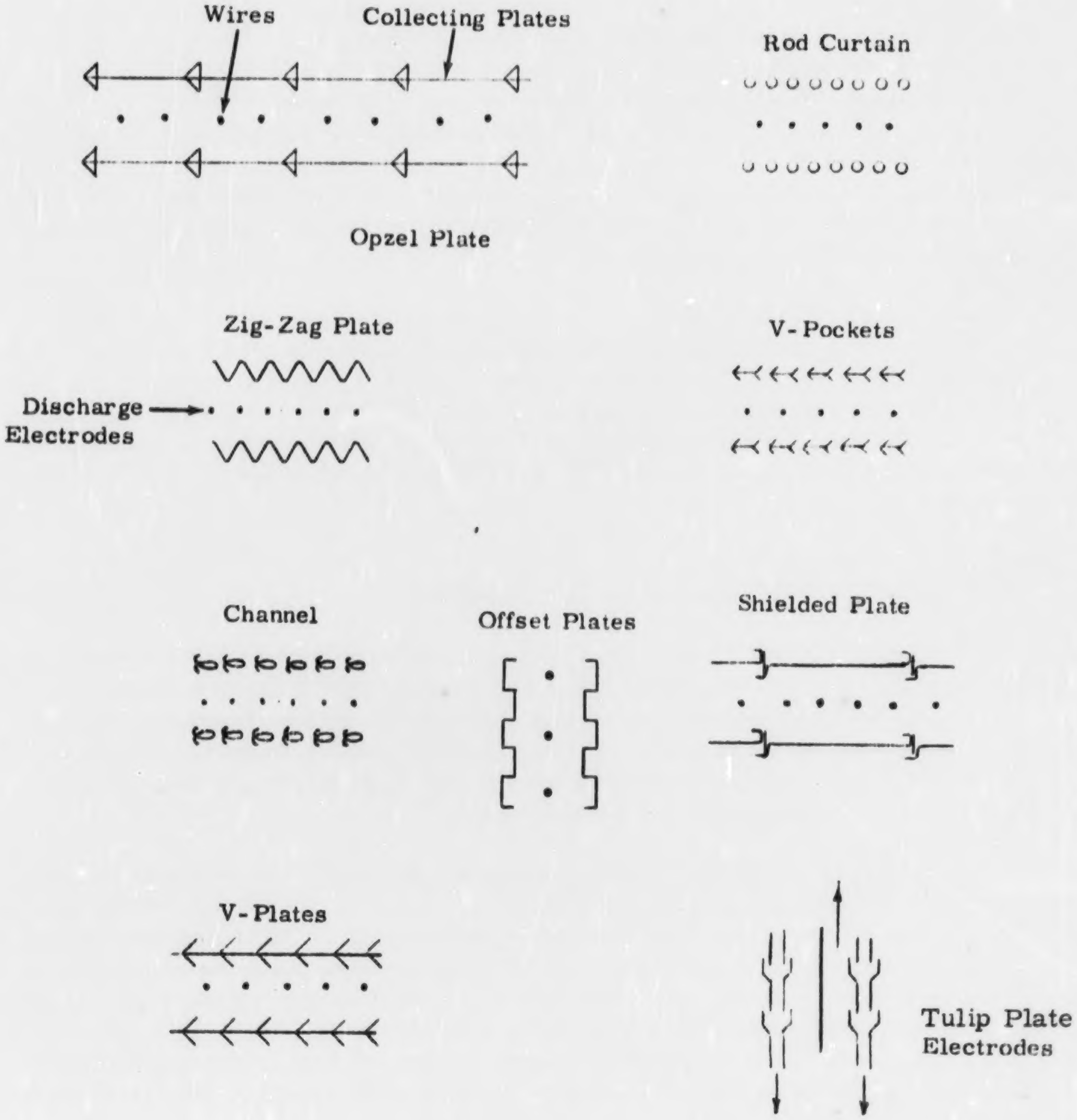

Figure 10.8. Various Types of Collection Electrodes.

Vee plates. A vee plate is a composite assembly of metal strips bent in the shape of a vee or chevron. The vees are spaced about $1\frac{1}{4}$ inch apart for the full length of the plate. The assembled plate is about 2 inches thick. The plates are hung so that the points of the vees face upstream. The spaces between the vee members act as quiescent zones in which the dust is precipitated with minimum reentrainment. The collecting plates in use today range from about 18 feet to 36 feet in height. An individual plate is 3 feet in the direction of gas flow. It is customary to fasten two plates together in order to make up a 6 foot section.

Rod curtain. Rod curtain collecting electrodes are solid metal rods which are hung vertically in a straight line, relatively close together. Relatively large collection areas are thus formed that are effectively shielded from the gas stream. These are very poor aerodynamically and are subject to high reentrainment losses. Their main advantage is the ability to withstand high temperatures (700° to 800°F) without much warping or distortion.

10.6 ELECTRODE CLEANING EQUIPMENT

Dust accumulates on both the collection and discharge electrodes and must be periodically removed for proper operation of the precipitators. The requirements for rapping are discussed in detail in the chapter on rapping and reentrainment. Methods of dust removal include impact, vibration, or liquid flushing. For most precipitators, mechanical means are used to remove the collected dust in the dry state.

Single impact rapper - (electromagnetic solenoid). Electrostatic solenoid rappers consist of a plunger which is lifted by energizing the solenoid. On release of the plunger by deenergizing the coil, it falls against an anvil which transmits the rap through a rod to the electrodes to be cleaned. Figure 10.9 illustrates the construction. Solenoid type rappers are used for both discharge electrode and collecting electrode cleaning. They are mainly used in connection with horizontal flow, dry type plate precipitators. When used for plate or discharge electrode rapping, they are located on top of the precipitator.

Solenoid rappers can also be spring actuated as well as gravity actuated, and in such instances, can be located in other than upright position

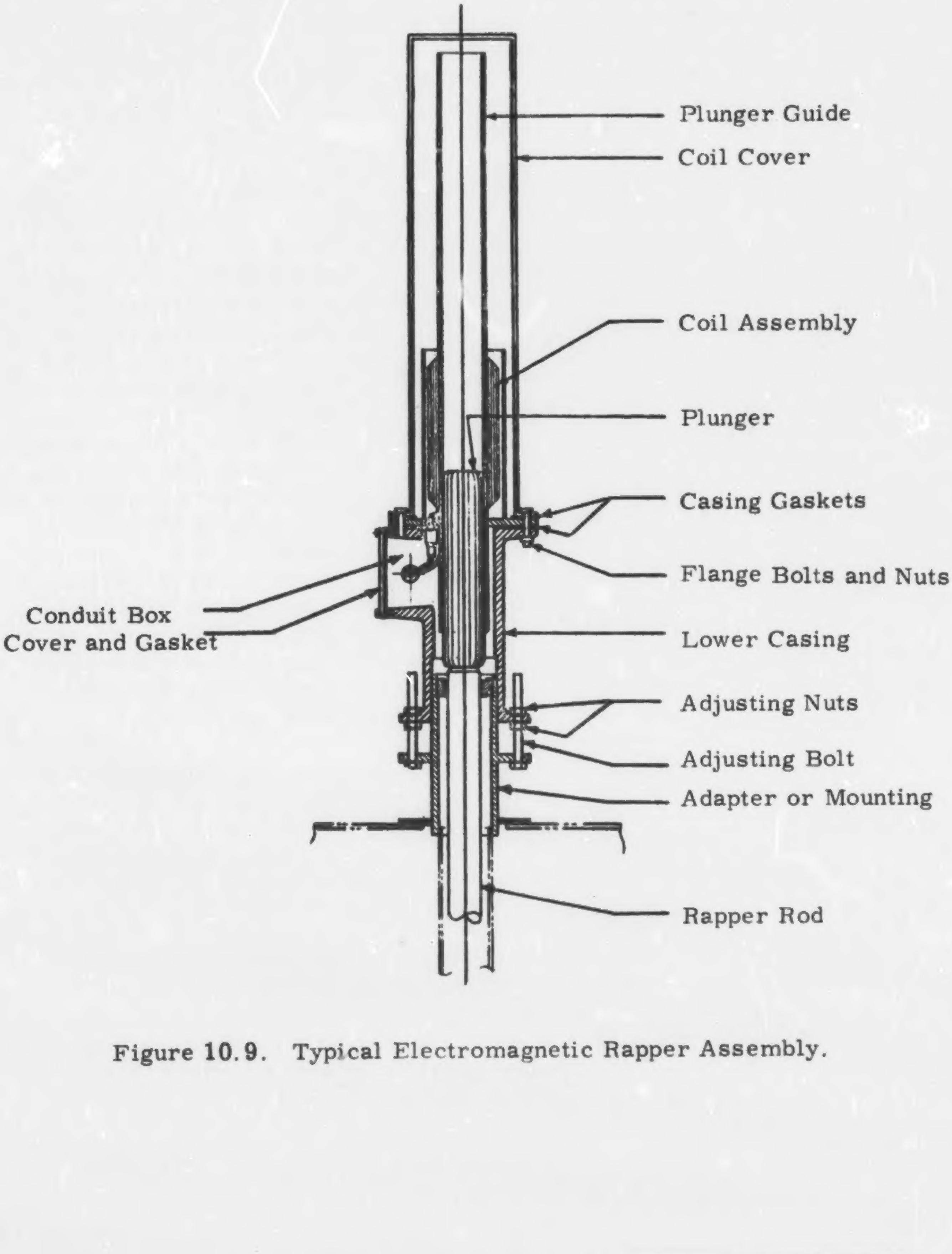

Figure 10.9. Typical Electromagnetic Rapper Assembly.

on the side or end for plate rapping. Control consists of varying the electrical energy, which changes the magnitude of the impulse, or the frequency of rapping. Final selection of magnitude and frequency is usually made after trials in the actual plant under operating conditions.[3] The acceleration of the rap can be as low as 5 g's, but raps from 30 g's to 50 g's are required for most fly ash precipitators.

Vibrators (electromagnetic). Electromagnetic vibrators consist of a balanced, spring loaded armature suspended between two synchronized electromagnetic coils. When energized, the armature vibrates at a high frequency. This vibrating energy is transmitted through a rapper rod to the electrodes and also collecting electrodes. When employed for discharge electrode cleaning, the rapper rod is provided with an electrical insulating section in order to isolate the high voltage electrode charge from ground. This device is used mainly in the vertical position for discharge electrode cleaning and is suitable for both horizontal and vertical flow dry type precipitators. Control consists of varying the electrical energy input, which changes the amplitude of vibrations, the operation time duration, and the frequency of vibration. The armature must be adjusted for the operating position required. Figure 10.10 is a typical electromagnetic vibrator installation.

Vibrators (eccentrically unbalanced motors). Mechanical vibrators consist of an electric motor equipped with adjustable cam weights mounted on a single shaft or on both shafts of a double ended motor. When operated, the eccentrically positioned cam weights set the entire assembly into vibration. The motor is mounted directly on the rapper shaft which transmits the generated vibration to the electrodes to be cleaned.

Vibrators are used for both discharge electrode and collecting electrode cleaning. They are used mainly in connection with horizontal-flow, dry-type plate precipitators. This type of rapper is used for either top, side, or end operation. Control consists of varying the degree of eccentricity by cam weight adjustment, the length of time operated, and the frequency of operation.

Single impact (motor-driven cams). This rapping system is usually used to clean dry-type horizontal flow precipitators. The mechanism consists of a motor-driven shaft running horizontally across the precipitator. Cams are located along the shaft which raise small hammers by their handles. When the rotating cam reaches the end of its lobe, the

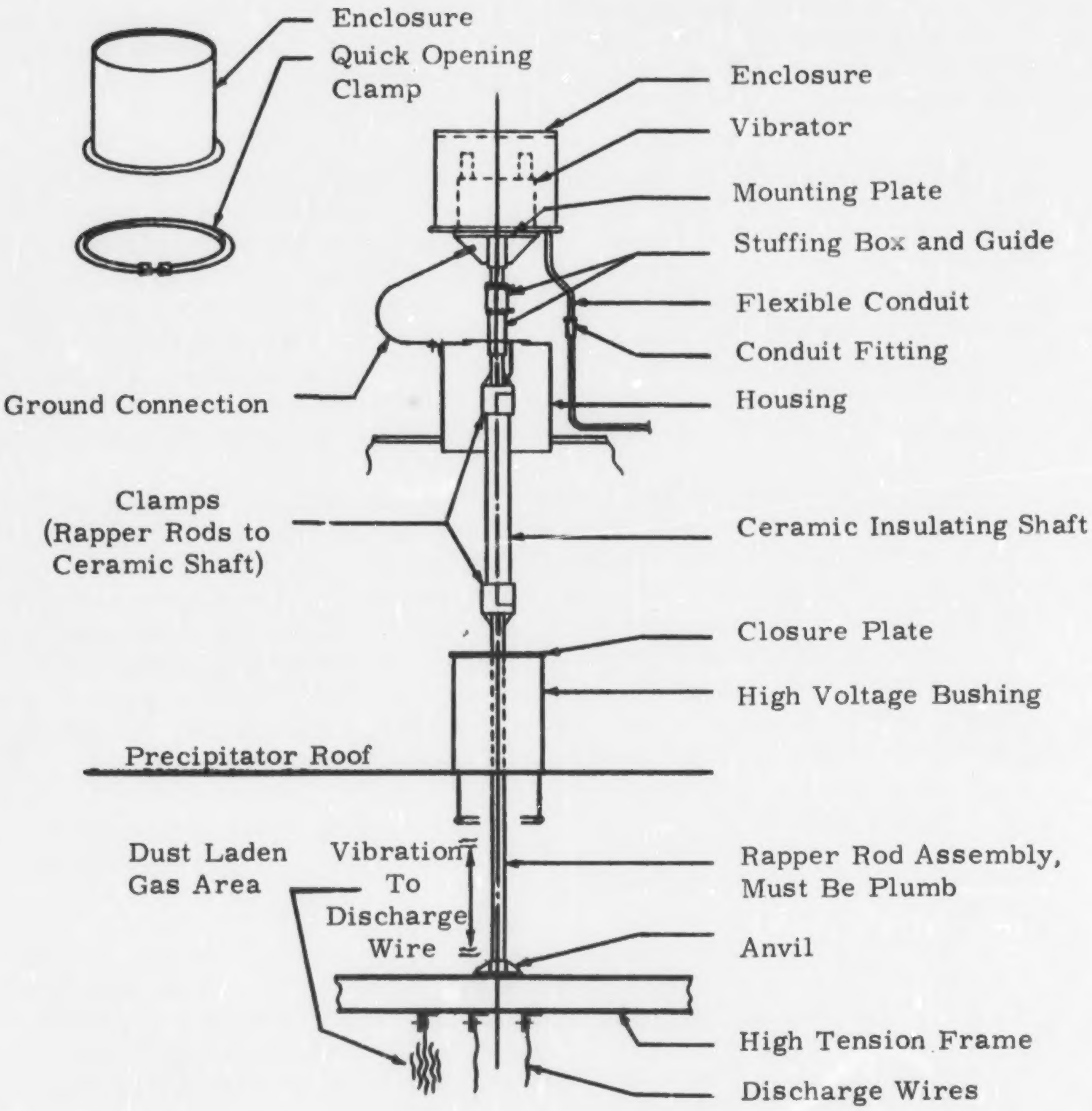

Figure 10.10. Typical Electromagnetic Vibrator Assembly.

hammer swings downward, striking an anvil located on the end of a single collecting electrode. The cam shaft can be located at any height along the plate ends. Rapping control is limited to adjustment of operating time and shaft speed.

Single impact (motor-driven swing hammers). This rapping system is limited to collecting electrode cleaning of dry type horizontal flow precipitators. The mechanism consists of a shaft running horizontally across the precipitator between banks of collecting plates. The shaft is oscillated by a motor-driven mechanical linkage. Hammer heads are connected to the shaft by spring leaf arms. The hammers strike against anvils attached to the ends of all collecting plates. The striking anvils are located near the bottom of the plates. The rapping blow can be varied by adjusting the arc of the hammer swing. Further control is obtained by operating time.

Single impact mechanical rappers. The mechanical arrangement for a mechanically actuated impact-type rapper is illustrated in Figure **10. 11.** The system consists of a cam shaft running across the precipitator. The cams located along the shaft engage the cam disc and raise the hammer rods. The hammer rods are released when the cams reach the end of their lobes and fall under gravitational forces, striking an anvil which is attached to the support structure of the electrodes being rapped. The system of rapping can be used on both discharge and collection electrodes. Rapping control is limited to operating time and shaft speed.

A variation of the mechanical rapper system is the use of swing hammers to provide the impact. These can be located on the sides or ends of precipitator as well as on the top.

Vibrators (air). The major components of a typical vibrator consist of a reciprocating piston in a sleeve type cylinder. The valve is of the centrally located pin type. The vibrator assembly is fastened directly to the end of a rapper rod which transmits the rapping energy to the electrodes to be cleaned. This device is used for both discharge electrode (employing an insulating section of rod) and collecting electrode cleaning. This type of rapper is used for both horizontal and vertical flow, dry type precipitators. For collecting electrodes, the vibrators can be used for either top, side, or end rapping since they operate in any position. For discharge electrode cleaning they are usually used as top rappers. Control consists of varying the air pressure, the duration of

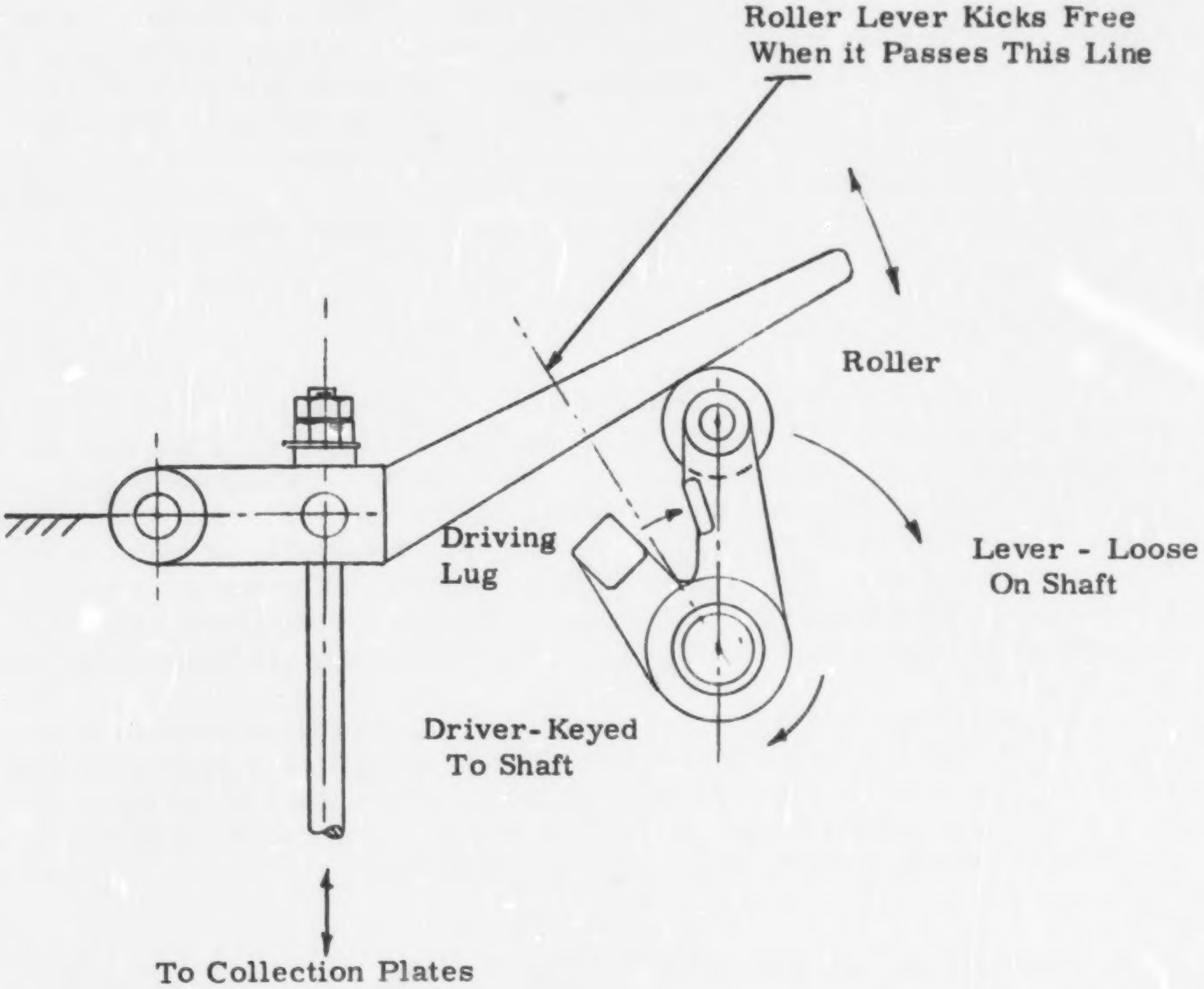

Figure 10.11. Mechanical Single Impact Rapper. Plates Are Raised and Dropped by the Action of the Rapper. Impact of the Plates in the Guide Supplies Rapping Force.

the rapping period, and the time elapsed between cleaning.

Water flush and liquid removal. Some electrostatic precipitators are used to precipitate mists from the gas stream. Most of these applications are found in chemical, petroleum, and paper plants. The mist droplets which collect on electrodes run together to form larger droplets, and then run down the electrode surface where they drain away. In some cases, water or other liquid is introduced at the top of the electrode to improve mist removal.[1] Tube electrodes are more adaptable than plates or rods for this application.[2] Because these electrodes do not require rapping, they can be made thinner, but may need to be fabricated from corrosion resistant material.[1]

10.7 HOPPER SYSTEMS

Hoppers are used to collect and store dry precipitate which is removed from the electrodes. The physical properties and quantity of the dust must be considered when designing hoppers. Heaters are sometimes required to prevent moisture condensation and caking of the dust. The outlet and slope of the sides must allow the dust to be removed adequately. If hoppers are allowed to overflow, collected dust will be reentrained in the gas thereby greatly reducing precipitator efficiency.[2] Baffles are frequently placed in hoppers to minimize undesirable gas flows which may reentrain dusts.[2]

If the precipitator system is operated with internal pressures less than ambient atmospheric, then air inleakage through the hopper can cause a reentrainment of the dust from the hoppers. Care must be taken to provide good seals around hopper doors and dust removal connections for systems operating under partial vacuum conditions.

10.8 DUST REMOVAL SYSTEMS

Container removal. This system is used on small installations collecting dry material in a hopper. The hoppers are usually of the conical or pyramidal type. The system consists of placing a transportable container below the hopper. The collected material stored in the hopper is transferred to the container through a simple manual valve or slide gate. When filled, the container is removed for emptying. In some instances the container is embodied as part of a truck.

Dry vacuum systems. In this system, dry bulk material is transferred from a precipitator hopper to a transport pipe system which is under vacuum. The material is metered from the hopper to the transport system through automatic rotary feeder valves or dump valves. The system vacuum is developed by an air pump. In order to maintain system fluidity, ambient air or hopper gas is induced as a carrier. The pump discharges the dust into a silo for storage.

Wet vacuum systems. In this system, dry dust is removed from a precipitator hopper into a transport pipe system which is maintained under vacuum by a water aspirator. The collected dust or ash is metered from the hopper into the transport system through automatic feeder valves or dump valves. In order to keep the dust suspended in the gas carrier, ambient air or additional hopper gas is induced into the transport line. The dry material being transported mixes with the water used for aspiration and forms a slurry. From this point the water-dust mixture is run to waste.

Screw conveyors. A screw conveyor system usually starts with an open screw in the bottom of a trough type hopper which moves the dry dust to the outside. At the turns in the system each screw run passes the dust on to each successive screw by a gravity drop. The dust is moved on to a system silo or directly to some mobile conveyance. A screw conveyor system is also applicable with a conical or pyramidal type hopper. A rotary valve is required when the system is operating under vacuum.

Scraper bottom. The precipitator hopper is a flat bottom pan. An endless belt type scraper moves the collected dust to one end where a screw conveyor is located. The screw moves the dust out of the hopper. Once outside, the dust is conveyed to some remote point by any form of system such as container removal, vacuum, or screw.

CHAPTER 10
BIBLIOGRAPHY

1. Strauss, W., Industrial Gas Cleaning, Pergamon Press, Long Island City, New York (1966).

2. White, H. J., Industrial Electrostatic Precipitation, Addison-Wesley, Reading, Massachusetts (1963).

3. Rose, H. E. and Wood, A. J., An Introduction to Electrostatic Precipitation in Theory and Practice, Constable and Company, London (1966).

CHAPTER 11
POWER SUPPLIES AND CONTROLS

The fundamental driving force that removes the dust from a gas stream in electrostatic precipitators is that between an electric field and a charged dust particle. Therefore, the electric field in the vicinity of the collection electrode should be maintained as high as practical in order to provide the maximum possible gas cleaning efficiency. The function of the power supply and related control system (power pack) is to provide optimum voltage and current conditions.

11.1 THE POWER SYSTEM

The power supply system consists of four components as shown in Figure 11.1: a step-up transformer, a high voltage rectifier, a control element, and a driving function or sensor for the control system. The step-up transformer is required because the voltage levels for modern precipitators can range from about 30 to 100 kV.

The high voltage rectifier is required to convert the high voltage ac power to varying direct current to be compatible with the electrostatic precipitator requirements.

One function of the control system is to vary the amplitude of the dc voltage that is to be applied to the electrode system. This control can be applied to either the primary or the secondary circuit in the power supply, but it is customarily utilized in the primary or low voltage side. The control system can be operated either manually or in one of several automatic modes. Automatic control systems are typically installed in all modern commercial installations. A well-designed automatic control system serves to maintain the voltage level at the optimum value, even when the dust characteristics and concentration exhibit dynamic behavior.

High voltage generation. Techniques for generating high voltage include the use of frictional types of high voltage machines, such as the Van de Graff generator, high frequency transformer, and the standard iron core voltage transformer. Both the frictional type generator and the high frequency transformers are too limited in current capacity for practical

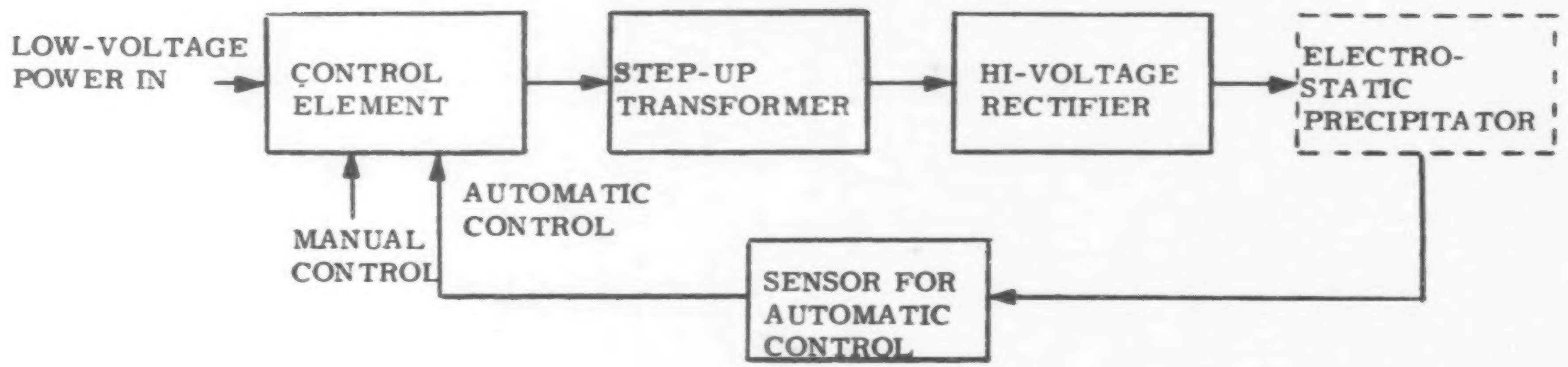

Figure 11.1. The Power Supply System for Modern Precipitators.

commercial precipitators, hence, the conventional high voltage power transformer is universally used as a means for converting the normal power line voltage to the values required for precipitator operation.

High voltage rectifiers. The high voltage rectifying equipment has passed through several stages of evolution to reach its present stage of development. The invention of the synchronous-mechanical rectifier in 1904 by Lemp[1] and utilized by Cottrell in 1907 was the first means for providing sufficient power at high voltage so that electrostatic precipitation became feasible. In this system, a high voltage alternating current is fed to a rotating spark gap that is driven in synchronism with the applied ac power. The phasing of the spark timer is such that ac is converted to pulsating dc. A schematic diagram of the mechanical rectifier, included primarily for historical purposes, is shown in Figure 11. 2.

Point A lines up with Point 1 when Point 1 is at a positive voltage. As the sine wave changes to where Point 1 becomes negative, the rotor turns to align Point B with Point 1 so that the output always maintains a voltage of the same polarity. It is imperative that the rotational speed of the spark gap maintain synchronism with the driving voltage.

Shortly after the development of the synchronous rectifier, Lodge[2] in England patented the use of mercury vapor rectifiers. However, high voltage rectifier tubes were not used commercially until 1920.

The first nonrotating (static) power supply utilizing rectifier tubes was installed in the early 1920's. Copper oxide rectifiers[3] were utilized in about 1928. Selenium rectifiers were introduced about 1939. These devices, with significantly smaller electrical losses, allowed the development of static power supplies that were economically competitive with the mechanical unit. A diagram of the static rectifying system is shown in Figure 11. 3 where either vacuum tubes or diodes act as the rectifying element.

More recent rectifier developments include high-voltage, high-efficiency vacuum tube and single-crystal silicon rectifiers. The silicon rectifiers are currently the most widely used for new installations since they provide high conversion efficiency and high reliability.

Voltage control. In the normal operating range, the transformer is linear, so that the output voltage is directly proportional to the input voltage. The output voltage can therefore be controlled by changing the voltage input to the

---

[1] Refer to the bibliography for this chapter.

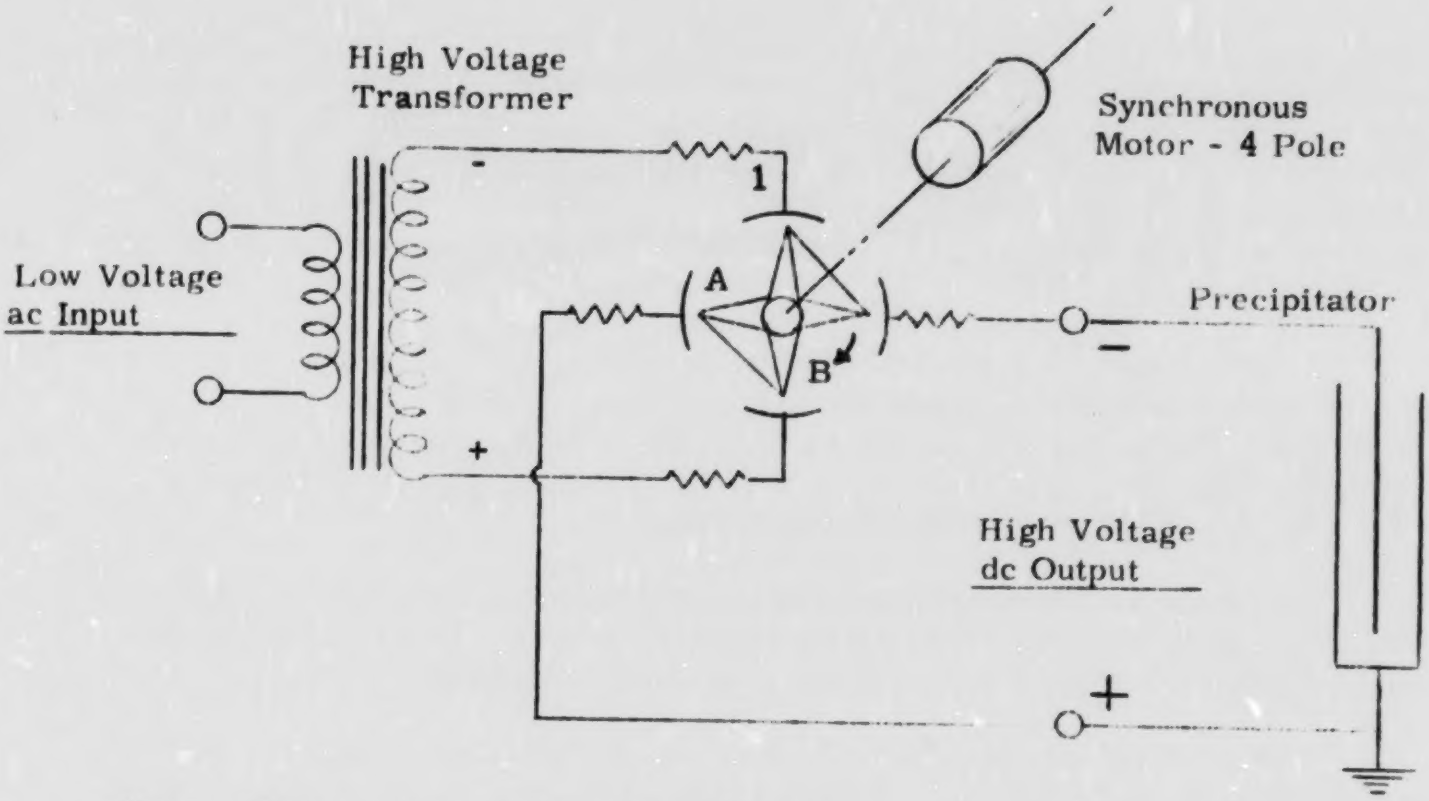

Note: Motor and transformer connected to same electrical source.

Figure 11.2. Full-Wave Mechanical Rectifier H-V Power Supply.

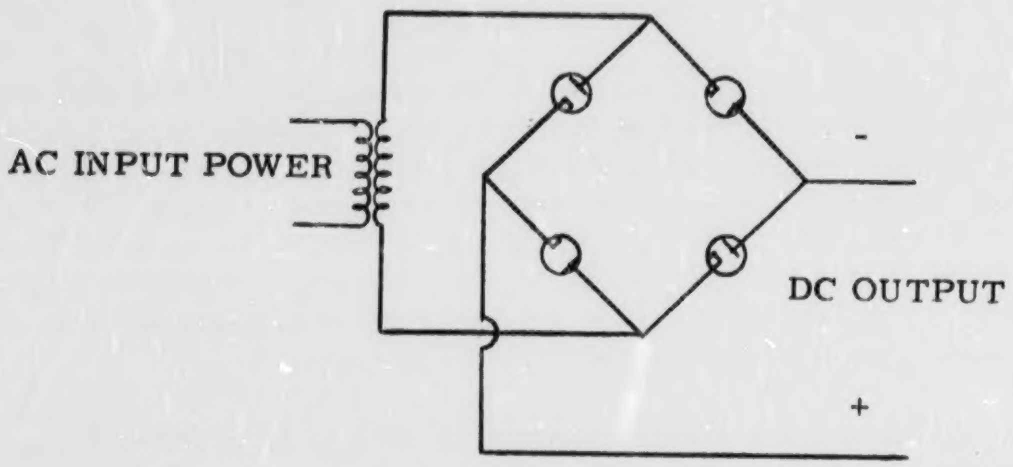

Figure 11.3. Vacuum Tube Rectifier.

transformer. Some common techniques for voltage control include tapped series dropping resistors, series rheostats, tapped transformer primaries, variable inductances or solid state control devices. Some installations use combinations of control elements where gross voltage control is accomplished by tapped devices and continuously variable devices such as rheostats or inductances provide the fine control. Some of the more modern control devices include saturable reactors (magnetic devices), silicon controlled rectifiers (SCR), and thyristors (four-element, solid-state devices). The reactive control elements in general lead to a more efficient power conversion subsystem than do the resistive ones.

The current limiting function is necessary to avoid catastrophic failure of the power supply under arcing conditions. When an arc exists between the corona wire and the collection electrode, the ionized path constitutes essentially a short circuit across the power supply. Without a means for current limiting, excessive current will flow which will lead to a catastrophic failure of the power supply. This protection can be provided by a variety of devices including resistors, various combinations of reactive elements or active devices in the control subsystem.

The signal to the control device determines the operational characteristics of the power supply so long as the design of the overall system is sufficient to provide the needed capability. This control signal can range from a simple manual setting of a passive device (tapped element) to a dynamic control signal related to current, voltage, spark rate, or combination of these. The shortcomings of manual control became evident early in the period of commercial application to precipitators. The voltage-current characteristics of the precipitator are related to the dust concentration and composition. Extremely heavy dust loads tend to quench the corona current in the input section of the unit and high resistivity dusts lead to increased voltage drops in the deposit layer, with the result that excessive sparking, back corona, or simply poor collection efficiency occurs. Therefore, the need for dynamic control becomes obvious.

Various combinations of the above parameters (voltage-current-spark rate) have been utilized in power supply automatic controls, but the predominant one currently used in this country is spark rate together with a current limit. The spark rate control establishes the applied voltage at a point where a fixed number of sparks occur per minute (typically 50-150 per corona section). The spark rate is a function of the applied voltage for a given set of precipitator conditions. The higher the voltage, the greater the spark rate. As the spark rate increases, a greater percentage of the input power is wasted in the spark current, and consequently less useful power is applied to dust collection. Thus, the spark rate control should be designed to maintain the precipitator at or near the optimum operating point. The optimum conditions correspond to the highest time average voltage on the precipitator.

As the dust conditions and concentration change, sparking conditions change. Specifically, a highly resistive dust can cause sparking to occur at a lower than normal applied voltage (this is discussed in detail in the section on particle collection). The automatic spark rate control adjusts the applied voltage downward to bring the collector into a more efficient operating range if high dust resistivity is encountered.

The spark rate control senses voltage or current surges caused by the sparks. A schematic diagram of one type of spark rate control is shown in Figure 11.4. The operation of the circuit is as follows: the current surge in the primary circuit, associated with a spark in the secondary, is sensed by the detector. This signal fires the thyraton V_1 which discharges capacitor C_1. When V_1 is turned off, capacitor C_1 charges through R_1 applying a voltage across the series combination of R_2 and C_2. Thus, with continual sparking, a voltage is developed across C_2 which is proportional to the spark rate of the unit. C_2 tends to discharge through resistor R_3 generating a signal V_s on the plate of diode V_2.

A reference signal V_b that opposes V_s is developed by voltage divider R_4 across battery B that is connected in series opposition to V_s. These two voltages are compared at the diode where an increasing voltage signal is developed across R_5 until V_s just exceeds V_b where the circuit establishes equilibrium. A detailed description of this circuit is given by Van Hoesen.[4]

In the case where the dust conditions are such that no sparking occurs, the voltage or current will increase up to the maximum capability of the power supply. In this case it may be necessary to include a maximum voltage or current limiter to avoid damage to the power supply.

Sectionalization. It has been experimentally determined that the overall collection efficiency of a spark rate limited installation can be improved by increasing the number of independently powered electrical sections

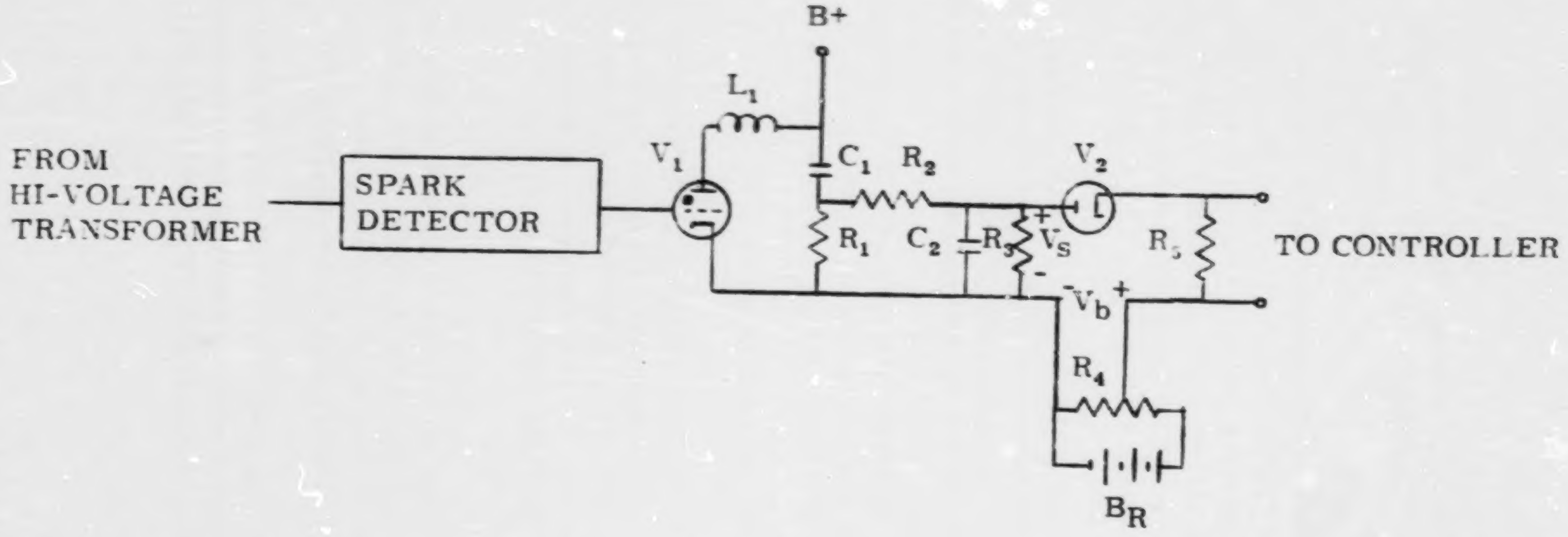

Figure 11.4. Spark Rate Control Circuit from Van Hoesen, et al.

(corona) in the precipitator.[5]

The spark rate in an electrostatic precipitator as given by White[6] follows an exponential relationship as shown below.

$$S = \exp b\,(V_p - V_i) \qquad (11.1)$$

where

S = spark rate sparks/min,
b = empirical constant,
V_p = peak voltage, and
V_i = initiation voltage (voltage for one spark per minute).

Thus, as the applied voltage increases above V_1, the spark rate increases accordingly. This increase in voltage leads to two conflicting effects. First, the increased voltage increases the charge and electric field in the precipitator, which tends to increase the collection efficiency. But, in contrast to this, a spark tends to short circuit the power supply and reduce the collection efficiency for the duration of the spark. The overall effect of these two factors is shown in Figure 11.5, where the maximum efficiency occurs at a spark rate of about 125 per min. This discussion specifically applies to a precipitator operating from a single power supply where one spark short circuits the entire collector unit.

Next, consider a similar situation where two independent power supplies are used, each supplying only one half of the collection area. The sparking condition for the entire precipitator will still follow the same spark rate equation above, but a spark will now disable only one-half of the precipitator. In this case, two sparks will be required to be as detrimental as one was in the original example, which leads to an effective spark rate of about 250 per minute. A further increase to ten electrical sections will similarly raise the overall effective spark rate to 1250. This increased spark rate will occur at a significantly higher applied voltage than the original single section case.

A numerical example will serve to show the changes in applied voltage to be expected. Consider the case where spark initiation occurs at an applied voltage of 33 kV and a spark rate of 125 per min occurs at an average voltage of 42 kV. Substitution into Equation 11.1 yields

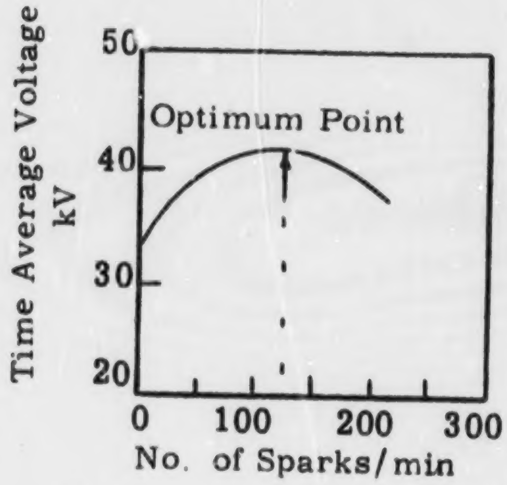

Figure 11.5. Optimum Operating Voltage for Single Section of a Precipitator (Reference 7).

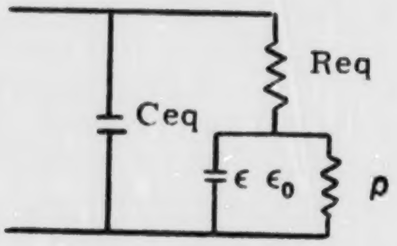

Figure 11.6. Equivalent Circuit of the Precipitator Collection Electrode System.

$$S = \exp b\,(V_p - V_i) \qquad (11.2)$$

$$125 = \exp[b(42 - 33)] = \exp(9b)$$

$$b = \frac{1}{9} \ln 125 = 0.536$$

The voltage required for a spark rate of 250 per min yields a value for the peak voltage of

$$V_p = \frac{1}{b} \ln S + V_i$$

which for S = 250 yields

$$V_p = 10.3 + 33 = 43.3 \text{ kV}$$

and similarly for S = 1250

$$V_p = 13.3 + 33 = 46.3 \text{ kV}$$

Thus, the effect of the increased sectionalization is seen to lead to a significant increase in the applied voltage, which generally leads to increased collection efficiency.

In addition to the sparking effect, increased sectionalization tends to isolate portions of the precipitator with mechanical defects such as broken or misaligned wires, and misaligned collection electrodes or other factors that tend to cause a reduction in the operating voltage of localized sections.

A further advantage of sectionalization of the precipitator power supply is the higher internal impedance associated with the smaller capacity power supplies. Higher impedance tends to limit the current and minimize the tendency for power arcs to develop.

The precipitator constitutes a capacitive load and the energy stored in the precipitator depends upon the capacitance of the section and the voltage to which it is charged.

If a spark occurs within a precipitator, the energy stored in the precipitator due to its capacitance tends to sustain the spark for a given time. However, the current drain during a spark is heavy relative to normal current flow from the power supply, and the spark would tend to be quenched when the energy from the precipitator has been dissipated in the spark.

However, if the power supply impedance is low, the power supply voltage can supply a sustaining value of current while the arc is maintained. Consequently, the precipitator capacitance may not be completely discharged during the interval that the power supply voltage reaches its minimum value. In such case, the spark would not be extinguished and a condition known as a power arc would develop. The current limit on the power supply normally quenches a power arc; however, considerable disruption of the precipitator occurs during the period of the arc. Low impedance power supplies are not as effective in spark quenching and power arcs can develop more frequently than in precipitators powered by high impedance supplies.

Waveform selection. Electrostatic precipitation theory shows that the collection efficiency is fundamentally related to two factors: the charge on the dust particles and the average value of the electric field in the collection zone. The charge on the particles is related to the peak value of the electric field in the charging region (field charging). The basis for the selection of the waveform should take these factors into consideration.

There are several choices of waveform including: pure dc, half-wave and full-wave rectification and pulsed supplies. Pure dc is seldom, if ever, used, primarily because of its poor spark quenching characteristics.

In general, half-wave power supplies provide a greater degree of sectionalization, although the sections are not completely independent, since control is normally associated with the transformer primary. Full-wave rectification is used where higher average currents are required, as for example, where large dust loading or extremely fine particles lead to a large space charge which limits current flow.

The effect of the voltage waveform on precipitator operation can be seen from the equivalent circuit, Figure **11.6**.

The dust layer constitutes a distributed capacitance, the magnitude of which is given by $C_d = \epsilon \epsilon_0$ where ϵ = relative dielectric constant and ϵ_0 = permittivity of free space and a resistance, given by the dust resistivity ρ. The effect of this combination is to provide a filtering action to the buildup of voltage which results in a delay in the voltage appearing across the dust layer. The higher the dust resistivity and the greater the dust capacitance, the greater the delay in charging. Thus, for a time varying applied voltage, the voltage appearing across the dust layer will in effect be filtered and will not follow the swing of the applied voltage.

The parallel capacitance C_{eq} constitutes the distributed capacitance of the precipitator due to the electrodes. The large area represented by the collection surface and the discharge wires can lead to an appreciable capacitance. If the wires are assumed to be a plate, the capacitance due to the geometry can be calculated from

$$C_{eq} = \frac{\epsilon_0 A}{d}$$

where ϵ_c = permittivity of free space, A = plate area, d = distance between electrodes. For a 10 cm plate-to-wire spacing and 1500 m^2 of plate area, the capacitance would be

$$C_{eq} = \frac{8.85 \times 10^{-12} \times 1500}{0.1} = 0.126 \mu \text{ F}$$

In practice, the capacitance must be around half this value for the given dimensions due to the effect of the discharge wires.

The equivalent resistance of the precipitator can be computed from

$$R_{eq} = \frac{V}{I}$$

For a precipitator of 1500 m^2 plate area, a current of 400 mA at an applied voltage of 40 kV would be typical. For these conditions

$$R_{eq} = \frac{40 \text{ kV}}{400 \text{ mA}} = 100 \times 10^3 \text{ ohms}$$

This equivalent resistance is not a constant since the voltage-current relationships in the corona systems are not linear. However, as a final approximation, the assumption of a constant resistance will serve to illustrate the operating conditions.

The time required for the charging and discharging of the capacitance represented by the equivalent circuit is determined by the value of the capacitance and resistance. The time constant can be computed from τ = RC =

$(0.126 \times 10^{-6} \times 100 \times 10^{3}) = 12.6 \times 10^{-3}$ sec, which means that about 12.6 milliseconds would be required for the charge in the capacitance to reach 63% of its final value if a steady dc voltage is applied.

Since the normal voltage source is a time varying one, the effective voltage applied to the precipitator electrodes would be a function of the applied voltage waveform and the precipitator impedance. Figure 11.7 shows the precipitator voltage resulting from a 60 Hz half-wave and full-wave supply and a 500 Hz pulsed voltage supply. The waveforms were computed on the basis of the equivalent circuit of Figure 11.6 and the values of capacitance and resistance given above.

As indicated in Figure 11.7, the capacitance of the precipitator maintains the applied voltage at some minimum value even though the applied voltage would go to zero for a half cycle in the absence of the precipitator capacitance.

The 500 Hz pulse power supply indicates the effect of the higher frequency. Since charging current is applied more frequently, the resultant precipitator voltage approaches that of a dc voltage.

Studies of the effect of waveform have shown that higher peak voltage can be applied before sparkover if the voltage rise rate is rapid. It can be shown from the equivalent circuit that the integrating effect of the dust layer prevents the voltage across it from rising as rapidly as the applied voltage. Consequently, since sparking is related to the electric field at the dust surface, a higher peak voltage can be applied before sparking occurs.

In general, the value of the peak voltage determines the maximum charge on a particle in the field charging mode. For optimum collection, the product of the average and maximum field should be as high as possible. This condition would be met by a rapid voltage rise rate.

However, the particle charge rate is also a very significant variable in terms of precipitator performance. Pulse type power supplies must provide sufficient pulse width for the particles to acquire their charge and this requirement tends to limit the effectiveness of pulse power supplies.

The practical high voltage power supply. The practical aspects of power supply requirements place additional requirements on the designer. The

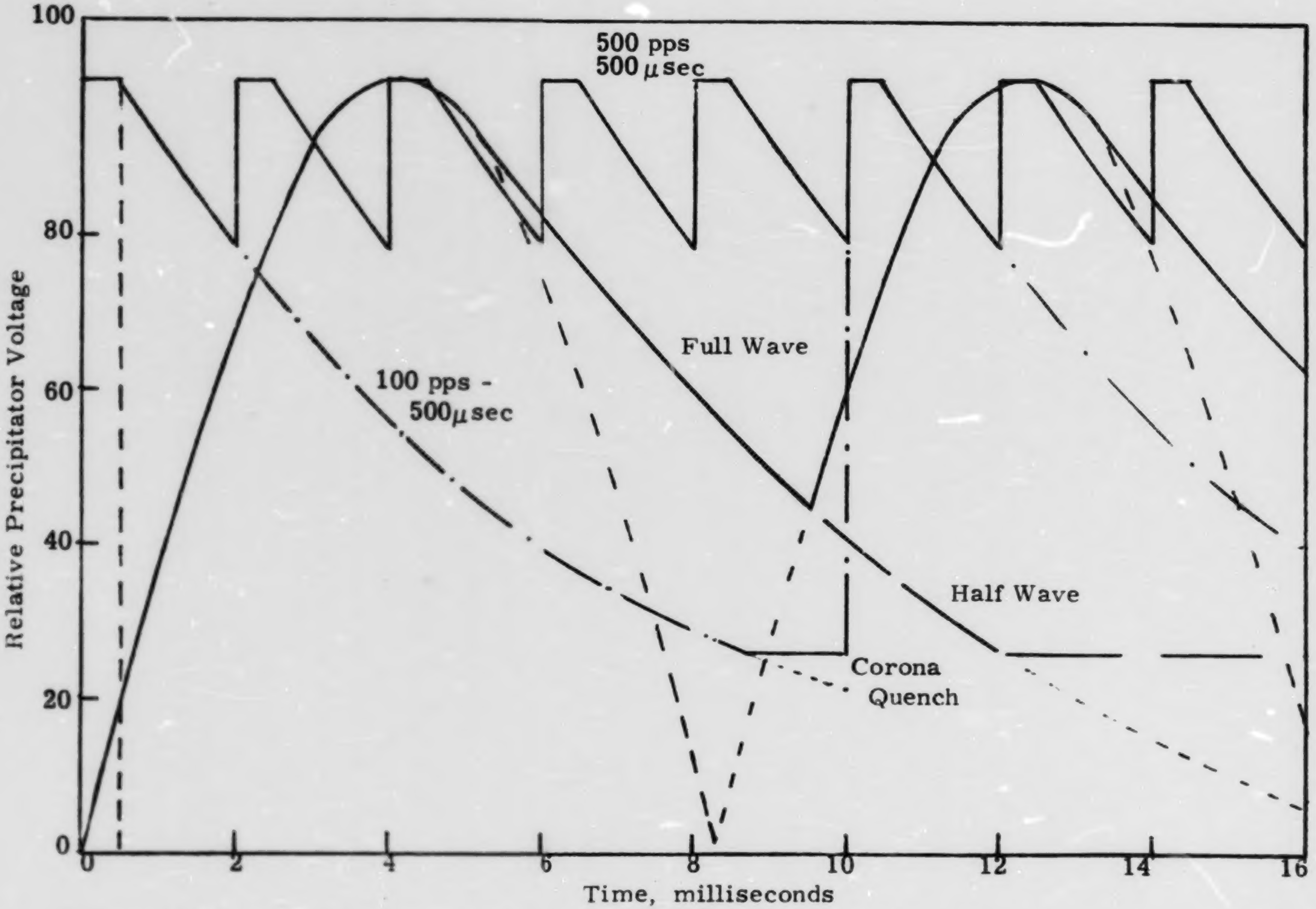

Figure 11.7. Time Response of the Precipitator Equivalent Circuit to Various Voltage Waveforms With the Same Peak Amplitude.

various alternative techniques for fulfilling these requirements provide some insight into the problems facing the designer of a precipitator power supply.

H-V transformers

H-V transformers for precipitation rectifiers are conservatively designed and ruggedly constructed to withstand high average ambient temperatures and continuously occurring electrical transients due to precipitator sparking.

The high voltage and power level requirements are best satisfied by liquid-immersed, self-cooled designs. The insulating and cooling liquid is usually transformer grade mineral oil. In some instances fire insurance regulations dictate use of nonflammable oil (Askarel). The latter material is expensive and requires special insulation system designs because of its electrical dielectric and solvent properties. Transformers 50 kVA and larger require extended cooling surfaces, in the form of convectors, to maintain low temperature rise.

The shell-type, single-phase transformer core and coil arrangement is normally used. Stacked cut core designs are common and in some instances tape-wound (cut "C") cores are used. The L-V primary winding is placed adjacent to the core and the H-V secondary winding is placed over the primary winding. Though a single-layer-type secondary winding can be used, it is advantageous to use two coils, which can be arranged to minimize electrical stress on the primary-secondary insulation. Numerous oil ducts are included in both primary and secondary windings to minimize thermal gradients and assure thorough impregnation. Surge screens are used at both ends of the secondary winding for protection against transient voltages. A grounded electrostatic shield between primary and secondary windings is useful for minimizing radio interference caused by precipitator corona and sparking. The core and coil structures also require adequate structural bracing to withstand mechanical stresses and shocks induced by precipitator short circuits and sparkover.

Mechanical rectifiers

Figures 11.2 and 11.8 illustrate typical FW and HW rectifier arrangements. The rotors are driven by an 1800 RPM synchronous motor and,

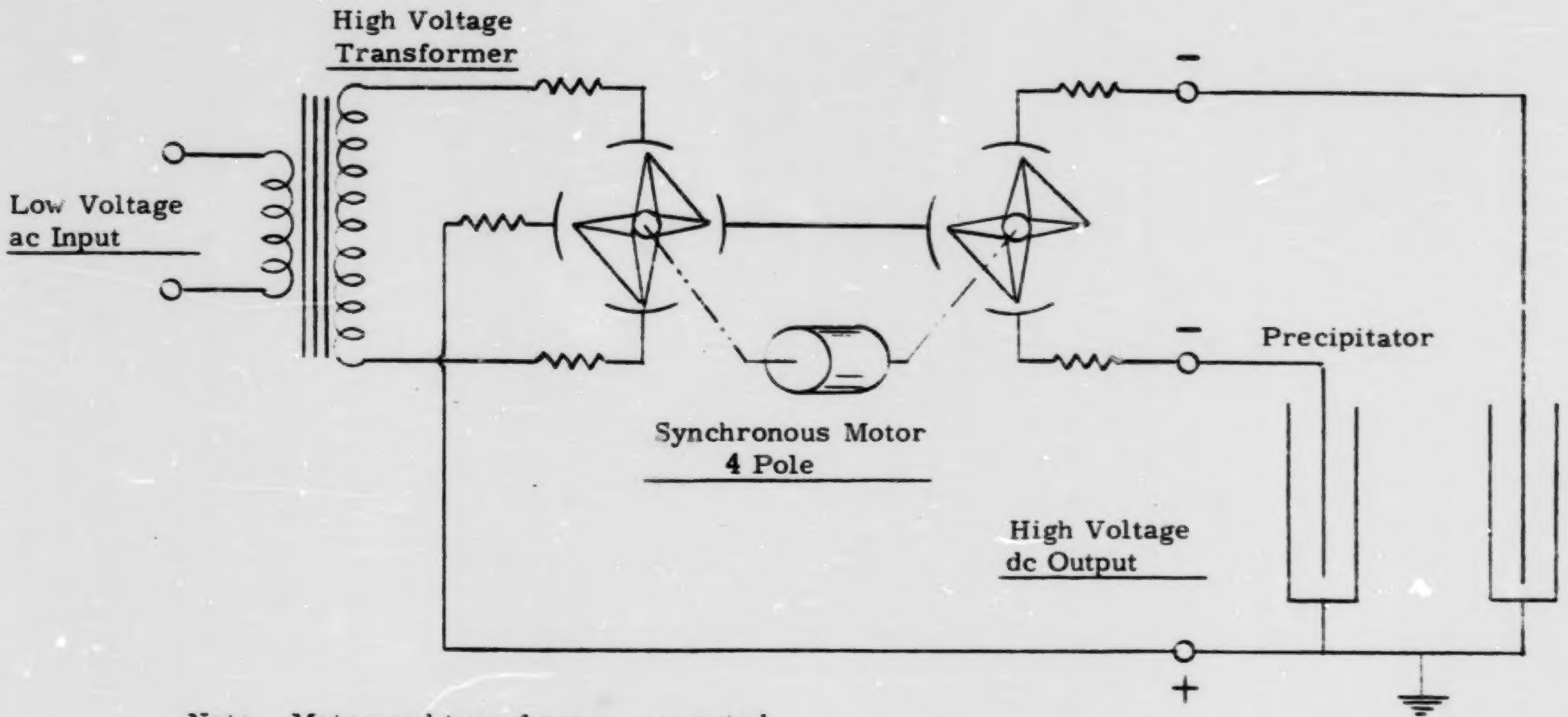

Note: Motor and transformer connected to same electrical source.

Figure 11.8. Half-Wave Mechanical Rectifier H-V Power Supply.

in effect, alternately switch H-V transformer connections to the precipitator once each half-cycle. In the HW rectifier, the second rotor essentially distributes alternate pulses to two precipitator sections. Because of high tip velocities, a small gap ($\sim \frac{1}{8}$") is needed between the rotor tips and arc shoes. These gaps (4 in series for FW and 6 in series for HW) introduce substantial voltage and power losses in the system, particularly when clearance increases to $\frac{1}{4}$" or $\frac{1}{2}$" due to tip burning. The intense electrical discharge in these gaps generates toxic gases, heat, and radio interference radiation. The former are dissipated by special ventilating systems, and the latter by grounded enclosures and radio interference chokes and filters. Quite often resistors (4K to 10K) are placed in the H-V rectifier leads to reduce severity of precipitator sparking transients.

These rectifiers are often driven with 3-phase reluctance-type synchronous motors of approximately 1 HP. These motors are essentially squirrel cage induction motors with salient poles milled in the rotor. Since these rotors do not have fixed magnetic polarity, special polarity sensing and transformer polarity reversing contractors are needed to insure negative H-V output. In the more modern designs permanent magnets were incorporated in the rotor structure. This change eliminated the special polarity controls and improved motor performance.

Electron tube rectifiers

Figure 11.9 illustrates the single-phase bridge commonly used for FW and HW energization. It will be appreciated that electron tube rectifiers offer considerable practical improvement over the mechanical rectifier in regard to electrical efficiency, noise, toxic gases, lack of moving parts, fixed polarity, and size.

The principal disadvantages are tube replacement costs, need for filament power, and some X-ray radiation. X-ray radiation is seldom a problem because it is soft and easily shielded by the steel rectifier enclosure provided for weather and H-V hazard protection. The filament power is provided by one or more small filament transformers which are oil immersed with the H-V transformer.

Tungsten filament tubes provide tube life of from 10,000 to 20,000 hours, by operating at a filament voltage just sufficient to satisfy the peak current requirements. Inherent current limitations of these tubes preclude

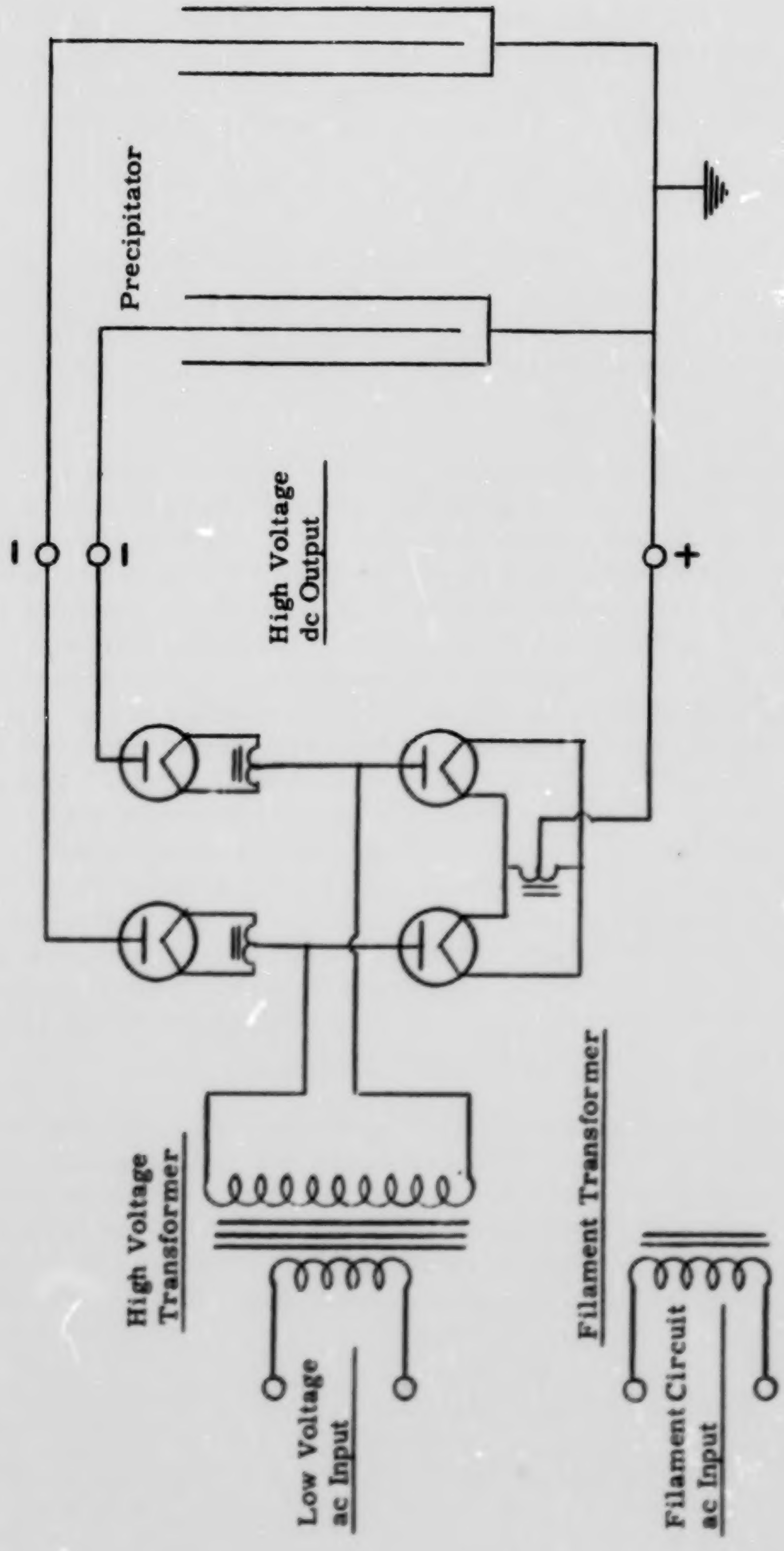

Figure 11.9. Tube Rectifier H-V Power Supply.

their use in rectifiers larger than 750 mA if reasonably long life is to be obtained. In most energization systems means are included to insure a one minute tube filament warmup before application of H-V and quite often voltage stabilizers are provided to closely regulate filament voltage.

Silicon rectifiers

In 1956, application of silicon rectifier elements to precipitation rectifiers quickly followed general commercial availability of the basic silicon devices. Rectifier failures were common at first, but have been essentially eliminated by appropriate design criteria and uniformity of rectifier junction manufacture.

Series strings of rectifier junctions are used as arms in single-phase bridge rectifier connection. Depending upon the characteristics of the rectifier junctions, transient voltage distribution is accomplished along the string by either resistance, capacitor, or resistor-capacitor networks. With development of the "avalanche diode," it is sometimes possible to obtain adequate transient voltage distribution solely through avalanche voltage limiting without resorting to a compensating network. The rectifier legs are composed of a sufficient number of 500 to 1200-V rectifier cells, each rated for approximately 1A average current. These cells are mounted on insulating boards with provision for simple connection in the circuit. It is general practice to immerse the silicon rectifier assemblies with the H-V transformer. This provides a compact package and an ideal ambient for the H-V elements. The insulating fluid can be either transformer oil or Askarel. In case of Askarel, a rectifier failure generally produces sufficient contamination to also ruin the H-V transformer. In most cases, air core inductors are included in the dc output leads of silicon rectifiers. These chokes serve to reduce severity of the precipitator sparking transients on the rectifier assembly by slowing voltage and current wavefronts.

H-V silicon rectifier assemblies have not been specified and typed like the H-V rectifier tubes. This is largely due to differences in rectifier junction manufacture and specialty of the precipitation rectifier application. As previously mentioned, several H-V rectifier modules are available and are used to replace mechanical and tube rectifiers. In general, these assemblies are for lower current sets, 500 mA or less.

Description of L-V control components

Manually operated rheostats were used as a variable series impedance means to vary energization levels in early electrical sets. In general, the control range was quite limited and also directly related to precipitator current requirements. This control situation was helped somewhat by use of primary taps on the H-V transformer and a tap switch which essentially changed the transformation ratio.

Power rheostats similar to field rheostats with cast iron grids were common. In some cases more modern strip or ribbon resistance elements were used in conjunction with power tap switches to vary resistance. Suitable resistance values ranged from 1 to 8 ohms depending upon current levels and power losses could run as high as 15 to 18 kW. The rheostats were constructed so that 20 to 40% of the total resistance was always in the circuit as ballast. This ballast performed the essential function of spark quenching.

Tapped input autotransformer

Use of tapped input autotransformers provides true voltage control at moderate costs. These arrangements often have a control range of ≅ 50% and permit relatively close adjustment by means of coarse and fine voltage tap switches. Operation of the tap switches momentarily de-energizes the system—generating transient electrical surges and often puffs from the precipitator. Ballast resistors are also incorporated for spark quenching.

Variable autotransformer

Variable autotransformers either manually or motor operated provide true voltage control without the circuit interruption of tap switching. Motor operated units also provide means to automatically raise and lower voltage in accordance with relay controls. These assemblies are prone to commutation difficulties, particularly when the brush remains stationary at one point on the winding for long periods of sparking operation. The usual voltage control range is ≅ 50% for precipitation rectifier control.

Induction regulator

The induction voltage regulator is essentially a variable transformer wherein secondary voltage is varied by changing magnetic flux linkages between primary and secondary windings. Its construction is similar to a wound rotor induction motor with a blocked rotor whose angular position can be varied to change magnetic coupling. It is usually connected in autotransformer fashion with the stator winding in shunt with the load and the rotor winding in series with the load. These regulators are usually motor operated, and hence adaptable to automatic control systems. Though rugged, and the most expensive of the three voltage control means, these regulators are also vulnerable to precipitator sparking. In this case, sparking transients cause rapid wear of the gear drive train resulting in noisy operation and jamming. The usual voltage control range is ≅ 50%.

Saturable reactor

The saturable core reactor provides a good means of control. Load power is controlled in accord with the dc current supplied to the control winding. Since control is accomplished by electrical signal, the saturable reactor is well-adapted for continuously controlled automatic systems. It is a static device and can be designed to provide long life under all sorts of electrical abuse.

Both full-range and partial-range reactors are used for power control purposes. The partial range reactor arrangements usually require fixed resistance in the primary circuit to limit short-circuit currents. With high-gain, full-range reactor designs, it is possible to combine the power control, ballast, and automatic fault current limiting functions in a single device.

Saturable reactors are not well-suited for use with mechanical rectifiers because phase shift effects seriously affect the rectifier phasing. They are also not well-suited for use in conjunction with monocyclic networks. High powered systems, 700 mA and larger, with saturable reactor controls are sometimes adversely affected by H-V sparking under light load. Basically, the spark transient unbalances core fluxes causing unsymmetrical H-V waveforms, which induce additional sparks. In bad situations, many cycles may be required to return to normal symmetrical operating conditions.

Thyristor

Phase control with back-to-back thyristors (silicon controlled rectifiers) is an excellent means to control precipitator energization levels.

Fast, full-range control is easily accomplished with negligible control power and the system is easily adapted to automatic control. Control is achieved by synchronous switching techniques and the switching devices (SCR's) have low losses in the "on" and "off" states. Successful application of thryristor phase control was realized in 1967. It is highly contingent upon selection of reliable, adequate devices, proper firing circuitry, and due consideration of electrical conditions in precipitator energization. Use of thyristors in conjunction with silicon rectifiers now permits electrical set conversion efficiencies $(\frac{KWdc}{KWac} \times 100)$ of 76% at 1500 mA, 50 kV power levels. The theoretical maximum conversion efficiency for a full-wave, single-phase rectifier is 81%, assuming lossless components.

Ballast elements

The circuit ballast function is simply satisfied by the fixed resistors of suitable rating. Resistors with ribbon or expanded metal grids prove reliable and operate at reasonably low temperatures without hot spots.

The monocyclic network originally proposed by Steinmetz is an excellent ballast element because it is an energy storage device. It is simply a resonant bridge circuit which draws power from the source only when load impedance is high. As such, it inherently limits power under short circuit precipitator conditions. Unfortunately, monocyclic networks are expensive to construct and they have the ability to severely overload components in the event of an open-circuit condition.

The ac reactor is another good ballast element which will limit fault currents quite efficiently. This is an inductive element, and some care is needed in its application to make certain it does not introduce high voltage transients into the system.

CHAPTER 11
BIBLIOGRAPHY

1. Lemp, H., U.S. Patent 774,090 (1904).

2. Lodge, Sir Oliver, U.S. Patent 803,180.

3. Stevens, S. A., et al., "High Voltage Supplies for Electrostatic Precipitators," Institute of Electrical Engineers, Colloquium on Electrostatic Precipitators, London (1965).

4. Van Hoesen, H. E., "Automatic Control of Electrical Precipitators," *Paper 58-229*, AIEE Winter General Meeting (Feb. 2-7, 1958).

5. Ramsdell, Roger, "Design Criteria for Precipitators," American Power Conference (April 23-25, 1968).

6. White, H. J., *Industrial Electrostatic Precipitation*, Addison-Wesley, Reading, Mass. (1963).

CHAPTER 12
MEASUREMENTS

12.1 MEASUREMENT OF GAS FLOW AND EFFICIENCY

Standardized procedures have been established by various organizations for the determination of the dust content of gases and the efficiency of dust collection equipment. Many of the standards are either based upon, or are similar to the ASME Performance Test Code PTC-27, 1957. Table 12.1 compares some specifications of six different measurement standards.

The usual procedure in dust sampling is to determine the gas velocity at a number of points in a cross section of the ductwork as in a standard pitot tube traverse. The individual readings are used to determine the required velocity for isokinetic sampling of the dust laden air. Alternatively, a null type pitot tube may be used to obtain isokinetic sampling. The mean velocity is used to calculate the total volume of the air per unit time. Dust samples are taken with a filter, and the change of weight gives the total weight of dust per unit time. The two results together give the mean dust concentration. Corrections are made as required for temperature, humidity, pressure, weight of filter media, condensation, etc.

12.2 VELOCITY AND GAS VOLUME

The choice of station for testing is governed by accessibility of the location and the expected uniformity of the gas flow. Ideally, the test station should be in a straight run of duct 8-10 diameters downstream from the nearest disturbance to gas flow such as an elbow or transformation, although in practical installations, it is seldom that such a sampling point is available. Alternate total gas flow calculations are sometimes made from stoichiometric calculations on the carbon dioxide-carbon balance of the fuel consumed, and also are sometimes made from the blower characteristics.

The sampling traverse is used for both velocity readings and dust sampling. The number of points in a traverse should be as large as economically feasible. The standards are not well established for the number of test points, as can be seen from the table. In a round duct or flue, the sampling points are taken at the centroids of equal area annular

Table 12.1

Comparison of Six Measurement Standards

Specification	Organization and Publication A. S. M. E. * PTC-27	I. G. C. I. * Pub. No. 1	V. D. I. * 2066	National Council for Paper Industries	Manufacturer No. 1	Manufacturer No. 2
Number of test points	12-20 if velocity range less than 2:1 and area more than 25 ft^2. Double or treble if velocity range >2:1	$\sqrt{\text{sq ft area}}$	Not specified	Same as A. S. M. E.	Same as A. S. M. E.	4 if less than 2 ft^2. 12 if between 2 and 25 ft^2. 20 if more than 25 ft^2.
Location of test points	In a straight run with uniform velocity	Same as A. S. M. E.	In a straight run at least ±3 hydraulic diameters long	In a stable flow pattern 8 to 10 diameters upstream and 3 to 5 diameters downstream to nearest disturbance	In a straight run with 10 times largest dimension upstream to nearest disturbance and with s.p. ≤ 1-in. w.g.	In a straight run with uniform velocity and 8 diameters upstream to the nearest disturbance
Array of test points (rectangular)	Centroids of equal areas	Same as A. S. M. E.	Same as A. S. M. E.	Same as A. S. M. E.	Same as A. S. M. E.	Same as A. S. M. E.
Array of test points (circular)	Centroids of quadrants of equal area anuli	Same as A. S. M. E.	Same as A. S. M. E.	Same as A. S. M. E.	Same as A. S. M. E.	Same as A. S. M. E.
Velocity measurement	Average of pitot tube traverse	Same as A. S. M. E.	Same as A. S. M. E.	Same as A. S. M. E.	Same as A. S. M. E.	Same as A. S. M. E.
Dust sampling nozzle	Thin-edged isokinetic, 1/4-in. diameter minimum	Isokinetic if particles larger than 5 microns. Taper less than 15°	Thin-walled isokinetic, aim within ±5° of flow	Isokinetic if particles larger than 5 microns. Aim within ±5° of flow.	Isokinetic	Isokinetic 1/4-in. diameter minimum
Tubing	Smooth, cleanable, short, airtight, above dew point	Same as A. S. M. E.	Short, airtight, corrosion resistant, and no electric charge	Not specified	Not specified	Smooth, corrosion resistant
Filters	99% collection efficiency, tare less than 20% of dust weight	99% collection efficiency	"complete capture"	Paper, alundum, membrane, glass wool, wet scrubber, or electrofilter	Paper, alundum, asbestos, or tar camera	Paper, alundum, glass cloth, membrane, impinger, or tar camera
Sampling pump	Adequate capacity	Same as A. S. M. E.	Same as A. S. M. E.	Not specified	Aspirator or pump	Vacuum pump
Dust calculation	Sum over all traverse points	Same as A. S. M. E.	Same as A. S. M. E.	Same as A. S. M. E.	Same as A. S. M. E.	Same as A. S. M. E.
Other	Preliminary runs to check instruments and personnel	Same as A. S. M. E.	Include estimate of error	5-10 min/pt 50-60 min total time	Sample at least one hour	Maximum velocity less than 1.5 times minimum

* A. S. M. E.: American Society of Mechanical Engineers.
I. G. C. I.: Industrial Gas Cleaning Institute.
V. D. I. Verein Deutscher Ingenieure (German Engineer Association).

quadrants as shown in Figure 12.1. For a rectangular cross section, the sampling points are taken at the centroids of equal area rectangular subdivisions of the duct. The velocity measurements are made by measuring the velocity pressure with a standard pitot tube. Special pitot tubes for extreme dust conditions may be used provided proper calibration factors are available.

It is important to select the location of the traverse carefully. Locations which have a high degree of turbulence or nonuniformity are undesirable, as are locations with very low velocities which would be difficult to measure accurately. Two location are required, one before the inlet to the dust collector and one after the outlet. The second location is often chosen at the inlet to the induced draft fan where the turbulence and nonuniformity are low and the velocity is high enough to be measured with a reasonable degree of accuracy. The selection of a point before the inlet to the dust collector is usually difficult, because the gas velocity right at the inlet is rather low for accurate measurement, and there is often a diffuser plate in the way. Any other spot upstream from the dust collector inlet is often either turbulent, nonuniform, inaccessible, or hot.

If it is necessary to run a pitot traverse close to the precipitator inlet, the traverse location should be downstream from a diffuser plate at least 5-10 hole diameters or mesh lengths, and far enough upstream from the electrostatic precipitator to prevent sparkover to the sampling probe.

12.3 DETERMINATION OF DUST CONCENTRATION

Samples of dust laden air are taken isokinetically at measured time intervals at the traverse points in the duct. The sample probe should be inserted to the location of the first traverse point with the velocity preadjusted to approximately the isokinetic rate. The probe should be pointed downstream, and the flow cut off until ready to sample. At the start of sampling, the probe is rotated into the flow and the sample flow started. The sampling rate is then checked for isokinetic flow and adjusted if necessary. Gas temperatures and pressures are recorded during the sampling at each point. The probe is held at the sampling point for a predetermined period of time, calculated to give a total dust collection sufficient for accurate weighing, but not less than 10 minutes at each traverse point. A minimum of about 100 milligrams of dust should be collected for accurate weighing. At the proper time, the probe is moved quickly to the next

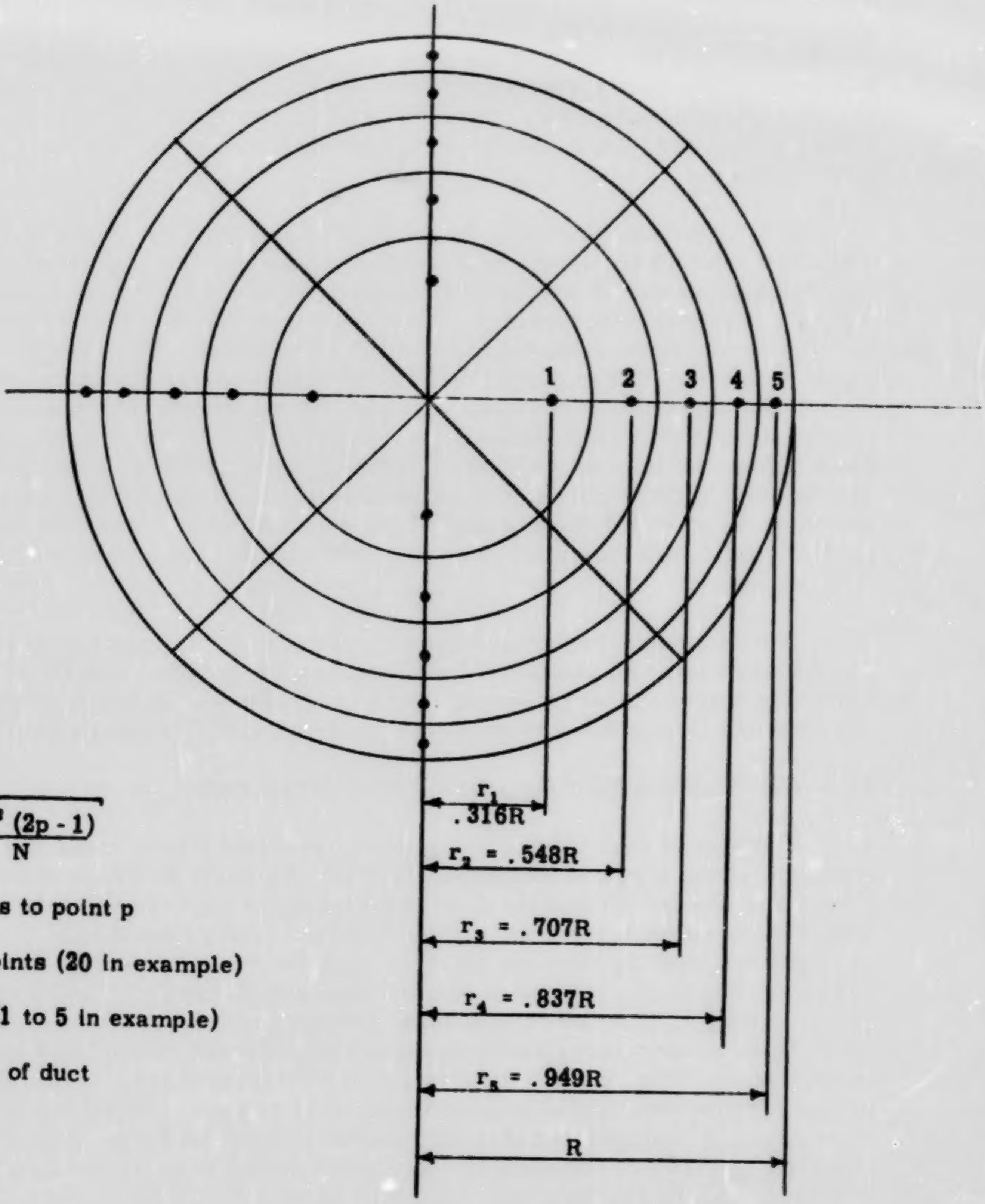

$$r_p = \sqrt{\frac{2R^2\,(2p-1)}{N}}$$

r_p = radius to point p

N = no. points (20 in example)

p = index (1 to 5 in example)

R = radius of duct

Figure 12.1. Sampling Points in a Round Duct.

traverse point and the process is repeated. The total run should cover the circuit of all traverse points twice. The weight of dust collected on the filter medium divided by the total sampling volume is then the mean weight per unit volume, or the mean concentration of dust in the gas stream. This mean concentration times the mean gas volume per unit time gives the total weight per unit time in the gas stream. Test runs made in the dust collector inlet and in the outlet give the required data to calculate the collection efficiency:

$$\eta = \frac{W_1 - W_2}{W_1}$$

where

W_1 = weight per unit time-dust collected at inlet, and
W_2 = weight per unit time-dust collected at outlet.

The sampling line includes the sampling probe, the filter holder, possibly a condenser if the gas is humid or a cooler if the gas is hot, a gas meter, a pump, and the necessary instrumentation to measure temperature, humidity, and pressure for the calculation of gas density. An Orsat apparatus or other gas analysis instrumentation may be used if information about the constituents of the gas is required, such as CO and CO_2 for carbon balance calculations or SO_2 and SO_3 for information on the effect of sulfur on resistivity.

The sample probe may be of a null pressure type so that isokinetic sampling can be achieved without reference to a previous velocity traverse.

The filter medium may be one of several types, according to the requirements of the particular situation:

1. Paper filter for dry gas at temperatures below 300°F.
2. Glass cloth filter for coarse dusts and temperatures to 750°F.
3. Alundum thimble for high temperature and chemical resistance.
4. Membrane filter for fine dusts to sizes below 1 micron.
5. Impinger trains for particle size distribution of insoluble dusts.
6. Electrostatic electrofilter for high efficiency at low sampling rates.
7. Tar camera (colorimetric filter for nonaqueous mists).

The filter selected should resist the conditions of temperature, pressure, and chemical attack to which it will be exposed, and should have a collection efficiency of greater than 99%. The filter must be protected against condensation during the test run. If the filter assembly is part of the sample probe, it should be held inactive in the gas stream long enough for it to warm up to the gas temperature so that condensation will not occur.

The following items are usually measured or calculated in testing dust collection equipment:

1. Gas volume

    a. Main stream - pitot traverse or stoichiometric calculation.
    b. Sample stream - gas meter, flowmeter or calibrated orifice.
    c. Corrections calculated for density.

2. Humidity - psychrometric dry bulb and wet bulb temperatures or cooled condensate.

3. Gas composition - Orsat or other gas analysis instrumentation.

4. Gas density - calculated from composition, temperature, humidity, and pressure.

5. Gas pressure - manometer and barometer.

6. Dust concentration - weight of sample collected by isokinetically sampled traverse.

7. Collection efficiency - calculated from concentrations at inlet and outlet of collector.

8. Dust properties - determined by analysis of dust sample (see ASME PTC-28, 1965).

    a. Size distribution - calculate from Stokes' law and terminal velocity distribution (ASME PTC-28, 1965).
    b. Specific gravity - ASTM C188-44: change in volume of kerosene or naptha with addition of dry sample.
    c. Moisture content - weight loss in drying oven.
    d. Water soluble content - weight loss after dissolving in water.
    e. Water soluble sulfate content - chemical analysis of solute.
    f. Resistivity - resistance of 5-mm layer of dust in a 3-in. diameter cup through a 1-in. electrode weighted to 10 gm/cm^2.

g. Specific surface - ASTM C204-55: calculate from air permeability.

Figure 12.2 shows one schematic arrangement of dust sampling apparatus for testing dust collectors. Other arrangements are possible, depending on the instrumentation available. Two setups are required, one upstream from the dust collector and one downstream. It would be desirable to run both upstream and downstream traverses simultaneously to insure exactly the same operating conditions for both runs. However, standards usually require only that the operating conditions be maintained constant.

12.4 COMPUTATION

The computation of results of dust collector tests requires careful attention to all corrections for temperature, humidity, density, and instrument calibration.

The gas velocity may be calculated from the pitot tube readings with necessary corrections. A standard pitot tube reads the impact, or velocity, pressure directly with no correction for calibration. All other types of velocity pressure tubes must be calibrated and the data corrected. The pitot tube velocity at each traverse point is calculated by the formula:

$$V = 1096.5\sqrt{\frac{p}{d}} \text{ ft/min}$$

where

p = the velocity pressure in inches water gage, and
d = the density of the gas calculated from the composition, temperature, and humidity of the gas.

$$\text{Density} = \frac{144p_s}{R\,(T_d + 460)\,2.036} \text{ pounds per cubic foot,}$$

where

p_s = static pressure, inches of mercury,
T_d = dry bulb temperature °F, and

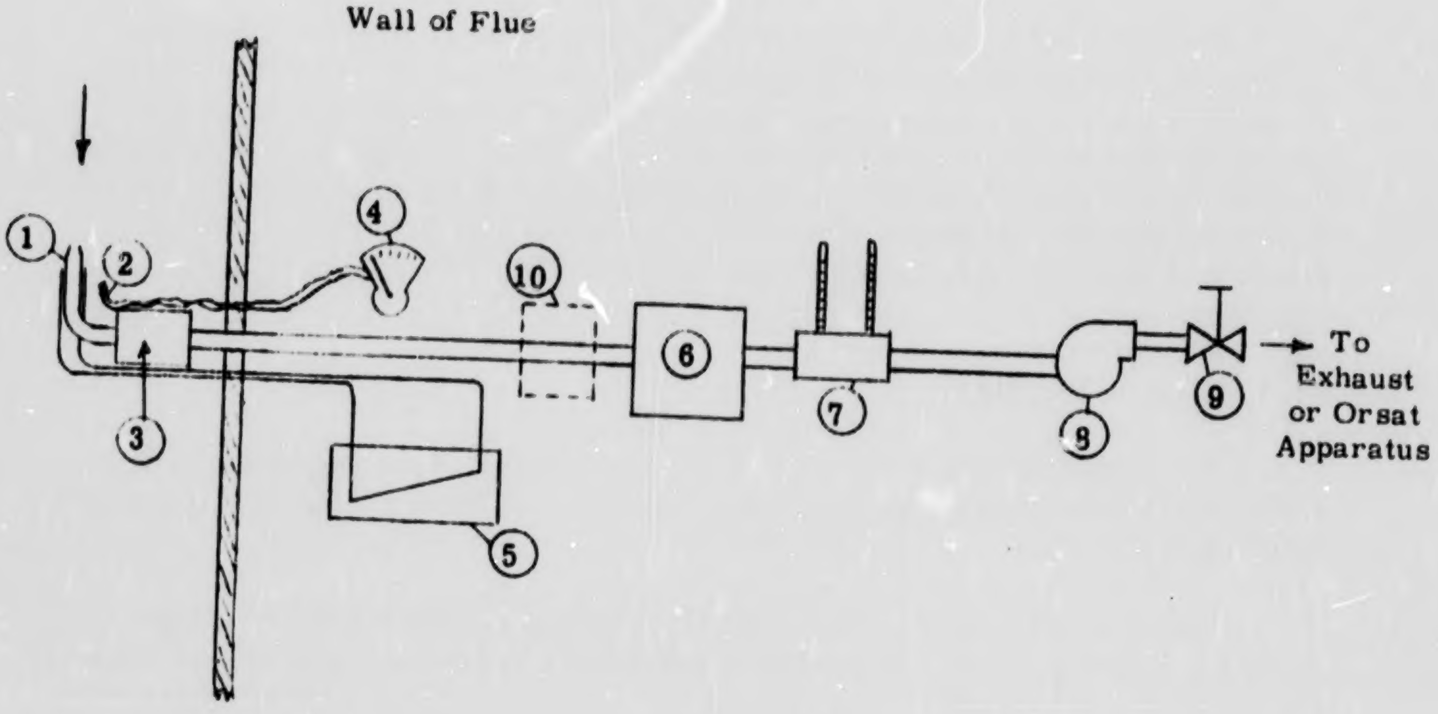

(1) Sample probe and pitot tube
(2) Thermocouple
(3) Filter holder
(4) Temperature readout
(5) Inclined manometer
(6) Flow meter
(7) Humidity measurement
(8) Pump or blower
(9) Flow control valve
(10) Cooler or condensate trap if required

Figure 12.2. Schematic Arrangement of Dust Sampling Apparatus.

R = gas constant calculated for composition of gas:
R = 53.3 for standard air, and
R = 52.4 for 12% CO_2 flue gas.

Note that turbulent fluctuations in the gas flow show up as variations in the velocity pressure and that the velocity varies as the square root of the pressure. If there are wide variations in velocity pressure readings, averaging the velocity pressures will not represent the average velocity. Therefore, pitot traverses should be made at locations where the turbulence is relatively small. The pitot tube manometer becomes unreliable when the velocity is below about 10 ft/sec (600 ft/min). Therefore, pitot traverses should be made at locations where the velocity is around 30-50 ft/sec (1800-3000 ft/min).

The total gas flow may be calculated either from the integration of the pitot tube traverse or from the stoichiometric relationships of combustion. The standard calculation for the mean velocity from a pitot tube traverse is simply the arithmetic mean of all the traverse points:

$$v_m = \frac{1}{n} \sum_{i=1}^{n} v_i$$

and the total gas flow is determined from the continuity equation:

$$Q = A v_m$$

where A is the actual measured cross-section area at the test section including the effect of errors in construction, warping of plates, and dust deposits. (Refer to the section on sources of error for comments on the use of the arithmetic mean velocity).

To determine the total gas flow from stoichiometric considerations, it is desirable to have the ultimate analysis of the fuel being burned, the operating conditions of the furnace, and an analysis of the flue gas composition. The total gas flow in cfm is given by

$$Q = \frac{Wc\tau}{60} \text{ cfm}$$

where

W_c = the weight of fuel burned per hour, and
τ = the volume of gas produced per pound of fuel.

The weight of fuel per hour may be obtained by weighing or calculating from

$$W_c = \frac{S\,(E_s - E_w)}{\eta H}$$

where

S = the rate of steam generation,
E_s = the enthalpy of steam,
E_w = the enthalpy of feed water,
η = the boiler efficiency, and
H = the heating value of fuel.

To determine τ, the volume of gas produced per pound of fuel, a material balance may be made by following a known and detectable chemical element throughout the system. Common examples of such elements are carbon and sulfur. The amounts of carbon and sulfur in the fuel are known from the chemical analysis of the fuel and the amounts of CO_2 and SO_2 in the exhaust gases are known from the tests on the gas with the Orsat apparatus or other analytical procedures. Trace elements can also be used.

The sample gas flow rate may be calculated from standard orifice meter formulae if orifices are used to meter the sample flow, or may be calculated from the calibration curves of whatever flow meter is used. Because immediate adjustment of sample flow to isokinetic sampling is required, curves or tables are required in the field for making these calculations rapidly.

The dust concentration by weight is determined as the ratio of the weight of dust to the weight of gas:

$$m = \frac{w_r}{w_g}$$

where

$$w_r = \text{weight of dust} = \sum_{i}^{n} w_i = \text{sum of traverse dust samples, and}$$

$$w_g = \text{weight of gas sampled} = \frac{\text{total volume of gas sampled}}{\text{density}} .$$

The collection efficiency can be calculated from the dust concentration in the inlet and outlet to the collector:

$$\eta = 1 - \frac{m_o}{m_i}$$

where

m_o = mass concentration, outlet, and
m_i = mass concentration, inlet.

A similar calculation using dust concentration by volume may be made, provided that the volumes are corrected to the same basis, that is, at the same temperature and pressure. Because this would represent equivalent densities, the calculation would be identical. Also, a similar calculation may be made using dust collected per unit time, provided the installation is operating under steady-state conditions. Because steady-state conditions imply the same weight and volume of gas per unit time, the calculation would again give an identical result.

12.5 SOURCES OF ERROR

Errors may occur in measurement, or in calculation, and also may be intrinsic due to random variations. Table 12.2 lists the sources of measurement errors. Some are unavoidable and irreducible, but some can be avoided or reduced to a small value.

Isokinetic sampling is essential to accurate sampling in order to obtain representative samples of all particle sizes. If the velocity into the sampling nozzle is greater than the velocity of the gas stream, the larger particles will be under-represented because they do not accelerate with the gas. If the velocity into the sampling nozzle is lower than the velocity of the gas stream, the larger particles will be over-represented because they ram

Table 12.2

Sources of Measurement Errors

1. **Errors due to probe**
    - a. **Anisokinetic sampling velocity**
    - b. **Probe not parallel to gas flow**
    - c. **Dust collected on walls or probe and sample line**
    - d. **Condensation in probe or sample line**
2. **Errors due to sample collector**
    - a. **Efficiency less than 100%**
    - b. **Condensation in collector**
3. **Errors in sample flow**
    - a. **Meter inaccuracy**
    - b. **Leaks**
4. **Errors in weighing**
    - a. **Hygroscopic loss or regain of sample or filter media**
    - b. **Loss of sample in handling**
    - c. **Scale accuracy**
5. **Errors in integrating**
    - a. **Variations over time or space of dust load or velocity**
    - b. **Integration error**
    - c. **Too few traverse points**
6. **Errors due to personnel**
    - a. **Reading and recording errors**
    - b. **Failure to comply with requirements**
    - c. **Calculation errors**

into the nozzles where smaller particles detour around the streamlines. Figure 12.3 shows the flow lines in the vicinity of a sampling probe.[1] It can be seen that a representative sample will be taken only when the sample flow is parallel to and equal in magnitude to the main gas flow—that is, isokinetic. It is difficult to obtain precise isokinetic sampling in the case of velocity variations, so some unavoidable error may occur.

A relationship between the accuracy of anisokinetic sampling and the ratio of sampling velocity to approach velocity has been developed by Ruping.[1] Figure 12.4 shows his curves of 1% and 5% error plotted on a semilog grid of sampling velocity ratio versus the dimensionless parameter:

$$k = \frac{gR}{w_s \; w_o}$$

where

R = the radius of sampling probe,
w_s = the settling velocity,
w_o = the approach velocity, and
g = the acceleration of gravity.

For all possible values of the dimensionless parameter, it is necessary to hold the sampling velocity within about ±2% of the isokinetic velocity for a 1% error, or within about ±6% of isokinetic velocity for a 5% error.

For a particular situation, the required range need not be quite as restricted. For example, for a 1/4-in. I. D. probe, an approach velocity of 8 ft/sec, and a 10-micron particulate matter of unit specific gravity, $k = 0.13$; and the allowable range of sampling velocity would be about +25% to -12% of isokinetic velocity for 5% accuracy. However, in a practical situation, a wide range of particle sizes will usually exist, hence a wide range of values of the parameter will result, and a narrow range of sampling velocities about isokinetic velocity will be required.

Isokinetic sampling also requires that the probe be parallel to the gas flow at all times. In a turbulent flow, this may not be possible. Standard methods usually call for aiming to within ±5° of parallel to the main gas flow. Note that the cosine of 5° is 0.996, so that the reduction in cross-section of the nozzle facing the gas stream will be only 0.4% at that aiming angle.

---

[1] Refer to the bibliography for this chapter.

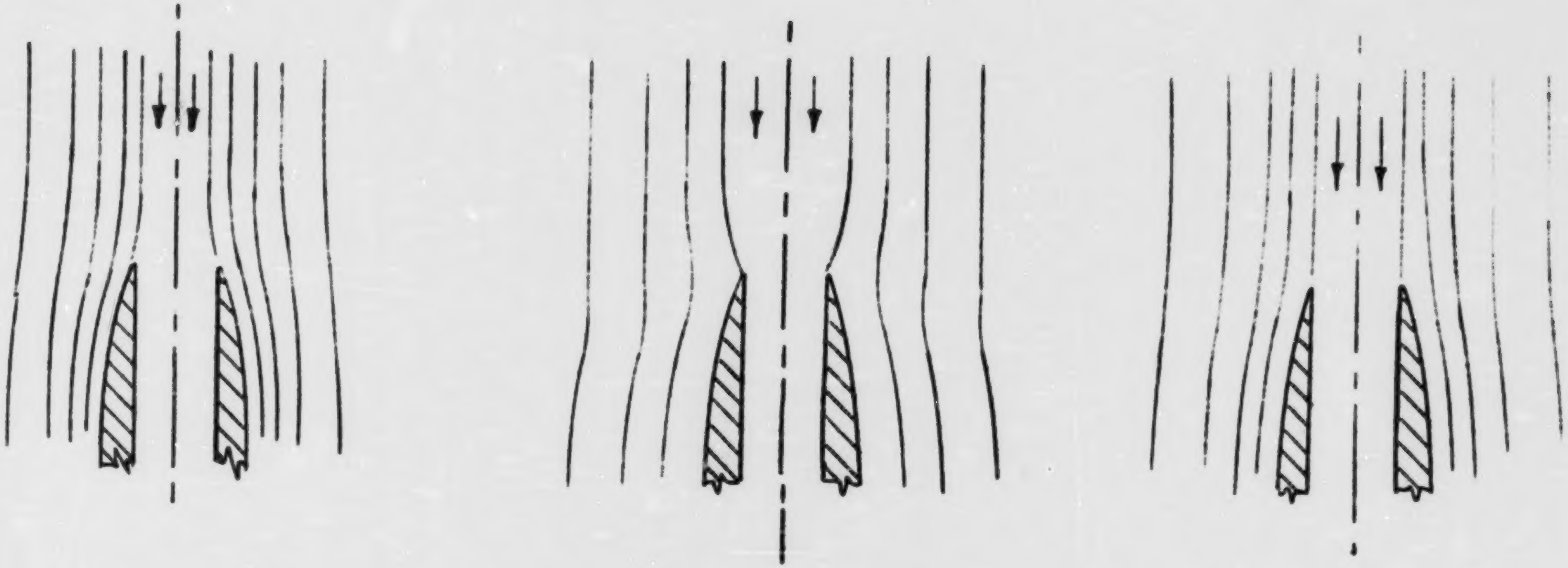

Local velocity greater than sampling velocity

Sampling velocity greater than local velocity

Isokinetic sampling

Figure 12.3. Flow Lines in the Vicinity of a Sampling Probe.

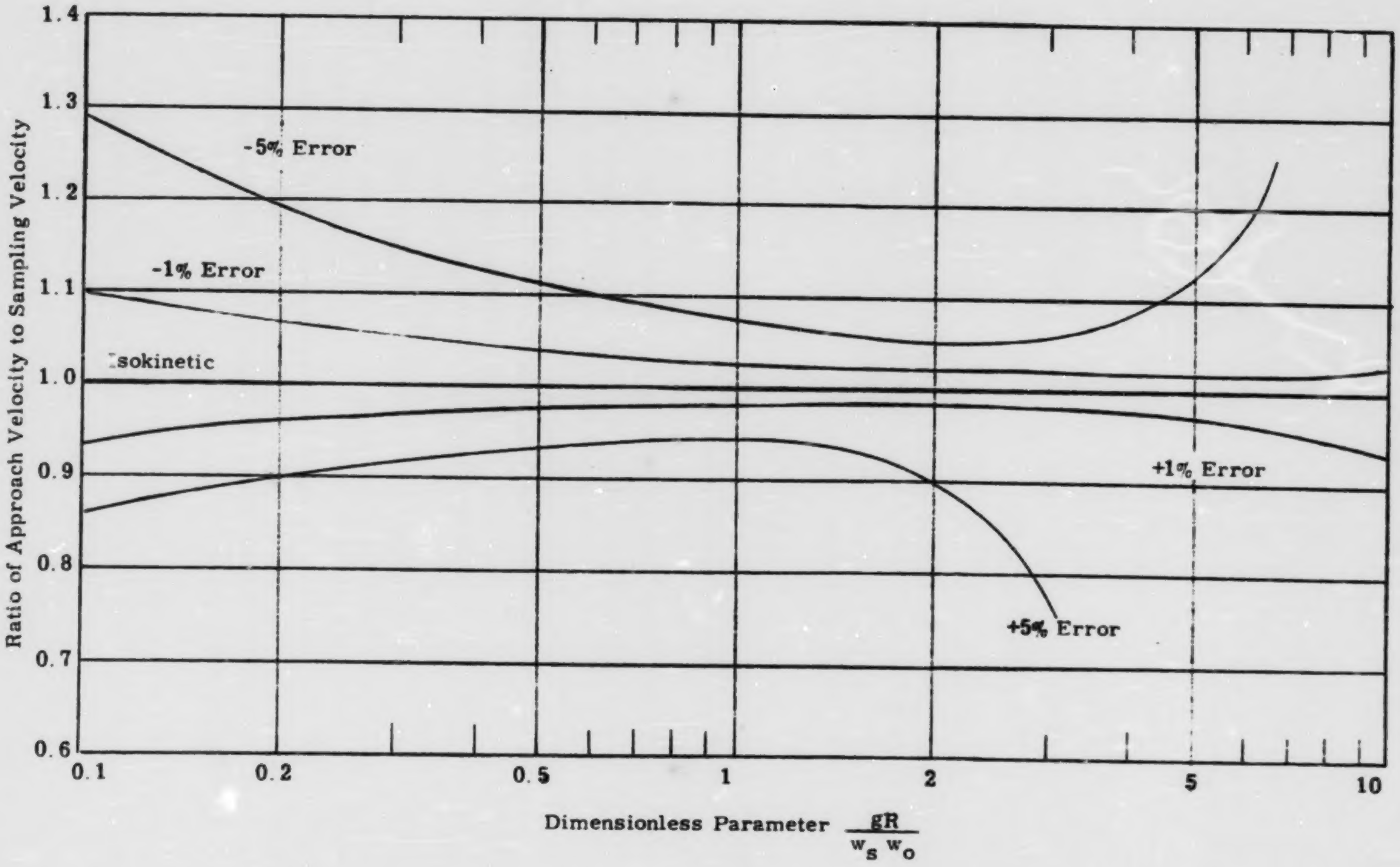

Figure 12.4. Accuracy of Anisokinetic Sampling.

Although the pitot tube itself is usually considered to be error free and to have a calibration factor of unity, the manometer used to read the velocity pressure is not free of error, especially if the gas flow is turbulent so that the manometer reading fluctuates. A slant tube manometer with draft gage oil of specific gravity 0.826 may have divisions down to 0.01 or 0.02 inch of water. Thus, the accuracy of reading the manometer will be about ±0.01 inch water gage with constant gas velocity. Figure 12.5 shows the range of apparent velocities for manometer accuracies of 0.01-in. w.g. and 0.1-in. w.g. Note that the limits diverge rapidly at low velocities. At densities different from that for standard air, the curves shown will shift slightly, but the shape will be similar. Also note that turbulent variations in velocity pressures on the order of ±0.1 in. w.g. can introduce appreciable error.

Errors due to the sample collector depend on the efficiency of collection for the size particles in the gas stream. Because most of the mass occurs in the larger particles, a small loss of mass in the smaller particles will not necessarily be important. Standards call for 99% efficiency of the sample collector.

Errors in measurement of the gas volume sampled depend upon the accuracy of the meter and its calibration.

Errors in temperature readings depend upon the calibration of the thermocouples, resistance thermometers or glass thermometers used, random errors due to temperature variations, and heat losses due to heat conduction through the thermometer stem or lead-in wires. In thermocouples, there is the added possibility of a deviation in the temperature of the cold junction. Table 12.3 shows the error limits for mercury thermometers for various scale divisions and temperature ranges.[2]

Errors in weighing depend upon the scale accuracy and the size of dust sample collected with respect to the tare weight of the filter. Care must be taken to avoid or compensate for hygroscopic loss or gain. Care must also be taken to include with the dust sample any dust deposited in the sampling nozzle and sampling tube. A weight and collection efficiency change can result from the paper thimble becoming charred if the gas temperature exceeds 300°F.

The existence of an error in the calculation of the mean value of either velocity or dust concentration is attributed in the literature to the

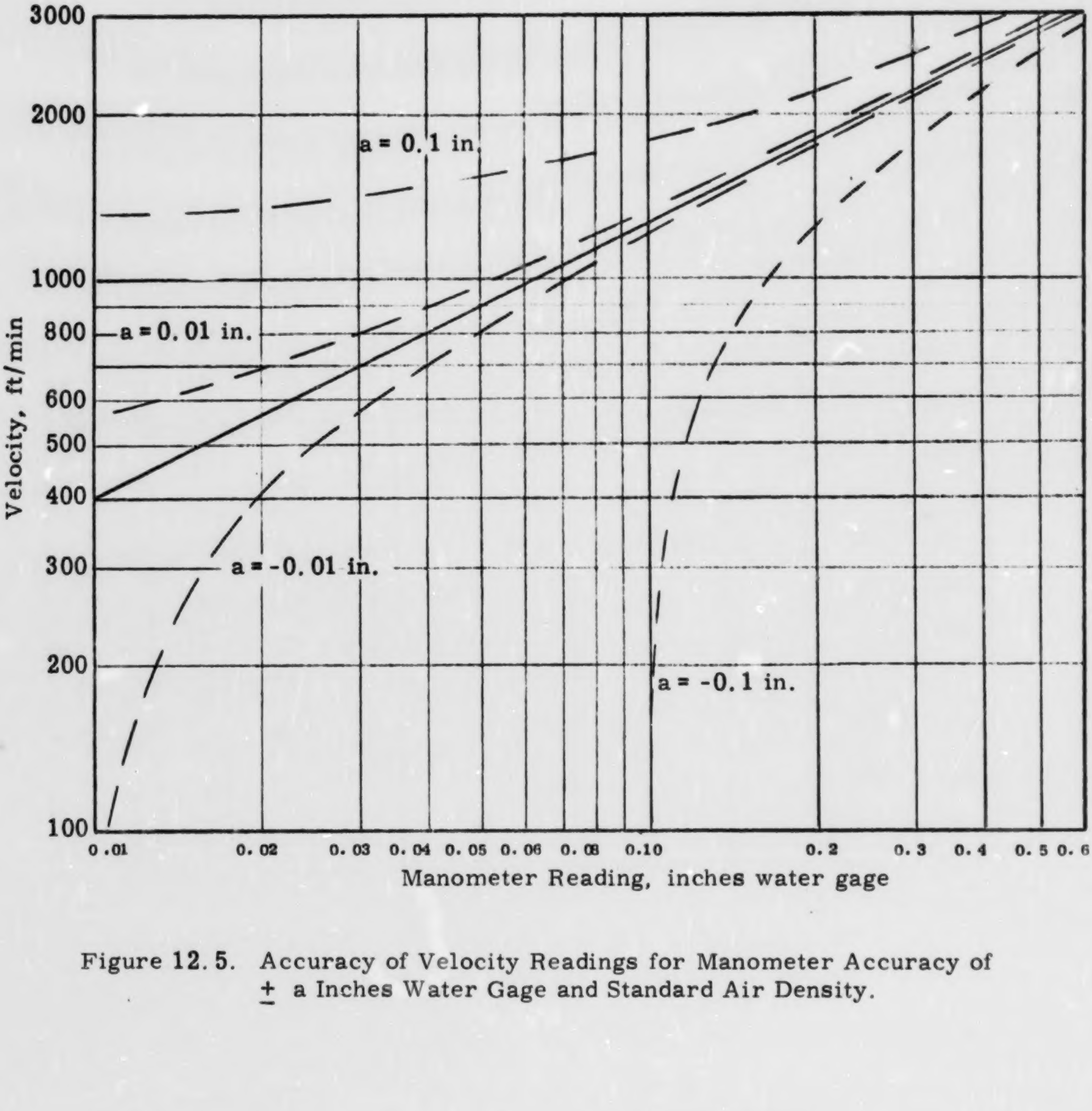

Figure 12.5. Accuracy of Velocity Readings for Manometer Accuracy of ± a Inches Water Gage and Standard Air Density.

Table 12.3

Permissible Error Limits for Glass/Mercury Thermometers

Range, °C		Error Limit ± °C for Scale Divisions of:								
From	To	.01	.02	.05	0.1	0.2	0.5	1	2	5 or 10
-58	0	-	-	-	0.3	0.4	0.7	1	2	3
0	50	.02	.04	0.1	0.15	0.2	0.5	0.7	1	2.5
50	100	-	.04	0.15	0.25	0.3	0.5	1	1.5	3
100	200	-	-	-	-	0.5	1	1.5	2	4
200	300	-	-	-	-	-	1.5	2	3	5
300	400	-	-	-	-	-	-	2.5	4	7
400	515	-	-	-	-	-	-	3	5	10
515	700	-	-	-	-	-	-	-	6	10
More than 700		-	-	-	-	-	-	-	-	10

random variations in time and space of the variable being measured. However, there is an additional systematic error due to the fact that the value of the velocity is zero at the wall and the present calculation techniques do not take this into account.

If the variable to be measured were perfectly random, a simple average of all the points would be a satisfactory estimate of the mean value. However, dust concentration and velocity are not perfectly random. The velocity in the core of the gas flow will be some average gas flow plus and minus turbulence, but near the walls, the turbulence will be damped out and viscous friction will diminish the flow velocity all the way to zero at the walls. The dust concentration in the core of the flow will be rapidly mixed by turbulence to some mean concentration plus and minus both time and space variation, but near the walls, the mixing effect will diminish with decreasing turbulence so that dust concentration can be expected to be lower near the walls, possibly close to zero. With large dust particles in the gas stream, the settling velocities may overcome the mixing effect of turbulence and a concentration stratification may occur with a heavy load of larger particles near the bottom of the duct.

The mathematical definition of a mean value of a variable over an area is as follows:

$$M = \frac{\int_{a_1}^{a_2} \int_{b_1}^{b_2} y dA}{A}$$

where

y = variable,
A = area, and
b, a = limits of A.

The problem of determining the mean velocity or the mean dust concentration is, therefore, a problem in numerical integration from a limited number of traverse points. If the function "y" were a simple linear function, the mean would be an arithmetic mean, or a simple average:

$$A.M. = \frac{1}{n} \sum_{i=1}^{n} y_i$$

If the variable were completely random, the arithmetic mean would be satisfactory. Because the gas flow is zero at the walls, the velocity readings at all traverse points located adjacent to a wall will be higher than the local mean and an average velocity calculated from the arithmetic mean will be 5% to 15% high. For example, suppose a traverse were made in a square duct with 25 traverse points and every point had a velocity of 100. Also suppose, for simplicity of calculation, that the boundary layer is parabolic and has a thickness equal to half the traverse spacing. An average velocity using the arithmetic mean would obviously be simply 100. However, by integration, a true mean velocity can be calculated.

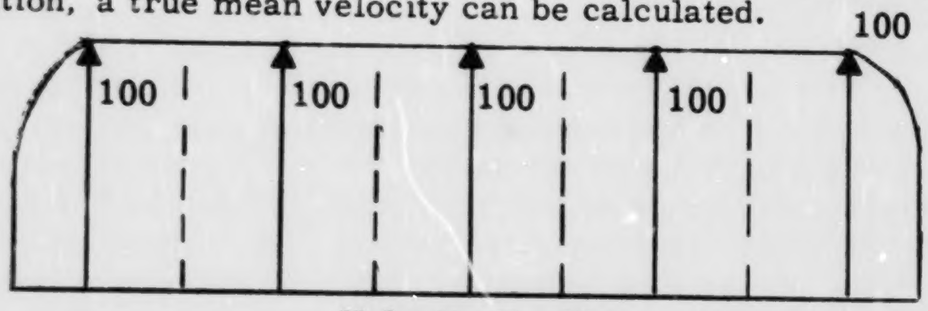

Velocity Profile

By elementary calculus, the mean ordinate of a parabola is 2/3 of the maximum. Therefore, the edge points of the traverse would have a true value as follows:

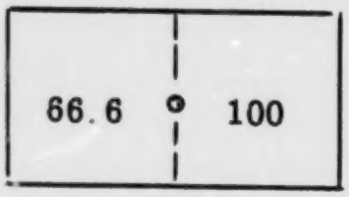

$$\frac{100 + 66.66}{2} = 83.33$$

Also by elementary calculus, it can be shown that the intersecting parabolas at the corners have a mean of 1/2 the maximum. Then the corner points would have a true value as follows:

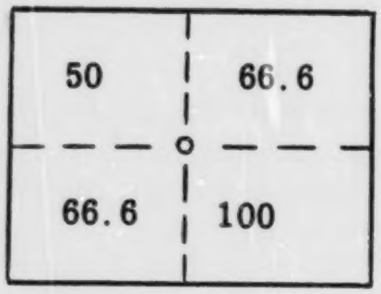

$$\frac{50 + 66.66 + 66.66 + 100}{4} = \frac{17}{24} \times 100 = 70.83$$

Then the corrected traverse would be as follows:

70.83	83.3	83.3	83.3	70.83
83.3	100	100	100	83.3
83.3	100	100	100	83.3
83.3	100	100	100	83.3
70.83	83.3	83.3	83.3	70.83

Calculated Mean Values

Then the overall average would equal

$$\frac{4 \times 70.83 + 12 \times 83.33 + 9 \times 100}{25} = \frac{2183.28}{25} = 87.33$$

or 12.66% less than the arithmetic mean. Also, duct dimensions may not be known with required accuracy because of construction errors and distortions of flues due to warping, temperature effects, dust buildup, etc. These may be common sources of error.

Obviously, the result would be different if the boundary layer thickness were different, but it is apparent that the cook-book use of the arithmetic mean in calculating an average value can lead to a large systematic error in the calculation of the average velocity in a rectangular duct. Research may be required to determine the relationship of a number of traverse points, boundary layer thickness, and accuracy. Where a high degree of accuracy is required, it is recommended that as many traverse points as is economically possible be used and that the boundary layer thickness be measured for calculation of the mean value as shown above. The foregoing remarks do not strictly apply to a pitot traverse in a round duct, because only four points will be in error in a standard equal annular area traverse, instead of the 16 erroneous points in the above example.

The distribution of dust in the duct work at the measuring point may be very nonuniform because the distribution can be distorted by transforms, elbows, turning vanes, and simple settling. Therefore, the required number of traverse points will depend on the degree of uniformity. However, a relatively inaccurate measure of dust concentration at the inlet to the precipitator will not greatly decrease the accuracy of the efficiency calculation.

Suppose the concentration at the inlet is about 100 times the concentration at the outlet, both measured with ± 10% accuracy. Then the minimum and maximum efficiency calculations would be as follows:

$$\eta_1 = 1 - \frac{1}{100 - 10} = 1 - \frac{1}{90} = 1 - 0.011 = 0.989$$

$$\eta_2 = 1 - \frac{1}{100 + 10} = 1 - \frac{1}{110} = 1 - 0.009 = 0.991$$

Thus $\eta = 0.99 \pm 0.001$.

Therefore, in efficiency calculations, the greatest accuracy is required in the determination of the outlet dust loading. Fortunately, the outlet can usually be measured at a point with fairly uniform air flow, fairly uniform dust distribution, and with velocities high enough for accurate readings of isokinetic sampling velocities.

It is theoretically impossible to obtain a truly representative sample of any aerosol with a wide range of particle sizes because of the differences in the trajectories of the different sizes. Large particles tend to settle out, but small particles tend to follow the gas flow. For example, the terminal velocities of spherical particles with unit specific gravity are approximately as follows:

Size, microns	Terminal Velocity
0.1	8×10^{-5} cm/sec or 2-1/2 inches/day
1	3×10^{-3} cm/sec or 4-1/2 inches/hour
10	0.3 cm/sec or 6-1/2 inches/min
100	25 cm/sec or 10 inches/sec
1000	400 cm/sec or 150 inches/sec

Thus, a 1-micron particle in a 250 cm/sec wind (8.2 ft/sec or 5.6 mph) is moving almost horizontally: arc tan $\frac{3 \times 10^{-3}\text{ cm/sec}}{250\text{ cm/sec}} = 0° 0' 2.5$ in. arc tan 0.000012, but a 100-micron particle in the same wind has an appreciable trajectory angle with respect to horizontal: arc tan $\frac{25\text{ cm/sec}}{250\text{ cm/sec}} =$ 5°40'. Therefore, from a theoretical point of view, it is not possible to aim a sampling probe at the correct angle for all particle sizes. However, from a practical point of view, an aiming error of only 5° is inconsequential. At extremely low gas velocities, however, the trajectory angle for large particles gets disastrously large.

No comment on errors due to personnel needs to be made other than to recommend the use of trained, experienced, reliable personnel for testing.

The total effect of all errors combined may be serious when the collection efficiency is low. Although there are many sources of error, and care must be taken to minimize their effect, the efficiency calculation is not very sensitive to these errors when the efficiency is high. If we assume the error in measurement is ±a for both inlet and outlet, we can derive the following relationship between true efficiency versus calculated efficiency.

$$\eta_{calc} = 1 + \frac{(1 \pm a)^2}{1 - a^2} (\eta - 1)$$

Figure 12.6 shows this relation plotted on an inverted log (1 - x) by log (1 - y) scale for measurement errors of ±10%, ±20%, and ±50%. Note that even a 20% measurement error at a calculated efficiency of 99.5% only represents a range of true efficiencies from 99.25 to 99.67%.

However, if the emission from a stack is specified, then the important factor is the accuracy with which one can measure the dust concentration at the outlet and the measurement errors apply directly.

12.6 MEASUREMENT OF RESISTIVITY

Since resistivity plays such an important role in governing precipitator performance, it is important that it be measured with sufficient accuracy so that its influence on precipitator performance can be determined.

There are a variety of methods utilized for determining resistivity. They are classified as laboratory measurements if the dust is extracted from the duct and measurement subsequently made in the laboratory, and in-situ if the resistivity measurement is made in the duct or in the presence of the gaseous atmosphere of the duct.

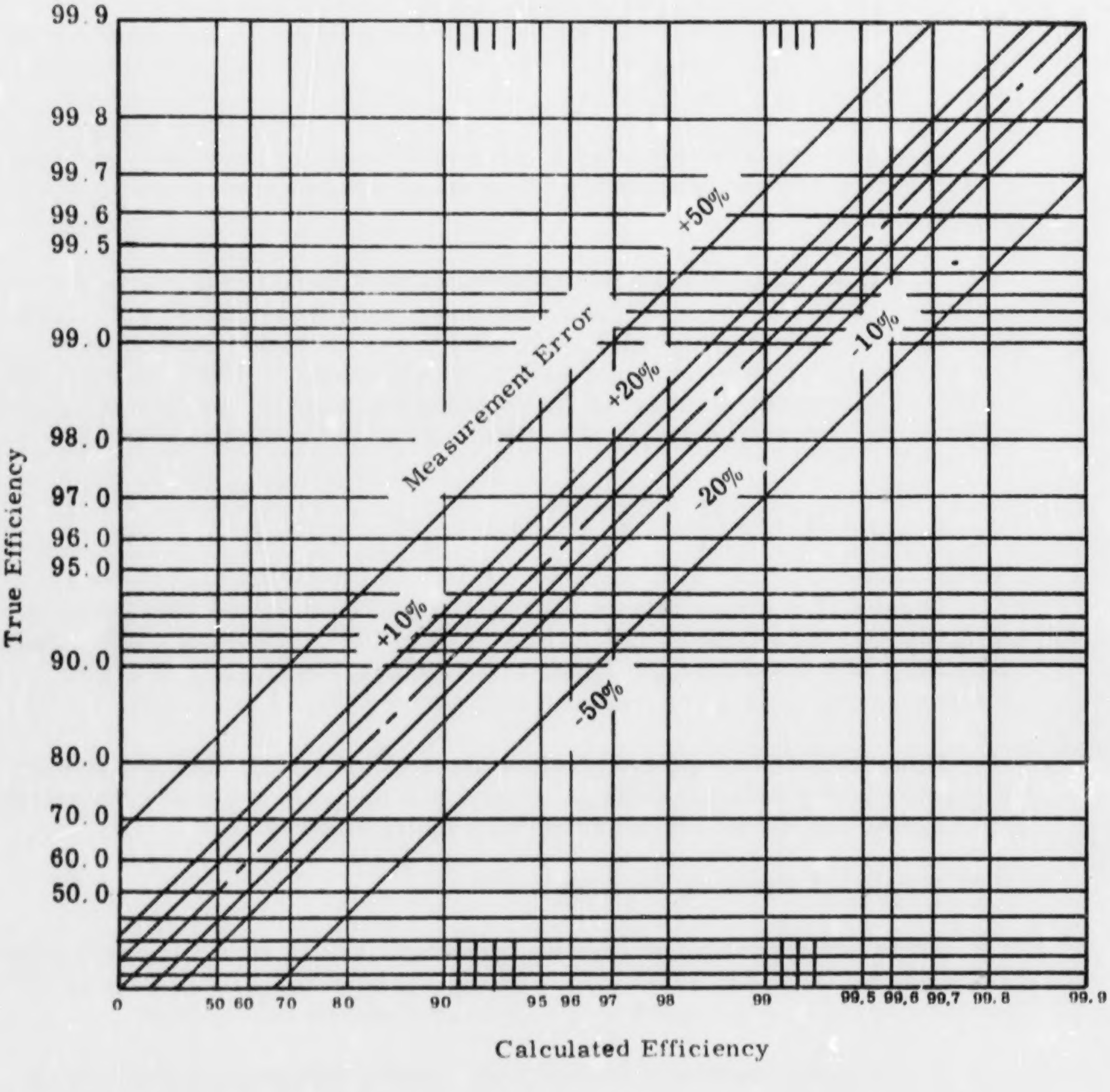

Figure 12.6. Relationship between True Efficiency Vs. Calculated Efficiency.

Laboratory techniques vary in the manner in which the resistivity is determined and in which the dust layer is deposited. The simplest method of resistivity measurement is to utilize a pair of plates which serve as the electrodes and measure the current and voltage while maintaining the cell at the temperature corresponding to that in the duct.

Figure 12.7 shows a high voltage conductivity cell that is used for laboratory measurement. The cell is normally mounted in an oven and its temperature controlled over the range of interest. Dust can be placed on the plate manually, or it can be electrostatically deposited by increasing the voltage on the point electrode so that a corona is formed. Once the deposit is formed, a plate is lowered onto the dust surface and the resistivity determined from the current-voltage readings.

Because of the dependence of resistivity on humidity as well as temperature, other types of laboratory measurement equipment are arranged to introduce moisture and perhaps other conditioning agents in a recirculating system. Dust is introduced into the system and, after sufficient time for equilibrium, is precipitated onto the plate of a high voltage conductivity cell. Resistivity is then measured by lowering a disc onto the dust surface, and the voltage and current measured for resistivity calculations.

Laboratory measurements have the inherent disadvantage that the atmosphere to which the dust is exposed during measurement is different from that in operation; also, the dust may have undergone chemical and physical changes after removal from the original source. Consequently, the resistivities determined by laboratory techniques can be in error by several orders of magnitude in the temperature range where surface conduction predominates. Figure 12.8 shows resistivity data taken on the same dust by laboratory and in-situ techniques. The values agree well in the temperature range where volume conduction predominates, but the laboratory data are considerably higher in the low temperature region. The disagreement between laboratory and in-situ data depends upon the nature of the dust and gas. Agreement can be good under some conditions, but very poor in others.

In-situ resistivity measurements are made under conditions in which the only atmosphere to which the dust is exposed is that present in the process. This eliminates uncertainties in attempting to duplicate the gaseous conditions and generally gives more reliable and reproducible results than those obtained by laboratory techniques.

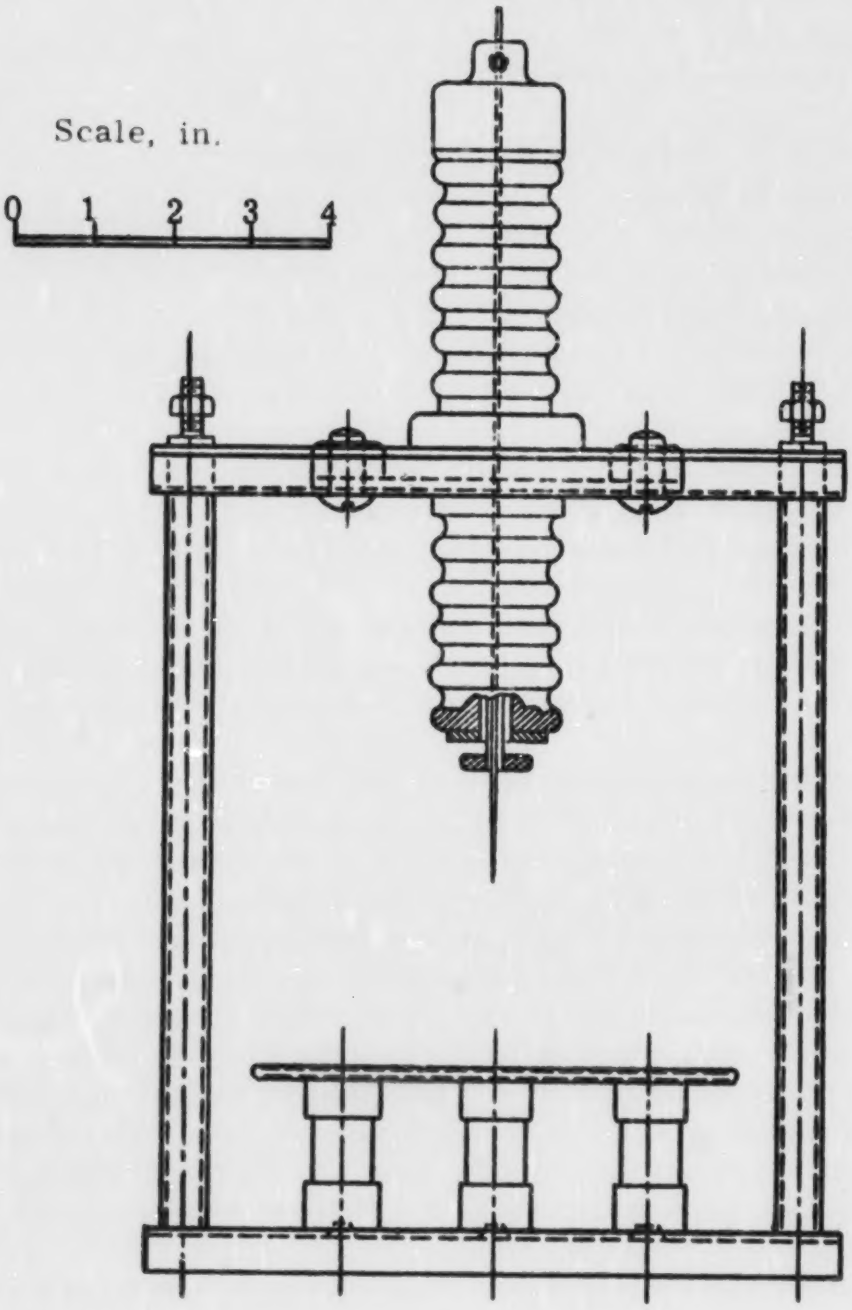

Figure 12.7. High Voltage Cell for Measurement of Dust Resistivity.

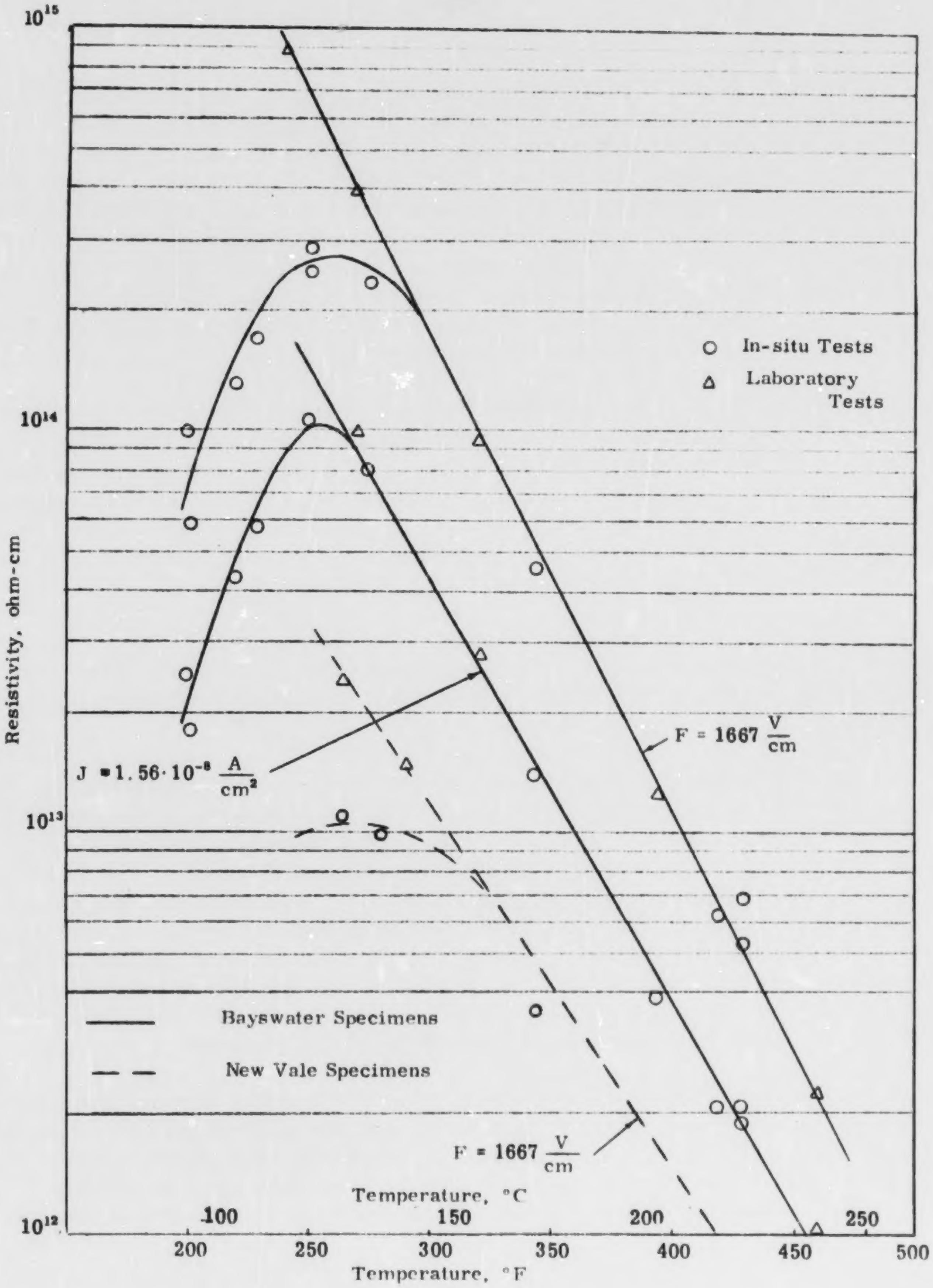

Figure 12.8. Resistivity-Temperature Relations (Reference 3).

Figure 12.9 is a schematic diagram of a typical in-situ resistivity probe. The apparatus consists of a point-plane cell at the end of the probe, which is inserted into the duct through openings of from 2-1/2" to 4" diameter. When a voltage sufficient to generate a corona is applied to the cell, dust is precipitated onto the plate. After sufficient time has elapsed to collect a dust layer, the point-plane disc is lowered onto the dust layer and the current and voltage are measured. The probe is then removed and the dust thickness measured. Resistivity can then be calculated from the dimensions of the probe, thickness of the dust layer, and the electrical data. Thermocouples on the probe are used to measure temperature.

Figure 12.10 is another type of in-situ resistivity probe. It differs from the first type discussed in that the dust and gas are drawn from the duct into a small cyclone separator where the dust is separated and deposited into a resistivity cell. The cell is composed of a central electrode and an outer cylindrical electrode on the inside of the cyclone dust hopper. The collected dust forms an annular layer between the two electrodes, and the resistivity is determined from resistance measurements.

The two types of resistivity measuring instruments differ in the size particle collected, and in the manner in which the deposit is formed. No data have been found which show comparative resistivity values measured by the two methods.

Cohen[4] reports that for some types of dust, the resistivity varies with aging time after collection. Figure 12.11 shows that for a particular dust the resistivity measured 10^{10} ohm-cm immediately on collection and rose to 10^{12} after 20 minutes. Laboratory resistivity values are shown on the same curve, and the data indicate that the in-situ resistivities approach the laboratory values after about 30 minutes. It is postulated that the change of resistivity with time is due to a change of the conducting film by chemical and/or physical interaction with the bulk of the dust particles. If so, it is interesting to note that the resistivity of the collected dust would also change with time, so that resistivity would be a dynamic rather than a static property.

Since the techniques for resistivity measurements are not standardized, the data should be interpreted cautiously, and the method used in the measurements identified. It should be especially noted that critical resistivity values in terms of precipitator operation should be identified with the method of measurement, since the values can vary by as much as two orders of magnitude.

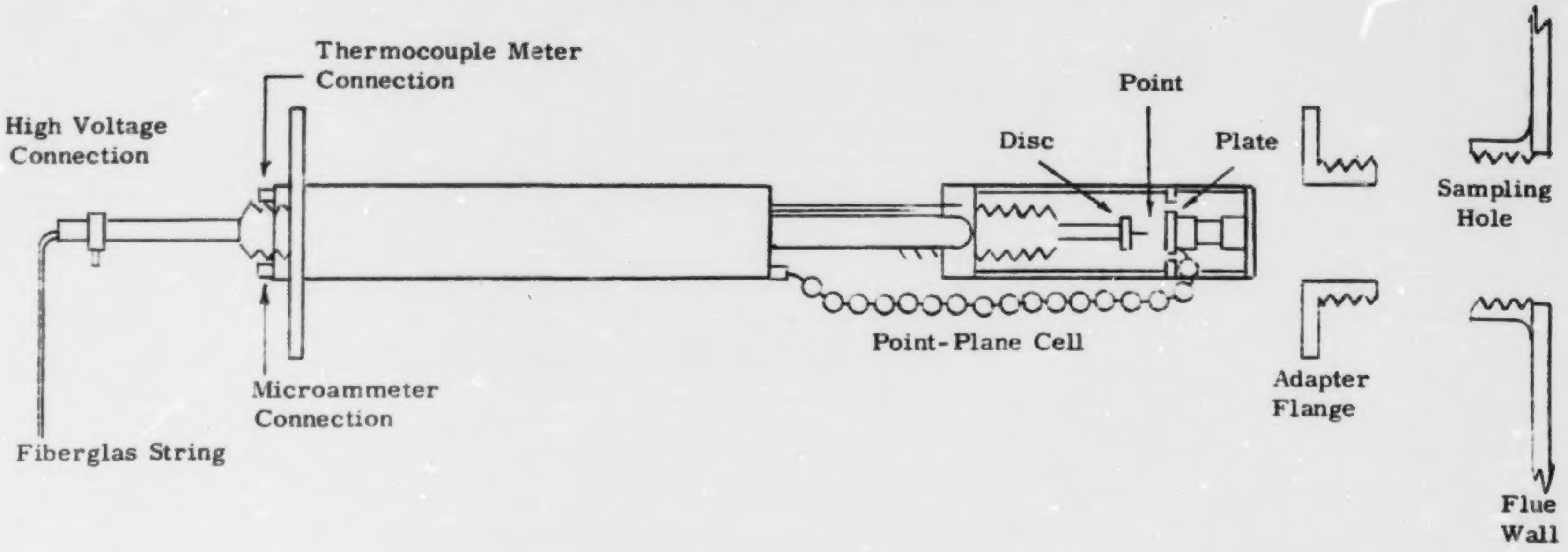

Figure 12.9. Resistivity Probe.

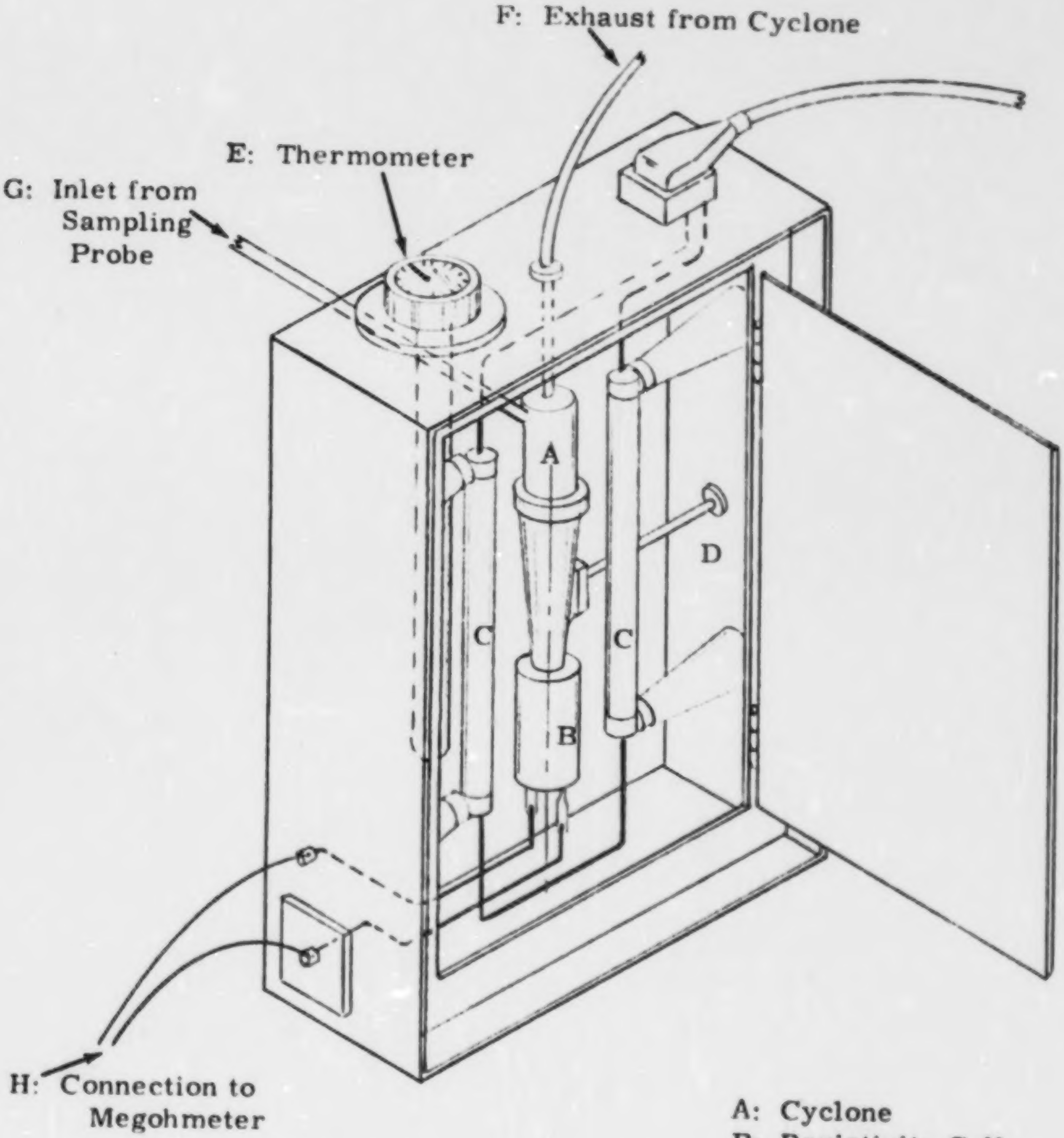

A: Cyclone
B: Resistivity Cell
C: Heater
D: Rapper

Figure 12.10. Diagram of Apparatus.

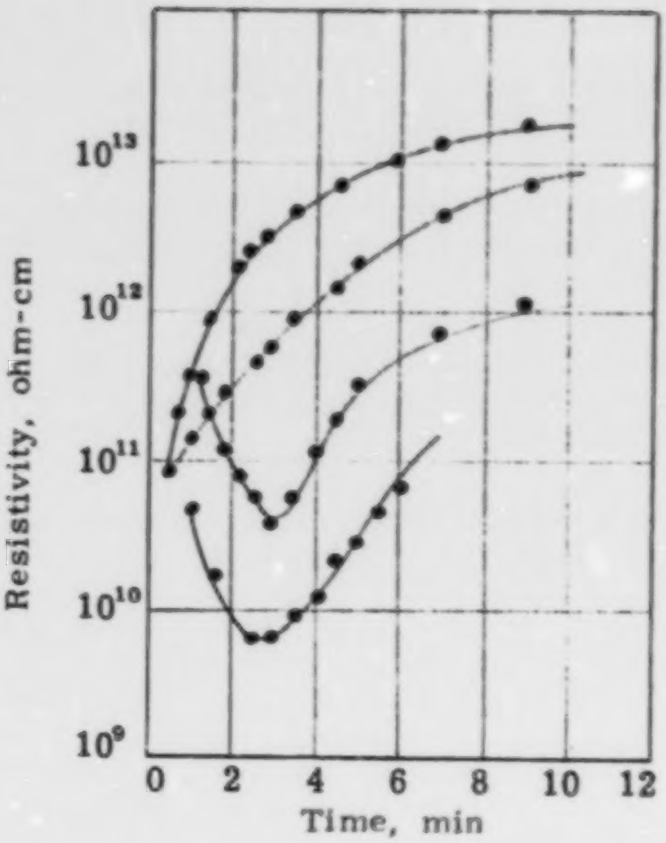

Figure 12.11. Resistivity Changes During Site Measurements on Four Different Power Stations. (Reference 4)

CHAPTER 12

BIBLIOGRAPHY

1. Verein Deutscher Ingenieure, VDI-2066 - Standards, "Performance and Measurements at Dust Collectors" (May 1966).

2. Darby, K. H. and Heinrich, D. O., "Conditioning of Boiler Flue Gases for Improving Efficiency of Electrofilters," Staub **26**, No. 11, pp 12-17 (1966).

3. Tassicker, O. J., Herceg, A. and McLean, K., "The Electrical Resistivity of Fly-Ash from Bayswater and Newvale," Bulletin No. 11, University of New South Wales (Dec. 1966).

4. Cohen, L. and Dickinson, R., "The Measurement of the Resistivity of Power Station Dust," J. Sci. Inst. **40**, p 72 (1963).

CHAPTER 13
TROUBLESHOOTING AND MAINTENANCE

When an electrostatic precipitator fails to achieve its design efficiency, it is necessary to examine the causes for its poor performance and take corrective action where possible. The number of causes for poor precipitator performance is so large that it is impractical to establish a rigid procedure for determining the exact problem. Rather it is a task of reviewing all aspects of the precipitator operation and arriving at possible trouble based on operating data and physical examination. Diagnosis of the problems and corrective action requires a good understanding of precipitation theory, as well as practical experience in precipitator operation.

Precipitator problems can arise either when the precipitator is brought on line, or after an extended period of operation. In the latter case, the difficulties may be associated with improper maintenance, changes in gas flow due to dust accumulation, misalignment or warping of the electrodes, or changes in the dust properties due to changes in the fuel or process parameters. In the former case problems are more likely to result from poor gas distribution, inadequate area of collecting surface, or inadequate energization.

Causes for precipitator problems can be classified generally as follows:

1) Electrical
2) Gas Flow
3) Rapping
4) Mechanical

Since an electrostatic precipitator operates on the basis of electric field and electric charge, it follows that the electrical energization must be adequate to provide for particle charging, maintenance of the electric-field, and for holding the collected dust to the collection plates. Field tests show a close correlation between efficiency and useful corona power. Figure 13.1 is a plot of efficiency of fly ash precipitators vs. corona power. This curve is useful as a guide to determining whether existing electrical energization is sufficient to achieve the desired efficiency.

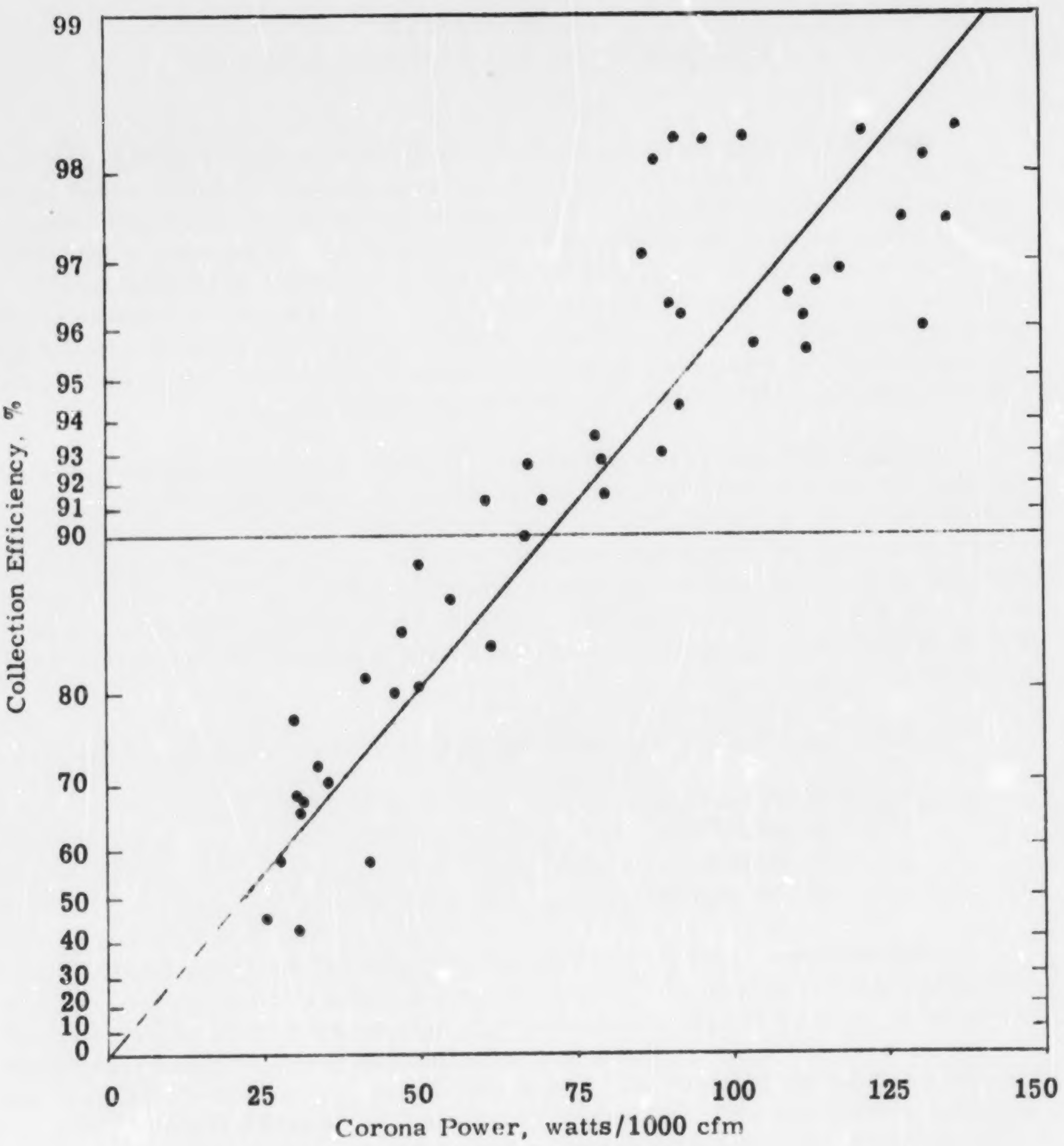

Figure 13.1 Relationship between Corona Power and Efficiency for Fly Ash Precipitators.

There are several possible causes for inability to achieve the required level of power input. The most common ones are

1) High dust resistivity
2) Excessive dust accumulations on the electrodes
3) Unusually fine particle size
4) Inadequate power supply range
5) Inadequate sectionalization
6) Improper rectifier and control operation
7) Misalignment of the electrodes

Normal power supply operation is indicated by voltages in the proper range as determined by the precipitator electrode spacing. Typical values for these currents range from 10 to 30 mA per 1000 sq ft of collecting surface. For most applications, the power supply output is controlled by the spark rate and is adjusted to give around 10 to 100 sparks per min per section. The setting of the spark rate should be such as to give maximum average high tension voltage, usually resulting in spark rates as shown above.

If a precipitator is operating in a spark rate limited condition but with low current and voltage, the problem commonly can be traced to high resistivity dust, electrode misalignment, or uneven corona due to buildup on the discharge electrode.

Because of the importance of resistivity in the precipitation process, in-situ resistivity measurements should be made as one of the first steps in troubleshooting. If the resistivity is found to be high (in excess of 10^{10} ohm-cm) most of the difficulty may be due to this cause. If this is not the case, other potential causes of abnormally low currents should be investigated.

High dust resistivity affects precipitator efficiency principally by limiting the voltage and current at which the precipitator operates. If the precipitator electrodes are clean, the high tension voltage can be increased until a sparking condition is reached. The maximum voltage is determined principally by the gas composition and precipitator dimensions.

If dust is deposited on the collection electrode, the voltage at which sparking occurs is decreased due to the increased electric field at the dust surface. If the resistivity of the dust layer is increased, the voltage at which sparking occurs will be further reduced. Finally, at very high values of dust resistivity, the voltage will be reduced sufficiently so that sparks will not propagate across the interelectrode space. Under these conditions, the gas in the interstitial regions of the dust layer will break down, resulting in a back corona. The positive ions, resulting from this corona, flow toward the discharge electrode and neutralize the negative charge previously applied to the dust particles.

Back corona results in an increase in current at low voltage and is manifested visibly as a diffuse glow at the surface of the dust layer. Visual verification of the presence of back corona is usually very difficult; however, it can be observed under very dark conditions.

Corrective procedures for precipitators that are limited by high resistivity include gas conditioning or alterations in temperature to reduce the resistivity of the dust. Some improvements can also be made by increased sectionalization.

If a precipitator is operating in a spark-limited mode with abnormally low voltage on dust with resistivities less than 10^{10} ohm-cm, the problems are likely to be associated with misalignment of the electrodes, uneven deposits on the discharge wire or broken corona wires.

Occasionally, precipitators are encountered that operate at the maximum voltage or current settings on the power supply with no sparking. This condition is likely to be associated with the collection of low resistivity dusts, where the electric field in the deposit is insufficient to initiate sparking. These installations are referred to as "power hogs." The fact that the precipitator is not sparking does not necessarily mean that the unit is underpowered. These installations may have sufficient power to provide adequate charging and collection electric fields without sparking. If low efficiencies are encountered and tests show that sufficient power is provided, then other disruptive conditions should be sought.

Other electrical problems encountered with precipitators are shorting of the high tension frame by dust accumulation in the hoppers, broken wires, insulator or "flower pot" bushing leakage, and broken down or leaky cables.

13.1 GAS FLOW

Uneven gas velocity distribution in a precipitator can reduce the efficiency several ways. First, because of the exponential relationship between gas velocity and efficiency, an uneven gas distribution flow results in a lower efficiency than would be predicted from the average. Second, uneven gas flow can cause scouring or erosion of the dust from the collection plates, thereby reducing efficiency. Third, poor gas flow patterns can result in dust fallout and accumulation on turning vanes and in the duct work. Such accumulations can further interfere with gas flow, and cause decreased performance. Plugging of distribution plates is also a commonly encountered problem which disrupts gas flow.

Evidence of poor gas flow quality (uniformity of flow) is obtained from a gas velocity distribution profile at the precipitator inlet. The IGCI recommends a gas quality such that 85% of the local velocities is within 25% of the mean with no single reading more than ± 40% from the mean. This is the minimum requirement for good precipitation.

Other types of gas flow problems commonly experienced are air inleakage into hoppers from the dust conveyor system and "gas sneakage" (see below) through the upper portion of the precipitator around the high tension frame. Air inleakage through the conveyor system results in reentrainment of collected dust which is carried back into the precipitator. Air inleakage can also occur through the precipitator shell or inlet flanges, if the precipitator operates at less than atmospheric pressure. Often sufficient air is bled into the system to cause intense sparking.

"Gas sneakage" is the term used to describe gas flow that constitutes a by-pass around the effective precipitator section. It can occur through dead passages of the precipitator above the collector plates, around the high tension frame, or through the hoppers. The gas sneakage problem usually accounts for only a few percent drop in efficiency unless it is exceptionally severe. The problem can be identified by measurement of gas flow in the suspected areas in a nonoperating or cold test. Corrective measures usually involve baffling to direct the gas into the active precipitator section.

Problems of reentrainment of dust from the hoppers by virtue of air inleakage or gas sneakage can often be identified by an increase in dust concentration at the bottom of the exit to the precipitator.

13.2 RAPPING

Rapping requirements for various types of dusts are discussed in the section on rapping and reentrainment. Unfortunately, there are inadequate data from which to determine rapping requirements based on variations in dust resistivity, current density and other dust conditions.

Rapping is needed on both the discharge and collection electrodes. The rapping forces can be either too mild or too severe and result in poor performance. Removal of the collected dust is best achieved when the intensity and frequency of rapping is such that the dust falls from the collection plates in sheets; hence too intense and frequent rapping can result in a clean plate with the collected dust reentrained rather than falling into the hopper. On the other hand, inadequate rapping can result in an excessive thickness of deposit on both collection and discharge electrodes, which can lead to other disruptive effects.

Inadequate rapping of the discharge electrodes can result in heavy dust build up with a localization of the corona, low corona current, and excessive sparking.

The presence of a deposit on the discharge electrodes can be a result of several factors, including poor gas flow and the conditions of the dust. Often deposits of up to two inches diameter can form. These deposits or donuts are generally composed of the finer dust particles and often cling tenaciously to the discharge wire. Deposits on the discharge wires do not necessarily result in poor performance, although depending on resistivity, power supply range, and uniformity of the deposit, it can constitute a source of reduced efficiency.

Rapping of both collection and discharge electrodes is only effective if the force is transmitted to the respective electrodes. Variations in the design of the support structure and in the electrodes themselves can also result in inadequate rapping. Recent investigations of rapping acceleration in fly ash precipitators have shown measured accelerations of approximately 5g's on the plates when accelerations of 30g's may be required. If practical, measurement of the rapping acceleration with accelerometer mounted on the plates can be used to check rapping adequacy. A common method of adjusting rappers is with the use of an optical dust measuring instrument in the precipitator exit gas stream.

The discharge electrodes should be kept as clean as practical. The rapping intensity in this case is limited only by mechanical damage to the electrodes and support structure.

13.3 HOPPERS AND ASH REMOVAL

Hoppers and ash removal systems often constitute problems in precipitator operation. If the hoppers become full, the precipitator may become short circuited by the collected dust. Often the power through the dust is sufficient to fuse the dust, and a large clinker-type structure called a "hornet's nest" is formed. This further interferes with ash removal and must be removed for proper operation. Most problems associated with the hoppers are in providing for proper flow of the dust. Improper adjustment of the hopper vibrators or failure of the conveyor system are the usual causes of the failure to empty the hoppers. In some instances it may be necessary to provide heat and/or thermal insulation for the hoppers to avoid moisture condensation and a related cementing of the collected dust.

Air leakage and gas sneakage as related to hoppers have been previously discussed.

13.4 TROUBLESHOOTING TECHNIQUES

The procedures used in locating precipitator troubles are principally those of measurement of those quantities that can be readily determined and a visual inspection and observation of the precipitator itself. Depending upon the severity of the problem, the difficulty will be more or less obvious. For example, if a precipitator is designed for 90-95% efficiency and is operating at 50-60%, the difficulties are gross ones. In contrast, the problems in increasing efficiency from 90-95% may involve subtle changes or improvements.

Gross difficulties with precipitators are usually those associated with inadequate electrical energization or excessive reentrainment. The following techniques are generally useful in pinpointing the causes of gross precipitator problems.

1) Measurement of high tension voltage, current, and spark rate.
2) Measurement of gas flow distribution.
3) Observation of the collecting plates for evidence of back corona.

4) Oscilloscope record of the high tension voltage to determine the duration of the corona current.

5) Direct observation of the collection plate for evidence of scouring or excessive reentrainment. (This requires construction of a glass plate and wiper for an access port and a means for illumination of the interelectrode space.)

6) Measurement of the dust distribution at the precipitator exit.

7) Careful examination of the general alignment and the conditions of the hoppers, insulators, and other components.

8) Measurement of the rapping accelerations.

9) Observation of the corona wire and the uniformity of the corona tufts.

13.5 MAINTENANCE

Maintenance of precipitators falls into the categories of preventive maintenance and maintenance to correct failures of some part of the system. Preventive maintenance schedules should be established to conform to the requirements for the particular installation. A typical maintenance schedule is given in Table 13.1 for a fly ash precipitator. The items covered will give an idea of the types of maintenance that need to be performed on a weekly to monthly basis.

Problems with failure of precipitator components are usually associated with power supply, wire breakage, failure of structural parts due to corrosion, fatigue, or rapper failure.

Power supply failures should be handled by only those personnel competent to service high voltage equipment. The types of failure that may be encountered are: (1) malfunction of the control circuit, (2) rectifier failure, or (3) transformer failure. Conventional high voltage servicing procedures should be used to identify the particular power supply problem.

The majority of the precipitators now in service utilize vacuum tube or solid-state rectifiers. Normal vacuum tube life ranges from 12,000 to

Table 13.1

Typical Maintenance Schedule

A. Annual Inspection

1. Internal inspection

   a. Observe dust deposits on collecting plates and wire before cleaning - a $\frac{1}{4}$" deposit is normal. If metal plates are clean, there is a possibility that a section is shorting out. If more than $\frac{1}{4}$" of dust is on plates, rappers are not cleaning.

   b. Observe dust buildup on wires.

   c. Interior corrosion - corrosion could indicate air leak through shell, or could indicate moisture carryover from air heater washer.

   d. Plate corrosion adjacent to door or near bottom of plate could indicate inleakage through doors.

   e. Check plates for alignment and equal spacing between plates.

   f. Measure to see that discharge wires hang midway between plates.

   g. Check for and replace broken wires.

2. Hopper inspection

   a. Check for dust buildup in upper corners of hoppers.

   b. Check anti-sway insulators to see that they are cleaned and not cracked.

   c. Check high tension weights - if one has dropped 3", this indicates broken wire.

   d. Check hopper bottom and valve for debris.

Table 13.1 - Maintenance Schedule (Continued)

3. Penthouse inspection
   - a. Check for corrosion due to condensation and/or leakage of flue gas into housing.
   - b. Excessive dust in penthouse indicates air sealing pressure too low.
   - c. Clean all high tension insulators.
   - d. Check that all high tension connections are secure.
   - e. Check that collars on high tension vibrator insulators are secure.
4. Transformer inspection
   - a. Check liquid level.
   - b. Clean high tension line, insulators, bushings, and terminals.
   - c. Check surge arrestors, spark gap should be $\frac{1}{32}$".
5. Control cabinet inspection
   - a. Clean and dress relay contacts.

B. Rappers and Vibrators Checked Quarterly

1. Rappers
   - a. Check distributor switch contacts for wear and lubricate.
   - b. Clean dust, dirt, and moisture from cabinet.
   - c. Check rapper assembly for binding at plunger or misalignment.

Table 13.1 - Maintenance Schedule (Continued)

2. Vibrators
    a. Check contacts on load cams to see that they are clean.
    b. Clean dirt, dust, and moisture from cabinet.
    c. Check vibrators to see that they operate at proper intervals.

C. Checks to Be Made Each Shift
    1. Electrical reading for each control unit should be recorded and checked for abnormal readings.
    2. Rapper controls should be checked to see that they operate.
    3. Vibrator controls should be checked.

20,000 hours, and servicing usually involves only replacement of defective rectifier tubes. Most solid state rectifiers are relatively trouble free and maintenance is not normally required. Transformer oil should be periodically inspected to determine its condition, however transformers generally last the life of the precipitator.

Insulators and flower pot bushings which hold the high tension frame must be kept clean and dry to prevent arcing. This is normally done by providing a source of clean, dry gas to the insulator compartment. Should the dusty, moist gas from the precipitator get into the insulator compartment, arcing would occur and ultimately result in the failure of the insulator.

One of the most common difficulties with electrostatic precipitators of the suspended wire electrode type is wire failure. Depending on the location of the break, the wire can fall in such a way as to short circuit an entire section and it must be removed before the section can be reenergized.

Wire failures can be caused by corrosion, excessive localized sparking or mechanical fatigue. It is often difficult to determine the exact cause of failure; the best procedure is to keep account of the location of the failed wire in the precipitator and the position of the break along the wire to determine if the failures are random or associated with a particular location in the unit. Corrosion failures generally occur around cooler areas where condensation can take place. Excessive air bled in around insulators can cause condensation leading to failure of the wires near the insulators. Electrical sparking in localized areas is also a common cause of failure. Normal sparking is a statistical phenomenon and the location of the spark can be at any position along the wire and in any wire. However, localized areas of high field strength can confine sparking to a particular area, and this will ultimately lead to failure at that position. Common faults leading to this type failure are misalignment of the electrodes or improper shielding around edges of collection plates. These conditions call for realignment of the plates, use of shrouds to reduce the field at critical locations, or removal of sources that might cause localized high fields.

Mechanical failure can occur because of movement of the wire under the influence of aerodynamic and electrical forces. If a wire is moved from the center of the field by an uneven gas flow, an electrical force will develop causing the wire to move further in the same direction. This movement could result in fatigue failure of the wires.

When it is recognized that a typical precipitator contains approximately 10,000-30,000 feet of wire, it is reasonable to expect some wire failure.

There have been some attempts to establish a normal failure rate in terms of the number of wire failures per year per 1,000 ft of wire; however, there is a wide variation in experience depending on application, and no standard or normal failure rate has been established.

Most industrial gases are corrosive under proper temperature conditions, and corrosion must be considered as a problem in the design and maintenance of electrostatic precipitators. This can be handled by the use of corrosion-resistant materials or by maintaining the temperature of the critical components above the dew point. Use of corrosion-resistant materials is practiced for precipitators used in the collection of sulfuric acid fume, in cement kiln precipitators operating at low temperatures, in some precipitators collecting dust from black liquor recovery boilers, and in some fly ash precipitators operating with high sulfur coal at low temperatures.

Because of the trend to lower exit gas temperatures in electric power generating stations, problems of corrosion have become more acute in that application. One of the major corrosion problems is that of the precipitator shell. In order to reduce corrosion to a minimum, it is customary to provide good insulation on the shell to keep its temperature as high as practical. This technique has been adequate within the range of temperatures and sulfur contents used.

In addition to the shell, corrosion can also occur at other locations. Air inleakage at joints can cause severe localized corrosion. The major consideration as far as maintenance is concerned is to maintain all corrosion-susceptible surfaces above the dew point and to prevent air inleakage into vulnerable areas of the precipitator.

BLANK PAGE

CHAPTER 14
ELECTROSTATIC AUGMENTATION AND UNUSUAL PRECIPITATION DESIGNS

Augmentation of particulate control devices by superposition of an electric field or by charging of the dusts has been studied to varying degrees. Also, the use of methods of establishing an electric field by space charge and alternative methods of particle charging have been subjects of continuing interest.

Electrostatic augmentation has been applied to fabric filters, packed bed filters, wet scrubbers, and mechanical collectors, using both conventional and alternative methods of establishing an electric field and particle charging.

The following discussion is limited to an examination of the concepts involved in electrostatically augmented particulate control devices and in unusual precipitator designs, as opposed to a critique of the implementation.

14.1 WET SCRUBBERS

The efficiency of wet particulate scrubbers is generally limited by the ability to capture the dust particles by the water droplets. Conventional high efficiency scrubbers are operated with relatively large pressure drops to achieve a high relative velocity between the dust particle and the water droplet. This high velocity is necessary to propel the dust particle across the boundary layer and to overcome the surface tension of the water drop so that the particle will be captured. Fine dusts require a very large pressure drop, and hence high energy requirements, because the mechanism that transports the dust particle through the boundary layer is primarily inertial.

One concept of electrical augmentation of wet scrubbers is to charge the water and dust with an opposite polarity in an attempt to utilize the attractive electrical forces to bring the dust and water droplets together.[1]

An analysis of the attractive forces involved between a 0.5μ diameter dust particle and 10μ water droplet exhibits a variation as shown in

---

[1] Refer to the bibliography for this chapter.

Figure 14.1. The particles and water droplets are considered to be oppositely charged to saturation in a relatively high electric field of 6 kV/cm. The force equation from electrostatics is

$$F = q \cdot q_2 / 4\pi \epsilon_0 r^2 \text{ Newtons}$$

The saturation charge for the dust and water droplet is 78 and 31,000 electronic charges, respectively. The attractive force as a function of separation distance is

$$F = \frac{5.65 \times 10^{-22}}{r^2} \text{ Newtons}$$

when the separation distance is measured in meters. The graph shows the attractive force for separation distances from 10 to 100μ. At 10μ, the dust particle will be within the boundary layer of the air around the water droplet and they will contact. At distances greater than 100μ, the force becomes negligible.

A reference force for the gravitational attractive force acting on a 50μ water droplet is included which causes this water droplet to fall toward the earth with a settling velocity of about 10 cm/sec. This suggests that the effect of the electrostatic attractive force is rather small, except for very close approaches.

The electrical force causes an increase in the relative velocity of the dust particle and the water droplet of only about 3.0 cm/sec for the example considered. While this is a rather small change in the relative velocity, the fact that the attractive force always exists will tend to increase the collection efficiency of the very small particles somewhat. Since this effect is rather small, it seems that it would be more desirable to install an electrostatic precipitator initially than to include both positive and negative charging fields in front of the high energy wet scrubber.

Another technique for augmentation of wet scrubbers is through the use of an electrostatic precipitator as an agglomerator to modify the particle size distribution of the dust to the scrubber.[2] Since the collection efficiency for scrubbers is greater for large particles, the reentrained black liquor fume from a paper mill recovery system is more easily collected after agglomeration. The tests reported were from a pilot scale test.

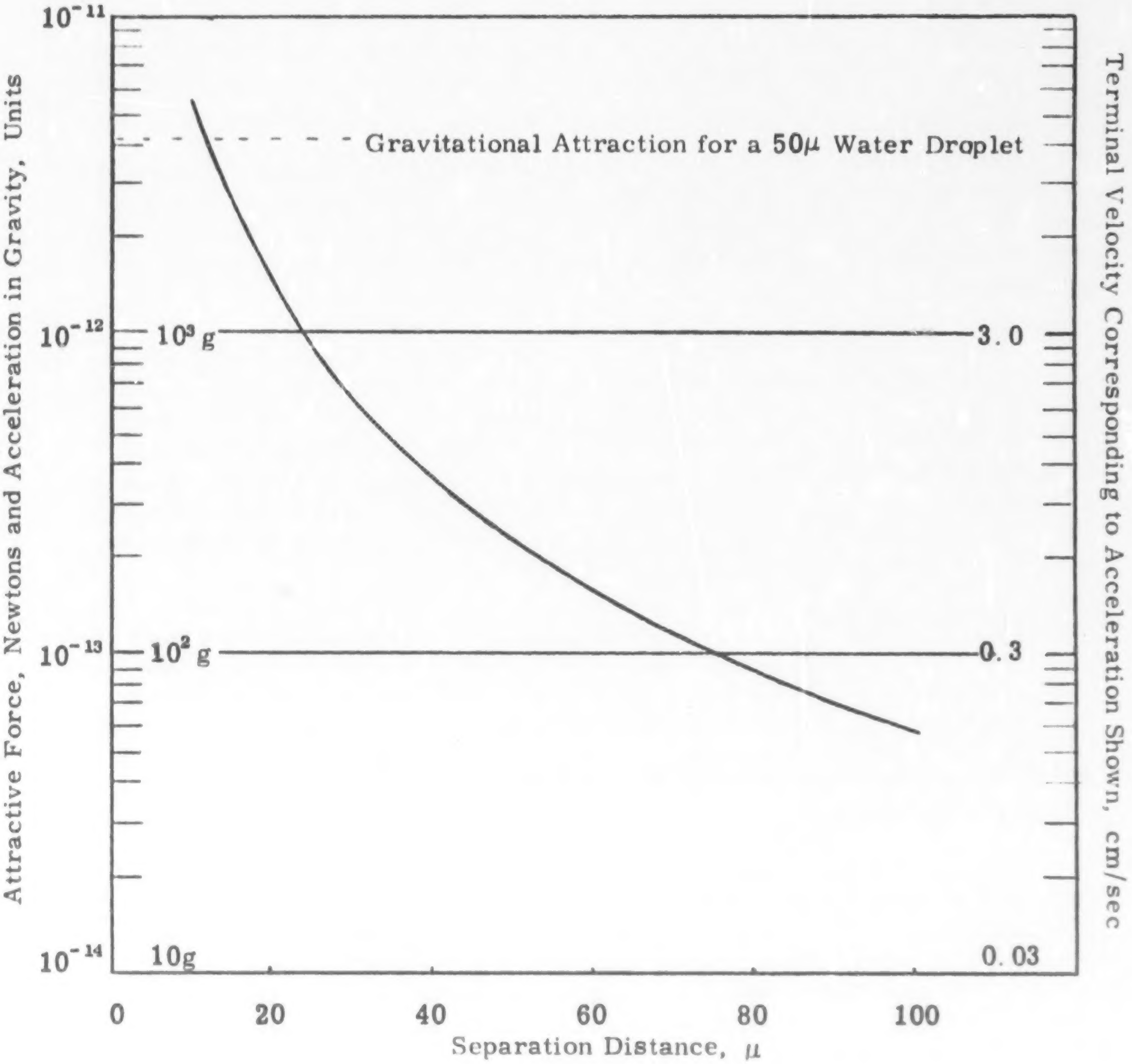

Figure 14.1. The Electrostatic Force between a 10μ Water Droplet and a 0.5μ Dust Particle Charged to Saturation in an Electric Field of 6 kV/cm.

14.2 ELECTROSTATICALLY AUGMENTED PACKED BED FILTERS

A packed bed filter is a particulate emission control device that is comprised of a column of loosely packed fibers, gravel or other filter material. The dust laden gases flow through this filter column to provide the opportunity for the dust particles to be collected on the filter medium. These packed bed filters characteristically provide rather poor efficiency for small particles.

The collection efficiency for this type of collector can be increased by the use of electrostatic augmentation. If the filtration region is immersed in an electrostatic field, the dust particles will be driven in a direction that tends to increase the probability of impact between the particles and the filter medium.

If the dust particles are initially uncharged, the electric field will induce an electrical dipole in each particle which tends to align each particle with the electric field.[3,4] This tends to orient the particle in such a way that the negative end of the dipole contacts the positive surface charge of the filter medium, and similarly, the positive ends tend to contact the negative surface charge of the medium (see Figure **14.1**). The result of this is that the collection efficiency is increased somewhat by the attractive force between the dust particles and the filter medium.

The filtration efficiency of packed bed filters can be further enhanced if the dust particles are electrically charged prior to introduction in the collector. If charged particles are introduced into the filter medium with a superimposed electric field, the dust particles are driven in the direction of the electric field. Thus, the probability of collection and the retentive forces for the dust particles are both increased by the addition of the electrostatic augmentation.

Particle collection theory for turbulent flow electrostatic precipitation shows that particles are captured only in the boundary layer of the gas stream adjacent to the collection electrodes. In conventional electrostatic precipitators, the interelectrode space is largely inactive for particle collection. This problem is significantly reduced in the augmented packed filter bed collector since the entire surface of the filter medium acts as the collection surface. This results in a significant increase in the collection area for a given volume of collector in comparison to that for a conventional precipitator.

The advantage of the loose packed filter bed is the low pressure drop required to maintain the gas flow. It seems probable from the above considerations that a reasonably high collection efficiency, even for the small particles, can be attained with electrostatic augmentation.

An obvious disadvantage to the electrostatically augmented bed filter is the inability of the system to be rapped for dust removal. The dust collector would require back flushing or filter media recycling for cleaning.

14.3 FABRIC FILTER

The collection efficiency and pressure drop in a fabric filter are related to the open area in the fabric and dust layer. As dust builds up in the fabric, the open area decreases leading to an increased collection efficiency and pressure drop. The efficiency of a fabric filter is essentially constant for a given dust and the resultant pressure drop is dependent on the gas flow rate.

Electrostatic augmentation of a fabric filter can take the form of charging the dust particles or establishing an electrostatic field across the dust layer, or both. The action of the electrostatic field is to provide a force between the dust particle and the dust layer such that openings appear to be smaller. Particles that would otherwise pass through the dust layer are therefore trapped, resulting in a somewhat higher efficiency and pressure drop.

Only limited studies have been made of electrostatic augmentation of fabric filters; the principal advantage noted has been a decrease in the time required to establish a dust layer and hence less time required to reach ultimate efficiency. Other studies have largely been inconclusive.

14.4 MECHANICAL COLLECTION

Consideration has been given to electrostatic augmentation of mechanical collection; however, since the mechanical collectors are basically of high gas flow type, there would appear to be little advantage to the addition of electrostatic augmentation since:

(1) the area of collecting surface would be small relative to the gas flow, hence in the standard efficiency equation, the contribution of the electrostatic field to the efficiency would be small; and

(2) the tendency toward reentrainment would be large.

14.5 SPACE CHARGE PRECIPITATION

Conventional electrostatic precipitator theory shows that the migration velocity of charged particles suspended in an electric field is proportional to the product of their charge and the value of the electric field as given by

$$w = qE_p/6\pi a\eta \qquad (14.1)$$

where q is the charge on the particle in Coulombs, E_p is the value of the electric field in the collection zone in volts per meter, a is the radius of the particle in meters, and η is the viscosity of the gas in kg-meter-second. This basic equation is valid for the particle velocity independent of the mechanisms used for either providing the charge or establishing the electric field.

The space charge precipitator[5,6,7] utilizes the distributed space charge of the charged particles, sometimes augmented by additional space charges provided by the introduction of charged water droplets as the source of the collection electric field. Conventional electrostatic precipitators of either the single-stage or two-stage type utilize collection electrodes connected to high voltage power supplies in addition to this space charge to provide the collection field.

The motivation for the development of space charge precipitators is to simplify the electrical requirements in the collection zone of the installation. Space charge precipitation is not a new concept in precipitation. The space charge has always contributed to the electric field in the collection zone; but the removal of that component of the collection field caused by the high voltage power supply is a new embodiment. However, it should be pointed out that the value of the electric field in the collection zone will always be smaller for the space charge collector than would result from a conventional precipitator of the same dimensions if all other factors remain the same. The removal of the electrical contributions from the power supply will result in a reduction in the collection field. Since the migration velocity is proportional to the collection field, this results in a decrease in the migration velocity. Therefore, it must be understood that the purpose for pursuing the development of space charge precipitators is to simplify the design of precipitators, not to improve their performance.

Two factors can be used to promote the development of space charge precipitators. The first is the absence of back corona in the collection zone and the second is the reduction of reentrainment when charged water droplets are utilized as part of the space charge. But it must be pointed out that these factors are not peculiar to space charge collectors. It is common knowledge that wet wall precipitators reduce the reentrainment of collected particles and that back corona is related to the current density and resistivity of the dust particles on the collection electrodes. Therefore, there are methods other than space charge precipitation available for the solution of these specialized problems.

The electric field in the collection zone of a wire and pipe precipitator as determined from conventional theory is

$$E(r) = -\left\{\left(\frac{r_0 E_0}{r^2}\right)^2 - \left(\frac{r_0^2}{r^2} - 1\right) \frac{i\rho}{2\pi\epsilon_0 \mu_i \rho_i}\right\}^{\frac{1}{2}} \qquad (14.2)$$

where $E(r)$ is the electric field value as a function of the radius r; r_0 is the radius of the corona glow region; i is the current per unit length of the corona wire; ρ and ρ_i are the respective space charges, total and ionic; μ_i is the mobility of the free ions; ϵ_0 is the permittivity of free space, and E_0 is the breakdown field strength of the gas in the precipitator. This equation shows that the electric field is caused by both the electrostatic term and the space charge term.

In the absence of an applied voltage, the electric field is caused exclusively by the distributed space charge. Gauss' law can be used to evaluate the value of the field for this special case. Thus

$$\int \epsilon_0 E ds = q. \qquad (14.3)$$

For the wire and pipe case, where the electric field is everywhere normal to the surface of the pipe and uniform, Equation 14.3 reduces to

$$E = q/\epsilon_0 A = \frac{\rho V}{\epsilon_0 A} = \frac{\rho \pi r^2 h}{2\pi r h \epsilon_0} = \frac{\rho r}{2\epsilon_0} \qquad (14.4)$$

where E is the value of the electric field at the pipe; q is the total space charge enclosed within the surface which is equal to the product of the space charge density, ρ, and the volume $\pi r^2 h$; A is the surface area of the cylinder; and ϵ_0 is previously defined.

A similar derivation for the parallel plate configuration yields

$$E\ (\text{parallel}) = \frac{\rho h}{2\epsilon_0} \qquad (14.5)$$

where h is the distance between the plates.

Equations **14.4** and **14.5** show that the value of the electric field is linearly related to the plate separation for a uniform charge density situation. Thus, theoretically, the collection efficiency for a space charge precipitator is independent of plate spacing. As the plate spacing increases, the electric field increases, which results in a linear increase in migration velocity, thus maintaining a constant collection efficiency. However, this collection efficiency is always less than that which theory predicts for a conventional precipitator since the electric field is increased by the applied voltage field.

Equations **14.4** and **14.5** show that the collection electric field is directly proportional to the space charge density for space charge precipitators. As the particles that provide the space charge are collected, the space charge density is reduced. The result of this is that the collection electric field is reduced by the amount of precipitate collected as the gas proceeds through the collector. The migration velocity and incremental collection efficiency approach zero as the total material collected approaches 100%.

This problem is overcome in some instances by the injection of charged water droplets at various positions within the collector. This technique reduces the problem of a reduced space charge, but does not eliminate it.

Some problems are encountered in the formation of these charged droplets. Spray nozzles typically form droplets of too great a diameter, while grown condensation nuclei require considerable equipment as well as additional corona sections.

Some merit is attributable to space charge precipitators in that the construction of the collection electrode system is simplified. This technique may find an application for the collection of particulate from small gas volume installations where extremely high collection efficiencies are not required.

A special case of the space charge precipitator that has been investigated utilizes laminar flow in the collection zone.[7] Since the collection efficiency of the space charge precipitator is independent of plate spacing, it is theoretically possible to build a collector with laminar flow rather than with the turbulent flow conditions existing in conventional installations. The motivation for this development is that the collection efficiency for laminar flow precipitation is linearly related to the collection electrode area to volume flow ratio rather than the exponential ratio associated with the Deutsch-Anderson equation for turbulent flow. Whereas the Deutsch-Anderson equation relates as follows:

$$\eta = 1 - \exp\left(-\frac{A}{v_g} w\right) \tag{14.6}$$

the laminar flow equation can be stated as

$$\eta = \frac{A}{v_g} w.$$

Thus it can be seen that the laminar flow equation predicts a 100% collection efficiency when $\frac{A}{v_g}$ becomes equal to the reciprocal of the migration velocity.

Initially, this approach appears to be extremely desirable. However, when viewed in the light of attainable migration velocities, some difficulties with the approach become apparent. Again, calling on conventional theory, the migration velocity is

$$w = qE_p / 6\pi a \eta$$

From Equation 14.5, the electric field for the parallel plate configuration is

$$E = \frac{\rho h}{2\epsilon_0}$$

Plate separations from laminar flow must be maintained at about 0.1 in. $\approx$ 2.5×10^{-3} meter. The space charge density can be estimated for a reasonable dust loading of about 10 grains/ft^3 = 2.3×10^{-5} gm/cm^3 = 0.23 gm/m^3. If this dust loading is brought about by a 1μ diameter particle with a density of 3 gm/cm^3, the number of particles per unit volume is determined by dividing the weight per unit volume of the gas by the weight of one particle. The weight and volume of unit density particles differ by a factor of 3.

$$V = \tfrac{4}{3}\pi a^3 = \tfrac{4}{3}\pi\ (5 \times 10^{-5}\ \text{cm})^3 = \frac{500\pi}{3} \times\ 10^{-15} = 5.22 \times 10^{-13}\ \text{cm}^3$$

The number of particles per cm is

$$\text{No/cm}^3 = \frac{2.3 \times 10^{-5}\ \text{gm/cm}}{15.66 \times 10^{-13}\ \text{gm}} = 4.4 \times 10^7\ \text{particles/cm}^3$$

$$= 4.4 \times 10^{13}\ \text{particles/m}^3$$

The charge per unit volume is estimated from the product of the charge per particle and the particle concentration. Assume a reasonable value of a charging field on the order of 5×10^5 V/m. The saturation charge for 1μ particles is about 260 electrons/particle = 4.2×10^{-17} Coulombs/particle. Thus,

$$\rho = \text{space charge density} = 1.4 \times 10^7\ \text{part/cm}^3 \times 4.2 \times 10^{-17}\ \text{Cou/part}$$

$$= 5.90 \times 10^{-10}\ \text{Cou/cm}^3 = 5.90 \times 10^{-4}\ \text{Cou/m}^3$$

Substituting into Equation 14.5

$$E = \frac{5.90 \times 10^{-4}\ \text{Cou/m}^3 \times 2.5 \times 10^{-3}\ \text{meter}}{2 \times 8.85 \times 10^{-12}\ \text{F/m}} = 0.83 \times 10^5\ \text{V/m}$$

$$= 8.3 \times 10^4\ \text{V/m} = 830\ \text{V/cm}$$

Customary values for the collection electric field range from 2 - 6 kV/cm.

The migration velocity for a particle collected in a field of 800 V/cm will be only one-fifth of that for one collected in a field of 4 kV/cm. Thus, the collection electrode area for a laminar flow space charge collector would be approximately the same as for a conventional turbulent flow collector for a collection efficiency of 99%.

If the laminar flow collector were contemplated for collecting larger particles, the problem becomes more acute. The space charge from large particles is reduced if the same dust loading is used. For example, if

10μ particles are used in the previous example, the volume of one particle is increased by a factor of 10^3, while the charge per particle is increased by a factor of 10^2 for a net reduction in space charge of a factor of 10 to 83 V/cm.

Electrostatic precipitation theory shows that the migration velocity of a charged particle suspended in an electric field is proportional to the product of the charge on the particle and the value of the electric field. In this example, the charge on the particle is of the same order of magnitude that would be encountered in conventional precipitators. The value of the collection electric field is about one-tenth that in conventional collectors. Therefore, the migration velocity of the particles would be only one-tenth that for conventional precipitators.

The idea of approaching laminar flow in the collection zone does have some merit, but the practical matter of constructing commercial sizes of these units with plate spacings of 0.1 in. places an extremely tight manufacturing tolerance on the installation.

CHAPTER 14
BIBLIOGRAPHY

1. Joubert, Jacques, "Contribution to the Problem of Determination of the Trajectory of a Conducting Particle Placed in a Hydrodynamic Field and an Electric Ionizing Field," University of Lyon, France.

2. Walker, A. B., "Enhanced Scrubbing of Black Liquor Boiler Fume by Electrostatic Pre-Agglomeration," JAPCA **13**, No. 12, p 622 (December 1963).

3. Zebel, G., "Deposition of Aerosol Flowing Past a Cylindrical Fiber in a Uniform Electric Field," J. Colloid Sci. **20**, pp 522-543 (1965).

4. Mazumder, M. K. and Thomas, K. T., "Improvement of the Efficiency of Particulate Filler by Superimposed Electrostatic Forces," Filtration and Separation, p 25 (Jan-Feb 1967).

5. Faith, L., et al., "Particle Precipitation by Space Charge in Tubular Flow," Ind. Eng. Chem. Fund. **6**, p 519 (1957).

6. Webber, M. E., "Experimental Studies on Space-Charge Precipitation," thesis submitted to the University of California at Berkeley (September 5, 1969).

7. Hanson, D. N. and Wilke, C. R., "Electrostatic Precipitator Analysis," Department of Chemical Engineering, University of California at Berkeley.